



**HAL**  
open science

## Extending full-plate tectonic models into deep time: Linking the Neoproterozoic and the Phanerozoic

Andrew S. Merdith, Simon E. Williams, Alan S. Collins, Michael G. Tetley,  
Jacob A. Mulder, Morgan L. Blades, Alexander Young, Sheree E. Armistead,  
John Cannon, Sabin Zahirovic, et al.

### ► To cite this version:

Andrew S. Merdith, Simon E. Williams, Alan S. Collins, Michael G. Tetley, Jacob A. Mulder, et al..  
Extending full-plate tectonic models into deep time: Linking the Neoproterozoic and the Phanerozoic.  
Earth Science Reviews, 2021, 214, 10.1016/j.earscirev.2020.103477 . insu-03710151

**HAL Id: insu-03710151**

**<https://insu.hal.science/insu-03710151>**

Submitted on 22 Mar 2023

**HAL** is a multi-disciplinary open access archive for the deposit and dissemination of scientific research documents, whether they are published or not. The documents may come from teaching and research institutions in France or abroad, or from public or private research centers.

L'archive ouverte pluridisciplinaire **HAL**, est destinée au dépôt et à la diffusion de documents scientifiques de niveau recherche, publiés ou non, émanant des établissements d'enseignement et de recherche français ou étrangers, des laboratoires publics ou privés.



Distributed under a Creative Commons Attribution - NonCommercial 4.0 International License

# 1 **Extending Full-Plate Tectonic Models into Deep Time: Linking the Neoproterozoic and the** 2 **Phanerozoic**

3  
4 Andrew S. Merdith<sup>1,\*</sup>, Simon E. Williams<sup>2</sup>, Alan S. Collins<sup>3</sup>, Michael G. Tetley<sup>1</sup>, Jacob A. Mulder<sup>4</sup>,  
5 Morgan L. Blades<sup>3</sup>, Alexander Young<sup>5</sup>, Sheree E. Armistead<sup>6</sup>, John Cannon<sup>7</sup>, Sabin Zahirovic<sup>7</sup> and R.  
6 Dietmar Müller<sup>7</sup>

7 <sup>1</sup> UnivLyon, Université Lyon 1, Ens de Lyon, CNRS, UMR 5276 LGL-TPE, F-69622, Villeurbanne, France

8 <sup>2</sup> Northwest University, Xi'an, China

9 <sup>3</sup> Tectonics and Earth Systems (TES) Group, Department of Earth Sciences, The University of Adelaide, Adelaide, SA 5005, Australia

10 <sup>4</sup> School of Earth, Atmosphere and Environment, Monash University, Clayton, Victoria 3168, Australia

11 <sup>5</sup> GeoQuEST Research Centre, School of Earth, Atmospheric and Life Sciences, University of Wollongong, Northfields Avenue, NSW 2522,  
12 Australia

13 <sup>6</sup> Geological Survey of Canada, 601 Booth Street, Ottawa, Ontario, Canada & Metal Earth, Harquail School of Earth Sciences, Laurentian  
14 University, Sudbury, Ontario, Canada

15 <sup>7</sup> Earthbyte Group, School of Geosciences, University of Sydney, Sydney, New South Wales, 2006, Australia

16 \* Corresponding author: [Andrew.merdith@univ-lyon1.fr](mailto:Andrew.merdith@univ-lyon1.fr)

## 17 18 **Abstract**

19  
20 Recent progress in plate tectonic reconstructions has seen models move beyond the classical idea of  
21 continental drift by attempting to reconstruct the full evolving configuration of tectonic plates and plate  
22 boundaries. A particular problem for the Neoproterozoic and Cambrian is that many existing  
23 interpretations of geological and palaeomagnetic data have remained disconnected from younger, better-  
24 constrained periods in Earth history. An important test of deep time reconstructions is therefore to  
25 demonstrate the continuous kinematic viability of tectonic motions across multiple supercontinent cycles.  
26 We present, for the first time, a continuous full-plate model spanning 1 Ga to the present-day, that  
27 includes a revised and improved model for the Neoproterozoic–Cambrian (1000–520 Ma) that connects  
28 with models of the Phanerozoic, thereby opening up pre-Gondwana times for quantitative analysis and  
29 further regional refinements. In this contribution, we first summarise methodological approaches to full-  
30 plate modelling and review the existing full-plate models in order to select appropriate models that  
31 produce a single continuous model. Our model is presented in a palaeomagnetic reference frame, with a  
32 newly-derived apparent polar wander path for Gondwana from 540 to 320 Ma, and a global apparent  
33 polar wander path from 320 to 0 Ma. We stress, though while we have used palaeomagnetic data when  
34 available, the model is also geologically constrained, based on preserved data from past-plate boundaries.  
35 This study is intended as a first step in the direction of a detailed and self-consistent tectonic

36 reconstruction for the last billion years of Earth history, and our model files are released to facilitate  
37 community development.

38

## 39 **1 Introduction**

40

41 Plate tectonics is a unifying theory of modern geology, explicitly connecting the evolution and processes  
42 that bridge the mantle, lithosphere, hydrosphere and atmosphere. Tectonic forces control the rates of  
43 uplift and erosion where continents collide or separate (England and Molnar, 1990) and modulate the flow  
44 of energy between oceans, lithosphere and mantle as continental configurations evolve (Bebout, 1995;  
45 Karlsen et al., 2019; Müller et al., 2008). Evolving plate tectonic configurations also determine changes in  
46 how species are distributed across different landmasses (McKenzie et al., 2014; Meert and Lieberman,  
47 2008) and infer the rates of chemical flux between the Earth's surface and the deep interior (Gernon et al.,  
48 2016; Jarrard, 2003).

49

50 Global reconstructions have traditionally focussed on the positions of the major continents and geological  
51 terranes preserved within them. Data acquired from modern oceans provide a powerful constraint on the  
52 breakup of the supercontinent Pangea over the last ca. 200 Ma, and form the basis of continuous models  
53 of plate configurations from the Mesozoic to present (e.g. Müller et al., 2016; Seton et al., 2012). These  
54 'full-plate' reconstructions use geological and geophysical data to determine the configurations and  
55 motions of both continental and oceanic lithosphere, and the nature of the plate boundaries that separate  
56 neighbouring plates. Together with the development of free software tools (Boyden et al., 2011; Müller et  
57 al., 2018), full-plate reconstructions permit quantitative estimates of tectonic processes through time  
58 within a continuous, consistent kinematic framework, opening up portions of Earth's history to  
59 quantitative analysis (e.g. Bower et al., 2013; Brune et al., 2017; Dutkiewicz et al., 2019; Hounslow et al.,  
60 2018; Karlsen et al., 2019; Meredith et al., 2019a).

61

62 Plate tectonic processes are thought to have been the dominant control on Earth's paleogeography  
63 possibly since 3.2 Ga (Brenner et al., 2020; Brown et al., 2020a; Cawood et al., 2018a; Gerya, 2014; Palin  
64 et al., 2020). Studies of the pre-Pangean Earth have led to the proposal that Pangea was preceded by the  
65 Proterozoic supercontinents Rodinia (Dalziel, 1991; Hoffman, 1991; Moores, 1991) and Nuna/Columbia  
66 (Meert, 2002; Rogers and Santosh, 2002; Zhao et al., 2002) and earlier Archaean 'supercratons' (e.g.  
67 Bleeker, 2003; Pehrsson et al., 2013; Smirnov et al., 2013), reflecting transient aggregations of  
68 continental blocks interspersed between other phases of Earth's history when the continents were more  
69 dispersed. The absence of a pre-Mesozoic ocean floor record necessitates that reconstructing the pre-

70 Pangean Earth relies on the fragmented geological record preserved within the continents. Early studies of  
71 Proterozoic supercontinents provide individual snapshots of continental configurations; though there are  
72 differences between competing interpretations. More recently, attempts have been made to reconcile  
73 Neoproterozoic continental motions within a continuous kinematic framework (Cawood et al., 2020;  
74 Collins and Pisarevsky, 2005; Li et al., 2008). To further infer the extent and nature of tectonic  
75 boundaries covering all of Earth's surface in the Proterozoic requires methodical extrapolation of  
76 available observations and is subject to major uncertainties. Despite this, these reconstructions are  
77 valuable in that they make testable predictions about regions and time periods where observations are  
78 lacking.

79

80 Full-plate models published over the last decade collectively span the last 1 Ga. However, each of these  
81 models cover different time periods or areas of the world and each model is based on different  
82 assumptions and hypotheses, and place differing emphases on subsets of the geological record. Thus,  
83 although continental motions and plate boundary evolution have been categorised in some manner for the  
84 past 1 Ga, there is no fully continuous model defining Earth's tectonic history for this time. A  
85 fundamental test of any tectonic reconstruction for the Precambrian is that the configurations of  
86 continents, terranes and plate boundaries can evolve continuously as to seamlessly merge with  
87 reconstructed configurations for more recent times that are better constrained and ultimately tied to the  
88 present-day Earth. The absence of such continuous reconstructions highlights a critical uncertainty for  
89 assessing interpretations of Neoproterozoic palaeogeography, tectonics and geodynamics.

90

91 Our key motivations for this study are three-fold. Firstly, a 1 Ga model will permit, for the first time,  
92 Neoproterozoic and Cambrian quantitative analysis that constrains (bio)geochemical and volatile fluxes,  
93 palaeoclimatic studies and the nature of earth systems, during times of biological evolution and extreme  
94 climate change (Gernon et al., 2016; Godd ris et al., 2017; Mills et al., 2011, 2019). Second, a full-plate  
95 model would be a starting point for future studies to constrain both the tectonic (e.g. supercontinent cycle  
96 (Li et al., 2019; Merdith et al., 2019b)) and geodynamic (e.g. core-lithosphere-mantle connection (Heron  
97 et al., 2020; Tetley et al., 2019)) nature and evolution of the Earth. Third, a consistent model for the  
98 Neoproterozoic and Cambrian that coherently links with younger models can be used as a framework to  
99 support future regional studies that test and enhance the resolution of the model or spawn alternative  
100 models that can be used for hypothesis testing. We stress that our reconstruction is intended to capture the  
101 main aspects of global tectonics across the last billion years and consequently lacks many details that  
102 could be incorporated for individual regions. Just as the earliest full-plate models for the Cenozoic and  
103 Mesozoic (Seton et al., 2012) and late Palaeozoic (Domeier and Torsvik, 2014) have provided valuable

104 open-access resources for numerous other studies to test and improve, we intend that the global  
105 framework provided by our reconstruction will form the basis for future studies that will generate  
106 improved reconstructions by incorporating new or different observations and ideas.

107

108 This paper is organised as follows: first, we provide a review of the concepts behind full-plate  
109 reconstructions, including the types of observations and assumptions on which they are based. We then  
110 summarise the previously published reconstruction models and justify which elements of these existing  
111 studies we have chosen to include in our reconstruction. Finally, we present the main outcome of our  
112 study: the first continuous and self-consistent full-plate model from 1 Ga to present day with a single set  
113 of polygons, Euler rotations and plate boundaries.

114

## 115 **2 Full-plate reconstruction models**

116 There are two broad categories of models that can be constructed to describe Earth's tectonic or  
117 palaeogeographic history. The first category we refer to as 'continental drift' type models (Fig. 1a), as  
118 they model the motion of continents drifting across the Earth's surface and tend to explicitly reflect  
119 palaeogeography rather than tectonic evolution. The second type we refer to as 'full-plate models' (Fig.  
120 1b), which, in addition to tracking the motion of continents, trace the evolution of plate boundaries and by  
121 implication, the evolution of tectonic plates themselves (Gurnis et al., 2012). In effect, continental drift  
122 type models are the precursor to full-plate models, but rather than supersede continental drift models, both  
123 types of models complement each other and provide different avenues for research. Continental drift type  
124 models are useful for analysing palaeomagnetic data, for contextualising regional studies or as a ground-  
125 breaking study where there is little preserved data on plate boundaries. Comparably, full-plate models are  
126 more encompassing, but are also much harder to iterate over and generate alternative models from. If one  
127 simply requires the distribution of continental crust and not of plate boundaries, then it is much easier and  
128 simpler to build a continental drift style model than categorically describe and model plate boundaries  
129 through time. However, both types of models use the same reconstruction framework.

130

### 131 **2.1 Reconstruction Framework**

132

133 The essential characteristic of any plate reconstruction is the reconstruction framework (or network  
134 (Domeier and Torsvik, 2017)), which is the organisation of data used to describe the motion of rigid  
135 objects on a sphere using Euler's rotation theorem (McKenzie and Parker, 1967; Morgan, 1968). In plate  
136 reconstructions, the rigid objects in motion are the plates themselves and, in addition to requiring the  
137 temporal and spatial components of moving plates (i.e. the time period of motion, latitude, longitude and

138 angle of rotation) the theorem also requires that each rotation be defined relative to another object. This  
139 rotation of one object relative to another forms the basis of a 'relative plate motion model'. It is also  
140 desirable for these relative rotations to be tied to something (relatively) immutable within, or around, the  
141 Earth (e.g. the core, mantle, or the spin-axis) thus, transforming the model into an 'absolute plate motion  
142 model'. For the Mesozoic and Cenozoic, plates are described in a relative framework due to the  
143 preservation of oceanic lithosphere within oceans formed since the breakup of Pangea. In this way each  
144 plate's motion history is described as moving relative to another plate, with the African plate typically at  
145 the top of the hierarchy (e.g. (Ross and Scotese, 1988; Torsvik et al., 2008); Fig. 2a, b). The motion of the  
146 African plate can then be defined absolutely (though using observations from many or all plates, and not  
147 just Africa) to the deep Earth through alternative methods such as hotspot chains (Müller et al., 1993;  
148 O'Neill et al., 2005), seismic imaging of subducted slabs (van der Meer et al., 2010), palaeomagnetic data  
149 (with or without true polar wander corrections, Torsvik et al., 2012) or methods jointly evaluating the  
150 characteristics of multiple constraints including plate velocities, hotspot chains and subduction trench  
151 migration (Tetley et al., 2019). Regardless of which method is chosen, the result is a global reference  
152 frame defined as a sequence of absolute motions of the African plate, which, together with the relative  
153 motions between plate-pairs arranged within a hierarchy (Fig. 2), define the absolute motions of all plates.  
154 An exception to all plates being tied to Africa occurs for the Mesozoic Pacific Ocean. Before 83 Ma (and  
155 the opening of the West Antarctic spreading centre) the motion of the Pacific plate is preserved and  
156 reconstructed absolutely to the spin axis through hotspot motion, rather than through Africa. Plate models  
157 can also be described in a purely relative framework, in which case a single continent (or plate) is fixed to  
158 its present-day position and all other continents or plates are rotated relative to the fixed plate. This  
159 approach is commonly used for localised studies or to easily highlight the difference between two  
160 contrasting models (Fig. 2c).

161

162 Before the Mesozoic era, it is not possible to use preserved, *in situ* oceanic lithosphere, hotspot motions  
163 and seismic imaging of slabs. Therefore, the logical arrangement of connections within the rotational  
164 framework changes (Domeier and Torsvik, 2017), however the general principles of plate reconstructions  
165 remain the same. For these times, the only quantitative information on the positions of plates is through  
166 palaeomagnetism, which describes the palaeolatitude of continents with respect to the Earth's spin axis. In  
167 these cases, where the absolute motions are more directly constrained than relative motions, rotation  
168 models traditionally favour a simpler hierarchy, rather than the complex hierarchies used for post-Pangea  
169 times (e.g Fig. 3a, b). The motion of major continents relative to the spin axis is determined using their  
170 own palaeomagnetic data (Fig. 3a, b). Within this data set, continents can be grouped together in localised

171 hierarchies where there is evidence that they have remained together or close to one another or, in  
172 instances where paleomagnetic data are lacking from some of the blocks if geological constraints permit.

173

174 Finally, although Euler's rotation theorem is based on the motion of rigid bodies, this is a simplification  
175 because the lithosphere is deformable. Recent advancements in plate modelling (Gurnis et al., 2018) have  
176 allowed for the development of deforming plate models where rigid plates are able to deform along their  
177 edges.

178

## 179 **2.2 Palaeolatitude**

180

181 Palaeolatitude is determined through the study of palaeomagnetic data and is the only method to  
182 quantitatively constrain the absolute latitudinal position of a continent for pre-Jurassic times. If sufficient  
183 data are present from a single continent, an apparent polar wander path (APWP) can be constructed that  
184 describes the motion of that continent through time (Torsvik et al., 2012). If there are very good  
185 geological constraints on the relative positioning between multiple continents, then poles from these  
186 continents can be merged to form composite apparent polar wander paths. This merging is done by  
187 rotating the poles of multiple continents into the coordinate frame of a single continent, typically found  
188 higher in the framework (e.g. Africa, Fig. 2a). If this process is done using all global data it is known as a  
189 global apparent polar wander path (GAPWaP). GAPWaPs provide the potential for a more rigorous  
190 description of the evolution of a suite of continents as more data are available.

191

192 There are, however, many caveats and uncertainties associated with GAPWaPs and APWPs that contain  
193 data sourced from more than one continent (e.g. APWP for Gondwana). In particular, they are strongly  
194 dependent on the relative position of continents, as even minor changes in these relative positions can  
195 result in large differences in the resulting wander paths. They also are directly dependent on the quality  
196 and abundance of palaeomagnetic data, thus a degree of subjectivity can be introduced by what criteria  
197 are used for selecting and filtering poles (Van der Voo, 1990; see a new approach in Wu et al., 2020). For  
198 example, in the Gondwana APWP of Torsvik et al. (2012) (and also for the APWP we construct in this  
199 paper), there is one pole for Gondwana between 440 and 400 Ma that constrains the motion of over half  
200 of all known continental crust at the time. In the Precambrian, the geological uncertainty of exactly how  
201 two cratons (or continents) fit together limits the usefulness of GAPWaPs and APWPs that are defined by  
202 multiple continents in conjunction with one another. Instead individual APWPs can be constructed using  
203 available palaeomagnetic data for continents and then these are all balanced together globally to produce

204 a coherent kinematic continental model (e.g. Li et al., 2008; Pisarevsky et al., 2014). In this manner, it is  
205 possible to build continental drift models purely from palaeomagnetic data.

206

### 207 **2.3 True Polar Wander**

208

209 True polar wander (TPW) is the motion of the entire solid Earth (mantle-lithosphere) with respect to the  
210 spin axis due to centrifugal forces from Earth's orbit acting on mass anomalies in the upper mantle,  
211 wherein positive anomalies are driven towards the equator and negative anomalies towards the poles  
212 (Evans, 2003). Since TPW is inherent in palaeomagnetic data, all APWP are a composite of both plate  
213 motions and some component of TPW. Thus, in the strictest sense, to properly use a plate model for  
214 geodynamic modelling, a correction that removes any component of detected TPW should be applied (i.e.  
215 the mantle reference frame). Further, as the mass anomalies in the mantle are thought to arise from the  
216 flow induced by subducted oceanic lithosphere and the associated return flows, TPW excursions are  
217 closely linked to the supercontinent cycle (Zhong et al., 2007).

218

219 Raub et al. (2007) identified three types of TPW summarised briefly below, though only the latter two are  
220 relevant here. Type 0 TPW operates on short ( $< 10^3$  a) timescales as a response to elastic deformation  
221 within the lithosphere arising from seismic events (Soldati et al., 2001) and so has a negligible effect on  
222 plate motions on the timescales pertinent here (Evans, 2003; Raub et al., 2007). Type 1 TPW is the most  
223 important to consider, and is broadly defined as the slow motion of the solid Earth (mantle and  
224 lithosphere) readjusting to mass anomalies in the mantle. Type 1 TPW is what is commonly detected and  
225 corrected in plate motion models (Steinberger and Torsvik, 2008; Torsvik et al., 2012) in order to  
226 constrain geodynamic relationships between deep Earth processes and tectonics (Mitchell et al., 2012).  
227 Type 2 TPW (Inertial-Interchange True Polar Wander, IITPW) was originally described by Kirschvink  
228 (1997) and is a hypothesis where the mantle and crust are rapidly displaced over large distances relative  
229 to the spin axis as the moment of minimum inertia ( $I_{min}$ ) approaches the maximum moment of inertia  
230 ( $I_{max}$ ) resulting in an interchange between the two (i.e.  $I_{min}$  becomes  $I_{max}$  and vice versa). IITPW has been  
231 linked to supercontinent breakup as continental lithosphere and subduction zones move away from the  
232 upwelling, known as a superswell, developing beneath the supercontinent, which is assumed to remain  
233 quasi-stable (Li et al., 2004). In the Li et al. (2004) model, the superswell is likely to maintain the  $I_{max}$ , but  
234 as all the continents move away  $I_{min}$  approaches  $I_{max}$ , thus they are speculated to interchange with each  
235 other.

236



237 The primary challenge of subtracting the effects of TPW from APW paths is identifying and separating  
238 TPW components from continental motion. Methods of detecting TPW vary, either isolating it directly  
239 from palaeomagnetic data (Mitchell et al., 2012) or deconstructing the APWP of continents by comparing  
240 the kinematic motions of all continental lithosphere on the globe to isolate TPW (Steinberger and Torsvik,  
241 2008). Both approaches require *a priori* assumptions stemming from the choice of plate model being  
242 analysed, which makes it impossible to apply a TPW correction from one model to another. For example,  
243 fitting a great circle to palaeomagnetic data following the approach of Mitchell et al. (2012) is dependent  
244 on knowing the relative continental configuration from which the palaeomagnetic data are sampled.  
245 Alternatively, deconstructing the motions of the continents after Steinberger and Torsvik (2008) is  
246 dependent on constraining absolute palaeolongitude to separate TPW from apparent polar wander. In  
247 order to support their arguments, both methods are dependent on having some form of absolute  
248 palaeolongitudinal control.

249

## 250 **2.4 Palaeolongitude**

251

252 There is no well-established method to compute the absolute palaeolongitude of any given plate that is  
253 applicable to pre-Jurassic times. However, two hypotheses have been proposed for establishing absolute  
254 palaeolongitude for pre-Pangea reconstructions (Torsvik and Cocks, 2017): (i) the plume generation zone  
255 method (PGZ) (Torsvik et al., 2014) and (ii) the orthoversion model of the supercontinent cycle (Mitchell  
256 et al., 2012).

257

258 The PGZ method is based on reconstructing the surface locations of kimberlites and large igneous  
259 provinces (LIPs) to the margins of the large low shear velocity provinces (LLSVPs) (Burke and Torsvik,  
260 2004; Torsvik et al., 2010a) situated on the core-mantle boundary (CMB) (Garnero et al., 2007; Li and  
261 McNamara, 2013). The foundation for this method is the observation that kimberlites and LIPs, when  
262 restored to a mantle reference frame at the time of eruption, are positioned preferentially above the  
263 margins of the LLSVPs (Burke and Torsvik, 2004; Torsvik et al., 2010a). LLSVPs are regions of  
264 anomalously slow (slower than ambient mantle) seismic velocities, close to the core–mantle boundary.  
265 Since large-scale mantle structure is intimately related to the supercontinent cycle, LLSVPs (Li and  
266 Zhong, 2009) are thought to exist for (at least) a similar time frame as the supercontinent itself (i.e.  
267 present-day LLSVPs are thought to have existed at least back to 320 Ma) (Li and Zhong, 2009), but not  
268 necessarily maintaining their present-day geometry (Flament et al., 2017; Zhang et al., 2010; Zhong and  
269 Rudolph, 2015).

270

271 The PGZ method to establish absolute palaeolongitude therefore assumes: (i) the geometric stability of  
272 the present-day positions of LLSVPs back to the time of interest, and (ii) that there is a positive statistical  
273 correlation with margins of LLSVPs and the extrusion of LIPs and kimberlites at the Earth's surface.  
274 Adopting the PGZ method allows one to position continents longitudinally by reconstructing the positions  
275 of LIPs and kimberlites to overlie the margins of LLSVPs while simultaneously utilising TPW-corrected  
276 palaeomagnetic data (Torsvik et al., 2014). In this way, models with explicitly defined and reproducible  
277 absolute plate motions can be created (Domeier and Torsvik, 2014). However, a number of recent studies  
278 have raised questions about the assumptions implicit in the PGZ approach. For example Flament et al.  
279 (2017) and correspondence by Torsvik and Domeier (2017), Doucet et al. (2020), Zhong and Rudolph  
280 (2015) and Zhong and Liu (2016) on long term LLSVP stability and Austermaier et al. (2014), Davies et  
281 al. (2015), with response by Doubrovine et al. (2016) on the statistical correlation. Consequently, while  
282 utilising the PGZ method for plate reconstructions in the Palaeozoic is currently an open area of research,  
283 the theoretical and practical application for Precambrian times remains untested.

284  
285 The other proposed method of determining absolute palaeolongitude for deep time reconstructions is  
286 known as the 'orthoversion model' and suggests that successive supercontinents coalesce orthogonally  
287 ( $90^\circ$  longitude) above the downwelling formed by subduction at the margin of the previous  
288 supercontinent (Mitchell et al., 2012). Mitchell et al. (2012) test their model by first determining the  
289 minimum moment of inertia ( $I_{min}$ ) during each phase of supercontinent assembly. This is done by rotating  
290 the available paleomagnetic data into a relative reference frame of a fixed continent (Africa for the  
291 Phanerozoic, Laurentia for the Neoproterozoic) and then fitting a great circle to the resulting poles.  $I_{min}$  is  
292 defined as the orthogonal axes (or pole) of the great circle and is taken to approximate the TPW axis.  
293 Mitchell et al. (2012) fitted great circles to palaeomagnetic data for a selection of time periods (1165–  
294 1015 Ma, 805–790 Ma, 550–490 Ma and 220–90 Ma) and calculated that the angle between each  
295 successive  $I_{min}$  was  $\sim 90^\circ$ ; as expected in the orthoversion model. The initial (palaeolongitudinal)  
296 placement of Pangea is constrained from its position at  $\sim 90$  Ma (centroid of  $I_{min}$  at  $0^\circ\text{N}$ ,  $10^\circ\text{E}$ ) when the  
297 most recent TPW episode finished (Steinberger and Torsvik, 2008). Therefore, during Rodinia and  
298 Gondwana, when  $I_{min}$  was  $90^\circ$  from present day, Mitchell et al. (2012) proposed that the centre of mass of  
299 both was positioned at  $100^\circ\text{E}$ .

300  
301 As with the PGZ, a number of limitations are apparent with the orthoversion model. In particular, the  
302 method of Mitchell et al. (2012) does not separate continental motion from true polar wander when  
303 calculating  $I_{min}$ , thus it assumes that during these times TPW is the primary signal recovered from  
304 palaeomagnetic data and not continental motion. Secondly, the orthoversion model is inherently

305 dependent on both the quality and abundance of palaeomagnetic data (e.g. the Rodinia  $I_{min}$  in Mitchell et  
306 al. (2012) is based on only three poles), as well as the continental configuration of the time (as the  
307 continental configurations can determine the relative position of palaeomagnetic data when rotated into a  
308 specific reference frame). Torsvik and Cocks (2017) highlight this succinctly by using slightly different  
309 palaeomagnetic data, and a slightly different Gondwana configuration to produce an  $I_{min}$  between 550 and  
310 490 Ma of 50°S, 64°E (compared to the estimate of Mitchell et al. (2012) of 30°S, 75°E). Finally, the  
311 calculation of  $I_{min}$  at each time step occurs within a fixed relative reference frame (i.e. Fig. 2c), meaning  
312 that the  $I_{min}$  itself cannot be restored to an absolute palaeogeographic position. Thus, the longitudinal  
313 centre of Rodinia at 100°E is not explicitly proven by Mitchell et al. (2012). Instead, since the calculated  
314 successive  $I_{min}$ 's are 90° apart, it is inferred to be in this location.

315

## 316 **2.5 Geology**

317

318 Geology is unfortunately silent on the absolute positioning of continents in time, except in circumstances  
319 such as the PGZ method discussed above. However, it contains a wealth of information of relative plate  
320 motions in the Mesozoic and Cenozoic (e.g. seafloor spreading), and in deeper time through the temporal  
321 evolution of sedimentary basins and facies, and tectonic affinities inferred from geochemistry, zircon  
322 arrays, magmatism and metamorphism. However, geology does have an advantage over palaeomagnetic  
323 data in that there are many different types of data available, especially from small and minor terranes in  
324 the Precambrian that are otherwise unconstrained palaeomagnetically. Given the wealth of geological  
325 data, especially in the Neoproterozoic, there is a general hierarchy of use that is a reflection of the scale of  
326 the problem. Our approach is to start by building a global framework and work progressively to finer  
327 resolution to inform the localised nature of that framework.

328

329 The first and most important geological data to gather is evidence of rifts and arcs, as they describe  
330 separation (usually leading to seafloor spreading) and convergence, respectively and can therefore put in  
331 place the framework for plate motions and subsequent interpretation of geological data. Secondly,  
332 identifying piercing points where geological boundaries can be matched on now separate continents (e.g.  
333 Appalachians and Gondwana forming orogenies), or ways of fitting two continents together in a stable  
334 configuration. These piercing points are important because reconstructing continental configurations with  
335 high confidence allows the generation of more rigorous APWPs and they help to constrain the location  
336 and orientation of both rifts and arcs on the periphery of continents. Unfortunately, due to deformation  
337 and progressive alteration of continental crust (e.g. changes of continent-ocean boundaries (COBs)), in  
338 pre-Gondwana times it is difficult to be more precise than matching the margins of large continents and

339 for smaller cratons and terranes it is almost impossible. A pertinent example of this are the four different  
340 proposed configurations of Australia and Laurentia during Rodinia (see reviews by Li et al., 2008;  
341 Merdith et al., 2017b), which all broadly match the same margins against each other (east coast of  
342 Australia with the west coast Laurentia, with or without an intervening continent) but place them in  
343 different relative positions.

344

345 After arcs and rifts, we can loosely (but not exhaustively) group geological features and data based on  
346 their applications. Sedimentary basins, dyke swarms, detrital minerals, geochemical signatures and fossils  
347 are typically used to determine provenance or latitudinal band and align once contiguous regions. The  
348 time-scales and conditions of metamorphism together with structural data can be used to infer the tectonic  
349 setting and polarity of collisional events or help constrain the nature of indeterminate plate margins such  
350 as transform boundaries. These types of data assist in increasing the resolution of a plate model by  
351 understanding the geology at smaller scales within the framework of a specific tectonic setting, such as an  
352 arc or rift. We stress here that the relationship between detailed regional geology and the broader  
353 framework of a plate model is not a ‘one-way street’ but is highly iterative. If, for example, a detailed  
354 geological study determines that an interval of magmatism and sedimentation that was originally  
355 interpreted as a failed rift, in fact led to seafloor spreading, then the broader scale tectonic framework and  
356 plate model must be re-evaluated. Finally, due to the qualitative nature of most geological data, the  
357 iteration and implementation of these data into the plate model typically necessitates qualitative decisions  
358 that others may disagree with. Iteration over the model continues until we approach tectonic congruency  
359 within the model (i.e. data-based iterations in one part of the world do not nullify data in other areas of the  
360 world). We stress that this does not mean our model is ‘correct’ or ‘true’, just that it is internally  
361 consistent with as much data as possible. Consequently, we consider the model presented here a viable,  
362 but non-unique interpretation of Neoproterozoic data.

363

364 A specific example of the importance of interpreting geology within a full-plate framework is given by  
365 recent work on the Stenian–Cryogenian evolution of the East African Orogen. Although arc-related  
366 magmatism has been recognised in the northern East African Orogen for a number of decades (e.g. Stern,  
367 1994), the recognition of similar-aged arc magmatism in the higher-grade southern East African Orogen  
368 of Madagascar, Southern India and East Antarctica has been more controversial and under-appreciated  
369 until recently (Archibald et al., 2018, 2017; Armistead et al., 2019; Plavsa et al., 2015; Ruppel et al.,  
370 2018). In one particular example, work over the last decade on Western Dronning Maud Land in East  
371 Antarctica has identified an extensive Stenian–Tonian juvenile arc system (named TOAST; (Elburg et al.,  
372 2015; Jacobs et al., 2015; Ruppel et al., 2018)). This discovery has gone hand-in-hand with the

373 recognition of a similar region in western Madagascar, known as the Dabolava Arc (Archibald et al.,  
374 2017; Tucker et al., 2011) (e.g. Fig. 8). These arcs are now separated by a considerable distance, but their  
375 reconstructed position in the Neoproterozoic and their similarity has led to us interpreting them as part of  
376 one continuous subduction system that was active for the Stenian and Tonian. In this manner, we now  
377 include TOAST as another part of Azania and have reworked a number of the plate boundaries in Merdith  
378 et al. (2017a) to reflect these new geological data and tectono-geographic interpretations.

379

## 380 **2.6 Kinematic considerations**

381

382 The final line of reasoning used to create full plate models are plate kinematic constraints. These are not  
383 defined explicitly through geological or geophysical data of the types outlined above, but rather come  
384 from the idea that the evolution of plate motions through time must follow the broad principles of plate  
385 tectonics in a way that would seem reasonable; for example, by equivalency with more recent and well-  
386 constrained plate motions. The most basic requirement is that continental blocks cannot pass through or  
387 significantly overlap other continents and we must be able to describe the position and motion of each  
388 continental block for as long as the crust within that block is thought to have existed. While this may  
389 seem obvious, these considerations present a powerful method for discriminating between competing  
390 reconstruction scenarios. Models constructed for deep time that cannot evolve towards more recent and  
391 present-day configurations of continents cannot be considered correct. Similarly, models requiring an  
392 implausible kinematic evolution in order to meet present-day configurations cannot be correct. A tangible  
393 example is Rodinia, for which a range of configurations could be permissible based on available  
394 paleomagnetic and geological data (see reviews in Evans, 2013; Li et al., 2008; Merdith et al., 2017b).  
395 However, analysing the sequence of plate motions required to translate each continent to their (better  
396 constrained) positions during the Palaeozoic is more plausible in some of these scenarios than others, such  
397 as not requiring individual terranes or blocks to cross multiple ocean basins or navigate their way around  
398 a stable continent (Merdith et al., 2017b). Further examples where kinematic constraints add useful  
399 insights are when constructing models that explicitly trace the evolution of plate boundaries and tectonic  
400 plates. An example is expressed in the logic of Domeier (2018) who inferred that the longitudinal position  
401 of Tarim, North China and South China during the late Cambrian–Devonian must have remained stable  
402 relative to one another, because palaeolatitudes from palaeomagnetic data overlapped and therefore must  
403 be consistent with their end position in the more well constrained Devonian–Triassic.

404

405 Finally, we take a uniformitarian view of tectonic evolution, in that we assume that plate tectonics and  
406 relative plate motions were operating on similar principles in the Neoproterozoic to what we can observe

407 in the Mesozoic and Cenozoic. During more recent times, the motion of plates remains relatively constant  
408 for time lengths on the order of 10–100 Ma, with changes in motion occurring comparatively quickly (< 3  
409 Ma) and tied to an event further afield, such as terrane collision in a subduction zone, subduction onset,  
410 rifting onset or ridge subduction (e.g. Austermann et al., 2011; Cawood et al., 2016; Cawood and Buchan,  
411 2007; Knesel et al., 2008). The representation of this within a conceptual framework is that a single  
412 continent or plate may move for time lengths on the order of 10–100 Ma around a single Euler pole,  
413 before a plate re-organisation event triggers a change in direction and velocity of the plate (Gordon et al.,  
414 1984). Within palaeomagnetic data, this approach is exemplified in Torsvik et al. (2008), where filtered  
415 compilations of data result in smooth APWP segments punctuated by cusps in motion and velocity, and  
416 more recently by Wu et al. (2020). For the Neoproterozoic, which has much more sparse palaeomagnetic  
417 data coverage than the Phanerozoic, the logic can be applied by linking changes in plate direction (as  
418 suggested or necessitated by palaeomagnetic data) directly to geological evidence of a change in tectonic  
419 regime within the region of interest (e.g. Merdith et al., 2017b).

420

## 421 **2.7 Synthetic Ocean Plates**

422

423 A complete full-plate model by definition includes a representation of the evolution of ocean basins  
424 through time. This is the most uncertain part of any full-plate model. With a few exceptions (e.g. Granot,  
425 2016), no pre-Jurassic ocean crust is preserved *in situ*, so that even where we can infer the presence of  
426 divergent plate boundaries (for example, following continental breakup), the precise geometry and  
427 spreading rates at these boundaries are conjectural. Consequently, there are no unique solutions to the  
428 definition of these boundaries and the synthetic ocean plates constructed from them. The main aim in the  
429 reconstruction of ancient ocean basins is to ensure that the synthetic plates and plate boundaries are at  
430 least consistent with sparse observations preserved on the continents.

431

432 Firstly, although we have little data on the creation of oceanic lithosphere for pre-Jurassic times, the  
433 geological record does preserve data on the consumption of oceanic lithosphere at subduction zones. The  
434 most important criteria that therefore must be met are that (i) (sub-) orthogonal divergence occurs at mid-  
435 ocean ridges and that (ii) convergence occurs at subduction zones (Domeier and Torsvik, 2014). The  
436 former of these two criteria typically occurs between continents during supercontinent breakup or when  
437 small terranes rift from a continent (Dalziel, 1997). The latter of these includes subduction along the  
438 margins of continents as well as within intra-oceanic arcs. Thus, these two criteria necessitate the  
439 extrapolation of known plate boundary positions (e.g. preserved continental arcs, rift zones) into larger  
440 areas to ensure the tectonic congruency of the model (in this case, that convergence or divergence at one

441 location doesn't nullify the same criteria in another location). It is this step, in particular, that requires  
442 significant iteration when constructing a model. Maintaining tectonic congruency for a model is best  
443 achieved when the extrapolation of plate boundaries is done as simply as possible. For example, in  
444 reconstructing an ocean basin without any continental crust (e.g. Pacific Ocean, Panthalassa Ocean), a  
445 triple junction is usually the simplest expression of a ridge system that ensures divergence in all directions  
446 and convergence at its margins (Domeier and Torsvik, 2014). The evolution of such a triple junction  
447 could also be seen in the Ediacaran opening of the Iapetus Ocean (e.g. Pisarevsky et al., 2008; Robert et  
448 al., 2020),

449

### 450 **3 Model selection and justification**

451

#### 452 **3.1 Existing plate models**

453

454 The selection of which full-plate model to assist in solving a problem is dependent on the nature of the  
455 problem, as each published plate model is constructed using a different approach and has a different  
456 reconstruction framework. For example, a study looking at absolute plate motions of the Cenozoic has  
457 little use for models connected to the Palaeozoic or Neoproterozoic. Instead, such studies typically  
458 include a comparison with previously published models as well as a rigorous mantle reference frame.  
459 Similarly, a study that traces the latitudinal distribution of continental arcs through the Phanerozoic has no  
460 need for a mantle reference frame and a study investigating the changes in net rotation through time  
461 would be concerned with small, localised improvements from regional models but more focussed on  
462 capturing the large scale changes that occur when continents breakup. Although newer plate models  
463 typically address the shortcomings of previous models or implement more refined updates of regional  
464 areas, this does not necessarily make them better for all applications. Older plate models have been more  
465 rigorously tested and used by the community and as one travels further back in geological time, the data  
466 are more ambiguous and can invite alternative interpretations. For the purpose of this study, the existing  
467 plate models we consider are only those that are publicly released with fully self-consistent with coherent  
468 plate motions and plate boundaries. Thus, we omit many models that provide only continental motions  
469 (Scotese, 2016; Torsvik and Cocks, 2016), alternative or regional Rodinia configurations (Evans, 2013) or  
470 regional refinements of global models for the Mesozoic and Cenozoic (e.g. Vaes et al., 2019).

471

472 The major step forward for producing full-plate models was the construction of open-source computer  
473 software specifically designed to work with full-plate reconstructions (e.g. GPlates; (Gurnis et al., 2012).  
474 Following their development, GPlates-compatible global models for the Early Jurassic to present (Seton

475 et al., 2012; Shephard et al., 2013) and a model for the Late Palaeozoic (Domeier and Torsvik, 2014) soon  
476 followed (hereafter, SET12 and DT14, respectively). Subsequent work by Matthews et al. (2016)  
477 (MAT16) bridged the gap between the Palaeozoic and Jurassic, linking a slightly modified version of  
478 DT14 with an updated SET12 model, the Müller et al. (2016) model (MUL16). Further back in time, two  
479 models for the Early Palaeozoic (500 to 410 Ma) now exist: Domeier (2016) (DOM16), which  
480 encompasses the evolution of the Iapetus and Rheic Oceans, as well as the motion of Gondwana, and  
481 Domeier (2018) (DOM18), which models the evolution of the first generations of Tethyan Oceans and  
482 Central Asian blocks (Siberia, North and South China, Tarim). For the Neoproterozoic, Merdith et al.  
483 (2017a) (MER17) produced a full-plate model from 1000 to 520 Ma, using the models of continental  
484 motion presented by Li et al. (2013, 2008) as a base. An alternative reconstruction from the late  
485 Palaeozoic to present-day has been presented by Young et al. (2019) (YOU19). YOU19 offers an  
486 alternative full-plate model for the Palaeozoic to the DT14 and MAT16 models that does not rely on the  
487 PGZ method. Finally, a deforming plate model was produced (Müller et al., 2019) (MUL19) that  
488 modelled rift and convergence deformation from 250 to 0 Ma. Table 1 summaries the main features of  
489 these models.

490

### 491 **3.2 Cenozoic and Mesozoic plate models**

492

493 We consider three plate models for the Cenozoic and Mesozoic: SET12, MUL16, and MUL19 (Fig. 4).  
494 The SET12 model spans from present-day to 200 Ma, with MUL16 and MUL19 extending back to 230  
495 and 240 Ma, respectively. The main geological constraint of these models are the magnetic lineations  
496 preserved in oceanic crust that describe the relative movement between the pairs of continents breaking  
497 apart during the fragmentation of Pangea. The evolution of the Atlantic, Indian, Southern, Arctic and  
498 Cenozoic Pacific oceans are consistent, to the first order, across all three models. Larger differences  
499 between the models arise in regions where oceanic crust has been subducted, upon which they then rely  
500 on a combination of geometric (e.g. assumption of symmetrical spreading), geological, seismic and  
501 palaeomagnetic data to constrain the motion and evolution of terranes that open and close ocean basins  
502 (e.g. Liu et al., 2010, 2008; Sigloch and Mihalynuk, 2013). In these regions, the tectonic histories, even  
503 for Cenozoic times, remain the subject of ongoing research and the scenarios embedded in the global  
504 models used in this study represent one candidate amongst many competing models. For example, the  
505 extent of subduction systems within the Tethyan domain and the nature of India-Eurasia collision is still  
506 hotly debated (Hu et al., 2016; Parsons et al., 2020; van Hinsbergen et al., 2020, 2012). Similar  
507 combinations of methods have been used to propose alternative interpretations for circum-Pacific regions,  
508 especially for the Cretaceous and earlier times in the northwest Pacific (Domeier et al., 2017;



509 Konstantinovskaya, 2002; Shapiro and Solov'ev, 2009; Vaes et al., 2019; Wu et al., 2016), the southwest  
510 Pacific (Hochmuth et al., 2015; Matthews et al., 2015; Schellart et al., 2006; Sutherland et al., 2020) and  
511 the northeast Pacific (Clennett et al., 2020; Sigloch and Mihalynuk, 2013). All of these regions invite  
512 competing models and alterations to existing global models and it is notable that many of the studies  
513 mentioned above have benefited from using the resources made available by previous global studies,  
514 beginning with SET12, as a starting point for detailed regional analysis.

515  
516 All three models employ a relative hierarchy (Fig. 2a), in which a fully relative plate motion model is tied  
517 to an absolute plate motion model through Africa. The relative hierarchies are similar across the models  
518 because of the preserved oceanic crust. These global relative motion hierarchies are then linked to an  
519 absolute reference frame tied to the mantle, though the details of these reference frames differ between  
520 models. SET12 uses a hybrid reference frame, using a moving hotspot reference frame for 100–0 Ma  
521 (O'Neill et al., 2005) and a true-polar wander corrected palaeomagnetic reference frame for 200–100 Ma  
522 (Steinberger and Torsvik, 2008). MUL16 also adopts a hybrid absolute reference frame, but uses the  
523 moving hotspot model of Torsvik et al. (2008) instead of that of O'Neill et al. (2005) based on an  
524 assessment of the geodynamic plausibility of a range of alternative mantle reference frames by Williams  
525 et al. (2015). MUL19 departs from both SET12 and MUL16 in that it uses an absolute reference frame  
526 derived by Tetley et al. (2019). The method of Tetley et al. (2019) optimises absolute plate motions  
527 through a joint inversion involving trench motion, fitting hotspot motion tracks and net rotation to  
528 determine the motion of Africa (at the top of the relative hierarchy) that simultaneously best fits all three  
529 criteria. Despite the emphasis on mantle reference frames in these previous global models, the same  
530 relative plate motion hierarchies can also be tied to a pure paleomagnetic reference frame (e.g. Cao et al.,  
531 2019; Torsvik et al., 2008).

532  
533 In this study, we rely on palaeomagnetic data as the main basis for linking absolute plate configurations  
534 continuously from the Cenozoic to the early Neoproterozoic, when tying plate configurations to the  
535 mantle is far more problematic. Nonetheless, some aspects of the more recent plate motions still rely on  
536 observations from hotspot trails—specifically, the motion of the Pacific Plate and other oceanic plates  
537 that have bordered it. During the Early Cretaceous, these plates lay within the Panthalassa ocean basin  
538 that was entirely surrounded by subduction zones, meaning that we cannot tie the motions of the oldest  
539 crust of the Pacific Plate to the continents by seafloor spreading anomalies.

540  
541 Finally, with regard to Mesozoic-Cenozoic global plate models, we note that MUL19, while containing  
542 the same relative framework as SET12 and MUL16, also contains deforming plates. In MUL19,

543 deformation of rifts and collisional zones are modelled explicitly, making it the first plate model to step  
544 away from the simplification of rigid plates that all other models assume. However, the reconstruction  
545 here relies on the simpler, rigid approximation used in SET12, MUL16, and other previous studies.

546

### 547 **3.3 Mid-late Palaeozoic plate models**

548

549 The progression of the three Palaeozoic plate models (all modelling 410–250 Ma) is slightly more  
550 nuanced than in the Mesozoic and Cenozoic because of the absence of preserved oceanic crust. DT14 is  
551 the original model and both MAT16 and YOU19 used DT14 as the basis of their Palaeozoic models and  
552 then connect to MUL16 for the Mesozoic and Cenozoic. In effect, MAT16 is the connection of DT14 (i.e.  
553 minimal changes) to MUL16, while YOU19 is an alternate version of DT14 for the Palaeozoic.

554

555 DT14 is heavily based on work by Torsvik et al. (2012) and models the amalgamation of Pangea through  
556 the collision of Laurussia and Gondwana and the evolution of the Palaeo-Tethys and opening of the  
557 Meso-Tethys oceans. The model has a flat hierarchy (Fig. 3a) with APWPs defined for each individual  
558 continent and each continent being tied directly to the spin axis. Domeier and Torsvik (2014) also use the  
559 PGZ method to constrain absolute palaeolongitude. Therefore, their model assumes the stable, immutable  
560 nature of the present-day LLSVPs within the mantle back to 410 Ma. DT14 is presented in both a mantle  
561 and a palaeomagnetic reference frame, with the mantle reference frame being corrected for TPW after  
562 Torsvik et al. (2014) .

563

564 MAT16 adopted the DT14 model, with minor amendments required to link it with MUL16 (see Matthews  
565 et al. (2016) for details). A key difference between the two models is that MAT16 translated the flat  
566 hierarchy of DT14 into a fully relative reference frame (i.e. converted the structure from Fig. 3a into Fig.  
567 2a), where the motion of all plates is tied to Africa, which is then tied to an absolute plate motion model.  
568 The absolute plate motion model of MAT16 is the same as in both MUL16 (i.e. a hybrid between  
569 hotspots, slabs and palaeomagnetic data) and DT14 (i.e. absolute latitude and longitude, corrected for  
570 TPW). Thus, MAT16 also invokes the PGZ method.

571

572 YOU19, while starting from MAT16 as a base, differs much more from MAT16 than MAT16 does from  
573 DT14. This is because YOU19 uses a different base assumption, leading to notable changes in the actual  
574 plate model itself. The most important difference is that YOU19 does not assume that LLSVPs were fixed  
575 and stable back to 410 Ma. They abandon the PGZ method for constraining palaeolongitude and thus  
576 argue that they can better accommodate geological and kinematic (plate speed and trench migration)

577 criteria more strongly than either DT14 or MAT16. The two key changes that YOU19 implemented  
578 (relative to DT14 and MAT16) are shifting Laurussia in latitude and longitude to be closer to its position  
579 in Pangea against Gondwana, thus removing a dextral motion between the Patagonian margin of South  
580 America and Laurussia (e.g. Fig. 2c), and removing easterly drift of South China during the  
581 Carboniferous–Permian. The implementation of both in DT14 (and then in MAT16) is a consequence of  
582 the PGZ method, since the longitudinal position of Laurussia and South China is based on fitting  
583 preserved eruptions to the edges of LLSVPs (Domeier and Torsvik, 2014). YOU19 argue that the  
584 interpretations of DT14 introduce unrealistic kinematic scenarios: 8000 km of relative dextral motion  
585 between Laurussia and the Patagonian margin of Gondwana (e.g. Fig 2c) at a relative plate velocity of 30  
586 cm/a and South China moving at plate speeds of 40 cm/a between 260 and 250 Ma in MAT16 (Young et  
587 al., 2019). The dextral motion between Gondwana and Laurussia of DT14 and MAT16 that that YOU19  
588 removed is not a transition from the Pangea B to Pangea A configuration, which is explicitly defined as  
589 dextral motion after Pangea formed (Domeier et al., 2012). Rather, all three models adopt a Pangea A  
590 configuration and include *some* component of dextral motion between Laurussia and Columbian–  
591 Mexican margin of Gondwana in the Devonian. However, the position of Laurussia in YOU19 is  
592 unsupported palaeomagnetically by  $\sim 30^\circ$  (Section 4.2 and 5.1), which is problematic as there is an  
593 abundance of data from both Laurentia and Baltica to constrain its position at this time.

594  
595 Recently, Wu et al. (2020) have also proposed an integrated geological and palaeomagnetic model for the  
596 amalgamation of Pangea. Their study used a different selection of palaeomagnetic data (all three mid-late  
597 Palaeozoic full-plate models discussed here used the compilation of Torsvik et al. (2012) as a base) and a  
598 new method of APWP generation that weighted poles based on their quality and uncertainty. The model  
599 of Wu et al. (2020) also suggested that the formation of Pangea was originally initiated by collision  
600 between Laurussia and a promontory of Gondwana consisting of the Variscan Massifs at ca. 400 Ma. In  
601 their model, the promontory formed by the scissor-like opening of the Palaeotethys Ocean off the  
602 northern margin of Gondwana. In principle this model would be very compatible with the one we present  
603 here, however as the model of Wu et al. (2020) is currently only palaeogeographic, we do not consider it  
604 as an option for merging in this study.

605  
606 YOU19, like MAT16, uses a relative plate hierarchy with Africa as the root of the hierarchy. Africa is  
607 connected to an absolute plate motion model using the Torsvik and Van der Voo (2002) APWP for the  
608 Palaeozoic, before the model transition to the absolute plate motion model of MUL16. Because the model  
609 has no absolute palaeolongitude control, YOU19 does not constrain or correct for TPW in the Palaeozoic  
610 and is therefore presented in a purely palaeomagnetic reference frame.

611

### 612 **3.4 Early Palaeozoic plate models**

613

614 Two separate models exist for part of the Early Palaeozoic between 500 and 410 Ma. Each of these two  
615 models focus on a separate area of the Earth at the time. DOM16 focuses on the evolution of the Iapetus  
616 and Rheic oceans and the amalgamation of Laurussia (Baltica, Laurentia and Avalonia). DOM18 models  
617 the evolution of Siberia, Gondwana, the terranes that now make up the Central Asian Orogenic Belt and  
618 the Chinese cratons (Tarim, North and South China). While each model focuses on a different area, the  
619 overarching assumptions and framework of both models are identical. Both models follow the approach  
620 of DT14, possessing a flat hierarchy with APWPs being defined for most continents, such that they all  
621 move independently from each other. The model extends the assumptions of the PGZ method back to 500  
622 Ma, using the location of LIPs and kimberlites to constrain absolute palaeolongitude. Both models  
623 therefore have a TPW correction, and are presented in a mantle and palaeomagnetic reference frame.

624

### 625 **3.5 Neoproterozoic**

626

627 Only one full plate model exists for the Neoproterozoic (MER17, Merdith et al., 2017a). MER17 is based  
628 on Li et al. (2013, 2008) and models the evolution of Rodinia; it's breakup and the amalgamation of  
629 Gondwana (1000–520 Ma). There are, however, a number of important considerations that differentiate  
630 MER17 from Phanerozoic full-plate models. Firstly, MER17 used a hybrid plate rotation hierarchy,  
631 defining two separate nodes that move independently from each other using palaeomagnetic data tied  
632 directly to the spin axis (India as one and Laurentia, as the centre of Rodinia, as the second) (Fig. 5a, b).  
633 In this model, India and Laurentia both act as separate roots that then constrain a series of relative plate  
634 rotations that collectively describe the rest of the world. Secondly, the continental drift model of Li et al.  
635 (2013) invokes the orthoversion model of determining palaeolongitude, where they fix the  $I_{min}$  of Rodinia  
636 to be at 100°E. As MER17 adopted these rotations as their base, there is an element of the orthoversion  
637 model preserved between models. However, MER17 also drastically changed the configuration of  
638 Rodinia, as well as the timing of breakup, compared to Li et al. (2013), relative rotations within the  
639 Laurentian (i.e. Rodinian) node and absolute rotation of Laurentia itself in order to fit geological and  
640 kinematic constraints. They did not recalculate TPW and the  $I_{min}$  of Rodinia, thus MER17 does not have a  
641 strict absolute palaeolongitude control. Finally, there is no correction for TPW in MER17 and no mantle  
642 reference frame; the model is presented purely in a palaeomagnetic reference frame.

643

644 **3.6 Model selection**

645

646 In order to produce a coherent global model, we must select from the models described above that best  
647 align with our goals: (i) open the Neoproterozoic and Cambrian up for quantitative tectonic analysis; (ii)  
648 create a framework that can support local or regional studies for the Neoproterozoic and (iii) a foundation  
649 for future studies looking at long timescale (> 10–100 Ma) trends in either tectonics or geodynamics.

650

651 As our aim is to produce a model back to 1 Ga, three choices are already made for us because they are the  
652 only models that exist for those time periods: MER17 for 1000–520 Ma, and DOM16 and DOM18 for  
653 500–410 Ma. For the remaining time period, MAT16 (an extension of DT14) and YOU19 are viable  
654 options. Both models link to the MUL16 model and choosing between them requires considering the  
655 reconstruction framework (e.g. hierarchy, reference frame) of our model with respect to our intent. To  
656 satisfy our goals, we need a model in a palaeomagnetic reference frame. We acknowledge the value and  
657 potential in exploring hypotheses for constraining palaeolongitude. However, since tectonic  
658 reconstruction models, such as the one we are presenting here, are a required starting point for exploring  
659 the long-term evolution of mantle, we have kept the model conservative by not assuming the fixity of  
660 LLSVPs or that TPW dictates supercontinent position. Therefore, we elect to leave palaeolongitude  
661 unconstrained by either PGZ or orthoversion methods. Thus, we selected the YOU19 model, as it has  
662 removed the absolute palaeolongitude controls adopted in MAT16. We stress that our approach is  
663 deliberately conservative and requires the fewest *a priori* assumptions, but anticipate that future  
664 developments will see improvements in the model presented and that a comparison of several end  
665 member models would be useful for evaluating the long-term connection between lithosphere and mantle.  
666 One promising way forward could be to optimise tectonic parameters, such as subduction zone migration  
667 and plate velocity in the manner of Tetley et al. (2019) to define a mantle reference frame. The model we  
668 present is an essential precursor for such techniques. Our model is constructed with a palaeomagnetic  
669 reference frame, that is, even at younger times, there is no mantle reference frame. For studies needing  
670 such a reference frame, which only exists since the Cretaceous, we suggest people use either SET12,  
671 MUL16 or MUL19.

672

673 **3.6.1 Our approach to plate modelling**

674

675 Here we outline our approach to merging individual plate models into a coherent global plate model  
676 spanning the past 1 Ga. As detailed above, our goal is a geologically constrained model within a  
677 palaeomagnetic framework. In addition to reconstructing plate motions, we also model plate boundaries,

678 which requires us to also focus on the relative motion between plates. The evolution of plate boundaries is  
679 commonly preserved in the geological record such as passive margins marking divergent boundaries and  
680 magmatic arcs recording convergence. Palaeomagnetic data, although providing a quantitative absolute  
681 constraint on the position of a craton, have varying uncertainty that allow some manipulation and  
682 flexibility. For example, continental drift models (and APWPs) typically fit the data as tightly as possible.  
683 However recent studies have analysed the effect of exploring both the temporal (i.e. age constraints) and  
684 statistical uncertainty to create alternative APWPs (Tetley et al., 2019; Wu et al., 2020). Given this, we  
685 use a hybrid approach that adopts parts of both the flat, palaeomagnetic hierarchy traditionally used for  
686 Precambrian reconstructions and the relative framework used in more recent times.

687  
688 Using this approach, our model has multiple clusters of related cratonic elements moving together (Fig.  
689 5a). Whether a specific cratonic element moves relative to another is dependent on their geological  
690 relationship. For example, if they are separated by an incipient ocean basin as indicated by geological data  
691 then we suggest that it is easiest for them to be moving relative to each other (within the bounds of  
692 whatever available palaeomagnetic data), because the relative relationship of divergence (expressed as a  
693 mid-ocean ridge) is preserved. The hierarchy is defined by geological precedence, where terranes move  
694 relative to blocks, blocks move relative to cratons and cratons move relative to 'supercontinents'. In this  
695 manner, generally (but not necessarily exclusively), crust with more preserved data should always be  
696 placed above crust with less preserved data in the hierarchy, because we have more confidence in the  
697 geological evolution (and also likely palaeomagnetic constraints) from these continents. Alternatively, if  
698 continents are separated by a large ocean basin, we form a new cluster. This cluster-approach has an  
699 added benefit in the more uncertain Neoproterozoic, as it means that we can simply introduce a new  
700 cluster for Rodinia, which has Laurentia as the root of the relative hierarchy, instead of maintaining  
701 Africa or the Congo craton at the top of the cluster (which are the roots of Pangea and Gondwana,  
702 respectively) and can also introduce a cluster for India and South China which, in our interpretation, move  
703 separately to Rodinia on the other side of the globe.

704  
705 A full-plate reconstruction models both continents (palaeomagnetic data) and plate boundaries (geological  
706 data). Therefore, we use both data simultaneously to iterate towards a solution. Palaeomagnetic data are  
707 used initially to build a continental drift framework (e.g. (Li et al., 2013, 2008)). If palaeomagnetic data  
708 are abundant and of high quality, then either an APWP or GAPWaP are constructed, which we do for the  
709 Phanerozoic. We then introduce geological data in the form of plate boundaries (e.g. compilation of rifts  
710 and arcs (Merdith et al., 2017b)) and use the compilation to manipulate the model in a manner that still  
711 fits the palaeomagnetic data, but also accommodates geological data. Structural and metamorphic

712 constraints are used here principally to infer (where possible): (i) polarity of subduction, (ii) collision  
713 timing and (iii) orientation of rifting. Once the broader tectonic framework is implemented, we begin  
714 introducing smaller blocks and terranes into this framework. This approach allows us to increase the  
715 resolution of the model within key areas while maintaining the tectonic coherency of the model as a  
716 whole. For example, where the broader tectonic framework models subduction leading to collision, the  
717 introduction of terranes and smaller blocks that preserve evidence suggesting a two-stage collision or  
718 accretion of an oceanic arc can be used to more finely model the plate boundary network. Other pieces of  
719 geological data, such as faunal provinces (e.g. Burrett et al., 1990), isotopic signatures (e.g. Collins et al.,  
720 2011) and detrital zircons (e.g. Cawood et al., 1999) are used here to assist with connecting disparate  
721 terranes to larger blocks that they share affinity with or to infer the presence of a plate boundary not  
722 directly preserved in the geological record (such as by a diverging fossil record).

723

724 Because our model contains geological data in the form of plate boundaries, we are particularly interested  
725 in ensuring the forwards and backwards compatibility of any decision made around geological data,  
726 especially for terranes or blocks that have limited palaeomagnetic data. For example, if the data support  
727 two or three interpretations in the early Neoproterozoic, but only one of those is consistent with an  
728 Ediacaran (or younger position), then we consider that position more reliable than the other two.  
729 However, we argue that this logic also works in reverse; if a number of positions are deemed viable in the  
730 Ediacaran for a terrane based on the data available, but only one of those also fits what data are available  
731 in the early Neoproterozoic, then we will use the older data to force an interpretation of the younger data  
732 (e.g. Evans, 2009). This argument is highlighted by the concept of ‘world uncertainty’ (the percentage of  
733 total crust (oceanic and continental) on the earth at any one time that is also preserved at present-day) of  
734 Torsvik et al. (2010b). Because time is asymmetrical, this means that the level of confidence we have at  
735 present-day is 100%, but decreases linearly back in time to ~70% at 200 Ma (i.e. 70% of all crust at 200  
736 Ma is no longer preserved). At 400 Ma, the world certainty is ~73% (Domeier and Torsvik, 2017), and  
737 using estimates of continental crustal volumes, at 600 Ma it is between 75 and 80% (Cawood et al.,  
738 2013a). Therefore, for the Mesozoic and Cenozoic, data from younger times are much more compelling to  
739 force interpretations of older data because of how much more confident one can be in the last 20 Ma.  
740 Comparably, the difference in this measure of uncertainty is much smaller between the Neoproterozoic  
741 and Cambrian, thus we suggest that models in this time period should simultaneously use older and  
742 younger data to iterate towards a solution.

743

#### 744 **4 Palaeomagnetic Data**

745

746 A major problem in comparing the Phanerozoic models is that they all use different rotational  
747 frameworks, including reference trees (i.e. flat vs hierarchical) and different absolute reference frames. In  
748 order to properly synthesise the DOM16, DOM18 and YOU19 models into a single reconstruction, we  
749 first need to lay a coherent groundwork in defining an absolute plate motion model for the largest  
750 continents during this time in order to merge the individual models. To do this, we first derive a new  
751 APWP for Gondwana (540–320 Ma) and GAPWaP for Pangea (320–0 Ma) using the palaeomagnetic  
752 compilation of Torsvik et al. (2012) to provide an absolute palaeomagnetic reference frame for 540 to 0  
753 Ma. We also apply the GAPWaP to the MUL16 portion (i.e. the Mesozoic and Cenozoic) of the YOU19  
754 model. We do this to ensure compatibility between the Cenozoic and Palaeozoic, and also because our  
755 goals for this model are broad scale (> 10–100 Ma) trends, mostly focussed on the Neoproterozoic. The  
756 method we follow to calculate our APWP and GAPWaP is outlined below. For the Neoproterozoic, and  
757 non-Gondwana constituents of the Palaeozoic, we use the compilations of palaeomagnetic data as  
758 presented in MER17, DOM16 and DOM18, along with some other additions. Palaeomagnetically derived  
759 alterations to the models are also discussed below.

760

#### 761 **4.1 APWP and GAPWaP construction**

762

763 The absolute reference frames for Gondwana (540–320 Ma) and Pangea (320–0 Ma) used in this study  
764 are derived using the method and velocity-optimised global palaeomagnetic data of Tetley (2018).  
765 APWPs are routinely constructed using poles assigned averaged or nominal ages, which particularly for  
766 older times, where palaeomagnetic constraint becomes increasingly limited, contribute to spurious  
767 apparent polar wander behaviours. This method directly evaluate individual palaeomagnetic pole age and  
768 associated uncertainty in combination with calculated pole A95 latitude and longitude uncertainties to  
769 derive optimised APWPs that minimise predicted plate velocities and plate velocity gradients  
770 (instantaneous accelerations). The resulting rate of apparent polar wander in optimised APWPs was  
771 reduced globally by an average of 56% by comparison to existing APWPs, resulting in predicted  
772 Phanerozoic plate motions displaying greater kinematic consistency with present-day plate motion  
773 behaviours.

774

775 Optimised APWPs were produced for the 15 major continental blocks of Amazonia, Australia, Colorado,  
776 East Antarctica, Greenland, India-Pakistan, Madagascar, Meseta, North America, Northeast Africa,  
777 Northwest Africa, Panama, Patagonia, Somalia, and Stable Europe. Applying the method as described in  
778 Torsvik et al. (2012, 2008) and the data provided in Torsvik et a. (2012), optimised continental pole data  
779 from all 15 continents were rotated from their individual source coordinate frames into a consistent South



780 African coordinate frame using the rotation model from this study. Now in a consistent coordinate frame,  
781 a GAPWaP for Pangea was produced using all poles aged 320-0 Ma (due to the collision of Laurussia and  
782 Gondwana during the Late Carboniferous), with a second GAPWaP produced using poles aged 540-320  
783 Ma associated with Gondwana (South America, Africa, India, Antarctica and Australia) only. For both  
784 GAPWaP reference frames, the *GMAP* software was used (Torsvik et al., 2012, 2008; Torsvik and  
785 Smethurst, 1989), applying a running mean method using a window size of 20 Ma and a step size of 10  
786 Ma.

787

## 788 **4.2 Palaeomagnetic compilation**

789

790 A compilation of palaeomagnetic data was used to constrain the position of all continental blocks during  
791 the Neoproterozoic and for non-Gondwanan continental blocks during the early and middle Palaeozoic.  
792 The Neoproterozoic data are presented in Table 2 and a GPlates compatible file of the data is also  
793 presented in the Supplementary Material. Figure 6a–c shows the great circle misfit of our model to the  
794 selected poles. As the majority of the data have already been used in the MER17, DOM16 and DOM18  
795 reconstructions, we point readers to those publications for in-depth discussion of the data. Here, we  
796 discuss two alterations to the base models that we implemented based on palaeomagnetic data: Tarim at  
797 ca. 700 Ma and Laurussia at ca. 420–400 Ma.

798

799 The MER17 model omitted Tarim prior to 700 Ma due to its pre-700 Ma palaeomagnetic data nullifying  
800 the position that placed it outboard of Australia. We rectify this and include a robust, time-sensitive  
801 geological argument for its position against India-South China during the Tonian (1000–720 Ma) and  
802 Cryogenian (720–635 Ma) (Section 5.4.2). The rationale for placing Tarim in this position is to allow for  
803 a significant 180° rotation required by paleomagnetic data. Two well-dated and high-quality poles; the  
804 760–720 Ma Qiaoenbrak Formation (Wen et al., 2013) and the 770–717 Ma Baiyisi Volcanics (Huang et  
805 al., 2005) are internally consistent and require Tarim to be inverted 180° from its present-day position  
806 (i.e. northern margin facing south). A third pole, assumed to be pre 700 Ma, from the Aksu Dykes (Chen  
807 et al., 2004) is rejected for poor age constraints and the possibility of remagnetisation (Wen et al., 2017).  
808 Comparably, three younger poles: the 635–550 Ma Sugetbrak Formation (Zhan et al., 2007), the ca. 635  
809 Ma Tereeken Cap Carbonate (Zhao et al., 2014) and the 621–609 Ma Zhamoketi Andesite (Zhao et al.,  
810 2014) are all consistent with each other and indicate that Tarim was in its present-day orientation. A  
811 recent pole by Wen et al. (2017) from the Lower Sugetbrak formation (640–615 Ma) stands in conflict  
812 with these three poles, suggesting a ~50° rotational difference in the orientation of Tarim, while  
813 maintaining the same palaeolatitude. Wen et al. (2017) dismiss the three earlier poles due to similarity to

814 Silurian–Devonian poles for the Sugetbrak Formation and possible remagnetisation for the latter two  
815 poles, respectively.

816

817 Successfully fitting the two older poles with either the three younger poles or the single pole of Wen et al.  
818 (2017) is not possible in a model in which Tarim is surrounded by continental lithosphere for the  
819 Neoproterozoic or in a scenario where Tarim is attached to the north-western or northern margin of  
820 Australia or the northern margin of India (e.g. instead of South China). An accommodation of the data can  
821 be obtained by placing Tarim in a ‘Missing-Link’ position (between Australia and Laurentia) with  
822 breakout and rotation of Tarim from ca. 700 Ma; as argued by Wen et al. (2018, 2017). However, beyond  
823 the kinematic issues with Missing-Link style models (Merdith et al., 2017b), it is difficult to account for  
824 the formation of the 760 Ma Aksu Blueschist if Tarim was located in the centre of an assembled Rodinia  
825 (see comment by Song and Li (2019) and reply by Wen et al. (2019)). In the present model, we use the  
826 pole of Wen et al. (2017) due to its greater reliability, though our model could easily be adapted to fit the  
827 other three poles if necessary (Section 5.4.2.). We also note that although we argue that India-South China  
828 were separate from the rest of Rodinia, our preferred Neoproterozoic position for Tarim is also  
829 compatible with models in which India-South China formed part of Rodinia (e.g. Cawood et al., 2013b).

830

831 In the YOU19 model, Laurussia was moved  $\sim 30^\circ$  further north in latitude relative to its position in DT14  
832 and MAT16 (Section 3.3). The consequence of this decision by YOU19 is that Laurussia is not in a  
833 palaeomagnetically constrained position in the late Silurian and early Devonian. For this model, in  
834 addition to the compilation of palaeomagnetic data in Torsvik et al. (2012), we also used palaeomagnetic  
835 data from mainland Baltica (Table 2) to constrain the late Silurian to early Devonian position of  
836 Laurussia. We implement these alterations to produce a coherent motion of Laurentia (later Laurussia)  
837 and Gondwana that fits palaeomagnetic data, while also ensuring that the relative motion between  
838 Gondwana and Laurussia is convergent, rather than dextral transform (e.g. Fig. 2c).

839

840

## 841 **5 Alterations to models**

842

843 We describe the alterations made to individual models separately for clarity, however, we stress that no  
844 single model was treated in isolation. Each alteration, whether during the Tonian or Devonian, was  
845 evaluated both forwards and backwards in time in order to ensure continuity with both older and younger  
846 geological and/or palaeomagnetic evidence. We begin our discussion with the alterations made to  
847 YOU19, followed by alterations to DOM16, DOM18 and MER17. The alterations to DOM16 and

848 DOM18 are discussed together, as the two models essentially form a single global model between 500  
849 and 410 Ma. The most significant changes, and the focus of much of the discussion, occurred in MER17.  
850 This is because, firstly, connecting this model with younger models in order to validate Neoproterozoic  
851 tectonic-geography is a primary goal of this study, and secondly, because many of the alterations are  
852 completely new and have never been incorporated into a plate model before. Figure 7a–b displays a  
853 latitudinal overview of the major and minor cratons in our model, with a comparison to the DOM-MAT  
854 models for the Phanerozoic, and the model of Li et al. (2013, 2008) for the Neoproterozoic. Figures 8, 9  
855 and 10 show overviews of our reconstruction at 1000 Ma, 500 Ma and present-day with relevant terranes  
856 and blocks highlighted.

857

## 858 **5.1 YOU19**

859 The primary change we made to YOU19 was the implementation of a new APWP for Gondwana from  
860 540 to 320 Ma and a GAPWaP for 320 to 0 Ma (Tetley, 2018). We also adjusted the position of Laurussia  
861 during the Devonian in order to better fit palaeomagnetic data and implemented an alternative position for  
862 Lhasa (against northwest Australia) that we consider to be more consistent with geological data in the  
863 Neoproterozoic (Section 5.4.1).

864

865 In the YOU19 reconstruction, Laurussia is rotated roughly 40° counter-clockwise compared to the DT14  
866 and MAT16 reconstructions (Fig. 11). While these changes improved the global kinematic integrity of the  
867 model (Young et al., 2019), the position of Baltica in this configuration conflicts with palaeomagnetic  
868 data, which indicates it lay at more southerly latitudes (Torsvik et al., 2012). We used the compilation of  
869 Torsvik et al. (2012) as a base, however, as many of the poles in that dataset for the late Silurian to early  
870 Devonian were taken from the British Isles (c.f. Jeleńska et al., 2015), we supplement it with some data  
871 from cratonic, continental Europe (Table 2, S. Pisarevsky pers. comm.). We modify the position of  
872 Laurussia from that used in YOU19 such that it fits the cluster of poles at this time (Fig. 11b). This  
873 modification places it in a similar latitudinal position to DT14 and MAT16 (e.g. Fig. 7a), however, we  
874 shift it further east relative to DT14, so that it is closer to its final position in Pangea. This position then  
875 satisfies the kinematic and structural issues outlined in YOU19, while maintaining Baltica and Laurussia  
876 at a palaeolatitude permitted by palaeomagnetic data.

877

878 The Lhasa block, currently preserved in the Tibetan Plateau between India and Tarim, is an E-W  
879 elongated block consisting of Precambrian metamorphic basement, overlain by predominantly Palaeozoic  
880 sedimentary rocks and Mesozoic and Cenozoic volcanic assemblages (Yin and Harrison, 2000; Zhu et al.,  
881 2013). The Precambrian basement is established only in the southern and central terranes of Lhasa (Zhu et

882 al., 2013) and in the Amdo micro-block that is preserved in the Mesozoic northern Lhasa terrane (e.g. Fig.  
883 10b). Lhasa is typically placed outboard of the Tethyan Himalayan terranes, off the northern margin of  
884 India within Gondwana (e.g. Domeier and Torsvik, 2014). However, an alternative position outboard of  
885 northwest Australia is also supported; a scenario consistent with tectonic affinities interpreted from zircon  
886 age spectra and Hf isotopic signatures (Burrett et al., 2014; Zhu et al., 2011). We find a position off  
887 northwest Australia more consistent with the Neoproterozoic geological record of Lhasa (Section 5.4.1)  
888 that preserves magmatism interpreted to represent the existence of a subduction zone and back-arc  
889 (Gynn et al., 2012; Hu et al., 2018), which would otherwise be impossible to produce if it was land-  
890 locked between India and South China. We therefore alter the position of Lhasa from YOU19 to outboard  
891 of NW Australia. For simplicity, we infer Lhasa's motion to follow the drift of the Cimmerian terranes,  
892 but recognise that the palaeolatitudes need further refinement in the Jurassic and Cretaceous following  
893 syntheses such as Li et al. (2017, 2016) and others.

894

## 895 **5.2 DOM16 and DOM18**

896

897 We sought to preserve, as closely as possible, the palaeolatitudes and the tectonic interpretations (i.e.  
898 history of collisions, rifting, subduction and ocean basin evolution) of the DOM16 and DOM18  
899 reconstructions. The position of Gondwana (both in Early Palaeozoic and the older times covered by  
900 MER17) has been adjusted to inherit the Gondwana position at 410 Ma from the new Gondwana APWP  
901 path described above. Relative rotations of smaller blocks to Gondwana were calculated from DOM16/18  
902 and translated into the new position of Gondwana. Further adjustments to all continental polygons have  
903 been implemented to smooth the transition from the late Palaeozoic configurations inherited from the  
904 adjusted YOU19 model (adj-YOU19). The following sections detail adjustments to the DOM16/18  
905 models made for the late Cambrian–Devonian.

906

907 Figure 11 shows a direct comparison between the DOM16/18 reconstructions and our adj-YOU19 model  
908 at 411/410 Ma. The primary differences between the models are longitudinal, as our adj-YOU19 model  
909 shifts Laurussia, Siberia, Kazak, Tairm and North China  $\sim 30^\circ$  longitudinally to the east compared to  
910 DOM16/18 (as well as when compared to DT14 and MAT16, which link closely to DOM16/18), in order  
911 to better model the amalgamation of Laurussia and Gondwana. This results in a far narrower Rheic Ocean  
912 at 410 Ma in our model and a much simpler collision between Laurussia and Gondwana (e.g. Wu et al.,  
913 2020; Young et al., 2019). This change is discussed further in context in the following section.

914

915 The motions of Baltica, Laurentia, and Siberia are tied directly to the spin axis through their own  
916 individual palaeomagnetic reference frame, in contrast to the younger parts of the reconstruction where  
917 we retain the hierarchy inherited from YOU19. For minor cratons (Tarim, North China, South China) and  
918 smaller blocks (e.g. Tianshan, Kara), we model their motion within a relative hierarchy for the practical  
919 reason that this makes it easier to preserve the consistency of their geological history, as they share  
920 multiple plate boundaries with Gondwana. For all these cratons and blocks, we sought to preserve the  
921 palaeolatitudes from the parent studies to a reasonable degree allowing for data uncertainties (e.g. Fig. 6).  
922 Figure 7 provides a quantitative comparison between the paleolatitudes of the DOM16/18 models and our  
923 incorporation of them into our adjusted reconstruction.

924

### 925 *5.2.1 Deviations from DOM16*

926

927 The key deviation between DOM16 and our model is a difference in the orientation of Baltica in the late  
928 Cambrian (Fig. 12a), where our model has Baltica rotated 90° counter clockwise relative to DOM16. As  
929 the DOM16 model only begins at 500 Ma it does not have to explicitly consider the earlier  
930 Neoproterozoic history of Baltica. In our opinion the position of Baltica in DOM16 is more congruent  
931 with an inverted Baltica (relative to Laurentia) during the Neoproterozoic (Hartz and Torsvik, 2002),  
932 where the southern-peri Urals are connected to Greenland. In comparison, MER17 connects Baltica to  
933 Rodinia through the Sveconorwegian margin in an upright position relative to the present-day (e.g.  
934 Cawood et al., 2003; Dalziel, 1992; Weil et al., 1998). The inverted Neoproterozoic Baltica position of  
935 Hartz and Torsvik (2002) results in simpler kinematic motions during the late Ediacaran and Early  
936 Palaeozoic, whereas the ‘traditional’ Neoproterozoic coupling of Baltica-Laurentia requires a more  
937 complex motion path in order to fit palaeomagnetic data. However, in our opinion the ‘upright’ coupling  
938 of Baltica and Laurentia is far more geologically and palaeomagnetically robust (Cawood and Pisarevsky,  
939 2006; c.f. Slagstad et al., 2019) in the Neoproterozoic than the alternative, and as such we adopt this  
940 configuration at ca. 600 Ma (as in MER17) during the opening of the Iapetus Ocean; necessitating a more  
941 complex kinematic evolution for Baltica between 600 and 470 Ma (Fig. 12a ,b). Our reconstruction of  
942 Baltica is therefore quite different to that of DOM16 during the late Cambrian and early Ordovician as we  
943 have to implement a ~90° rotation between 520 and 475 Ma of Baltica to fit the same series of  
944 palaeomagnetic data at 470 Ma as DOM16.

945

946 Baltic palaeomagnetic data compiled by Meert et al. (2014), Torsvik et al. (2012) and Domeier (2016)  
947 were used to ensure its latitudinal position remained valid between 550 and 470 Ma (Table 2).  
948 Importantly, only two poles—one from the Andarum Shale (Torsvik and Rehnström, (2001) categorised

949 as C-grade quality by Meert (2014)) and the other from the Narva sediments, (Khramov and Iosifidi,  
950 (2009), categorised as B-grade quality by Meert (2014))—are identified for Baltica between 530 and 480  
951 Ma, both with a nominal age of 500 Ma. Despite coeval ages, the poles are  $\sim 35^\circ$  apart from one another  
952 and Meert (2014) identified unresolved issues, specifically: few samples constraining the pole and a  
953 (possible) effect of inclination shallowing (even after correction for inclination shallowing a  $\sim 25^\circ$   
954 mismatch remains). A strict fitting of the Narva sediments pole would require Baltica to rotate by  $\sim 2^\circ/\text{Ma}$   
955 between 550 and 500 Ma; a situation we consider implausible and likely reflecting underlying issues in  
956 the palaeomagnetic data. As such, our model does not fit either pole explicitly, though our reconstructed  
957 position of Baltica is consistent with the latitude suggested by the inclination data of both poles. By 460–  
958 440 Ma, our model closely resembles the DOM16 model, with similar sized Rheic oceans, latitudinal  
959 positions and orientations of Gondwana, Baltica and Laurentia (Fig. 12c, d). At 410 Ma, when DOM16  
960 finishes, the only difference is the relative position of Laurasia and Gondwana due to differences in  
961 palaeolongitude (Fig. 2c; 11). In our model, Laurussia is much closer to Gondwana resulting in a far  
962 narrower Rheic Ocean at 410 Ma than in DOM16/18, DT14 and MAT16 (e.g. Fig. 2c, see also Wu et al.  
963 (2020)).

964  
965 The width of the Rheic ocean is poorly constrained (c.f. Dalziel and Dewey, 2019; Domeier, 2018; Wu et  
966 al., 2020) especially because of palaeolongitudinal uncertainty. The problem is compounded by the fact  
967 that there is only one reliable palaeomagnetic pole constraining our Gondwana APWP between 430 and  
968 400 Ma (Aïr intrusives in Niger, age at 410 Ma, (Hargraves et al., 1987)), meaning the early Devonian  
969 portion of the APWP has large uncertainty. Because of this uncertainty, the methods used to create  
970 APWPs tend to dampen the effect of this pole (which is true for our APWP). Nonetheless, even with the  
971 effect of this pole being dampened, reconstructed palaeomagnetic data (without considering longitudinal  
972 constraints) at 410 Ma allow placement of Laurussia and Gondwana to within a few thousand kilometres  
973 of one another (e.g. Fig. 11a, see also Wu et al. (2020)). At first glance, this seems problematic, because  
974 one might expect that the forces related to subduction zones modelled along the craton margins facing  
975 each other would draw the cratons to each other. DOM16, DT14 and MAT16 (along with Torsvik et al.,  
976 (2014)) solve this problem by changing the palaeolongitude of Laurussia to  $90^\circ$  east relative to  
977 Gondwana, allowing for a much wider ocean basin. This position is justified and necessitated in these  
978 models by their use of the PGZ method, where Laurussia is reconstructed over the eastern arm of the  
979 present-day position of the Pacific LLSVP. However, this position then requires  $> 8000$  km of dextral  
980 motion between Laurussia and the Patagonian margin of Gondwana from 400 and 340 Ma (e.g. Fig. 3c).  
981 As we do not adopt the PGZ method, our position of Laurussia at 410 Ma relative to Gondwana is much  
982 closer to its final collision place and the resulting relative motion between Laurussia and Gondwana

983 between 410 and 340 Ma is of sub-orthogonal–orthogonal collision along the southern Appalachian zone  
984 (Hopper et al., 2017), with some dextral transform motion between north-east Laurentia and the northwest  
985 margin of Gondwana (e.g. Murphy et al., 2011) and between southern Baltica and north Gondwana (e.g.  
986 Arthaud and Matte, 1977). From 340 to 320 Ma YOU19, MAT16 and DT14 have a similar configuration  
987 between Laurussia and Gondwana. We stress that while our model this differs from the adopted DOM16  
988 model, it is not a particularly novel interpretation and many continental reconstructions show a similar  
989 scenario (e.g. McKerrow et al., 2000; Scotese, 2004; Stampfli and Borel, 2002). A more detailed  
990 geological and kinematic justification of this interpretation is presented in Young et al. (2019) and a  
991 discussion of the palaeomagnetic challenges in amalgamating Pangea are presented in Domeier et al.  
992 (2020, 2012) which we encourage interested readers to.

### 993 994 *5.2.2 Deviations from DOM18*

995  
996 Two salient points made by Domeier (2018) pertaining to relative longitude and his model are also of  
997 interest here, and worth reiterating when merging DOM18 into the adj-YOU19 model and then extending  
998 the adj-YOU19 model into the Neoproterozoic. Firstly, a long lived south-dipping subduction zone,  
999 preserved in the northern Kazakhstan terranes of Urumbai, Selety and Erementau (Degtyarev, 2011;  
1000 Domeier, 2018; Windley et al., 2007) was longitudinally distributed from Siberia through to the  
1001 northernmost margin of Gondwana (i.e. North Australia, Papua New Guinea) and secondly, the broader  
1002 framework of Baltica-Siberia-Gondwana provides geological, spatial and temporal limits on the evolution  
1003 of this area. These two aspects of the model allowed DOM18 to infer with some certainty the relative  
1004 palaeolongitude of many of the smaller terranes within the broader absolute palaeolongitudinal constraints  
1005 imposed by (principally) Siberia, Baltica, Laurentia and Gondwana. Likewise, even though we do not  
1006 adopt the absolute longitudinal framework of DOM18, we can use the positions of the major cratons to  
1007 provide a relative control on the possible kinematic evolution of the Chinese cratons and terranes. We  
1008 follow DOM18 by reconstructing a quasi-stable south-dipping subduction zone to delimit the northerly  
1009 extent of the Palaeo-Tethys Ocean and this, coupled with the palaeomagnetic data from these cratons and  
1010 terranes between 500 and 410 Ma, make longitudinal re-ordering of these blocks unlikely. The  
1011 unlikelihood of longitudinal re-ordering is one of the main constraints and pieces of evidence that lead to  
1012 significant revision of the positions of Tarim and North China in MER17 that are discussed in the  
1013 following section (5.4).

1014  
1015 The relative positions of terranes (Tianshan, Qaidam-Qilian, Kunlun etc.) can also be considered in a  
1016 similar manner to how we conceive of the relative ordering of the Chinese cratons during the Early

1017 Palaeozoic. In particular, the ca. 470 Ma suturing of Tianshan-Chu Yili (Alexeiev et al., 2019) and the  
1018 440–430 Ma suturing of Kunlun, Qaidam, Qilian and Alxa to Tarim (Xiao et al., 2009) both necessitate  
1019 an internally consistent relative position between these terranes and Tarim and Siberia in order to be  
1020 consistent with the geological record. That is, relative to present-day Tarim, Tianshan, Chu-Yili and other  
1021 Kazakh terranes should be reconstructed somewhere north of the *northern* margin of Tarim during the  
1022 Ediacaran–Ordovician, but south of Siberia. Similarly, Kunlun, Qaidam, Qilian and Alxa need to be  
1023 reconstructed to the *south* and *east* of Tarim in the same time period. In a plate model framework, this  
1024 means that the longitudinal structure of the Proto-Tethyan ocean basin should reconstruct (from west to  
1025 east): Siberia—Chu-Yili-Kazakh-Tianshan—Tarim—Alxa-Qaidam-Qilian-Kunlun—North China—South  
1026 China (e.g. Fig. 13f, g). Further back in time, we also maintain this same configuration to minimise any  
1027 terrane re-organising, such that their relative positioning is broadly reminiscent of present-day (e.g. Figs.  
1028 9; 16). In this manner, we use these relative longitudinal constraints to infer a configuration for the nuclei  
1029 of these terranes in the Neoproterozoic, thereby connecting the present-day with their Precambrian  
1030 history.

1031  
1032 The fundamental difference between DOM18 and our implementation of the model is the longitudinal  
1033 width of the Proto-Tethyan ocean basin, bounded by Siberia in the west, Gondwana in the east and south  
1034 and the aforementioned south-dipping subduction zone in the north (e.g. Fig. 13b, c, f, g). The latitudinal  
1035 extent of the ocean basin remains similar in both models (30–50°), constrained by palaeomagnetic data  
1036 from Gondwana, Siberia and the Chinese cratons (e.g. Table 2, Fig. 13a, d, e, h). In our model, this ocean  
1037 basin is much wider (longitudinally) in the late Cambrian and Ordovician than in DOM18, narrowing in  
1038 size as it evolves due to our implemented easterly drift of Siberia from the Cambrian through to the  
1039 Devonian. The size of the ocean basin is then similar at 410 Ma (Fig. 11), due to the adopted similarity of  
1040 the YOU19 from the DT14 reconstruction (Young et al., 2019). The key reason for the difference in width  
1041 at 500 Ma is because DOM18 places Laurussia further east at 500 Ma than we do (Section 5.2.1). This  
1042 then forces a narrower ocean basin between 500 and 410 Ma in DOM18 than in our model. The following  
1043 paragraphs will discuss the regional longitudinal constraints of this ocean basin by considering the  
1044 position of Gondwana and Siberia.

1045  
1046 The Early Palaeozoic position of Siberia in our model is a function of palaeomagnetic data and its  
1047 position in, and breakout from, Rodinia. In isolation, the simplest explanation of Siberia’s journey is that  
1048 sometime during the late Tonian–Cryogenian (750–700 Ma) Siberia rifted off the northern margin of  
1049 Laurentia (somewhere near Greenland, see Pisarevsky and Natapov (2003) and Pisarevsky et al. (2013)).  
1050 At this time Siberia was located equatorially and rotated 60° clockwise from its present-day orientation



1051 (Pisarevsky et al., 2013). Palaeomagnetic data are sparse for the remainder of the Neoproterozoic, with  
1052 the few calculated poles having either poor age constraints or unresolved tectonic coherence with the  
1053 Siberian craton (Pavlov et al., 2015), and are therefore typically omitted from syntheses (Cocks and  
1054 Torsvik, 2007; Li et al., 2008; Merdith et al., 2017a). However, from the mid-Cambrian the  
1055 palaeomagnetic record of Siberia is reasonable (Cocks and Torsvik, 2007) and broadly congruent with the  
1056 palaeolatitude of the 750 Ma pole (that is, equatorial–sub-equatorial). From the mid-Cambrian, the data  
1057 suggest a slow northward drift and counter-clockwise rotation (Cocks and Torsvik, 2007), with the  
1058 orientation of Siberia at ca. 530 Ma inverted relative to present-day. This then requires a ~120° clockwise  
1059 rotation between 720 and 530 Ma in order to fit its Neoproterozoic position (Metelkin et al., 2012). For  
1060 the Cryogenian and Cambrian, Siberia's motion can be inferred indirectly using data from Baltica, as  
1061 outlined in the next paragraph.

1062  
1063 The position of Baltica is constrained by clusters of palaeomagnetic data during the Ediacaran and early  
1064 Cambrian. Furthermore, its latitudinal position places limits on the possible position of Siberia. The  
1065 equatorial excursion of Baltica in the latest Ediacaran places Baltica at a latitude similar to Siberia. As  
1066 they cannot be positioned on the same longitude (Merdith et al., 2017a), Siberia must be located either  
1067 longitudinally east or west of Baltica between 600 and 500 Ma (with Laurentia also occurring on a similar  
1068 palaeolatitude but further east than either Siberia or Baltica). Domeier (2018) presented similar arguments  
1069 for the second latitudinal excursion of Baltica (it returns to a high latitude during the Ordovician–Silurian)  
1070 when it collided with Laurentia to form Laurussia at ca. 440–430 Ma. He argued that the overlapping  
1071 palaeolatitudes of Siberia and Baltica at this time then requires Siberia to be located more easterly than  
1072 Baltica by ca. 470 Ma (Domeier, 2018). We also adopt this logic, thus providing a rough relative  
1073 longitudinal framework for Laurentia-Baltica-Siberia relations from 700 to 450 Ma.

1074  
1075 Our model requires the motion of Siberia to be predominantly longitudinal between 700 and 450 Ma (the  
1076 available palaeomagnetic data do not suggest more than 30° latitudinal movement). We constrain this to  
1077 two broad phases of movement, defined by Baltica's two latitudinal excursions (at ca. 560 Ma and 450  
1078 Ma). In the first excursion (750–550 Ma), we keep Siberia longitudinally between Laurentia and Baltica,  
1079 because to move it further east than Baltica at 550 Ma would require relative plate motion greater than 30  
1080 cm/a, which we deem unlikely. By 470 Ma palaeomagnetic data from Baltica suggest it has started  
1081 drifting north again, so we therefore reconstruct Siberia to also be moving east longitudinally between  
1082 550 and 470 Ma, such that by 470 Ma it is located along the same longitude as Baltica; by 450 Ma it is  
1083 further east than Baltica, such that Laurussia can form by 430 Ma. Our model is therefore similar to that  
1084 of DOM18 in concept and adherence to available observations, however the different absolute

1085 longitudinal positions create a notably different ocean basin in the late Cambrian and Ordovician, within  
1086 which the Chinese cratons and terranes are then arranged.

1087

1088 Domeier (2018) does not explicitly consider the Neoproterozoic or Early Palaeozoic evolution of the  
1089 Chinese cratons in his model. At 500 Ma, the DOM18 model places North China off the northern margin  
1090 of India, and South China off northern Australia. However, retaining these relationships in the  
1091 Neoproterozoic is invalidated by what Neoproterozoic palaeomagnetic data exists for each craton (e.g. Fu  
1092 et al., 2015; Li et al., 2004), and also conflicts with interpreted geological histories (Cawood et al., 2018b,  
1093 2013b). Consequently, our model, which balances both older and younger times, alters the kinematic  
1094 evolution in order to fit older constraints (Fig. 13, Sections 5.4.1 and 5.4.2).

1095

## 1096 **5.4 MER17**

### 1097 *5.4.1 Australia, North China, Lhasa and Tasmania*

1098 Significant alterations to MER17 were made between 1000 and 900 Ma along the north-western, western  
1099 and south-western margins of Laurentia, affecting the motions and positions of Australia, North China,  
1100 Siberia, Tasmania and Lhasa. We adopt the model of Wen et al. (2018) in having a dextral shear zone  
1101 between Australia-Antarctica (A-A) and Laurentia during the early Tonian. Wen et al. (2018) argued for  
1102 placing Tarim against the eastern margin of Laurentia, separating Laurentia from Australia in a ‘Missing  
1103 Link’ position (cf. (Li et al., 2008, 1995), with the dextral shear zone transecting Tarim. However, we  
1104 consider this position for Tarim is incompatible both with geological data (the 760 Ma Aksu Blueschist  
1105 (C.-L. Zhang et al., 2013)) and with the kinematic constraints that would be necessary to move Tarim  
1106 from this position to its Palaeozoic position (e.g. Meredith et al., 2017b). We therefore use the alteration of  
1107 Wen et al.’s (2018) model presented in Mulder et al. (2018b), who place a dextral boundary separating the  
1108 Antarctic crust of Australian affinity exposed in Terre Adélie Land from the Antarctic crust of Laurentian  
1109 affinity in the Nimrod Igneous Province (Fig. 14a, see also Goodge et al., (2017)).

1110

1111 North China and northern Australia share a similar Mesoproterozoic and early Tonian sedimentary record  
1112 and both preserve contemporaneous ca. 1.33–1.31 Ga magmatism (Bodorkos et al., 2020; Yang et al.,  
1113 2020; Zhang et al., 2017) that is interpreted as a large igneous province. Yang et al. (2019) also  
1114 demonstrated the similarity in detrital zircon ages and hafnium isotope compositions between the Tonian  
1115 strata of both areas. We find that this position of North China in the latest Mesoproterozoic is remarkably  
1116 compatible with the few reliable palaeomagnetic data for North China in the Neoproterozoic (e.g. Fig 6,  
1117 (e.g. Fig. 6, Fu et al., 2015) and places North China in a position readily compatible with its Palaeozoic  
1118 constraints where the same species of distinctive tommotiid fossils have recently been reported (Pan et al.,

1119 2018). A distinct Sino-Australian Cambro–Ordovician faunal province was identified by Burrett et al.  
1120 (1990) that suggests some proximity in the early Palaeozoic. Cambrian–Ordovician rifting in the Arafura  
1121 Basin north of northern Australia may represent the initial separation of North China from this margin of  
1122 Gondwana (Ahmad and Munson, 2013). Palaeomagnetic data necessitate some relative motion between  
1123 Australia and North China in the Early Palaeozoic from its inferred Mesoproterozoic–Neoproterozoic  
1124 position (e.g. Domeier, 2018). Given there is no evidence of orogenesis between North China and  
1125 northern Australia in the Phanerozoic, we infer that North China slowly drifts off this margin from the  
1126 Cambrian, remaining in close enough proximity to share the identified Cambro–Ordovician faunal  
1127 provinces (e.g. Fig. 13).

1128

1129 Dong and Santosh (2016) and Dong et al. (2014) describe a 1000 to 900 Ma suture between the Qinling  
1130 Terrane and North China, preserved as the Kuanping Ophiolite (Fig. 14a–c). As Siberia and Australia are  
1131 reconstructed adjacent to each other in Rodinia (Pisarevsky et al., 2013), the position of North China  
1132 along the northern margin of Australia suggests that the Qinling terrane could feasibly be an extension of  
1133 the Central Angara terrane, where there is a similarly aged (but sparsely described) ophiolite, the  
1134 Ribnaya-Panimba ophiolite (Vernikovskiy et al., 2004, 2003). In our model, the subduction zones  
1135 represented by these two ophiolites consume the oceanic lithosphere between Australia, Siberia and  
1136 Laurentia (the Kuanping Ocean) during the early Tonian. Mulder et al. (2018b) ceased motion at 900 Ma  
1137 in their model but, we adjust this cessation to 930 Ma wherein the Qinling Terrane rotates to fit against  
1138 the North China block. This is because we also reconstruct the Lhasa block along the western margin of  
1139 Australia ((Zhu et al., 2011), see Section 5.1) and here magmatism is preserved from ca. 925 Ma (Gynn  
1140 et al., 2012, 2006; Hu et al., 2018; Zeng et al., 2018) (Fig. 14d,e). Consequently, we suggest that this  
1141 subduction initiated after the closure of the interior Kuanping Ocean and collision of North China-  
1142 Australia-Antarctica with Siberia-Laurentia along the Qinling-Central Angaran Terrane. The subduction  
1143 zone then connects northwards through to subduction preserved in Taimyr outboard of Siberia  
1144 (Vernikovskiy et al., 2004; Vernikovskiy and Vernikovskaya, 2001) and southward into an oceanic arc  
1145 outboard of the Mawson Craton of Antarctica, possibly preserved in the southernmost Tonian Oceanic  
1146 Arc Super Terrane (TOAST) or between Indo-Antarctica and Australia-Antarctica). In our model,  
1147 Australia sits in a typical SWEAT (South West United States, East Antarctica) configuration (Moore,  
1148 1991). We made this change to better fit the arguments put forward by Mulder et al. (2018b), while still  
1149 maintaining integrity of relative plate kinematics following the reasoning of Merdith et al. (2017b).

1150

1151 Our revised model also incorporates recent refinements to the Proterozoic and early Palaeozoic  
1152 paleogeography of the Western Tasmania Terrane. The Western Tasmania Terrane, comprising the

1153 Proterozoic geology of Tasmania and the East and West South Tasman Rises (Berry et al., 2008),  
1154 occupies an important position in deciphering the geological relationship between Laurentia and  
1155 Australia-Antarctica in Rodinia, and also in understanding the transition between Rodinia to Gondwana.  
1156 The Western Tasmania Terrane represents an exotic Proterozoic microcontinent that was accreted onto  
1157 the Pacific margin of eastern Gondwana in the late Cambrian during the Ross-Delamerian orogenic cycle  
1158 (Berry et al., 2008; Cayley, 2011). The terrane has geological affinities with the central Transantarctic  
1159 Mountains of East Antarctica and the western margin of Laurentia, including overlapping  
1160 Palaeoproterozoic basement ages, contemporaneous Mesoproterozoic magmatic and fluid-flow events,  
1161 and correlated Mesoproterozoic sedimentary strata (Berry et al., 2008; Fioretti et al., 2005; Halpin et al.,  
1162 2014; Mulder et al., 2015, 2018b). Based on these geological connections, the Western Tasmania Terrane  
1163 was likely located between East Antarctica and western Laurentia within an assembled Rodinia. The  
1164 breakout of the Western Tasmania Terrane from its central position within Rodinia is recorded by  
1165 widespread Tonian–Ediacaran sedimentation and rift-related magmatism (Mulder et al., 2020). The onset  
1166 of Neoproterozoic rifting of the Western Tasmania Terrane is marked by 780–750 Ma intraplate  
1167 magmatism (Black, 1997; Calver et al., 2013) and latest Tonian (750–730 Ma) siliciclastic and carbonate  
1168 sedimentation (Calver et al., 2014; Mulder et al., 2018a). Following deposition of Cryogenian rift-related  
1169 strata and glaciogenic intervals (Calver, 2011; Calver et al., 2014) a final pulse of Neoproterozoic rifting  
1170 is recorded by voluminous ca. 580 Ma rift-related basalts in northwest Tasmania (Direen and Crawford,  
1171 2003; Meffre et al., 2004). Geological correlations permit the Western Tasmania Terrane to have  
1172 remained attached to either the western margin of Laurentia or the eastern margin of Australia-Antarctica  
1173 following the opening of the Pacific Ocean (Fig. 10f), prior to being isolated as a microcontinent during  
1174 ca. 580 Ma rifting and accretion onto its present-day position along the margin of Gondwana by the late  
1175 Cambrian (Fig. 10g; Berry et al., 2008; Mulder et al., 2020). We follow Mulder et al. (2020) in having  
1176 Tasmania rift from the Antarctic margin (rather than the alternative scenario of Laurentia), thus implying  
1177 that some further unknown micro-continents rifted from the western margin of Laurentia at the same time  
1178 in order to account for that passive margin (e.g. Fig. 14f, g Macdonald et al., 2013) (see also Colpron et  
1179 al., 2002; Cox et al., 2018; Eyster et al., 2019).

1180

#### 1181 *5.4.2 India-South China Accretionary Belt*

1182 We preserve the MER17 interpretation of a tight India-South China connection (after Cawood et al.,  
1183 2013b). This possible connection was suggested previously by Jiang et al. (2003) who noted the similarity  
1184 between sequence stratigraphy in rift basins preserved in both South China and the Indian Lesser  
1185 Himalaya (Fig. 15a), as well as by Hofmann et al. (2011) who suggested a geological similarity based on  
1186 detrital zircon analysis. Arguments for this connection are succinctly summarised in Cawood et al.

1187 (2018b) and are not repeated here—instead we focus our discussion of this margin on the relative position  
1188 of outboard terranes during the Neoproterozoic (Fig. 15), which are based predominantly on their  
1189 Palaeozoic positions (Domeier, 2018). Here we have sought to preserve their relative internal positions in  
1190 order to minimise reshuffling of terranes during the Neoproterozoic (e.g. Fig. 16). For example, Kunlun,  
1191 which is currently preserved south of Tarim and west of Qaidam-Qilian, is always reconstructed with the  
1192 same internal consistency. Although we note that this may not be an accurate reflection of the ordering  
1193 and positioning of the terranes, it ensures consistency within the model and minimises terrane shuffling  
1194 which can preclude unrealistic scenarios, where terranes have to kinematically skirt one another  
1195 precariously. Figure 16 gives a schematic overview of our conceptualisation and implementation of this  
1196 model.

1197

1198 Following Alessio et al. (2018) and Armistead et al. (2019), the northwest margin of India is here  
1199 interpreted as an extensive Stenian-Tonian accretionary margin that extends as far as the Omani basement  
1200 and northernmost Madagascar. The pre-Ediacaran basement rocks in Rajasthan and Pakistan share  
1201 similarities with those of Oman. Granitoids have been dated from Rajasthan and from Nagar Parkar in  
1202 eastern Sind (Pakistan) at ca. 1.1 Ga (Meert et al., 2013; Raza et al., 2012). There is no evidence of older  
1203 crust occurs west of the Western Margin Fault of the Aravalli-Delhi Orogen, where the Marwar terrane  
1204 accreted to India in the latest Mesoproterozoic (Meert et al., 2010) (Fig. 15b). Tonian granitoids and  
1205 rhyolites occur in inliers through northwest India and Pakistan, where they cluster into crystallisation ages  
1206 of ca. 990–970 Ma (Haldar and Deb, 2001; Pandit et al., 2003), ca. 860–820 Ma (Davies and Crawford,  
1207 1971; Deb et al., 2001; Just et al., 2011; Van Lente et al., 2009) and ca. 775–760 Ma (Ashwal et al., 2013;  
1208 Gregory et al., 2009; Meert et al., 2013; Van Lente et al., 2009). The latter magmatic and extrusive phase  
1209 forms one of the largest felsic igneous provinces on the planet—the Malani Igneous Suite—which is also  
1210 traced to the Seychelles (Fig. 15c–e) (Torsvik et al., 2001; Tucker et al., 2001). Arc accretion continued  
1211 outboard to Oman where two main phases of subduction and arc magmatism occur, at ca. 850 Ma and ca.  
1212 770 Ma (Blades et al., 2019a). The latter phase focussed in the southern Mirbat area and interpreted here  
1213 as the arc that formed ocean-ward of the more back-arc Malani Igneous Suite. Further outboard still, and  
1214 later accreting onto the Indian margin, the Bobakindro Terrane of northern Madagascar (Armistead et al.,  
1215 2019) consists of juvenile magmatism that dates from ca. 750–705 Ma (Armistead et al., 2019; Collins,  
1216 2006; Thomas et al., 2009).

1217

1218 Many terranes currently preserved north of South China and south of Siberia have Neoproterozoic or  
1219 older cores. They have not been previously considered in global models (Li et al., 2008; Merdith et al.,  
1220 2017a) due to the sparsity of data and small size of terranes, which invites many competing and

1221 conflicting interpretations of their history. However, in the construction of this continuous plate model,  
1222 where spatial and temporal continuity is vital, the most compatible Tonian position for these terranes was  
1223 outboard of the afore-discussed large accretionary subduction zone of South China and India. This  
1224 position places them in the most favourable kinematic, palaeomagnetic and geologically plausible  
1225 positions for their (more well constrained) Palaeozoic journeys (e.g. Charvet et al., 2011; Domeier, 2018;  
1226 Xiao et al., 2013). Below we summarise some geological evidence for this, with particular reference to  
1227 the Tarim Craton, as it is the only block that has multiple reliable palaeomagnetic data from the  
1228 Neoproterozoic that act as a another line of evidence. We also note that Huang et al. (2019) recently  
1229 proposed a location outboard of Greenland for the Yili-Tianshan Block on the basis of similar detrital  
1230 zircon age spectra. However, more work would have to be done to determine whether this Tonian position  
1231 is consistent with the kinematic evolution necessary for these blocks to fit their Palaeozoic constraints.

1232  
1233 Early Tonian age (1000–900 Ma) magmatism and high-pressure metamorphism is preserved in the  
1234 basements of the Qilian-Qaidam (Qi-Qa), Kunlun and Tianshan-Chu Yili terranes (Song et al., 2012;  
1235 Tung et al., 2007; Wu et al., 2017). Importantly Song et al. (2012) identified an early Tonian event  
1236 preserved in a high-pressure metamorphic belt in Qi-Qa. Here, a ~200 km linear belt of granitic gneisses,  
1237 metamorphosed in the Palaeozoic, have crystallisation ages between ca. 1000 and 900 Ma (Song et al.,  
1238 2012). Zircons recovered from pelitic and psammitic gneisses from the same belt possess multiple  
1239 generations of growth, as suggested through cathodoluminescence imaging, and return ages of the (first  
1240 generation) to between ca. 940 and 900 Ma (Song et al., 2012). These are interpreted to represent a period  
1241 of granulite facies metamorphism from a continental arc indicating that subduction was active during the  
1242 Early Tonian (Song et al., 2012). Song et al. (2012) and others (e.g. Zhang et al., 2008) suggested a link  
1243 between these two blocks and South China on the basis of similar-aged magmatism and metamorphism.  
1244 However, as the Qi-Qa preserves a different Palaeozoic tectonic history to South China, as opposed to  
1245 fragments of older lithosphere preserved in the Panxi-Hannan Belt of the Yangtze Craton, we suggest that  
1246 a subduction zone was located outboard of Qi-Qa while a secondary, smaller ocean was closing between  
1247 Qi-Qa and the accretionary orogen of the Panxi-Hannan Belt (Fig. 11a–c). Upon the suturing of Yangtze  
1248 with Cathaysia (ca. 900 Ma, Fig. 11b), subduction relocated outboard of South China and began to close  
1249 the ocean between Qa-Qi and South China. Similar to the Qi-Qa, the Kunlun terrane preserves scattered  
1250 magmatic ages of S-type granites and protoliths of orthogneiss and amphibolites ranging between ca.  
1251 1000 and 900 Ma (Chen et al., 2008; He et al., 2018; and Chen et al., 2006a; 2006b—both cited in Chen  
1252 et al., 2008; He et al., 2018). We interpret these rocks and ages as an extension of the same subduction  
1253 zones outboard of Qi-Qa, and extend it further to the south where (again) similar-aged magmatism is also  
1254 preserved in the North Tianshan and Chu-Yili (Degtyarev et al., 2017).

1255

1256 The Kazakh terranes (including Krygyz Tianshan and Chu-Yili, Fig. 15a) have poorly constrained  
1257 Neoproterozoic histories, with only a handful of ages from outcropping magmatic rocks and sedimentary  
1258 successions. We predominantly follow the summary of Degtyarev et al. (2017) in offering a possible  
1259 tectonic interpretation of their Neoproterozoic geological history that is linked to the wider globe.  
1260 Degtyarev et al. (2017) note that there are two broad categories of Precambrian terranes preserved in the  
1261 Krygyz-Tianshan-Yuli area; the Issedonian and Ulutau-Moyunkum terranes. The Issedonian terranes,  
1262 preserved in the northeast of the western Central Asian Orogenic Belt, include Chu-Yili and the Chinese  
1263 Central Tianshan and are characterised by late Mesoproterozoic magmatism (e.g. Degtyarev et al., 2011),  
1264 thick (> 1000 m) 1050–950 Ma quartzite-schist successions followed by ongoing magmatism from ca.  
1265 960–890 Ma (e.g. Degtyarev et al., 2008; Gao et al., 2015; Huang et al., 2015). Comparably, the Ulutau-  
1266 Moyunkum terranes are preserved only in the west (in Krygyz) within Krygyz Middle Tianshan and  
1267 Krygyz North Tianshan (e.g. Fig. 10b), and consist of a Palaeoproterozoic basement, with predominantly  
1268 sedimentary Mesoproterozoic and early Neoproterozoic rocks (Degtyarev et al., 2017). Magmatism,  
1269 between 840 and 760 Ma (Kröner et al., 2012) and granulite facies metamorphism from 800–760 Ma  
1270 (Degtyarev et al., 2017; Tretyakov et al., 2016) are recorded only in the late Tonian. Both sets of terranes  
1271 preserve distinct differences in their Mesoproterozoic histories, minor differences in the Early  
1272 Neoproterozoic histories but similar histories from the mid-Neoproterozoic (ca. 700 Ma) onwards,  
1273 suggesting proximity sometime during the late Tonian (800 to 700 Ma?) (Degtyarev et al., 2017). We  
1274 interpret the Issedonian terranes to be the southernmost extent of the subduction zone spanning Qi-Qa and  
1275 Eastern Kunlun, as the magmatism preserved in the Issedonian terranes has a continental arc signature  
1276 (Huang et al., 2014) and is broadly coeval. Comparably, the Ulutau-Moyunkum terranes, which share  
1277 Mesoproterozoic similarities to Tarim and record no magmatism in the early Neoproterozoic, are located  
1278 on the opposite side (lower plate) of a closing ocean basin. This culminates with the collision of Tarim  
1279 (with the Ulutau-Moyunkum terranes) and the combined India-South China continent at ca. 800–760 Ma  
1280 along the Issedonian margin (Fig. 11d, e). The sparse data and age constraints from these terranes means  
1281 much of their Neoproterozoic history is conjectural. Although the specific orientation and positioning of  
1282 the terranes along the margin is speculative our interpretation is that it places the Kazakh terranes in a  
1283 favourable position for their Palaeozoic evolution which is, comparably, much better constrained.

1284

1285 Two clusters of Neoproterozoic-aged palaeomagnetic data from Tarim make it difficult to elucidate a  
1286 consistent position with other palaeomagnetic data from Rodinian constituents. Three poles from the  
1287 Tonian and Cryogenian require a 90° rotation of Tarim in order to fit the younger pole of Wen et al.  
1288 (2017), or a 180° rotation to fit the cluster of three poles in the Ediacaran to Cambrian (see Merdith et al.

1289 (2017a) and Section 4.2 for a discussion). Within a self-consistent kinematic plate boundary framework,  
1290 this motion is not permissible if Tarim is positioned either against north-western Australia (e.g. Zhang et  
1291 al., 2012) or as an extension of the ‘Missing-Link’ model (Li et al., 2004 for the original proposal of the  
1292 “Missing-Link” model; Wen et al., 2018, 2017). A plausible position where these palaeomagnetic criteria  
1293 are met, along with satisfying key geological evidence, such as the 800–760 Ma Aksu Blueschist  
1294 preserved on the northern margin of Tarim(C.-L. Zhang et al., 2013), is outboard of the India-South China  
1295 accretionary belt, where it acts as the final piece of continental lithosphere accreted to the margin. In our  
1296 model, we suggest the metamorphism recorded by the Aksu Blueschist marks the accretion of Tarim to  
1297 Chu-Yili and the Tianshan (see Xia et al. (2017) for the most recent discussion, but see also data and  
1298 discussion from Zhang et al. (2012, 2009). To accommodate the change in position suggested by the  
1299 palaeomagnetic data, we introduce a  $\sim 120^\circ$  rotation of Tarim and Southern Tianshan away from this  
1300 margin, such that Tarim’s southern margin collides with the outboard margin of Alxa-Qaidam-Qilian, so  
1301 its northern margin faces an open ocean basin, allowing it to rift northward facing as Gondwana forms  
1302 towards its more well constrained Palaeozoic position (Fig. 16).

1303

1304 To support this interpretation of Tarim’s evolution we present the following geological observations in  
1305 support of this model. Firstly, there is an absence of extensive magmatism on either the northern or  
1306 southern margin of the Tarim craton between 1000 and 850 Ma, which makes it difficult to include as a  
1307 part of the upper-plate circum-Rodinian subduction girdle (Cawood et al., 2016). Previous studies,  
1308 including MER17, place Tarim on the margin of Rodinia typically also include the Chu Yili and Tianshan  
1309 crust attached in a quasi-present-day configuration to the northern margin of Tarim. In such cases their  
1310 record of Tonian magmatism supports the interpretation that they formed part of the circum-Rodinian  
1311 subduction girdle (Ge et al., 2014) however, this location is inconsistent with available palaeomagnetic  
1312 data (e.g. (Wen et al., 2018). Secondly, rift related granitoids preserved in the Southern Tianshan  
1313 (Degtyarev et al., 2017; Gao et al., 2015) are here interpreted as evidence of the re-adjustment of Tarim  
1314 between 730 and 680 Ma to account for the change in palaeolatitude and orientation inferred from  
1315 palaeomagnetic data (Fig. 11e). In addition, extensive rifting in the southwest of Tarim (Wang et al.,  
1316 2015) is interpreted to reflect the rearrangement of subduction after Tarim/India-South China  
1317 amalgamation. This motion is similar to the adjustment of Baltica relative to Laurentia in the latest  
1318 Mesoproterozoic proposed by Cawood et al. (2010) to account for the Valhalla Orogeny. Xiao et al.  
1319 (2010) summarise the geology and geochronology of rocks found in the Beishan area of China which  
1320 record a protracted and complex history of multiple arc development and accretion through the late  
1321 Neoproterozoic and Early Palaeozoic. Rocks in the Beishan area (Alxa, Fig. 15, 16) range from low-grade  
1322 sedimentary metamorphic assemblages to gneiss and eclogite complexes and intrusive granitic bodies that



1323 have late Neoproterozoic–Cambrian ages (Xiao et al., 2010). These rocks, inferred to represent an active  
1324 subduction zone and accretionary complex, are unconformably overlain by Cambrian–Ordovician  
1325 sediments. The earliest record of metamorphism in the area are from a series of SHRIMP U-Pb ages taken  
1326 from the metamorphic rims of zircons of an eclogite unit at ca. 830–800 Ma (Yang et al., 2006).

1327

1328 With respect to the palaeomagnetic issues of Tarim we raised earlier (Section 4.2), we find that our  
1329 conceptual model of this rotation of Tarim (e.g. Fig. 16) can fit either set of palaeomagnetic data equally  
1330 as well, with the key factor being the time of subduction in the Beishan area. Under the cluster of three  
1331 poles, the motion of Tarim occurs more quickly and peak subduction (possibly resulting in a collision?)  
1332 would be earlier (ca. 650 Ma), while to fit the pole of Wen et al. (2017) it would occur later at between  
1333 600 and 550 Ma. Based on the review of Xiao et al. (2010), we infer that the geological data support the  
1334 later interpretation more strongly however, given the novelty of this scenario and the absence of  
1335 identifiable piercing points, it could be revised in the future to fit the alternative scenario.

1336

1337 Late Neoproterozoic–Early Cambrian rifting events are inferred to have occurred within all the terranes  
1338 (Kunlun, Qa-Qi, Chu Yili and Tianshan) that we have placed on this Indian-South Chinese accretionary  
1339 margin, however, the high degree of reworking and suturing of crust from the terranes, coupled with the  
1340 small size of these terranes makes it difficult to pin down precise rift times. We stress that our  
1341 interpretation here is preliminary, especially when compared to specialised reviews of the tectonics of this  
1342 area (Kroner et al., 2007; Wilhem et al., 2012; Windley et al., 2007; Xiao et al., 2013; Yakubchuk, 2017).  
1343 We reiterate that our intention here is to provide a possible framework that connects and contextualises  
1344 these terranes within a consistent kinematic and tectonic evolution between the Neoproterozoic and  
1345 Palaeozoic (Fig. 16), which can be more tightly refined in the future. Ordovician–Silurian sutures  
1346 between Qa-Qi-Kunlun and surrounding cratons preserve late Neoproterozoic–Cambrian ophiolites (Jian  
1347 et al., 2014; Shi et al., 2018; Song et al., 2013, 2009) thus necessitating the existence of ocean basins, but  
1348 there are few dates of ocean basin initiation. Xu et al. (2015) date Qilian-Qaidam continental rift basalts  
1349 to 600–580 Ma, constraining ocean basin formation to the latest Ediacaran–earliest Cambrian, with the  
1350 oldest ophiolite (the Yushigou Ophiolite) preserved in these terranes dated to 550 Ma (Shi et al., 2004).  
1351 Evidence of rifting is more sparse in Kunlun, however, similar stratigraphy, ages and geochemistry of  
1352 metavolcanic deposits between Kunlun and Qaidam-Qilian (Yuan et al., 2004) suggest coeval rifting is  
1353 reasonable, though not definite. We follow some recent work (Peng et al., 2019; Zhao et al., 2018) in  
1354 having separation of Tarim and these terranes in the late Ediacaran (550 Ma here, as a response to the  
1355 closure of the Mozambique Ocean between India and Congo). Our model closely resembles the schematic  
1356 framework outlined by Qiantao et al. (2001), while also following Domeier (2018) in maintaining a very

1357 close affinity between Kunlun, Q-Q and Alxa for the Early Palaeozoic, such that they conceptually form a  
1358 single elongated terrane that rifts off Gondwana at ca. 550 Ma and collides along the southern margin of  
1359 Tarim by 440 Ma.

1360

1361 Comparably, rifting on the northern margin of Tarim is easier to constrain. Thick, late Neoproterozoic  
1362 sedimentary sequences capped with carbonate and an unconformity on the Ediacaran–Early Cambrian  
1363 imply a prolonged rift phase with breakup at ca. 550–540 Ma (Zhao et al., 2014; Zhu et al., 2017).  
1364 Similarly, sedimentary assemblages preserved in the South Tianshan orogen are dated from 540–520 Ma  
1365 (Alexeiev et al., 2020; Safonova et al., 2016), suggesting that ocean basin formation between Tarim and  
1366 Krygyz Middle Tianshan begins in the Early–Middle Cambrian. Further north, the relationship between  
1367 the Kryguz North Tianshan and Chu-Yili is also reasonably well established (e.g. Windley et al., 2007;  
1368 Xiao et al., 2013). Late Ediacaran–Early Cambrian magmatism preserved in Chu-Yili and North Tianshan  
1369 (Alexeiev et al., 2011; Degtyarev et al., 2017; Kroner et al., 2007) is interpreted to represent development  
1370 of multiple contemporaneous arcs (e.g. Alexeiev et al., 2020). The Ordovician-aged sutures between Chu-  
1371 Yili and North and Central Tianshan (Windley et al., 2007) are defined by ophiolitic slithers, implying an  
1372 ocean basin (or a back-arc) existed between these terranes. We infer that in the late Neoproterozoic to  
1373 Early Cambrian, the Kazakh and Tianshan terranes that accreted outboard of India-South China were  
1374 fragmented and rifted off this margin forming a collage (not dissimilar to modern southeast Asia, or the  
1375 NE Pacific in the Mesozoic, e.g. Sigloch and Mihalynuk (2013) that eventually re-assembled in the  
1376 Ordovician. We model the time of fragmentation at 550 Ma, because this is the time of collision between  
1377 India and Congo along the East African Orogen, so we infer that subduction relocated outboard of the  
1378 northern margin.

1379

1380 Palaeomagnetic data from South China do not permit a fixed fit between South China and Gondwana for  
1381 the early Palaeozoic. The data do, however, permit a close spatial relationship between them (<1000 km).  
1382 Palaeomagnetic data from South China suggest it moved from mid to lower latitudes between the  
1383 Cambrian and Devonian (Domeier, 2018; Han et al., 2015). Furthermore, shallow marine faunal data and  
1384 detrital zircon arrays suggest that between the Cambrian and Devonian, South China shifted from an  
1385 Indian-Himalayan-Iran affinity (Burrett et al., 1990) to Sibumasu-Australian affinity (Cocks and Fortey,  
1386 1997; Metcalfe, 2013, 2011), broadly consistent of the positions necessary to fit the palaeomagnetic data.  
1387 Rift sequences in South China and in northern India (Himalayan terranes) are similar, but diverge strongly  
1388 after the early Cambrian (Jiang et al., 2003), providing some kinematic support for invoking for relative  
1389 motion between South China and Gondwana. The Sanya Block of Hainan Island (Fig. 15f) is linked  
1390 through detrital zircon provenance and middle Cambrian trilobites to western Australia and Antarctica

1391 rather than South China in the Neoproterozoic (Cawood et al., 2018b; Xu et al., 2014). The presence of  
1392 Early Ordovician trilobites in the Sanya block also common to South China and Australia (Torsvik and  
1393 Cocks, 2009) support a close relationship between the three domains by this time (Cawood et al., 2018b).  
1394 A late Cambrian–Ordovician (520–450 Ma) metabasaltic arc assemblage in Hainan Island (Xu et al.,  
1395 2008, 2007) is interpreted to be the northerly extension of the Kunguan Orogen that sutured Australia-  
1396 Antarctica and India (e.g. Xu et al., 2014). We introduce divergent motion between Gondwana and South  
1397 China at 550 Ma, coinciding with the rift-to-drift sequences of Jiang et al. (2003). This divergent motion  
1398 moves South China from a position outboard of Northern India at 550 Ma to one that is slightly further  
1399 east and adjacent to western Australia at 500 Ma, accounting for the arc assemblage in Hainan as well as  
1400 similar faunal patterns.

1401

#### 1402 5.4.3 ANS-Azania-TOAST

1403 We suggest that, to a first order, the central Arabian-Nubian Shield (ANS) accreted on the kernel of  
1404 Azania and formed a semi-continuous archipelago outboard of the eastern margins of the Congo Craton  
1405 and Sahara Metacraton (SM) (Fig. 17; Collins and Pisarevsky, 2005; Merdith et al., 2017a). Geological  
1406 details and a regional plate model of the accretion of the ANS and Azania are adopted from Collins et al.  
1407 (in revision), Blades et al. (2019a) and Johnson et al. (2011), though here we extend Azania to the south  
1408 by attaching portions of the Tonian Aged Ocean Arc Super Terrane (TOAST—Jacobs et al. (2017,  
1409 2015)). The similarity in ages, petrology of rocks and  $\delta^{18}\text{O}$  from zircons between the Dabolava Suite in  
1410 Madagascar (Archibald et al., 2018) and TOAST (Jacobs et al., 2017, 2015; Wang et al., 2020) suggest a  
1411 similar tectonic environment. As the southern tip of Azania is reconstructed to be adjacent to the location  
1412 of the TOAST terrane in Gondwana, at the nexus between the East African Orogen and the  
1413 Pinjarra/Kuunga Orogen, there is also a strong palaeogeographic argument for attaching TOAST to  
1414 Azania, as their Rodinian reconstructed position requires no alteration for their position in Gondwana  
1415 (Fig. 17b).

1416

#### 1417 5.4.4 Hoggar, Borborema, Avalonia and Ganderia

1418 The Hoggar Block is preserved between the Sahara Metacraton (SM) and the West African Craton  
1419 (WAC) in northwest Africa and records a long Neoproterozoic history of accretion of island arcs and  
1420 continental ribbons. The model incorporated here is based on fieldwork by Cabby et al. (1989), Black et al.  
1421 (1994) and Liégeois et al. (1994) and involves three main constituents of present-day Hoggar (from west  
1422 to east): IOGU-IGU, LATEA and the Air Block (Fig. 18a, b).

1423

1424 The broad tectonic framework of the Hoggar block is an accretionary margin consisting of at least 23  
1425 individual terranes that were slowly compressed between two large tectonic units—the WAC and the  
1426 SM—as Gondwana amalgamated. The Air block, preserved in the east, is an amalgamation of three  
1427 closely related terranes: the Aouzegueur, Barghot and Assodé-Issalane terranes. The first two terranes  
1428 accreted onto the margin of the SM by 650 Ma, with the Aouzegueur terrane preserving a tonalite-  
1429 trondhjemite-granodiorite (TTG) suite dated at ca. 730 Ma and the Barghot terrane recording calc-alkaline  
1430 granitoids from ca. 730 to 660 Ma, with a post nappe pluton preserving a U-Pb zircon age of  $664\pm 8$  Ma,  
1431 interpreted to provide a minimum age for deformation (Liégeois et al., 1994). Both these terranes were  
1432 metamorphosed to greenschist or amphibolite facies and were cut by east-verging thrusts. In contrast, the  
1433 Assodé-Issalane terranes exhibit younger magmatism (ca. 640–580 Ma) and amphibolite-facies  
1434 metamorphism. They are thrust east over the Barghot terrane. Both Black et al. (1994) and Liégeois et al.  
1435 (1994) suggest that the Aouzegueur terrane collided first with the SM, followed by the Barghot terrane,  
1436 which is positioned slightly further south than the former, through an east-dipping subduction zone  
1437 underneath the two terranes (Fig. 18). Following collision, the Assodé-Issalane terrane (which until this  
1438 time we position slightly west of the former terranes) was thrust above of the Barghot terrane in response  
1439 to the closure of the ocean between the WAC and the SM. Our reconstruction implies that this motion  
1440 was predominantly transpressive, along the dextral Raghane shear zone with plutons dating from ca. 630  
1441 to 580 Ma (Liégeois et al., 1994).

1442  
1443 Further west from the Air block in central Hoggar, the LATEA terranes (Laouni, Azrou-n-Fad, Tefedest  
1444 and Egéré-Aleksod) all consist of Archaean to Palaeoproterozoic basement, but preserve no  
1445 Mesoproterozoic or early Neoproterozoic rocks. LATEA was a passive cratonic unit for most of the  
1446 Neoproterozoic and acted as a nucleus for the accretion of juvenile terranes. The earliest Neoproterozoic  
1447 activity is the accretion of the ca. 900 Ma juvenile Iskel island arc to the western margin of LATEA, with  
1448 subduction inferred to be west dipping away from LATEA (Liégeois et al., 2003). The protolith of an  
1449 eclogitic unit, currently preserved along the shear zone delineating the Iskel arc and LATEA, is dated to  
1450 ca. 870 to 850 Ma by U-Pb dating from zircons extracted from syn-to-late kinematic plutons (Caby et al.,  
1451 1982). The combined In-Ouzzal and Iforas granulite units (IOGU/UGI), which are Palaeoproterozoic  
1452 continental ribbons, preserve few Tonian rocks. From ca. 700 to 640 Ma magmatism is recorded  
1453 throughout the entire region, suggesting that subduction occurred along both margins of the terranes  
1454 (Caby, 2003) (Fig. 18d, e). At 630 Ma, collision between the IOGU/UGI terranes and the LATEA block  
1455 occurred, forming the combined present-day central-western Hoggar region.

1456

1457 The final tectonic events of this area involve a two-step amalgamation process of Western and Central  
1458 Hoggar (i.e. IOGU/UGI and LATEA) to the Air Shield and SM, and the collision between this landmass  
1459 (Hoggar and the SM) and the WAC, where collisional deformation is preserved in the Pharusian and  
1460 Dahoymede belts (Merdith et al., 2017a) (Fig. 18f, g). Here, subduction is inferred to have occurred away  
1461 from the WAC (i.e. underneath Hoggar) due to the absence of magmatic rocks preserved on the WAC.  
1462 Continual dextral deformation is preserved throughout Hoggar until ca. 530 Ma, suggesting that there was  
1463 still relative motion until the Cambrian (Liégeois et al., 2003; Paquette et al., 1998). The major regime of  
1464 the Hoggar block between the Ediacaran and early Cambrian was transpressive, resulting in extensive  
1465 faulting and upwelling of the asthenosphere; causing partial melting of lower Archaean crust in some  
1466 areas (Hadj-Kaddour et al., 1998). We interpret the final amalgamation of Hoggar to occur at ca. 580 Ma,  
1467 as this is the age of the syntectonic, deformed plutons found among the shear zones that bind the SM and  
1468 the WAC. Here, a suite of ages include: Rb-Sr whole rock ages from dykes affected by the transpressive  
1469 event yield an age of  $592\pm 6$  Ma (Hadj-Kaddour et al., 1998); a  $583\pm 7$  Ma U-Pb age on zircons extracted  
1470 from the syn-to-late tectonic, elongated Imezzarene pluton (Lapique et al., 1986); a  $594\pm 4$  Ma and  
1471  $593\pm 17$  Ma U-Pb age of zircon extracted from the Ohergehém and Adaf plutons, respectively (Henry et  
1472 al., 2009). Fezaa et al. (2010) identified younger (ca. 575–555 Ma) deformation in the Murzoq area of  
1473 Hoggar, however, they suggested that it was unrelated to the main convergence between WAC and SM.

1474

1475 The Borborema block sits between Congo-SF and the Nigeria-Benin Shield in a reconstructed Gondwana  
1476 (Fig. 18a). This small block consists of Archaean–Proterozoic basement that was strongly reworked and  
1477 deformed during the Gondwana amalgamation events between Africa and Amazonia (dos Santos et al.,  
1478 2010). Magmatism in the Transversal Domain of Central Borborema is thought to represent a local, early  
1479 Tonian orogeny called the Cariri Velhos Orogeny (da Silva Filho et al., 2002; dos Santos et al., 2010).  
1480 Late Stenian rift deposits are preserved in the Cariri Velhos belt, suggesting that the Pernambuco-Alagoas  
1481 domain (PEAL) (the crystalline basement of Southern Borborema) originally rifted from this margin  
1482 (Guimarães et al., 2012), before the ocean inverted and closed. Our model places the Northern and  
1483 Transversal Domains of Borborema fixed to the Nigeria-Benin-SM blocks, while the PEAL closed the  
1484 small Stenian aged relict ocean basin as it collided with the northern and central Borborema provinces by  
1485 ca. 920 Ma (Caxito et al., 2014a), forming the Cariri Velhos Orogen. An ocean basin remained on the  
1486 southern margin of PEAL until the Ediacaran, as the final collision between Borborema and SF did not  
1487 occur until this time forming the Sergipano belt, which preserves relict oceanic crust (e.g. Caxito et al.,  
1488 2014b; Ganade de Araujo et al., 2014) (e.g. Fig. 9). To accommodate the Tonian closure, while  
1489 maintaining an open ocean basin to the south of PEAL, we follow Caxito et al. (2014a, 2016) who  
1490 suggested that the synchronous rifting and aulacogen formation preserved in SF (Pedrosa-Soares et al.,

1491 2001), which in our model is reconstructed to be adjacent to PEAL, are relicts of the divergent motion  
1492 necessary to achieve this.

1493

1494 The Avalonian terranes, currently preserved in the east coast of modern day North American and western  
1495 Europe, have a well-documented Neoproterozoic history (e.g. Murphy and Nance, 1989). The Avalonian  
1496 terrane is interpreted to be underlain by ca. 1.0 Ga juvenile basement on the basis of 1.3–0.8 Ga Sm-Nd  
1497 depleted mantle model ages in in younger Neoproterozoic rocks (Murphy et al., 2000; Thorogood, 1990).  
1498 These younger rocks consist of magmatic gneiss and plutonic complexes, along with tuffs, pelitic schists  
1499 and quartzites. U-Pb ages of the complexes and tuffs range from ca. 750–650 Ma (Bevier et al., 1993;  
1500 Doig et al., 1993; Keppie and Dostal, 1998; Krogh et al., 1988; O’Brien et al., 2001) and detrital zircons  
1501 from the (meta-)sedimentary rocks suggest they were sourced from a juvenile arc (metapelites, Murphy,  
1502 2002) and a cratonic source (quartzite), typically inferred to be Amazonia or the WAC (Nance et al.,  
1503 2008). This magmatism is followed by amphibolite–granulite metamorphism from 660–630 Ma (Keppie  
1504 et al., 1998; Strachan et al., 2007). Younger magmatism (ca. 640–550 Ma) is more voluminous and  
1505 includes abundant arc derived volcanic, plutonic complexes and coeval volcanic-sedimentary successions  
1506 (Bevier et al., 1993; Compston et al., 2002; Doig et al., 1993; Nance et al., 2008; O’Brien et al., 2001;  
1507 White et al., 2020). Subduction does not continue into the Cambrian, instead a clastic platform and  
1508 transition to rift environment begins to form, culminating in the opening of the Rheic Ocean (Domeier,  
1509 2016; Nance et al., 2008; Nance and Linnemann, 2008).

1510

1511 To a first order, Ganderia and Carolina, both preserved in North America, record a similar Neoproterozoic  
1512 history to Avalonia, differing predominantly in that key metamorphic and magmatic events are ca. 30–  
1513 40 Ma younger than in Avalonia (Hibbard et al., 2007; Nance et al., 2008; van Staal et al., 2012).  
1514 Depleted mantle model ages from Sm-Nd isotopes also hint at the presence of ca. 1.2–0.8 Ga juvenile  
1515 crust in Carolina (Hibbard et al., 2007). However, the principal period of magmatism in both Ganderia  
1516 and Carolina is preserved from 650 to 580 Ma and is inferred to have occurred in an ocean-arc  
1517 environment (Hibbard et al., 2007). Metamorphism, up to eclogite facies, occurs at the end of this period  
1518 and continues into the earliest Cambrian (580–540 Ma) (Barker et al., 1998; Shervais et al., 2003).  
1519 Younger magmatism (to ca. 520 Ma, White et al., 2002) linked to the rifting and opening of the Rheic  
1520 Ocean, is only preserved in Ganderia (Hibbard et al., 2007). Finally, the Suwannee terrane of Florida is  
1521 linked tectonically to both the West African Craton and Amazonia throughout the Neoproterozoic  
1522 (Dallmeyer, 1989), lacking the Neoproterozoic arc development preserved in Avalonia, Ganderia and  
1523 Carolina. Instead, 550 Ma calc-alkaline volcanic rocks are inferred to represent the remnants of a  
1524 continental arc (Heatherington et al., 1996).

1525

1526 We follow the model of Nance et al. (2008) and Murphy et al. (2004) for the Neoproterozoic evolution of  
1527 these terranes. An early Tonian (1–0.8 Ga) oceanic arc outboard of Baltica-Ama-zonia-WAC dipping  
1528 under the Rodinian plate, formed the earliest portions of crust preserved in these terranes (Fig. 18c–e).  
1529 The relative positioning of the terranes follows that of DOM16, with East Avalonia most easterly (Fig.  
1530 18b), then West Avalonia, and Ganderia and Carolina furthest west, with Ganderia sitting oceanward of  
1531 Carolina. This arrangement follows the same logic outlined in Section 5.2.2, as by maintaining this  
1532 relative positioning we avoid having to laterally re-organise the terranes during the Palaeozoic. This is  
1533 slightly different from the positioning in Nance et al. (2008), who model West Avalonia more easterly  
1534 (relative to a fixed WAC) than East Avalonia and invoke wrench-tectonics to laterally translate the  
1535 terranes. Nonetheless, at ca. 750 Ma this subduction polarity reversed and the adjacent ocean basin  
1536 between WAC-Baltica began to subduct underneath Avalonia. We model Ganderia and Carolina slightly  
1537 further away from the active subduction front—behind Western Avalonia, to account for their lack of  
1538 Cryogenian magmatism. This arc front collided with WAC at ca. 650 Ma when the subduction ceased and  
1539 reset outboard of the now amalgamated Avalonian-WAC continent as a continental arc (Fig. 18f, g). This  
1540 subduction continued until the Cambrian when the area transitioned into a rift environment when the  
1541 Rheic Ocean opened.

1542

1543 This last phase our model is preliminary and needs further development, though we hope that it provides a  
1544 framework that can assist with testing alternative scenarios. By fitting the latitude of the ca. 520–500 Ma  
1545 poles of Baltica (Section 5.2.1), subduction must consume most of the relic ocean basin immediately  
1546 north of the Avalonian margin of Gondwana between 550 and 520 Ma. The magmatism in Ganderia  
1547 easily accounts for this, however Baltica needs to be further east at 520 Ma, otherwise it must undergo  
1548 4000 km of dextral motion (relative to Gondwana) to allow for the initial stages of the Rheic Ocean  
1549 opening at ca 500 Ma (e.g. Domeier, 2016; von Raumer and Stampfli, 2008), which we suggest is not a  
1550 reasonable scenario. As such, our model places a subduction zone slightly outboard of Avalonia, but  
1551 acknowledge that this is a simplification that needs further refinement.

1552

## 1553 **6 Plate Model**

1554

1555 Having discussed the motions of the evolution of continental configurations in previous sections, here we  
1556 discuss the more speculative elements of the reconstruction—the oceanic plates and plate boundaries. For  
1557 further in-depth discussion of the continental portions of the model, in particular the major Gondwana  
1558 forming sutures and evolution of the post-Cambrian world, we point readers to the studies that produced

1559 the base models used here (MER17, DOM16/18, YOU19, DT14). We also provide in our supplementary  
1560 material the associated plate model files (SM2), as well we a tectonic summary of seafloor production and  
1561 consumption rates, mid-ocean ridge length and subduction zone length (SM3).

1562

## 1563 **6.1 Synthetic ocean plates**

1564

1565 The construction of synthetic ocean plates is required to maintain tectonic congruency (Section 2.7) but,  
1566 with few exceptions (e.g. ophiolites), there is no direct evidence of the configuration or tectonic  
1567 parameters (e.g. spreading rate, asymmetry) of oceanic crust for the pre-Mesozoic due to the constant  
1568 subduction of oceanic lithosphere. However, we know that oceanic crust typical of present-day (i.e.  
1569 MORB) did exist in the Palaeozoic and Neoproterozoic, as evidenced by ophiolitic remains preserved in  
1570 orogens (Furnes et al., 2014). We therefore use one key assumption when constructing oceanic plates: we  
1571 assume that the production (rate of motion, orthogonal spreading etc.) and subduction of oceanic crust in  
1572 the Neoproterozoic was fundamentally similar to the Cenozoic. We note that this may not be a valid  
1573 assumption for the early Neoproterozoic, since abundant ophiolite preservation only occurs after Rodinia  
1574 breakup (Stern and Miller, 2018) and pre-1 Ga ophiolites suggest thicker oceanic crust (Moores, 2002)  
1575 which, along with secular changes in Earth's heat loss (Brown et al., 2020b) could have an influence on  
1576 spreading and subduction dynamics. Nonetheless, we maintain that if available palaeomagnetic and  
1577 geological data can be reconciled within a uniformitarian framework of oceanic crust production and  
1578 destruction, then our model becomes a useful reference model for future models that explore alternative  
1579 hypotheses. Measurements of seafloor production, crustal consumption, ridge length and subduction zone  
1580 length are provided in the supplementary material.

1581

### 1582 *6.1.1 Early Tonian until Rodinia breakup (1000-750 Ma)*

1583

1584 In our model, three prominent ocean basins existed in the early Tonian: the Mirovoi Ocean (McMenamin  
1585 et al., 1990; Meert and Lieberman, 2008), the Mawson Sea (Meert, 2003; Meert and Lieberman, 2008)  
1586 and the Mozambique Ocean (Fig. 8) (Collins et al., 2003; Collins and Pisarevsky, 2005). These ocean  
1587 basins have been defined previously in the same context as they appear in our model, however, given  
1588 differences between our model and the original publications, the geographical boundaries of each ocean  
1589 are slightly different.

1590

1591 We define the Mirovoi Ocean as the large ocean bordering Rodinia in its west and India-South China and  
1592 the Sahara Metacraton in the north east and south east respectively. The Mirovoi is the largest and most



1593 prominent ocean basin for the Neoproterozoic in our model, existing until ca. 520 Ma with the opening of  
1594 the Proto-Tethyan Ocean and Ran Sea (Fig. 9, Hartz and Torsvik, 2002). It is (conceptually) equivalent to  
1595 the external Panthalassic and Pacific oceans of the Phanerozoic, as it consists almost entirely of oceanic  
1596 lithosphere and is ringed by subduction for the majority of its existence. At 1000 Ma, we model a triple  
1597 junction spreading ridge located roughly in the centre of the ocean basin. The triple junction provides  
1598 three directions of spreading to account for convergence in three areas: (i) the closure of the ocean basin  
1599 separating India-South China from Tarim, Qaidam-Qilian, Lut, Afghanistan, Kunlun and Tarim (*this*  
1600 *study*); (ii) the Taimyr subduction zone outboard of *northern* Siberia (Metelkin et al., 2012; Vernikovskiy  
1601 et al., 2004) and the Valhalla Orogen outboard of Greenland (Cawood et al., 2010), and; (iii) the Proto-  
1602 Avalonian-Cadomian subduction zone outboard of Baltica and Amazonia (Murphy et al., 2000) that  
1603 extends northwards to Sao Francisco and further north where it is preserved in the Iskel Island Arc of  
1604 Hoggar (Liégeois et al., 2003).

1605  
1606 The spreading arms of the triple junction span north, east-southeast and southwest. The northern arm  
1607 separates Siberia and the India-China accretionary zone and extends partway into the Mawson Sea. The  
1608 east-southeastern arm extends towards India, where we connect it via a transform fault to the mid-ocean  
1609 ridge in the Mozambique Ocean. The southwestern arm intersects the Proto-Avalonian subduction zone.  
1610 We model this configuration (triple junction) as being stable through the early Tonian until ca. 870–850  
1611 Ma, where a plate-reorganisation event occurs. We link this organisation to a change in kinematics of  
1612 Rodinia, suggested through palaeomagnetic data. At this time, palaeomagnetic data from the Baltica  
1613 (Walderhaug et al., 2007) suggest that Rodinia had drifted to southerly latitudes, before returning to  
1614 equatorial latitudes by ca. 750 Ma (Eyster et al., 2019). MER17 modelled significant relative dextral  
1615 motion between Congo-SF-Azania and Rodinia during this time (870–750 Ma) as well, as suggested by  
1616 palaeomagnetic data (Evans et al., 2016). Geological data from Congo-Azania also supports the rotation,  
1617 with onset of sedimentation interpreted to be a rift event in the Damara region (Armstrong et al., 2005;  
1618 McGee et al., 2012) and the onset of a massive subduction system outboard of Azania (Archibald et al.,  
1619 2017; Handke et al., 1999). During this transition (850–800 Ma), we model the Mirovoi Ocean as a single  
1620 spreading ridge, orientated sub-parallel to the *north*-facing arm in the original triple junction, extending  
1621 northwards toward Siberia and intersecting an oceanic arc outboard of Baltica.

1622  
1623 For the Tonian, until 750 Ma, the South China-India continent moved to polar latitudes on the north-  
1624 eastern side of the Mirovoi Ocean basin. Comparably, Siberia started dextral motion relative to Rodinia,  
1625 from a position near Australia-North China to one near Greenland (Pisarevsky et al., 2013). To account  
1626 for this motion, alongside ongoing subduction in the Taimyr region of Siberia, we have extended the

1627 spreading ridge from the Mozambique Ocean into the Mirovoi Ocean (running E-W) and have a northern  
1628 arm accounting for divergence between Tarim and the Taimyr subduction zone. This interpretation  
1629 necessitates the presence of a triple junction, with a third ridge arm intersecting the subduction zone  
1630 outboard of Baltica, similar to the configuration at the start of the Tonian.

1631

1632 The Mawson Sea is defined as the ocean basin between Australia and India-South China that closed with  
1633 the amalgamation of Gondwana (Meert, 2003). In the early Tonian, this basin is large in our model,  
1634 necessitated by MER17s removal of India-South China from Rodinia. The large size is because relative  
1635 longitude prevents India-South China (at this point in time travelling north from the equator) from being  
1636 any closer to Australia, as Azania occupied the same latitude as India and lay between India and  
1637 Australia. We model a single spreading ridge in the centre of the ocean basin, accounting for the  
1638 subduction on the India-South China margin as suggested in the Eastern Ghats of India and accretion of  
1639 the Ruker Terrane to Indo-Antarctica (e.g. Corvino et al., 2008; Liu et al., 2017). In South China, this  
1640 subduction is more sparse, but recent work has suggested that part of present-day Vietnam is associated  
1641 with the southwestern Yangtze craton (Minh et al., 2020) and could record the late Tonian portion of a  
1642 subduction system and be the focus of future work. At 930 Ma the spreading direction of the ridge  
1643 changes, to compensate for the southerly drift of Rodinia. The change in spreading direction coincides  
1644 with the docking of North China-Australia-Antarctica with Laurentia as the final amalgamation event of  
1645 Rodinia (Mulder et al., 2018b). At this time we model subduction initiating outboard of Australia (against  
1646 Lhasa, (e.g. Guynn et al., 2006) and into the ocean outboard of Antarctica further *south*. Preserved  
1647 evidence of subduction here is sparse due to ice cover in Antarctica. However, this area of the ocean (just  
1648 outboard of the western margin of the Mawson craton) is positioned at the centre of Antarctica in the  
1649 nexus between the TOAST terrane and Mawson craton, so it could be possible some arcs are preserved in  
1650 Antarctica. Further south, this subduction zone transitions into a transform boundary and separates  
1651 relative motion between Azania-Congo and Rodinia between 930 Ma and 850 Ma. We model continual  
1652 spreading in the Mawson Sea until 850 Ma, at which time the ocean basin begins to close and we do not  
1653 model an active ridge. By 750 Ma the Mawson Sea is extremely narrow, with only 2500–3500 km of  
1654 ocean basin separating Australia and India. A narrow ocean basin is supported geologically by the strong  
1655 evidence suggesting that a large sinistral shear zone was present outboard of western Australia and  
1656 Antarctica during the Cryogenian and Ediacaran, suggesting that there was close proximity without  
1657 collision between Australia-Antarctica and another continent (Collins, 2003; Fitzsimons, 2003; Halpin et  
1658 al., 2017; Merdith et al., 2017b; Powell and Pisarevsky, 2002).

1659

1660 The Mozambique Ocean is described as the ocean that closed with the collision of India and Congo along  
1661 the East African Orogen reacted to Gondwana amalgamation during the Cryogenian and Ediacaran (e.g.  
1662 Collins and Pisarevsky, 2005). For the sake of continuity, we refer to this ocean as the Mozambique in the  
1663 Tonian as well. A small ocean (in our model, roughly equivalent in size to the Tasman Sea between  
1664 Australia and New Zealand), termed ‘Neomozambique Ocean’ also closed with the formation of the East  
1665 African Orogen, however this ocean was located between ANS-Azania-TOAST and Congo (Fig. 8).

1666

1667 Geographically, the location of the Mozambique ocean is difficult to determine in the early Tonian due to  
1668 overlapping latitudes between Azania and India (they are separated longitudinally by  $\sim 120^\circ$  in our  
1669 model). In our model there is no spreading in this ocean basin at this time, because Congo-Azania was  
1670 latitudinally stable while India-South China moves towards the North Pole on a different longitude,  
1671 accounted for by spreading in the Mirovoi Ocean. The spreading ridge in the Mawson Sea at ca. 900 Ma  
1672 extends sufficiently south so that the ocean lithosphere generated here is subducted during closure of the  
1673 Mozambique Ocean. We model active spreading in a clearly defined Mozambique Ocean beginning at  
1674 850 Ma, by which time India-South China had a similar longitude to Azania-Congo, making it easier to  
1675 delineate the geographical extent of the ocean distinct from the Mawson Sea. Between 820 and 750 Ma  
1676 the ocean basin closes rapidly, in order to fit palaeomagnetic constraints at 750 Ma that show India at  
1677  $\sim 60^\circ\text{N}$  (Gregory et al., 2009; Torsvik et al., 2001) and Congo at  $15^\circ\text{S}$  (Meert et al., 1995) (placing Azania  
1678 at the equator).

1679

1680 At 800 Ma, we model the birth of the Pacific/Panthalassic Ocean, here defined as the ocean basin  
1681 separating Laurentia from North China, Australia and Antarctica, which most likely opened as Rodinia  
1682 broke-up (although terrane migration across this ocean basin cannot be ruled out, e.g. Mulder et al.  
1683 (2020)). We note here that the pre-Mesozoic Pacific Ocean is already universally referred to as the  
1684 Panthalassic Ocean. Consequently, we refer to the ocean separating North China-Australia-Antarctica and  
1685 Laurentia between Rodinia and Gondwana times (ca. 800–520 Ma) as the proto-Pacific Ocean, the ocean  
1686 surrounding Gondwana as the Panthalassic Ocean (‘Panthalassa’, ca. 520–200 Ma) and the ocean that has  
1687 existed from 200 Ma to present-day as the Pacific Ocean, noting that all three of these oceans essentially  
1688 refer to the same ocean basin (in a geographical sense) that existed between North China-Australia-  
1689 Antarctica and Laurentia. From 800 to 720 Ma we have a single ridge system separating Australia-  
1690 Antarctica and Laurentia. This ridge produces a highly angular divergence, with spreading rates faster  
1691 towards northern Australia and Canada than in Antarctica, resulting in a wider ocean basin in the north  
1692 and narrower in the south. These variable spreading rates are required fit the ca. 750 Ma palaeomagnetic

1693 data, which require Australia to be ‘upright’ (same orientation as present-day) and perpendicular to  
1694 Laurentia (Wingate and Giddings, 2000).

1695

1696 *6.1.2 late Tonian–Cambrian (Rodinia breakup–Gondwana Assembly, 720–520 Ma)*

1697

1698 By 720 Ma, continental motions around the Mirovoi Ocean are latitudinally stable with no polar  
1699 excursions thus, the simplest way to account for the necessary subduction is with a stable triple junction.

1700 At this time, we show subduction along the western margin of the Mirovoi Ocean, outboard of Siberia in  
1701 the Taimyr region, as well further south outboard of the WAC and Baltica where the Avalonian and

1702 Cadomian terranes were coalescing (Murphy et al., 1999; Murphy and Nance, 1989) and along the  
1703 *northern* margin of the Sahara Metacraton in the east. This latter subduction zone is speculative since

1704 there are no known rocks of this age in the Sahara Metacraton (Blades et al., submitted). The Mirovoi  
1705 ocean basin does not grow appreciably during the Ediacaran due to onset of subduction around its

1706 periphery, however, at 590 Ma Baltica begins moving north, resulting in the consumption of the Mirovoi  
1707 Ocean basin and necessitating a change in mid-ocean ridge configuration. At this point we model a single

1708 ridge parallel to the Gondwanan margin, from Amazonia in the west towards India in the northeast. This  
1709 ridge also accommodates the final motion of India as it collides with Congo. It is difficult to identify

1710 when the Mirovoi Ocean ceased to exist, but by ca. 490 Ma, expansion in the Proto-Tethyan ocean basin  
1711 outboard of northwest Gondwana (e.g. Fig. 12), as well as the easterly drift of Siberia amalgamates the

1712 Siberian subduction zones outboard of North China and Chu-Yili-Tianshan, probably indicating that the  
1713 majority of Mirovoi crust produced during the Cryogenian and Ediacaran has been consumed.

1714

1715 An obvious issue with this discussion on the size of the Mirovoi is the longitudinal uncertainty between  
1716 the position of Congo and Laurentia during the Ediacaran. This uncertainty is because the distance

1717 between these two cratons dictates the size of the Adamastor Ocean (between Kalahari and Congo),  
1718 which grew at expense of the Mirovoi Ocean. Earliest evidence of subduction in the Damara belt exists

1719 from 650 Ma, with final closure occurring at 550 Ma. A conservative convergence rate of 40–60 km/Ma  
1720 (roughly equivalent to present-day Pacific convergence rates) would make the ocean basin at 4000–6000

1721 km wide, roughly equivalent to the present-day Atlantic Ocean (this width is similar in our model to that  
1722 of the Adamastor Ocean). However, faster divergence during Rodinia breakup would increase the size of

1723 this ocean basin, in turn reducing the size of the Mirovoi Ocean during the Ediacaran, similar to how the  
1724 size of the modern Pacific Ocean would become smaller or larger depending on the changing size of the

1725 Atlantic Ocean.

1726

1727 The Mawson Sea remains very small in size during the Cryogenian due to the close proximity between  
1728 India and Australia-Antarctica. There is no active ridge, instead a transform fault separates the two  
1729 continents. There is little evidence of subduction-related magmatism on either cratonic Australia or India  
1730 or this time (e.g. Halpin et al., 2017), suggesting the intervening lithosphere that eventually closed with  
1731 Gondwana amalgamation could have also involved a more complex scenario of terrane accretion. The  
1732 veracity of that statement is strongly dependent on the configuration and relative positioning of other  
1733 terranes that are typically reconstructed to the north-western margin of Australia in the late Palaeozoic,  
1734 such as Sibumasu and Indochina (Metcalf, 2011) or other terranes preserved in Antarctica that are  
1735 speculated to have rifted off the Indo-Antarctica and accreted to the western margin of the Mawson  
1736 Craton (Daczko et al., 2018; Mulder et al., 2019). Neither set of terranes are yet considered explicitly in  
1737 our model. By 520 Ma Australia-Antarctica is sutured with India, closing any remnants of the Mawson  
1738 Sea.

1739  
1740 Both the Mozambique and NeoMozambique oceans close orthogonally from 720 to 550 Ma due to the  
1741 continual southward motion of India towards Congo-SM. We do not model an active spreading ridge  
1742 during this time, as subduction is only preserved on the African side of the collision (Collins and  
1743 Pisarevsky, 2005). The presence of an earlier ridge does, however, suggest that at least two ridges (in our  
1744 model they are extinct) were subducted during the East African Orogeny.

1745  
1746 The Proto-Pacific Ocean grows predominantly longitudinally during the Cryogenian–Cambrian. In our  
1747 model, we show separation between Australia-Antarctica-North China and Laurentia using a single ridge  
1748 system that propagates southwards, around *southern* Laurentia to eventually separate the Kalahari Craton  
1749 and DML at ca. 700 Ma. We maintain a single ridge system until the Ediacaran, although when Kalahari  
1750 begins drifting from Laurentia, we follow Merdith et al. (2017b) in inferring a ridge jump to re-align  
1751 spreading between Australia and Laurentia with the incipient ridge separating Kalahari and Laurentia.  
1752 This ridge jump also assists with reconciling the necessary motion of Australia to Ediacaran  
1753 palaeomagnetic data, which require a  $\sim 35\text{--}45^\circ$  counter-clockwise rotation from its present-day orientation  
1754 (Schmidt and Williams, 2010). At 580 Ma we model a triple junction in the Proto-Pacific Ocean that  
1755 coincides with the equatorial excursion of Baltica and cessation of triple junction spreading in the  
1756 Mirovoi Ocean. The arms of this triple junction intersect sub-perpendicular to subduction outboard of  
1757 Laurentia, a transform fault outboard of North China and another transform boundary outboard of Baltica.

1758  
1759 Between 500 and 410 Ma, we refer to the ocean as the Panthalassic Ocean and for this time interval we  
1760 extended the triple junction of YOU19 backwards through DOM16 and DOM18. We found at 500 Ma

1761 when Cuyania rifts off the promontory of Laurentia (Domeier, 2016), that the position of the triple  
1762 junction and orientation of the ridges extended backwards from YOU19 was parallel to the direction of  
1763 spreading separating Cuyania from Laurentia. While coincidental, given the arbitrary nature of pre-  
1764 Mesozoic ocean plates, we find it useful to use the configuration at this time as a transition from the  
1765 Proto-Pacific Ocean to the Panthalassic Ocean.

1766

## 1767 **7 Conclusions**

1768

1769 We present here the first continuous full-plate model from 1 Ga to present-day. The model traces the  
1770 kinematic evolution of all cratonic crust and links the Neoproterozoic to the Phanerozoic, encompassing  
1771 an entire supercontinent cycle, and enabling quantitative analysis of tectonic features for deep time. We  
1772 present the model in a palaeomagnetic reference frame, including a new APWP for Gondwana from 540  
1773 to 320 Ma and a GAPWaP from 320 to 0 Ma. For the Neoproterozoic, the model uses a hybrid hierarchy,  
1774 where relative plate motions are tied to a key plate, forming distinct nodes. This cluster-approach allows  
1775 for the model to be iterated, constructed and modified in the future more easily in light of sparse  
1776 palaeomagnetic data, but abundant geological data. Our revised Neoproterozoic model incorporates a late  
1777 amalgamation of Rodinia with a novel configuration, in particular through the removal of India, South  
1778 China and Tarim from the supercontinent. We incorporate major plate re-organisation events at ca. 850  
1779 Ma and again at ca. 750–700 Ma, corresponding to the counter-clockwise rotation of Congo-Sao  
1780 Francisco-Sahara Metacraton relative to Rodinia and the initial closing of the Mozambique Ocean and  
1781 coeval opening of the Proto-Pacific Ocean, respectively. Our model also includes preliminary  
1782 interpretations of the Neoproterozoic history of many regional areas, such as terrane amalgamation  
1783 outboard of India-South China, Hoggar and Avalonia, that then link coherently with their more  
1784 established Phanerozoic histories. We reiterate that this model is a non-unique solution of global  
1785 palaeogeography and tectonics for the Neoproterozoic but we hope it can provide a framework on which  
1786 future studies can build upon. To facilitate this, we include in our supplementary material (SM3) the  
1787 tectonic parameters of seafloor production and consumption as extracted from the model.

1788

1789 Because our model has continuous plate boundaries, it enables a range of new scientific experiments such  
1790 as those seeking to link plate boundary processes to other aspects of the Earth system. This includes  
1791 experiments related to the biosphere, hydrosphere and atmosphere investigating events surrounding  
1792 oxygenation of Earth's atmosphere, Snowball Earth and animal radiation (e.g. (Gernon et al., 2016;  
1793 Godd ris et al., 2017; He et al., 2019; Hoffman et al., 1998; Hoffman and Schrag, 2002; Lenton et al.,  
1794 2016; Mills et al., 2019) and those studying the deep Earth (e.g. Heron et al., 2020). There are a number

1795 of limitations of this study, in particular, we do not address TPW in this model. Most previous studies  
1796 looked at TPW purely from a palaeomagnetic framework, however the incorporation of geological data in  
1797 the form of plate boundaries in this model (and others like it) open up opportunities for to analyse whole-  
1798 lithospheric motion from other directions (e.g. Tetley et al., 2019).

1799

## 1800 **Acknowledgements**

1801

1802 The authors thank Sergei Pisarevsky for advice on palaeomagnetic data. ASM is currently supported by  
1803 the Deep Energy Community of the Deep Carbon Observatory and the Richard Lounsbery Foundation.  
1804 ASM, SEW, RDM and SZ were supported by Australian Research Council grant IH130200012. ASC and  
1805 MLB are supported by Australian Research Council grants FT120100340 and LP160101353. MGT was  
1806 supported by European Research Council Grant Agreement 617588 and Agence Nationale de la  
1807 Recherche project ANR-18-ERC1-0005. JAM is supported by ARC grant FL160100168. AY and SA are  
1808 supported by an Australian Government Research Training Program Scholarship. SZ was supported by  
1809 Australian Research Council grant IH130200012, a University of Sydney Robinson Fellowship. SZ and  
1810 RDM were supported by Alfred P. Sloan grants G-2017-9997 and G-2018-11296 through the Deep  
1811 Carbon Observatory. JC and RDM were also supported by the AuScope National Collaborative Research  
1812 Infrastructure System (NCRIS) program. pyGPlates and GPlates development is funded by the AuScope  
1813 National Collaborative Research Infrastructure System (NCRIS) program. The authors are grateful for  
1814 thorough reviews by D. J. J. van Hinsbergen, C. Scotese and B. Murphy, all of which greatly improved  
1815 the focus and clarity of the manuscript.

1816

1817

1818 Table 1

Model	Time (Ma)	Scope	Reference Frame			LLSVPs	Hierarchy Structure
			Palaeomagnetic	Mantle	Details		
SET12	200–0	Global	No	Yes	TPW corrected palaeomagnetic data (200–100 Ma). Hotspot motion (100–0 Ma).	No assumption.	Branching.
DT14	410–250	Global	Yes	Yes	TPW corrected mantle reference from 410–250 Ma.	Assumes stable and long-lived.	Flat.
MUL16	230–200	Global	No	Yes	TPW corrected palaeomagnetic data (200–100 Ma). Hotspot motion (100–0 Ma).	No assumption.	Branching.
MAT16	410–0	Global	Yes	Yes	TPW corrected mantle reference from 410–0 Ma.	Assumes stable and long-lived.	Branching.
<i>DOM16</i>	500–410	Gondwana-Laurentia-Baltica	Yes	Yes	TPW corrected mantle reference from 500–410 Ma.	Assumes stable and long-lived.	Flat.
<i>MER17</i>	1000–520	Global	Yes	No		No assumption.	Nodal.
<i>DOM18</i>	500–410	Gondwana-Siberia-China	Yes	Yes	TPW corrected mantle reference from 500–410 Ma.	Assumes stable and long-lived.	Flat.
<i>YOU19</i>	410–0	Global	Yes	Yes	TPW corrected mantle reference frame from 250–0 Ma.	No assumption.	Branching.
MUL19	250–0	Global	No	Yes	Optimisation method after Tetley et al. (2019).	No assumption.	Branching.
This model	1000–0	Global	Yes	No		No assumption.	Nodal from 1000–410 Ma. Branching from 410–0 Ma.

1819



1820 **Table 2**

Key	Rockunit	OldAge	YoungAge	Glat	Glon	Plat	Plon	A95	Reference
<i>Laurentia</i>									
L1	Gunbarrel Intrusions combined	780	776	45	-110	14.6	127	3.2	Harlan et al. (2008).
L2	Uinta Formation	800	750	41	-110	0.8	161.3	4.7	Weil et al. (2006).
L3	Galeros - Carbon Canyon	764	750	35.15	-111.8	-0.5	166	9.7	Weil et al. (2004); Eyster et al. (2019).
L4	Kwagunt Formation	759	743	36.15	-112	14.2	163.8	3.5	Eyster et al. (2019).
L5	Kwagunt Formation 2	748	736	36.15	-112	18.2	166	7	Weil et al. (2004).
L6	Franklin Dykes	727	712	75	-82	8.4	163.8	2.8	Denyszyn et al. (2009).
L7	Long Range Dykes	617	613	53.5	-57.5	-19	175.3	17.4	Murthy et al. (1992); Hodych et al. (2004); Age: Kamo and Gower (1994).
L8	Skinner Cove Formation	554	548	50	-60	15	157	9	McCausland and Hodych (1998).
L9**	Andres Red Beds	423	393	41	-74	13	105	9	Miller and Kent (1988).
L10**	Wabash Reef	423	415	40.85	-85.7	17	125	5.3	McCabe et al. (1985); Torsvik et al. (1996).
L11**	Rose Hill formation	433	427	39	-79	19.1	128.3	5.8	French and Van der Voo (1979).
L12**	Ringgold Gap Sediments	456	433	34.51	-85.06	24	146.6	7.7	Morrison and Ellwood (1986).
L13**	Tablehead Group Limestone mean	470	456	48.33	-58.43	13.4	149.3	3.9	Hodych (1989); Hall and Evans (1988); Deutsch and Prasad (1987); Torsvik et al. (1996); Torsvik et al. (2012).
L14**	St George Group Limestone	485	456	48.3	-59	17.5	152.4	4.3	Deutsch and Prasad (1987).
L15**	Oneota Dolomite	485	470	43.41	-91.23	10.3	166.5	11.9	Jackson and Van der Voo (1985).

L16**	Moore Hollow sediments	500	490	31	-99	-0.6	163	8.5	Far and Gose (1991).
L17**	Morgan Creek	497	470	30.25	-98.5	10.6	158	9.7	Loucks an Elmore (1986).
L18**	Point Peak	497	485	30.5	-99	5.2	165.8	6	Van der Voo et al. (1976).
L19**	Taum Sauk Limestone	497	485	37.55	-90.31	-3.4	175.1	7.1	Dunn and Elmore (1985).
L20**	Roywe dolomite	497	485	34.25	-97.11	12.6	157.3	4.3	Nick and Elmore (1990).
L21**	Florida Mountains	497	485	32.05	-107.37	-5.4	168.7	10	Geissman et al. (1991).
L22**	Tapeats Sandstone	520	497	36.11	-113.99	2.3	162.6	3.3	Elston and Bressler (1977).
L23**	Mount Rigaud and Chatham-Grenville	534	530	45.28	24.2	-11.9	184.5	6.2	McClausland et al. (2007).
<i>Baltica</i>									
B1	Southern Sweden Dykes	946	935	59	16	-0.9	240.7	6.7	Elming et al. (2014); Pisarevsky and Bylund (1998).
B2	Branton-Algo Anorthosite	927	905	58.5	6.5	5	249	3.9	Stearn and Piper, (1984); Age: Scherstén et al. (2000).
B3	Rogaland Igneous Complex	883	855	58.5	6	-46	238	18.1	Walderhaug et al. (2007).
B4	Hunnedalen Dykes	875	821	59	6.75	-41	222	10	Walderhaug et al. (1999).
B5	Egersund Dykes	619	613	58.5	6	-31.4	224.1	15.6	Walderhaug et al. (2007).
B6	Kurgashlya Formation	570	560	53.3	57.5	-51	135	4.9	Lubnina et al. (2014).
B7	Bakeevo Formation	570	560	54.5	58.2	-42	119	5.3	Lubnina et al. (2014).
B8	Winter coast sediments	558	552	65.5	40	-25.3	132.5	2.8	Popov et al. (2002); Age: Martin et al. (2000).
B9	Zolotitsa sediments I, Russia	560	550	65.5	40	-31.7	112.9	2.4	Popov et al. (2005).

B10	Verkhotina sediments	560	550	65.5	40	-32.2	107.1	2	Popov et al. (2005).
B11	Zolotitsa sediments II	560	550	65.5	40	-28.3	109.9	3.8	Iglesia Llanos et al. (2005).
B12	Zigan Formation	552	544	53.7	56.7	-16	138	3.7	Levashova et al. (2013).
B13	Swedish Limestone (1N)	467	458	58.3	13.9	3	35	13.4	Torsvik & Trench (1991).
B14	Swedish Limestone	480	470	58	13	30	55	9	Torsvik & Trench (1991).
B15	Swedish Limestone (1R)	480	470	59	15	18	46	5.1	Torsvik & Trench (1991).
B16	Narva Limestones	485	470	59	31	18	55	4	Khramov and Iosifidi (2009).
B17	St Petersburg Limestone	480	470	58	30	33	58	3.6	Smethurst et al., (1998).
B18+	Gotland Follingbo Limestone	430	420	57.5	18.5	21	164	6	Claesson (1979).
B19+	Dniestr Silurian Lmst.	428	416	48.6	27	14.3	169.3	7.4	Jelenska et al. (2005).
B20+	Gotland Medby Limest.	427	417	57.5	18.5	23	171	8	Claesson (1979).
B21+	Ringerike Sandst. Norway	426	410	60	10.2	19	164	6.7	Douglass. (1988).
B22+	Tiverskaya Series	419	411	48.6	27	0	149	13.3	Jelenska et al. (2015).
B23+	Ivaniev and Dniestr Sediments	419	393	48.7	26	-1	175	9.6	Lubnina et al (2007).
B24+	Devonian Seds. Podolia	416	406	48.7	26	-3.7	145.5	6.7	Smethurst and Khramov (1992).
B25+	Dniestrovskaya Series	416	407	48.6	27	2.3	158.4	7.4	Jelenska et al. (2005).
B26+	Zilair Sediments, Russia	411	375	54	59	-2	161	3.1	Danukalov et al. (1983).
B27+	Eifelian sedimentary rocks, Russia	398	392	50	5	19	173	2.9	Minibaev and Sulutdinov (1991).

B28+	Bashkirea Sediments, Russia	398	385	54	59	-7	162	4.8	Danukalov et al. (1983).
B29+	Kola Dykes, Russia	390	370	68	33	11	147.6	11.1	Veselovsky and Arzamastsev (2011).
<i>Siberia</i>									
S1	Ust-Kirba Formation	960	930	60	137.2	8.1	2.6	10.4	Popov et al. (2002).
S2	Kitoi Dykes	762	754	52	103	0.4	21.8	6.1	Pisarevsky et al. (2013).
S3	Kesyussa Formation	542	535	71	122.5	-37.6	165	5.2	Pisarevsky et al. (1997).
S4-	Moyero River sediments	459	439	68	104	-14	124	8	Gallet and pavlov (1996).
S5-	Angara River sediments*	460	450	58.5	99.8	-29.5	140.2	6.4	Pavlov et al. (2012).
S6-	Kulumbe section	466	456	68	88.8	-24.1	152.4	3.3	Pavlov et al. (2008).
S7-	Stolobovaya section	466	456	62.1	92.5	-22	158	4	Pavlov et al. (2008).
S8-	Moyero River sediments	468	458	68	104	-23	158	4	Gallet and Pavlov (1996).
S9-	Angara River sediments	473	463	58.5	99.8	-35.2	153.2	3.6	Pavlov et al. (2012).
S10-	Moyero River sediments	474	464	68	104	-30	157	4	Gallet and Pavlov (1996).
S11-	Guragir Formation	475	465	68	88.8	-30.9	152.7	3.2	Pavlov and Gallet(1998).
S12-	Angara River sediments	480	470	58.5	99.8	-36.4	158.2	6.5	Pavlov et al. (2012).
S13-	Moyero River sediments	483	473	67.5	104	-33.9	151.7	2.2	Gallet and Pavlov (1996).
S14-	Uigur and Nizhneiltyk Formations	488	478	68	88.8	-35.2	127.2	4.9	Pavlov and Gallet (1998).

S15-	Moyero River sediments	488	478	68	104	-40	138	9	Gallet and Pavlov (1996).
S16-	Kulumbinskaya Formation	505	495	68	88.8	-36.1	130.7	6	Pavlov and Gallet (1998).
S17-	Moyero River sediments	505	495	68	104	-37	138	9	Gallet and Pavlov (1996).
S18	Yunkyulyabit-Yuryakh Formation	512	502	70.9	122.6	-36.4	139.6	4.6	Pisarevsky et al. (1997).
S19-	Kulumbe River section	512	502	68	88.4	-41.9	135.8	2.3	Pavlov and Gallet (1998).
S20-	Khorbusuonka Amgan and Mayan seds.	512	502	71.5	124	-43.7	140.5	2.6	Gallet et al. (2003).
S21-	Nyuya and Lena River sediments	437	427	60.6	116.3	-17.6	102	3.2	Powerman et al. (2013).
S22-	Nyuya and Lena River sediments	438	428	60.7	116.3	-18.6	101.9	4.6	Shatsillo et al. (2007).
S23-	Lena River sediments	454	444	60.5	116.4	-21	109	17.3	Torsvik et al. (1995).
S24-	Nyuya River sediments	456	446	60.6	116.3	-31.3	129.5	3.6	Powerman et al. (2013).
S25-	Kudrino section	466	456	57.7	107.99	-21.1	143.4	5	Pavlov et al. (2008).
S26-	Krivaya Luka Formation	469	459	59.7	118.1	-25.6	117.9	5.1	Iosifide et al. (1999).
S27-	Krivaya Luka Formation	469	459	59.7	118.1	-28.2	127.1	2.5	Iosifide et al. (1999).
S28-	Krivolutsky Suite	470	460	57.6	107.8	-32.6	137	8.3	Rodionov et al. (2003).
S29-	Lena River sediments	473	463	59.8	118.1	-32	139	3.1	Torsvik et al. (1995).
S30-	Lena River redbeds	475	465	60	114	-25	137	9	Rodionov et al. (1966).
S31-	Surinsk Formation	485	475	58.3	109.61	-42.2	128.1	5.8	Surkis et al. (1999).

S32-	Verkholensk Formation	506	496	58.5	109.8	-37.69	124	4.5	Rodionov et al. (1998).
S33-	Maya River sediments	515	505	60	132	-45.8	115	5	Pavlovl et al. (2008).
<i>West Australia</i>									
WA1	Browne Formation	830	730	-26	126	44.5	141.7	6.8	Pisarevsky et al. (2007).
WA2	Hussar Formation	800	730	-26	126	62.2	85.8	10.3	Pisarevsky et al. (2007).
WA3	Mundine Dykes	758	752	-23	115.8	45.3	135.4	4.1	Wingate and Giddings (2000).
<i>North Australia</i>									
NA1	Johnny's Creek Member	780	660	-24	133	15.8	83	13.5	Swanson-Hysell et al. (2012).
<i>South Australia</i>									
SA1	Angepena Formation	660	640	-32	138	47.1	176.6	5.3	Williams and Schmidt (2015).
SA2	Yaltipena Formation	650	635	-31.5	139	44.2	172.7	8.2	Sohl et al. (1999).
SA3	Elatina Formation, MEAN	645	635	-32	137.5	49.9	164.4	13.5	Embleton and Williams (1986); Schmidt et al. (1991); Schmidt and Williams (1995); Sohl et al. (1999).
SA4	Nuccaleena Formation	635	610	-31	139	32.3	170.8	2.9	Schmidt et al. (2009).
SA5	Brachina Formation	620	590	-32.2	138	46	135.4	3.3	Schmidt and Williams (2010).
SA6	Bunyeroo Formation	590	570	-31.6	138.4	18.1	196.3	8.8	Schmidt and Williams (1996).
SA7	Wonoka Formation	575	555	-31.3	138.6	5.2	210.5	4.9	Schmidt and Williams (2010).
<i>North China</i>									

NC1	Huaibei Sills 890 Ma	913	876	34	117	-52.3	149.3	3.5	Fu et al. (2015).
NC2	Wudaotang and Xinji Fm	541	521	35.6	110.5	18.5	341.9	6.5	Huang et al. (1999).
NC3	Hebei and Shandong Sediments	541	501	36	118	21.2	335.2	12.4	Zhao et al. (1992).
NC4	NE Sino-Korean Massif	541	485	35.6	110.5	26.8	334.5	8.9	Gao et al. (1983) (recalculated by Zhao et al. (1992)).
NC5-	Zhangxia and Xuzhuang Fms	510	496	35.6	110.5	37	326.7	5.5	Huang et al. (1999).
NC6-	Zhaogezhuang area carbonates	490	467	39.7	118.5	32.9	294.6	4.7	Yang et al. (2002).
NC7-	Changshan and Gushan Fms	496	485	35.6	110.5	31.7	329.6	5.4	Huang et al. (1999).
NC8-	Hebei and Shandong Sediments	499	461	36	118	28.8	310.9	12.3	Zhao et al. (1992).
NC9-	Liangjiashan and Lower Majiagou Fm	485	470	35.6	110.5	37.4	324.3	8.5	Huang et al. (1999).
NC10-	Jinghe	470	456	35.6	110.5	31.5	327.7	7	Huang et al. (1999).
NC11	Upper Majiagou Formation	470	456	35.6	110.5	27.9	310.4	9.2	Yang et al. (1996).
NC12-	Tianjinshan and Miboshan Formations	480	464	37.2	105.5	31.8	326.5	9.5	Huang et al. (1999).
<i>South China</i>									
SC1	Yanbian Dykes A	830	818	26.5	101.5	45.1	130.4	19	Niu et al. (2016).
SC2	Xiaofeng Dykes	812	792	31	111	13.5	91	10.9	Li et al. (2004).
SC3*	Yanbian Dykes B	814	798	26.5	101.5	14.1	32.5	20.4	Niu et al. (2016).
SC4	Liantuo Formation	735	705	30.8	111	9.9	160.3	4.6	Jing et al. (2015) and Evans et al.

									(2000), combined.
SC5	Nantuo Formation	641	631	28.5	110	7.5	161.6	5.9	Zhang et al. (2013); Zhang and Piper (1997).
SC6	Doushantuo Formation	614	590	30.8	111	25.9	185.5	6.7	Zhang et al. (2015).
SC7-	Douposi Formation (Wangcang)	510	496	32.1	106.2	-39.5	185.1	8.3	Lixin et al. (1998).
SC8-	Douposi Formation (Guangyuan)	510	496	32.4	106.3	-51.3	166	8.3	Yang et al. (2004).
SC9-	Shiqian Redbeds	440	425	27.5	108	4.9	194.7	5.6	Opdyke et al. (1987).
SC10-	Shiqian Redbeds	440	425	27.5	108	14.9	196.1	5.1	Huang et al. (2000).
SC11-	Pagoda Formation	458	445	32.4	106.3	-45.8	191.3	3.6	Han et al. (2015).
<i>Congo</i>									
C1	Luakela Volcanics A	770	757	-11.5	24.25	-40.2	122	14.1	Wingate et al. (2010).
C2	Mbozi Complex	773	713	-9.2	32.8	-46	145	6.7	Meert et al. (1995).
<i>Sao Francisco</i>									
SF1	Bahia Dykes (N+R)	928	912	-14	-39	7.3	106.4	6.2	Evans et al. (2016).
<i>Tarim</i>									
T1*	Sugetbrak Formation	635	550	40.9	79.4	19.1	149.7	9.3	Zhan et al. (2007).
T2*	Zhamoketi Andesite	621	609	41.5	87.8	-4.9	146.7	3.9	Zhao et al. (2014).
T3	Lower Sugetbrak Formation	640	615	41	79.5	-21.1	87.4	7	Wen et al. (2017).



T4*	Tereeken Cap Carbonate	640	630	41.5	87.8	27.6	140.4	9.9	Zhao et al. (2014).
T5	Qiaoenbrak Formation, Aksu	760	720	40.8	79.5	-6.3	17.5	9.1	Wen et al. (2013).
T6*	Aksu Dykes	819	795	41.15	80.1	19	128	4.5	Chen et al. (2004).
T7	Baiyisi Volcanics	770	717	41.6	86.54	-17.7	14.2	6	Huang et al. (2005).
T8-	Ordovician Limestones	485	470	41.3	83.4	-20.4	180.6	8.5	Fang et al. (1996).
T9-	Aksu-Kalpin-Bachu area sediments	455	445	40.6	78.9	-40.7	183.3	4.8	Sun and Huang (2009).
T10	Red Sandstone	433	427	40.6	79.4	12.8	159.8	7.3	Zhao et al. (2014)(2014) average of three poles from Fang et al. (1996); Li et al. (1990); Fang et al. (1998).
<i>India</i>									
I1	Malani Igneous Suite Grand Mean	770	734	26	72	69.4	75.7	6.5	Meert et al. (2013).
I2	Bhander and Rewa formations	650	530	26	78	47.3	212.7	5.8	McElhinny et al. (1978).
I3*	Jodphur Group	570	520	27	73	1	164	6.7	Davis et al. (2014).
<i>Seychelles</i>									
SE1	Mahe Dykes	753	747	-4.7	55.5	54.8	57.6	12.1	Torsvik et al. (2001).
<i>Rio de la Plata</i>									
RP1	Sierra de las Animas Complex	582	574	-34	-55.3	12.2	78.9	14.9	Rapalini et al. (2015).
RP2	Sierra de los Barrientos Redbeds	600	500	-37.8	-59	15.1	72.6	12.4	Rapalini et al. (2006).

<i>West African Craton</i>									
WAC1	Djebel Boho Volc.	547	526	30.4	-6.7	-27.3	207.1	14.9	Robert et al. (2017).
WAC2	Fajjoud and Tadoughast Volc.	572	551	30.2	-7.8	-21.9	211	15.6	Robert et al. (2017).
WAC3*	Adrar-n-takoucht Volc	577	564	30.4	-7.8	57.6	115.6	15.7	Robert et al. (2017).
<i>East Avalonia</i>									
EAV1#1	Treffgarne volcanics	482	472	52	-5	-56	126	5.5	Trench et al. (1992).
EAV2#	Stapeley volcanics	471	463	52.6	-3	-26.6	216.1	4.9	McCabe and Channell (1990).
EAV3#	Builth igneous and sediments	468	460	52.1	-3.3	-11	198	10	McCabe et al. (1992).
EAV4#	Tramore volcanics	461	449	52.1	-7.4	-11	198	8.5	Deutsch (1980); Trench and Torsvik (1991).
EAV5#	Borrowdale volcanics	448	438	54.4	-3.2	-8.1	186.2	6.9	Millward and Evans (2003); Channell and McCabe (1992).
EAV6#2	Midlands Minor Intrusives	442	432	52.5	-1.5	-52.5	181.5	10.4	Vizan et al. (2003).
EAV7#2	Browgill redbeds	439	433	54.3	-2.5	-13.6	133.9	12.4	Channell et al. (1993).
EAV8#2	Tortworth volcanics	437	431	51.7	-2.5	7	124	4.7	Torsvik et al. (1994).
EAV9#2	Mendips volcanics	435	429	51.2	-2.5	-13	91	8.8	Torsvik et al. (1993).
<i>Ganderia</i>									
GAN1#	Bourinot Group	510	496	46.1	-60.4	-21	160	8.1	Johnson and Van der Vood (1985).

<i>West Avalonia</i>									
WAV1#	Nahant intrusives	490	488	42.4	-70.9	-34	140	3.9	Thompson et al. (2010).
WAV2#	Dunn Point volcanics	463	457	45.8	-62.1	2	130	4.1	Johnson and Van Der Voo (1990); Hamilton and Murphy (2004).
WAV3#	Cape St. Mary sills	443	439	46.8	-54	10	140	9	Hodych and Buchan (1998).
<i>Carolinia</i>									
CAR1# <sub>2</sub>	Cid Formation metasediments	450	445	35	-80.2	29.6	122.1	5.1	Vick et al. (1987).
CAR2# <sub>2</sub>	Uwharrie and Cid Formation metaseds	450	445	35.5	-80	20	80	14.2	Noel et al. (1988).
<i>Cuyania</i>									
CUY1#	Pavon Formation sediments	458	452	-34.6	-68.6	-3.6	166.4	6.6	Rapalini and Cingolani (2004).
<p>* pole not fit by model  # from compilation of Domeier (2016)  + from compilation of S. Pisarevsky (<i>Pers. Comm.</i>)  - from compilation of Domeier (2018)  ** from compilation of Torsvik et al. (2012)  1 inclination only used  2 no upper age constraint (fits inclination data)  Glat, sample site latitude; Glon, sample site longitude; Plat, pole latitude; Plon, pole longitude; A95, 95% confidence ellipse.</p>									

1821

1822

1823 **Figure and Table Captions**

1824 Table 1

1825 Summary of main reconstruction features of the full-plate reconstructions discussed in text. Italicised  
1826 models are the models used in construction of the model presented in this study.

1827

1828 Table 2

1829 Summary of palaeomagnetic data

1830

1831 Figure 1

1832 Schematic comparison of evolution of plate tectonic modelling. (a) ‘Continental drift’/palaeogeographic  
1833 type models and (b) full-plate models; (i)–(iv) identify separate plates. Palaeomagnetic data are the  
1834 primary constraint of the movement of continents in both (a) and (b) however, the inclusion of geological  
1835 data into the model in (b) preserves the relative type of motion between two continents (divergence,  
1836 convergence or transform) and allows for the construction of plate boundaries.

1837

1838 Figure 2

1839 Overview of the rotational framework of a relative plate motion model. (a) Schematic of the ‘tree’ like  
1840 hierarchy (e.g. Ross and Scotese, 1988) from the Matthews et al. (2016) reconstruction, where the motion  
1841 of all plates are defined relative to the African plate at 50 Ma. (b) A simplified map view of the hierarchy  
1842 in (a). The African stage pole (blue hexagon) is at the top of the hierarchy and connected to the absolute  
1843 plate motion model that describes the movement of the African plate (in this case, as a proxy for the entire  
1844 globe) to the deep earth. (c) Example of plate motion with a continent (Africa) fixed in its present-day  
1845 position. Fixed plate presentations enable observations of relative motions between the fixed continent or  
1846 plate and another. Hence, they are useful to constrain relative plate motions and also compare two or  
1847 more different plate models. In this instance, a key difference between the model of Young et al. (2019)  
1848 and Matthews et al. (2016) is highlighted in the spatial relationship between Laurussia and Gondwana at  
1849 410 Ma. In Domeier and Torsvik (2014) (which is preserved in Matthews et al. (2016)) Laurussia is  
1850 proximal to southwest Gondwana while in Young et al. (2019) it is positioned to the northwest. ADR,  
1851 Adria; AFR, Africa; ARB, Arabia; AUS, Australia; BAL, Baltica (cratonic Europe); BM, Burma; CAR,  
1852 Caribbean; E.QT, East Qiangtang; EUR, Europe; GRN, Greenland; IC, Indochina; IND, India; JAP,  
1853 Japan; KOH, Kohistan arc; LHA, Lhasa; LHR, Lord Howe Rise; MAD, Madagascar; MBL, Marie Byrd  
1854 Land; MEX, Mexico; NAM, North America; NC, North China; NEA, Northeast Africa; NWA, Northwest  
1855 Africa; NZ, New Zealand; PAC, Pacific; PHL, Philippines; PNG, Papua New Guinea; SAL, Salado  
1856 Microplate; SAM, South America; SC, South China; SEA, Southeast Asia; SIB, Siberia; SOM, Somalia;  
1857 SPN, Spain; TAU, Taurides; W.QT, West Qiangtang.

1858

1859 Figure 3

1860 Overview of the rotational framework of an absolute plate motion model. (a) Schematic of a flat hierarchy  
1861 where the motion of all plates is defined relative to Africa. (b) Map view of the schematic at 450 Ma from  
1862 Domeier (2018, 2016). Many different plates (blue hexagons) sit at the top of the hierarchy and connect  
1863 to the deep earth. AFR, Africa; ANT, Antarctica; AUS, Australia; BAL, Baltica; C, Carolina; CY, ; EA,  
1864 East Avalonia; G, Ganderia; IC, Indochina; IND, India; K-T, Kazakh-Tianshan; LHA, Lhasa; MAD,  
1865 Madagascar; NAM, North America; NC, North China; NEA, Northeast Africa; NWA, Northwest Africa;  
1866 SAM, South America; SC, South China; SIB, Siberia; SOM, Somalia; T, Tarim; WA, West Avalonia.

1867

1868 Figure 4

1869 ‘Family-tree’ of full-plate models and some of the key underlying continental drift type models leading to  
1870 their development. We stress that more recent models are not necessarily better nor replace older models,  
1871 rather typically present some alternative interpretation of key data or are based on different assumptions.

1872 See text for more details. The model presented here bridges the MER17, DOM16, DOM18 and YOU19  
1873 models into a single continuous plate model. X-axis not to scale. Cr, Cryogenian, and; Ed, Ediacaran.

1874

1875 Figure 5

1876 Overview of the rotational framework of a hybrid plate motion hierarchy. (a) In this case, two different  
1877 nodes or clusters sit at the top of their respective branches of the hierarchy and ground regional relative  
1878 plate motions. (b) Map view of the schematic at 900 Ma from this study. Two different plates (India and  
1879 Laurentia; blue hexagons) sit at the top of the hierarchy and connect to the deep earth, with regional plate  
1880 motions being defined relative to each.

1881

1882 *Figure 6*

1883 Summary of the fit of palaeomagnetic data to our model for 1000 to 400 Ma (omitting poles used to  
1884 construct the Gondwana APWP). Misfit is the minimum great circle distance (in degrees) within the valid  
1885 time range between the palaeomagnetic pole and the geographic north pole. The error bar on each point is  
1886 the pole 95% confidence limit ( $A95$ ). Solid line is the mean misfit of all poles, with the dashed lines  
1887 representing the standard deviation of the mean. Poles marked as ‘not used’ or ‘inclination only’ in Table  
1888 2 are not included in this figure. (a) Poles from the constituent cratons of western Gondwana and the  
1889 Avalonian terranes; (b) poles from the constituent cratons of eastern Gondwana and present-day Asia,  
1890 and; (c) poles from Laurussia and Siberia.

1891

1892 Figure 7

1893 Comparison of palaeolatitude of major cratons (a) and Chinese cratons (b) from 1000–0 Ma between  
1894 three models; (i) This model, M2020; (ii) DOM16/18 (500–410 Ma) and MAT16 (410–0 Ma), and; (iii)  
1895 Li et al. (2013, 2008) (1000–550 Ma). The notable excursion at 800 Ma in the Li et al. (2013, 2008)  
1896 model is due to their adoption of IITPW at this time (Li et al., 2004).

1897

1898 Figure 8

1899 Distribution of continental crust, ocean basins and plate boundaries in our plate model at 0 Ma, based on  
1900 MUL16. Tan polygons are areas of continental lithosphere in the Neoproterozoic that we model, blue  
1901 polygons are areas of present-day continental lithosphere. Abbreviations as Figures 8 and 9. A,  
1902 Amazonia; Ant, Antarctica; AUS, Australia; BP, Borborema Province; CCT, Chinese Central Tianshan;  
1903 Cu, Cuyania; CY, Chu Yili; K, Kalahari; KMT, Krygyz Middle Tianshan; KNT, Krygyz North Tianshan;  
1904 KST, Krygyz South Tianshan; N-B, Nigeria-Benin; NC, North China; P, Paranapanema; ANS, Arabian  
1905 Nubian Shield; Qa, Qaidam; Qi, Qilian; RDLP, Rio de la Plata; SC, South China; SM, Sahara  
1906 Metacraton; T, Tarim; WAC, West African Craton.

1907

1908 Figure 9

1909 Distribution of continental crust, ocean basins and plate boundaries in this plate model at 500 Ma, based  
1910 on DOM16 and DOM18 (e.g. Figs. 12 and 13). Tan polygons are areas of continental lithosphere in the  
1911 Neoproterozoic that we model, blue polygons are areas of present-day continental lithosphere that are  
1912 inferred to exist during the Neoproterozoic, but without having firm geological evidence or that have been  
1913 effected by subsequent deformation (e.g. the distance between a present-day coastline and COB). Green  
1914 polygons represent a schematic interpretation of congruent continental lithosphere, with intervening crust  
1915 being subsequently deformed during future tectonic cycles. Abbreviations as Figure 8, in addition to; A-  
1916 C, Avalonia-Cadomia; Af, Afghanistan; B, Baltica; C, Congo; CMT, Central Mongolian Terrane; H,  
1917 Hoggar; I, India; S, Siberia.

1918

1919 Figure 10

1920 Distribution of continental crust, ocean basins and plate boundaries in our plate model at 1 Ga. Tan  
1921 polygons are areas of continental lithosphere in the Neoproterozoic that we model, blue polygons are  
1922 areas of present-day continental lithosphere that are inferred to exist during the Neoproterozoic, but

1923 without having firm geological evidence or that have been affected by subsequent deformation (e.g. the  
1924 distance between a present-day coastline and COB). Green polygons represent a schematic interpretation  
1925 of congruent continental lithosphere, with intervening crust being subsequently deformed during future  
1926 tectonic cycles. A-Ant, Austral-Antarctica; Az, Azania; BP, Borborema Province; CA, Central Angara  
1927 Terrane; CLB, Coats Land Block; Dabo. Arc, Dabolava Arc; DML, Dronning Maud Land; eSTR, Eastern  
1928 South Tasman Rise; IOGU, In Ouzal Granulite Unit; IGU, Iforas Granulite Unit; KMT(I), Krygyz Middle  
1929 Tianshan (Issedonian); KMT(UM), Krygyz Middle Tianshan (Ulutau-Moyunkum); KNT(I), Krygyz  
1930 North Tianshan (Issedonian); Mad, Madagascar; NAC, North Australian Craton; NeoMoz. Ocean,  
1931 NeoMozambique Ocean; NC, North China; p-ANS, proto-Arabian Nubian Shield; PH, Panxi-Hannan  
1932 Belt; Ra, Rayner Province; Ru, Ruker Block; SAC, South Australian Craton; SB, Southern Borborema;  
1933 SL, Sri Lanka; Tas, Tasmania; wSTR, Western South Tasman Rise.

1934

1935 *Figure 11*

1936 Comparison of our model (a, b) with Domeier (2018, 2016) (c, d) at 411–410 Ma to highlight the  
1937 latitudinal changes implemented for Laurussia in our model. Dark outline of Laurussia and Lhasa  
1938 (italicised labels) in (a) are their original positions in YOU19. Palaeomagnetic data are shown at time of  
1939 best fit for both models (i.e. map projection view of Fig. 6). Tan polygons are areas of continental  
1940 lithosphere in the Neoproterozoic that we model, blue polygons are areas of present-day continental  
1941 lithosphere that are inferred to exist during the Neoproterozoic, but without having firm geological  
1942 evidence or that have been affected by subsequent deformation (e.g. the distance between a present-day  
1943 coastline and COB). Green polygons represent a schematic interpretation of congruent continental  
1944 lithosphere, with intervening crust being subsequently deformed during future tectonic cycles. The  
1945 DOM16/18 models extend until 410.1 Ma (so we display it at 411 Ma), while YOU19 begins at 410 Ma.  
1946 NC, North China; SC, South China; T-K-Qi-Qa, Tarim-Kunlun-Qilian-Qaidam.

1947

1948 *Figure 12*

1949 Comparison of the evolution of the Rheic Ocean between our model (a, 500 Ma; c, 440 Ma) and DOM16  
1950 (b, 500 Ma; d, 440 Ma) during the early Palaeozoic. We point out the rotational difference (but similar  
1951 latitude) in Baltica at 500 Ma in our model relative to DOM16, discussed in text. Palaeolongitude is  
1952 constrained absolutely in DOM16 but not in our model. Subduction polarities are not provided in the  
1953 GPlates files of DOM16. Tan polygons are areas of continental lithosphere in the Neoproterozoic that we  
1954 model, blue polygons are areas of present-day continental lithosphere that are inferred to exist during the  
1955 Neoproterozoic, but without having firm geological evidence or that have been affected by subsequent  
1956 deformation (e.g. the distance between a present-day coastline and COB). Green polygons represent a  
1957 schematic interpretation of congruent continental lithosphere, with intervening crust being subsequently  
1958 deformed during future tectonic cycles. IO, Iapetus Ocean.

1959

1960 *Figure 13*

1961 Comparison of our model (a, c) with DOM18 (b, d) to highlight changes made. Annamia (Indochina,  
1962 Sibumasu) is not explicitly modelled in our reconstruction. L, Lut (Iran); F, Farah (Afghanistan); T,  
1963 Tarim. Tan polygons are areas of continental lithosphere in the Neoproterozoic that we model, blue  
1964 polygons are areas of present-day continental lithosphere that are inferred to exist during the  
1965 Neoproterozoic, but without having firm geological evidence or that have been affected by subsequent  
1966 deformation (e.g. the distance between a present-day coastline and COB). Green polygons represent a  
1967 schematic interpretation of congruent continental lithosphere, with intervening crust being subsequently  
1968 deformed during future tectonic cycles. Al, Alxa; An, Annamia; A-S, Altai-Sinai; SC, South China; K,  
1969 Kunlun; KMT, Krygyz Middle Tianshan; KNT, Krygyz North Tianshan; NC, North China; Qa-Qi,  
1970 Qaidam-Qilian; Ql, Qinling; T, Tarim.

1971

1972 *Figure 14*

1973 Snapshots of plate reconstructions showing our updated model for Australia-Laurentia at key time  
1974 intervals, along with palaeomagnetic data. (a) 1000 Ma; (b) 975 Ma; (c) 950 Ma; (e) 925 Ma; (f) 900 Ma;  
1975 (h) 580 Ma and (i) 560 Ma. The Tonian model (a–f) follows arguments laid out in Mulder et al. (2018b),  
1976 while the Ediacaran-Cambrian evolution is after Mulder et al. (2020). Times in these panels reflex the  
1977 nominal time of best fit for each pole. Tan polygons are areas of continental lithosphere in the  
1978 Neoproterozoic that we model, blue polygons are areas of present-day continental lithosphere that are  
1979 inferred to exist during the Neoproterozoic, but without having firm geological evidence or that have been  
1980 affected by subsequent deformation (e.g. the distance between a present-day coastline and COB). Green  
1981 polygons represent a schematic interpretation of congruent continental lithosphere, with intervening crust  
1982 being subsequently deformed during future tectonic cycles. CLB: Coats Land Block; DML, Dronning  
1983 Maud Land; eSTR: Eastern South Tasman Rise; MO, Mirovoi Ocean; MS, Mawson Sea; Tas: Tasmania;  
1984 wSTR: Western South Tasman Rise; RDLP: Río de la Plata; WAC, West African Craton.

1985

1986 *Figure 15*

1987 (a) Regional map at present day of Central Asian Orogenic Belt with modelled terranes highlighted in tan.  
1988 Light tan terranes are not explicitly modelled but are referred to in the main text. Black areas represent the  
1989 cratonic components. For the Kazakh area, we use polygons consistent with their Palaeozoic structure.  
1990 The size, orientation and distribution of crust in these terranes in the Neoproterozoic is unknown due to  
1991 the subsequent reworking of the terranes. Therefore, the precise position (along a margin), orientation,  
1992 size and shape of these terrane polygons in the reconstruction figures are speculative and should be  
1993 treated cautiously. (b–f) Evolution of the India-South China system during the Tonian–Cryogenian at key  
1994 times. Tan polygons are areas of continental lithosphere in the Neoproterozoic that we model, blue  
1995 polygons are areas of present-day continental lithosphere that are inferred to exist during the  
1996 Neoproterozoic, but without having firm geological evidence or that have been affected by subsequent  
1997 deformation (e.g. the distance between a present-day coastline and COB). Green polygons represent a  
1998 schematic interpretation of congruent continental lithosphere, with intervening crust being subsequently  
1999 deformed during future tectonic cycles. ADO = Aravalli-Delhi Orogen; Af, Afghanistan; Aus-Ant,  
2000 Australia-Antarctica; Ca, Cathaysia; DML-CLN, Dronning Maud Land-Coats Land Block; I, India; I-A,  
2001 Indo-Antarctica; KNT (I/UM), Krygyz North Tianshan (Issendonian/Ulutau-Moyunkum); KMT (I/UM),  
2002 Krygyz Middle Tianshan (Issendonian/Ulutau-Moyunkum); MIP, Malani Igneous Province; MO, Mirovoi  
2003 Ocean; MzO, Mozambique Ocean; NC, North China; NeoMzO, Neomozambique Ocean; Qa, Qaidam;  
2004 Qi, Qilian; Ru, Ruker; SC, South China; SM, Sahara Metacraton; T, Tarim; WAC, West African Craton;  
2005 Y, Yangtze.

2006

2007 *Figure 16*

2008 Schematic of our model for India-South China at key time steps, showing accretion of the Yangtze Craton  
2009 and numerous smaller terranes and blocks to a large, Tonian subduction zone outboard of the north-  
2010 western India and the northern margin of South China and their subsequent fragmentation and rifting off  
2011 during the Ediacaran–Early Cambrian. (a) early Tonian; (b) late Tonian; (c) Cryogenian–Ediacaran, note  
2012 if the model were adopted to fit the cluster of three palaeomagnetic poles from Tarim then collision would  
2013 be at ca. 650 Ma, and; (d) Ediacaran–Cambrian. Af, Afghanistan; Al-Qi-Qa, Alxa, Qilian, Qaidam; ANS,  
2014 Arabian Nubian Shield; CY, Chu Yili; DML-CLB, Dronning Maud Land-Coats Land Block; EAO, East  
2015 African Orogen; I, India; I-A, Indo-Antarctica; KMT (I/UM), Krygyz Middle Tianshan  
2016 (Issendonian/Ulutau-Moyunkum); KNT (I/UM), Krygyz North Tianshan (Issendonian/Ulutau-  
2017 Moyunkum); SC, South China; T, Tarim.

2018

2019 *Figure 17*

2020 Amalgamation of the Arabian-Nubian Shield (ANS) after Blades et al. (2019b, 2015), Armistead et al.  
2021 (2019) and Collins et al. (in revision) and the incorporation of the ANS, Azania and TOAST into  
2022 Gondwana along the East African Orogen at: (a) 800 Ma and (b) 520 Ma. Tan polygons are areas of

2023 continental lithosphere in the Neoproterozoic that we model, blue polygons are areas of present-day  
2024 continental lithosphere that are inferred to exist during the Neoproterozoic, but without having firm  
2025 geological evidence or that have been affected by subsequent deformation (e.g. the distance between a  
2026 present-day coastline and COB). Green polygons represent a schematic interpretation of congruent  
2027 continental lithosphere, with intervening crust being subsequently deformed during future tectonic cycles.  
2028 Thick black lines follow the suture of the East African Orogen and Kuunga Orogen. ANS, Arabian-  
2029 Nubian Shield; EAO, East African Orogen; SF, Sao Francisco; SM, Sahara Metacraton.

2030

2031 *Figure 18*

2032 Amalgamation of Hoggar after Cabby et al. (1989), Black et al. (1994) and Liégeois et al. (1994),  
2033 Borborema and Peri-Gondwanan terranes after Nance et al. (2008) at key time slices. (a) map of key  
2034 terranes in a reconstructed Gondwana (dark blue terranes are oceanic terranes); (b) map of reconstructed  
2035 Peri-Gondwanan terranes at 650 Ma; (c) 1000 Ma; (d) 900 Ma; (e) 860 Ma; (f) 700 Ma; (g) 640 Ma; (h)  
2036 580 Ma; (i) 550 Ma and (j) 520 Ma. Tan polygons are areas of continental lithosphere in the  
2037 Neoproterozoic that we model, blue polygons are areas of present-day continental lithosphere that are  
2038 inferred to exist during the Neoproterozoic, but without having firm geological evidence or that have been  
2039 affected by subsequent deformation (e.g. the distance between a present-day coastline and COB). Green  
2040 polygons represent a schematic interpretation of congruent continental lithosphere, with intervening crust  
2041 being subsequently deformed during future tectonic cycles A, Aouzegueur; A-I, Assodé-Issalane; Am,  
2042 Amazonia; ANS, Arabian-Nubian Shield; B, Baltica; BP, Borborema Province; C, Congo; C-B, Central  
2043 Borborema; IGU, Iforas granulite unit; IOGU, In Ouzzal granulite unit; IO, Iapetus Ocean; LATEA,  
2044 Laouni, Azrou-n-Fad, Tefedest and Egéré-Aleksod terranes; MO, Mirovoi Ocean; Moz. O, Mozambique  
2045 ocean; N-B, Niger-Benin Block; P, Paranapanema; PG, Peri-Gondwanan terranes; S-B, Southern  
2046 Borborema; SF, Sao Francisco; SM, Sahara Metacraton; WAC, West African Craton.

2047

2048 References

2049

2050 Ahmad, M., Munson, T.J., 2013. Geology and mineral resources of the Northern Territory. Northern  
2051 Territory Geological Survey Special Publication 5.

2052 Alessio, B.L., Blades, M.L., Murray, G., Thorpe, B., Collins, A.S., Kelsey, D.E., Foden, J., Payne, J., Al-  
2053 Khirbash, S., Jourdan, F., 2018. Origin and tectonic evolution of the NE basement of Oman: a  
2054 window into the Neoproterozoic accretionary growth of India? *Geol. Mag.* 155, 1150–1174.  
2055 <https://doi.org/10.1017/S0016756817000061>

2056 Alexeiev, D.V., Biske, G.S., Kröner, A., Tretyakov, A.A., Kovach, V.P., Rojas-Agramonte, Y., 2020.  
2057 Ediacaran, Early Ordovician and early Silurian arcs in the South Tianshan orogen of Kyrgyzstan.  
2058 *J. Asian Earth Sci.* 190, 104194. <https://doi.org/10.1016/j.jseaes.2019.104194>

2059 Alexeiev, D.V., Kröner, A., Kovach, V.P., Tretyakov, A.A., Rojas-Agramonte, Y., Degtyarev, K.E.,  
2060 Mikolaichuk, A.V., Wong, J., Kiselev, V.V., 2019. Evolution of Cambrian and Early Ordovician  
2061 arcs in the Kyrgyz North Tianshan: Insights from U-Pb zircon ages and geochemical data.  
2062 *Gondwana Res.* 66, 93–115. <https://doi.org/10.1016/j.gr.2018.09.005>

2063 Alexeiev, D.V., Ryazantsev, A.V., Kröner, A., Tretyakov, A.A., Xia, X., Liu, D.Y., 2011. Geochemical  
2064 data and zircon ages for rocks in a high-pressure belt of Chu-Yili Mountains, southern



2065 Kazakhstan: Implications for the earliest stages of accretion in Kazakhstan and the Tianshan. *J.*  
2066 *Asian Earth Sci.* 42, 805–820. <https://doi.org/10.1016/j.jseaes.2010.09.004>

2067 Archibald, D.B., Collins, A.S., Foden, J.D., 2017. Tonian arc magmatism in central Madagascar: the  
2068 petrogenesis of the Imorona-Itsindro Suite. *The Journal of.*

2069 Archibald, D.B., Collins, A.S., Foden, J.D., Payne, J.L., Macey, P.H., Holden, P., Razakamanana, T.,  
2070 2018. Stenian–Tonian arc magmatism in west–central Madagascar: the genesis of the Dabolava  
2071 Suite. *J. Geol. Soc. London* 175, 111–129. <https://doi.org/10.1144/jgs2017-028>

2072 Armistead, S.E., Collins, A.S., Merdith, A.S., Payne, J.L., Cox, G.M., Foden, J.D., Razakamanana, T., De  
2073 Waele, B., 2019. Evolving marginal terranes during Neoproterozoic supercontinent  
2074 reorganisation: constraints from the Bemarivo Domain in northern Madagascar. *Tectonics.*  
2075 <https://doi.org/10.1029/2018TC005384>

2076 Armstrong, R.A., Master, S., Robb, L.J., 2005. Geochronology of the Nchanga Granite, and constraints  
2077 on the maximum age of the Katanga Supergroup, Zambian Copperbelt. *J. Afr. Earth. Sci.* 42, 32–  
2078 40. <https://doi.org/10.1016/j.jafrearsci.2005.08.012>

2079 Arthaud, F., Matte, P., 1977. Late Paleozoic strike-slip faulting in southern Europe and northern Africa:  
2080 Result of a right-lateral shear zone between the Appalachians and the Urals. *GSA Bulletin* 88,  
2081 1305–1320. [https://doi.org/10.1130/0016-7606\(1977\)88<1305:LPSFIS>2.0.CO;2](https://doi.org/10.1130/0016-7606(1977)88<1305:LPSFIS>2.0.CO;2)

2082 Ashwal, L.D., Solanki, A.M., Pandit, M.K., Corfu, F., Hendriks, B.W.H., Burke, K., Torsvik, T.H., 2013.  
2083 Geochronology and geochemistry of Neoproterozoic Mt. Abu granitoids, NW India: Regional  
2084 correlation and implications for Rodinia paleogeography. *Precambrian Res.* 236, 265–281.  
2085 <https://doi.org/10.1016/j.precamres.2013.07.018>

2086 Austermann, J., Ben-Avraham, Z., Bird, P., Heidbach, O., Schubert, G., Stock, J.M., 2011. Quantifying  
2087 the forces needed for the rapid change of Pacific plate motion at 6Ma. *Earth Planet. Sci. Lett.* 307,  
2088 289–297. <https://doi.org/10.1016/j.epsl.2011.04.043>

2089 Austermann, J., Kaye, B.T., Mitrovica, J.X., Huybers, P., 2014. A statistical analysis of the correlation  
2090 between large igneous provinces and lower mantle seismic structure. *Geophys. J. Int.* 197, 1–9.  
2091 <https://doi.org/10.1093/gji/ggt500>

2092 Barker, C.A., Secor, Jr., T., D., Pray, J.R., Wright, J.E., 1998. Age and Deformation of the Longtown  
2093 Metagranite, South Carolina Piedmont: A Possible Constraint on the Origin of the Carolina  
2094 Terrane. *J. Geol.* 106, 713–726. <https://doi.org/10.1086/516055>

2095 Bebout, G.E., 1995. The impact of subduction-zone metamorphism on mantle-ocean chemical cycling.  
2096 *Chem. Geol.* 126, 191–218. [https://doi.org/10.1016/0009-2541\(95\)00118-5](https://doi.org/10.1016/0009-2541(95)00118-5)

2097 Berry, R.F., Steele, D.A., Meffre, S., 2008. Proterozoic metamorphism in Tasmania: Implications for  
2098 tectonic reconstructions. *Precambrian Res.* 166, 387–396.

2099 <https://doi.org/10.1016/j.precamres.2007.05.004>

2100 Bevier, M.L., Barr, S.M., White, C.E., Macdonald, A.S., 1993. U–Pb geochronologic constraints on the  
2101 volcanic evolution of the Mira (Avalon) terrane, southeastern Cape Breton Island, Nova Scotia.  
2102 *Can. J. Earth Sci.* 30, 1–10. <https://doi.org/10.1139/e93-001>

2103 Black, L.P., 1997. Dating Tasmania’s oldest geological events. Australian Geological Survey  
2104 Organisation.

2105 Black, R., Latouche, L., Liégeois, J.P., Caby, R., Bertrand, J.M., 1994. Pan-African displaced terranes in  
2106 the Tuareg shield (central Sahara). *Geology* 22, 641–644.  
2107 2.3.CO;2">[https://doi.org/10.1130/0091-7613\(1994\)022<0641:PADTIT>2.3.CO;2](https://doi.org/10.1130/0091-7613(1994)022<0641:PADTIT>2.3.CO;2)

2108 Blades, M.L., Alessio, B.L., Collins, A.S., Foden, J., Payne, J.L., Glorie, S., Holden, P., Thorpe, B., Al-  
2109 Khirbash, S., 2019a. Unravelling the Neoproterozoic accretionary history of Oman, using an  
2110 array of isotopic systems in zircon. *J. Geol. Soc. London*. <https://doi.org/10.1144/jgs2018-125>

2111 Blades, M.L., Collins, A.S., Foden, J., Payne, J.L., Stüwe, K., Hassan, M., Abu-Alam, T., submitted. Age  
2112 and Hafnium Isotope Evolution of Sudanese Butana and Chad Illuminates the Stenian to  
2113 Ediacaran Evolution of the Southeast Sahara Metacraton. *Precambrian Res.*

2114 Blades, M.L., Collins, A.S., Foden, J., Payne, J.L., Xu, X., Alemu, T., Woldetinsae, G., Clark, C., Taylor,  
2115 R.J.M., 2015. Age and hafnium isotopic evolution of the Didesa and Kemashi Domains, western  
2116 Ethiopia. *Precambrian Res.* 270, 267–284. <https://doi.org/10.1016/j.precamres.2015.09.018>

2117 Blades, M.L., Foden, J., Collins, A.S., Alemu, T., Woldetinsae, G., 2019b. The origin of the ultramafic  
2118 rocks of the Tulu Dimtu Belt, western Ethiopia--do they represent remnants of the Mozambique  
2119 Ocean? *Geol. Mag.* 156, 62–82.

2120 Bleeker, W., 2003. The late Archean record: a puzzle in ca. 35 pieces. *Lithos* 71, 99–134.  
2121 <https://doi.org/10.1016/j.lithos.2003.07.003>

2122 Bodorkos, S., Crowley, J.L., Clauoué-Long, J.C., Anderson, J.R., Magee, C.W., 2020. Precise U–Pb  
2123 baddeleyite dating of the Derim Derim Dolerite, McArthur Basin, Northern Territory: old and  
2124 new SHRIMP and ID-TIMS constraints. *Aust. J. Earth Sci.* 1–15.  
2125 <https://doi.org/10.1080/08120099.2020.1749929>

2126 Bower, D.J., Gurnis, M., Seton, M., 2013. Lower mantle structure from paleogeographically constrained  
2127 dynamic Earth models. *Geochem. Geophys. Geosyst.* 14, 44–63.  
2128 <https://doi.org/10.1029/2012GC004267>

2129 Boyden, J.A., Müller, R.D., Gurnis, M., Torsvik, T.H., Clark, J.A., Turner, M., Ivey-Law, H., Watson,  
2130 R.J., Cannon, J.S., 2011. Next-generation plate tectonic reconstructions, in: Keller, G.R., Baru, C.  
2131 (Eds.), *Geoinformatics: Cyberinfrastructure for the Solid Earth Sciences*. Cambridge University  
2132 Press, Cambridge, pp. 95–113.

- 2133 Brenner, A.R., Fu, R.R., Evans, D.A.D., Smirnov, A.V., Trubko, R., Rose, I.R., 2020. Paleomagnetic  
2134 evidence for modern-like plate motion velocities at 3.2 Ga. *Science Advances* 6, eaaz8670.  
2135 <https://doi.org/10.1126/sciadv.aaz8670>
- 2136 Brown, M., Johnson, T.E., Gardiner, N.J., 2020a. Plate Tectonics and the Archean Earth. *Annu. Rev.*  
2137 *Earth Planet. Sci.* 48, 291–320. <https://doi.org/10.1146/annurev-earth-081619-052705>
- 2138 Brown, M., Kirkland, C.L., Johnson, T.E., 2020b. Evolution of geodynamics since the Archean:  
2139 Significant change at the dawn of the Phanerozoic. *Geology* 48, 488–492.  
2140 <https://doi.org/10.1130/G47417.1>
- 2141 Brune, S., Williams, S.E., Müller, R.D., 2017. Potential links between continental rifting, CO<sub>2</sub> degassing  
2142 and climate change through time. *Nat. Geosci.* 10, 941–946. [https://doi.org/10.1038/s41561-017-](https://doi.org/10.1038/s41561-017-0003-6)  
2143 [0003-6](https://doi.org/10.1038/s41561-017-0003-6)
- 2144 Burke, K., Torsvik, T.H., 2004. Derivation of Large Igneous Provinces of the past 200 million years from  
2145 long-term heterogeneities in the deep mantle. *Earth Planet. Sci. Lett.* 227, 531–538.  
2146 <https://doi.org/10.1016/j.epsl.2004.09.015>
- 2147 Burrett, C., Khin Zaw, Meffre, S., Lai, C.K., Khositanont, S., Chaodumrong, P., Udchachon, M., Ekins,  
2148 S., Halpin, J., 2014. The configuration of Greater Gondwana—Evidence from LA ICPMS, U–Pb  
2149 geochronology of detrital zircons from the Palaeozoic and Mesozoic of Southeast Asia and China.  
2150 *Gondwana Res.* 26, 31–51. <https://doi.org/10.1016/j.gr.2013.05.020>
- 2151 Burrett, C., Long, J., Stait, B., 1990. Early-Middle Palaeozoic biogeography of Asian terranes derived  
2152 from Gondwana. *Geological Society, London, Memoirs* 12, 163–174.  
2153 <https://doi.org/10.1144/GSL.MEM.1990.012.01.14>
- 2154 Cabby, R., 2003. Terrane assembly and geodynamic evolution of central–western Hoggar: a synthesis. *J.*  
2155 *Afr. Earth. Sci.* 37, 133–159. <https://doi.org/10.1016/j.jafrearsci.2003.05.003>
- 2156 Cabby, R., Andreopoulos-Renaud, U., Gravelle, M., 1982. Cadre géologique et géochronologique U/Pb sur  
2157 zircon des batholites précoces dans le segment pan-africain du Hoggar central (Algérie). *Bulletin*  
2158 *de la Société Géologique de France S7-XXIV*, 677–684. [https://doi.org/10.2113/gssgfbull.S7-](https://doi.org/10.2113/gssgfbull.S7-XXIV.4.677)  
2159 [XXIV.4.677](https://doi.org/10.2113/gssgfbull.S7-XXIV.4.677)
- 2160 Cabby, R., Andreopoulos-Renaud, U., Pin, C., 1989. Late Proterozoic arc–continent and continent–  
2161 continent collision in the pan-African trans-Saharan belt of Mali. *Can. J. Earth Sci.* 26, 1136–  
2162 1146. <https://doi.org/10.1139/e89-097>
- 2163 Calver, C.R., 2011. Neoproterozoic glacial deposits of Tasmania, in: Arnaud, E., Halverson, G.P.,  
2164 Shields-Zhou, G. (Ed.), *The Geological Record of Neoproterozoic Glaciations*. Geological  
2165 Society of London, pp. 649–658. <https://doi.org/10.1144/M36.64>
- 2166 Calver, C.R., Everard, J.L., Berry, R.F., Bottrill, R.S., Seymour, D.B., 2014. Proterozoic Tasmania.

2167 Geological Evolution of Tasmania: Geological Society of Australia Special Publication 24, 33–  
2168 94.

2169 Calver, C.R., Meffre, S., Everard, J.L., 2013. Felsic Porphyry Sills in Surprise Bay Formation Near  
2170 Currie, King Island, Dated at 775 Ma (LA-ICPMS, U-Pb on Zircon). Tasmanian Geological  
2171 Survey.

2172 Cao, W., Williams, S., Flament, N., Zahirovic, S., Scotese, C., Dietmar Müller, R., 2019.  
2173 Palaeolatitudinal distribution of lithologic indicators of climate in a palaeogeographic framework.  
2174 *Geol. Mag.* 156, 331–354. <https://doi.org/10.1017/S0016756818000110>

2175 Cawood, P.A., Buchan, C., 2007. Linking accretionary orogenesis with supercontinent assembly. *Earth-*  
2176 *Sci. Rev.* 82, 217–256. <https://doi.org/10.1016/j.earscirev.2007.03.003>

2177 Cawood, P.A., Hawkesworth, C.J., Dhuime, B., 2013a. The continental record and the generation of  
2178 continental crust. *GSA Bulletin* 125, 14–32. <https://doi.org/10.1130/B30722.1>

2179 Cawood, P.A., Hawkesworth, C.J., Pisarevsky, S.A., Dhuime, B., Capitanio, F.A., Nebel, O., 2018a.  
2180 Geological archive of the onset of plate tectonics. *Philos. Trans. A Math. Phys. Eng. Sci.* 376.  
2181 <https://doi.org/10.1098/rsta.2017.0405>

2182 Cawood, P.A., Nemchin, A.A., Leverenz, A., Saeed, A., Balance, P.F., 1999. U/Pb dating of detrital  
2183 zircons: Implications for the provenance record of Gondwana margin terranes. *GSA Bulletin* 111,  
2184 1107–1119. [https://doi.org/10.1130/0016-7606\(1999\)111<1107:UPDODZ>2.3.CO;2](https://doi.org/10.1130/0016-7606(1999)111<1107:UPDODZ>2.3.CO;2)

2185 Cawood, P.A., Nemchin, A.A., Smith, M., Loewy, S., 2003. Source of the Dalradian Supergroup  
2186 constrained by U–Pb dating of detrital zircon and implications for the East Laurentian margin. *J.*  
2187 *Geol. Soc. London* 160, 231–246. <https://doi.org/10.1144/0016-764902-039>

2188 Cawood, P.A., Pisarevsky, S.A., 2006. Was Baltica right-way-up or upside-down in the Neoproterozoic?  
2189 *J. Geol. Soc. London* 163, 753–759. <https://doi.org/10.1144/0016-76492005-126>

2190 Cawood, P.A., Strachan, R., Cutts, K., Kinny, P.D., Hand, M., Pisarevsky, S., 2010. Neoproterozoic  
2191 orogeny along the margin of Rodinia: Valhalla orogen, North Atlantic. *Geology* 38, 99–102.  
2192 <https://doi.org/10.1130/G30450.1>

2193 Cawood, P.A., Strachan, R.A., Pisarevsky, S.A., Gladkochub, D.P., Murphy, J.B., 2016. Linking  
2194 collisional and accretionary orogens during Rodinia assembly and breakup: Implications for  
2195 models of supercontinent cycles. *Earth Planet. Sci. Lett.* 449, 118–126.  
2196 <https://doi.org/10.1016/j.epsl.2016.05.049>

2197 Cawood, P.A., Wang, W., Zhao, T., Xu, Y., Mulder, J.A., Pisarevsky, S.A., Zhang, L., Gan, C., He, H.,  
2198 Liu, H., Qi, L., Wang, Y., Yao, J., Zhao, G., Zhou, M.-F., Zi, J.-W., 2020. Deconstructing South  
2199 China and consequences for reconstructing Nuna and Rodinia. *Earth-Sci. Rev.* 204, 103169.  
2200 <https://doi.org/10.1016/j.earscirev.2020.103169>

- 2201 Cawood, P.A., Wang, Y., Xu, Y., Zhao, G., 2013b. Locating South China in Rodinia and Gondwana: A  
2202 fragment of greater India lithosphere? *Geology* 41, 903–906. <https://doi.org/10.1130/G34395.1>
- 2203 Cawood, P.A., Zhao, G., Yao, J., Wang, W., Xu, Y., Wang, Y., 2018b. Reconstructing South China in  
2204 Phanerozoic and Precambrian supercontinents. *Earth-Sci. Rev.* 186, 173–194.  
2205 <https://doi.org/10.1016/j.earscirev.2017.06.001>
- 2206 Caxito, F. de A., Uhlein, A., Dantas, E.L., 2014a. The Afeição augen-gneiss Suite and the record of the  
2207 Cariris Velhos Orogeny (1000–960 Ma) within the Riacho do Pontal fold belt, NE Brazil. *J.*  
2208 *South Amer. Earth Sci.* 51, 12–27. <https://doi.org/10.1016/j.jsames.2013.12.012>
- 2209 Caxito, F. de A., Uhlein, A., Stevenson, R., Uhlein, G.J., 2014b. Neoproterozoic oceanic crust remnants  
2210 in northeast Brazil. *Geology* 42, 387–390. <https://doi.org/10.1130/G35479.1>
- 2211 Caxito, F.A., Uhlein, A., Dantas, E.L., Stevenson, R., Salgado, S.S., Dussin, I.A., Sial, A. da N., 2016. A  
2212 complete Wilson Cycle recorded within the Riacho do Pontal Orogen, NE Brazil: Implications for  
2213 the Neoproterozoic evolution of the Borborema Province at the heart of West Gondwana.  
2214 *Precambrian Res.* 282, 97–120. <https://doi.org/10.1016/j.precamres.2016.07.001>
- 2215 Cayley, R.A., 2011. Exotic crustal block accretion to the eastern Gondwanaland margin in the Late  
2216 Cambrian--Tasmania, the Selwyn Block, and implications for the Cambrian--Silurian evolution of  
2217 the Ross, Delamerian, and Lachlan orogens. *Gondwana Res.* 19, 628–649.
- 2218 Channell, J.E.T., McCabe, C., 1992. Palaeomagnetic data from the Borrowdale Volcanic Group: volcano-  
2219 tectonics and Late Ordovician palaeolatitudes. *J. Geol. Soc. London* 149, 881–888.  
2220 <https://doi.org/10.1144/gsjgs.149.6.0881>
- 2221 Channell, J.E.T., McCabe, C., Woodcock, N.H., 1993. Palaeomagnetic study of Llandovery (Lower  
2222 Silurian) red beds in north-west England. *Geophys. J. Int.* 115, 1085–1094.
- 2223 Charvet, J., Shu, L., Laurent-Charvet, S., Wang, B., Faure, M., Cluzel, D., Chen, Y., De Jong, K., 2011.  
2224 Palaeozoic tectonic evolution of the Tianshan belt, NW China. *Sci. China Earth Sci.* 54, 166–184.  
2225 <https://doi.org/10.1007/s11430-010-4138-1>
- 2226 Chen, Y., Xu, B., Zhan, S., Li, Y., 2004. First mid-Neoproterozoic paleomagnetic results from the Tarim  
2227 Basin (NW China) and their geodynamic implications. *Precambrian Res.* 133, 271–281.  
2228 <https://doi.org/10.1016/j.precamres.2004.05.002>
- 2229 Claesson, C., 1979. Early Palaeozoic geomagnetism of Gotland. *Geologiska Föreningen i Stockholm*  
2230 *Förhandlingar* 101, 149–155. <https://doi.org/10.1080/11035897909452573>
- 2231 Clennett, E.J., Sigloch, K., Mihalyuk, M.G., Seton, M., Henderson, M.A., Hosseini, K.,  
2232 Mohammadzaheri, A., Johnston, S.T., Müller, R.D., 2020. A Quantitative Tomotectonic Plate  
2233 Reconstruction of Western North America and the Eastern Pacific Basin. *Geochem. Geophys.*  
2234 *Geosyst.*, Geological Association of Canada Special Paper 21, 2011-11.

- 2235 <https://doi.org/10.1029/2020GC009117>
- 2236 Cocks, L.R.M., Fortey, R.A., 1997. A new Hirnantia fauna from Thailand and the biogeography of the  
2237 latest Ordovician of south-east Asia. *Geobios Mem. Spec.* 30, 117–126.
- 2238 [https://doi.org/10.1016/S0016-6995\(97\)80017-4](https://doi.org/10.1016/S0016-6995(97)80017-4)
- 2239 Cocks, L.R.M., Torsvik, T.H., 2007. Siberia, the wandering northern terrane, and its changing geography  
2240 through the Palaeozoic. *Earth-Sci. Rev.* 82, 29–74.
- 2241 <https://doi.org/10.1016/j.earscirev.2007.02.001>
- 2242 Collins, A.S., 2006. Madagascar and the amalgamation of Central Gondwana. *Gondwana Res.* 9, 3–16.
- 2243 <https://doi.org/10.1016/j.gr.2005.10.001>
- 2244 Collins, A.S., 2003. Structure and age of the northern Leeuwin Complex, Western Australia: Constraints  
2245 from field mapping and U–Pb isotopic analysis. *Aust. J. Earth Sci.* 50, 585–599.
- 2246 <https://doi.org/10.1046/j.1440-0952.2003.01014.x>
- 2247 Collins, A.S., Blades, M.L., Merdith, A.S., Foden, J.D., in revision. A late Tonian plate reorganization  
2248 event revealed by a full-plate Proterozoic reconstruction. *Communications Earth and*  
2249 *Environment*.
- 2250 Collins, A.S., Kröner, A., Fitzsimons, I.C.W., Razakamanana, T., 2003. Detrital footprint of the  
2251 Mozambique ocean: U–Pb SHRIMP and Pb evaporation zircon geochronology of  
2252 metasedimentary gneisses in eastern Madagascar. *Tectonophysics* 375, 77–99.
- 2253 [https://doi.org/10.1016/S0040-1951\(03\)00334-2](https://doi.org/10.1016/S0040-1951(03)00334-2)
- 2254 Collins, A.S., Pisarevsky, S.A., 2005. Amalgamating eastern Gondwana: The evolution of the Circum-  
2255 Indian Orogens. *Earth-Sci. Rev.* 71, 229–270. <https://doi.org/10.1016/j.earscirev.2005.02.004>
- 2256 Collins, W.J., Belousova, E.A., Kemp, A.I.S., Murphy, J.B., 2011. Two contrasting Phanerozoic orogenic  
2257 systems revealed by hafnium isotope data. *Nat. Geosci.* 4, 333–337.
- 2258 <https://doi.org/10.1038/ngeo1127>
- 2259 Colpron, M., Logan, J.M., Mortensen, J.K., 2002. U–Pb zircon age constraint for late Neoproterozoic  
2260 rifting and initiation of the lower Paleozoic passive margin of western Laurentia. *Can. J. Earth*  
2261 *Sci.* 39, 133–143.
- 2262 Compston, W., Wright, A.E., Toghiani, P., 2002. Dating the Late Precambrian volcanicity of England and  
2263 Wales. *J. Geol. Soc. London* 159, 323–339. <https://doi.org/10.1144/0016-764901-010>
- 2264 Corvino, A.F., Boger, S.D., Henjes-Kunst, F., Wilson, C.J.L., Fitzsimons, I.C.W., 2008. Superimposed  
2265 tectonic events at 2450 Ma, 2100 Ma, 900 Ma and 500 Ma in the North Mawson Escarpment,  
2266 Antarctic Prince Charles Mountains. *Precambrian Res.* 167, 281–302.
- 2267 Cox, G.M., Halverson, G.P., Denyszyn, S., Foden, J., Macdonald, F.A., 2018. Cryogenian magmatism  
2268 along the north-western margin of Laurentia: Plume or rift? *Precambrian Res.* 319, 144–157.

2269 <https://doi.org/10.1016/j.precamres.2017.09.025>

2270 da Silva Filho, A.F., Guimarães, I.P., Van Schmus, W.R., 2002. Crustal Evolution of the Pernambuco-

2271 Alagoas Complex, Borborema Province, NE Brazil: Nd Isotopic Data from Neoproterozoic

2272 Granitoids. *Gondwana Res.* 5, 409–422. [https://doi.org/10.1016/S1342-937X\(05\)70732-2](https://doi.org/10.1016/S1342-937X(05)70732-2)

2273 Daczko, N.R., Halpin, J.A., Fitzsimons, I.C.W., Whittaker, J.M., 2018. A cryptic Gondwana-forming

2274 orogen located in Antarctica. *Sci. Rep.* 8, 8371. <https://doi.org/10.1038/s41598-018-26530-1>

2275 Dallmeyer, R.D., 1989. Contrasting accreted terranes in the southern Appalachian Orogen, basement

2276 beneath the Atlantic and Gulf Coastal Plains, and West African orogens. *Precambrian Res.* 42,

2277 387–409. [https://doi.org/10.1016/0301-9268\(89\)90021-1](https://doi.org/10.1016/0301-9268(89)90021-1)

2278 Dalziel, I.W., 1992. On the organization of American plates in the Neoproterozoic and the breakout of

2279 Laurentia. *GSA Today* 2.

2280 Dalziel, I.W.D., 1997. Neoproterozoic-Paleozoic geography and tectonics: Review, hypothesis,

2281 environmental speculation. *GSA Bulletin* 109, 16–42. [https://doi.org/10.1130/0016-](https://doi.org/10.1130/0016-7606(1997)109<0016:ONPGAT>2.3.CO;2)

2282 [7606\(1997\)109<0016:ONPGAT>2.3.CO;2](https://doi.org/10.1130/0016-7606(1997)109<0016:ONPGAT>2.3.CO;2)

2283 Dalziel, I.W.D., 1991. Pacific margins of Laurentia and East Antarctica-Australia as a conjugate rift pair:

2284 Evidence and implications for an Eocambrian supercontinent. *Geology* 19, 598–601.

2285 Dalziel, I.W.D., Dewey, J.F., 2019. The classic Wilson cycle revisited. Geological Society, London,

2286 Special Publications 470, 19–38. <https://doi.org/10.1144/SP470.1>

2287 Danukalov, N.F., Kondruchina, L.S., Chernikov, A.P., 1983. Paleozoic paleomagnetism of the South and

2288 Central Urals. *BF AN SSSR, Ufa*.

2289 Davies, D.R., Goes, S., Sambridge, M., 2015. On the relationship between volcanic hotspot locations, the

2290 reconstructed eruption sites of large igneous provinces and deep mantle seismic structure. *Earth*

2291 *Planet. Sci. Lett.* 411, 121–130. <https://doi.org/10.1016/j.epsl.2014.11.052>

2292 Davies, R.G., Crawford, A.R., 1971. Petrography and age of the rocks of Bulland Hill, Kirana Hills,

2293 Sarghoda District, West Pakistan. *Geol. Mag.* 108, 235–246.

2294 <https://doi.org/10.1017/S001675680005158X>

2295 Davis, J.K., Meert, J.G., Pandit, M.K., 2014. Paleomagnetic analysis of the Marwar Supergroup,

2296 Rajasthan, India and proposed interbasinal correlations. *J. Asian Earth Sci.* 91, 339–351.

2297 <https://doi.org/10.1016/j.jseaes.2013.09.027>

2298 Deb, M., Thorpe, R.I., Krstic, D., Corfu, F., Davis, D.W., 2001. Zircon U–Pb and galena Pb isotope

2299 evidence for an approximate 1.0 Ga terrane constituting the western margin of the Aravalli–Delhi

2300 orogenic belt, northwestern India. *Precambrian Res.* 108, 195–213.

2301 [https://doi.org/10.1016/S0301-9268\(01\)00134-6](https://doi.org/10.1016/S0301-9268(01)00134-6)

2302 Degtyarev, K., Yakubchuk, A., Tretyakov, A., Kotov, A., Kovach, V., 2017. Precambrian geology of the

- 2303 Kazakh Uplands and Tien Shan: An overview. *Gondwana Res.* 47, 44–75.  
2304 <https://doi.org/10.1016/j.gr.2016.12.014>
- 2305 Degtyarev, K.E., 2011. Tectonic evolution of Early Paleozoic island-arc systems and continental crust  
2306 formation in the Caledonides of Kazakhstan and the North Tien Shan. *Geotectonics/Geotektonika*  
2307 45, 23–50. <https://doi.org/10.1134/S0016852111010031>
- 2308 Degtyarev, K.E., Shatagin, K.N., Kotov, A.B., Sal’Nikova, E.B., Luchitskaya, M.V., Tret’yakov, A.A.,  
2309 Yakovleva, S.Z., 2008. Late Precambrian volcanoplutonic association of the Aktau-Dzhungar  
2310 massif, Central Kazakhstan: Structural position and age, in: *Doklady Earth Sciences*. Springer  
2311 Nature BV, p. 879.
- 2312 Degtyarev, K.E., Tret’yakov, A.A., Ryazantsev, A.V., Kotov, A.B., Sal’nikova, E.B., Aleksandrov, P.A.,  
2313 Anisimova, I.V., 2011. Stenian granitoids of the west Kyrgyz Ridge (North Tien Shan): Position,  
2314 structure, and age determination. *Dokl. Earth Sci.* 441, 1484–1488.  
2315 <https://doi.org/10.1134/S1028334X11110134>
- 2316 Denyszyn, S.W., Halls, H.C., Davis, D.W., Evans, D.A.D., 2009. Paleomagnetism and U–Pb  
2317 geochronology of Franklin dykes in High Arctic Canada and Greenland: a revised age and  
2318 paleomagnetic pole constraining block rotations in the Nares Strait region. *Can. J. Earth Sci.* 46,  
2319 689–705. <https://doi.org/10.1139/E09-042>
- 2320 Deutsch, E.R., 1980. Magnetism of the Mid-Ordovician Tramore Volcanics, SE Ireland, and the Question  
2321 of a Wide Proto-Atlantic Ocean. *J. Geomagn. Geoelectr.* 32, SIII77–SIII98.  
2322 [https://doi.org/10.5636/jgg.32.Supplement3\\_SIII77](https://doi.org/10.5636/jgg.32.Supplement3_SIII77)
- 2323 Deutsch, E.R., Prasad, J.N., 1987. Ordovician paleomagnetic results from the St. George and Table Head  
2324 carbonates of western Newfoundland. *Can. J. Earth Sci.* 24, 1785–1796.  
2325 <https://doi.org/10.1139/e87-170>
- 2326 Direen, N.G., Crawford, A.J., 2003. Fossil seaward-dipping reflector sequences preserved in southeastern  
2327 Australia: a 600 Ma volcanic passive margin in eastern Gondwanaland. *J. Geol. Soc. London* 160,  
2328 985–990. <https://doi.org/10.1144/0016-764903-010>
- 2329 Doig, R., Murphy, J.B., Nance, R.D., 1993. Tectonic significance of the Late Proterozoic Economy River  
2330 gneiss, Cobequid Highlands, Avalon Composite Terrane, Nova Scotia. *Can. J. Earth Sci.* 30, 474–  
2331 479. <https://doi.org/10.1139/e93-035>
- 2332 Domeier, M., 2018. Early Paleozoic tectonics of Asia: Towards a full-plate model. *Geoscience Frontiers*  
2333 9, 789–862. <https://doi.org/10.1016/j.gsf.2017.11.012>
- 2334 Domeier, M., 2016. A plate tectonic scenario for the Iapetus and Rheic oceans. *Gondwana Res.* 36, 275–  
2335 295. <https://doi.org/10.1016/j.gr.2015.08.003>
- 2336 Domeier, M., Font, E., Youbi, N., Davies, J., Nemkin, S., Van der Voo, R., Perrot, M., Benabbou, M.,



- 2337 Boumehdi, M.A., Torsvik, T.H., 2020. On the Early Permian shape of Pangea from  
2338 paleomagnetism at its core. *Gondwana Res.* <https://doi.org/10.1016/j.gr.2020.11.005>
- 2339 Domeier, M., Shephard, G.E., Jakob, J., Gaina, C., Doubrovine, P.V., Torsvik, T.H., 2017. Intraoceanic  
2340 subduction spanned the Pacific in the Late Cretaceous-Paleocene. *Sci Adv* 3.  
2341 <https://doi.org/10.1126/sciadv.aao2303>
- 2342 Domeier, M., Torsvik, T.H., 2017. Full-plate modelling in pre-Jurassic time. *Geol. Mag.* 1–20.  
2343 <https://doi.org/10.1017/S0016756817001005>
- 2344 Domeier, M., Torsvik, T.H., 2014. Plate tectonics in the late Paleozoic. *Geoscience Frontiers* 5, 303–350.  
2345 <https://doi.org/10.1016/j.gsf.2014.01.002>
- 2346 Domeier, M., Van der Voo, R., Torsvik, T.H., 2012. Paleomagnetism and Pangea: The road to  
2347 reconciliation. *Tectonophysics* 514–517, 14–43. <https://doi.org/10.1016/j.tecto.2011.10.021>
- 2348 Dong, Y., Santosh, M., 2016. Tectonic architecture and multiple orogeny of the Qinling Orogenic Belt,  
2349 Central China. *Gondwana Res.* 29, 1–40. <https://doi.org/10.1016/j.gr.2015.06.009>
- 2350 Dong, Y., Yang, Z., Liu, X., Zhang, X., He, D., Li, W., Zhang, F., Sun, S., Zhang, H., Zhang, G., 2014.  
2351 Neoproterozoic amalgamation of the Northern Qinling terrain to the North China Craton:  
2352 Constraints from geochronology and geochemistry of the Kuanping ophiolite. *Precambrian Res.*  
2353 255, 77–95. <https://doi.org/10.1016/j.precamres.2014.09.008>
- 2354 dos Santos, E.J., Van Schmus, W.R., Kozuch, M., Neves, B.B. de B., 2010. The Cariris Velhos tectonic  
2355 event in Northeast Brazil. *J. South Amer. Earth Sci.* 29, 61–76.  
2356 <https://doi.org/10.1016/j.jsames.2009.07.003>
- 2357 Doubrovine, P.V., Steinberger, B., Torsvik, T.H., 2016. A failure to reject: Testing the correlation  
2358 between large igneous provinces and deep mantle structures with EDF statistics. *Geochem.*  
2359 *Geophys. Geosyst.* 17, 1130–1163.
- 2360 Doucet, L.S., Li, Z.-X., Gamal El Dien, H., Pourteau, A., Murphy, J.B., Collins, W.J., Mattielli, N.,  
2361 Olierook, H.K.H., Spencer, C.J., Mitchell, R.N., 2020. Distinct formation history for deep-mantle  
2362 domains reflected in geochemical differences. *Nat. Geosci.* 13, 511–515.  
2363 <https://doi.org/10.1038/s41561-020-0599-9>
- 2364 Douglass, D.N., 1988. Paleomagnetism of Ringerike Old Red Sandstone and related rocks, southern  
2365 Norway: implications for pre-Carboniferous separation of Baltica and British terranes.  
2366 *Tectonophysics* 148, 11–27. [https://doi.org/10.1016/0040-1951\(88\)90157-6](https://doi.org/10.1016/0040-1951(88)90157-6)
- 2367 Dunn, W.J., Elmore, R.D., 1985. Paleomagnetic and petrographic investigation of the Taum Sauk  
2368 Limestone, southeast Missouri. *J. Geophys. Res., Geodyn. Ser.* 90, 11469.  
2369 <https://doi.org/10.1029/JB090iB13p11469>
- 2370 Dutkiewicz, A., Dietmar Müller, R., Cannon, J., Vaughan, S., Zahirovic, S., 2019. Sequestration and

2371 subduction of deep-sea carbonate in the global ocean since the Early Cretaceous. *Geology* 47, 91–  
2372 94. <https://doi.org/10.1130/G45424.1>

2373 Elburg, M.A., Andersen, T., Jacobs, J., Läufer, A., Ruppel, A., Krohne, N., Damaske, D., 2015. One  
2374 Hundred Fifty Million Years of Intrusive Activity in the Sør Rondane Mountains (East  
2375 Antarctica): Implications for Gondwana Assembly. *J. Geol.* <https://doi.org/10.1086/684052>

2376 Elming, S.-Å., Pisarevsky, S.A., Layer, P., Bylund, G., 2014. A palaeomagnetic and <sup>40</sup>Ar/<sup>39</sup>Ar study of  
2377 mafic dykes in southern Sweden: A new Early Neoproterozoic key-pole for the Baltic Shield and  
2378 implications for Sveconorwegian and Grenville loops. *Precambrian Res.* 244, 192–206.  
2379 <https://doi.org/10.1016/j.precamres.2013.12.007>

2380 Elston, D.P., Bressler, S.L., 1977. Paleomagnetic poles and polarity zonation from Cambrian and  
2381 Devonian strata of Arizona. *Earth Planet. Sci. Lett.* 36, 423–433. [https://doi.org/10.1016/0012-](https://doi.org/10.1016/0012-821X(77)90067-X)  
2382 [821X\(77\)90067-X](https://doi.org/10.1016/0012-821X(77)90067-X)

2383 Embleton, B.J.J., Williams, G.E., 1986. Low palaeolatitude of deposition for late Precambrian periglacial  
2384 varvites in South Australia: implications for palaeoclimatology. *Earth Planet. Sci. Lett.* 79, 419–  
2385 430. [https://doi.org/10.1016/0012-821X\(86\)90197-4](https://doi.org/10.1016/0012-821X(86)90197-4)

2386 England, P., Molnar, P., 1990. Surface uplift, uplift of rocks, and exhumation of rocks. *Geology* 18,  
2387 1173–1177. [https://doi.org/10.1130/0091-7613\(1990\)018<1173:SUUORA>2.3.CO;2](https://doi.org/10.1130/0091-7613(1990)018<1173:SUUORA>2.3.CO;2)

2388 Evans, D., 2003. True polar wander and supercontinents. *Tectonophysics.* [https://doi.org/10.1016/S0040-](https://doi.org/10.1016/S0040-1951(02)00642-X)  
2389 [1951\(02\)00642-X](https://doi.org/10.1016/S0040-1951(02)00642-X)

2390 Evans, D.A.D., 2013. Reconstructing pre-Pangean supercontinents. *Bull. Am. Assoc. Hist. Nurs.*

2391 Evans, D.A.D., 2009. The palaeomagnetically viable, long-lived and all-inclusive Rodinia supercontinent  
2392 reconstruction. *Geological Society, London, Special.*

2393 Evans, D.A.D., Li, Z.X., Kirschvink, J.L., Wingate, M.T.D., 2000. A high-quality mid-Neoproterozoic  
2394 paleomagnetic pole from South China, with implications for ice ages and the breakup  
2395 configuration of Rodinia. *Precambrian Res.* 100, 313–334. [https://doi.org/10.1016/S0301-](https://doi.org/10.1016/S0301-9268(99)00079-0)  
2396 [9268\(99\)00079-0](https://doi.org/10.1016/S0301-9268(99)00079-0)

2397 Evans, D.A.D., Trindade, R.I.F., Catelani, E.L., D'Agrella-Filho, M.S., Heaman, L.M., Oliveira, E.P.,  
2398 Söderlund, U., Ernst, R.E., Smirnov, A.V., Salminen, J.M., 2016. Return to Rodinia? Moderate to  
2399 high palaeolatitude of the São Francisco/Congo craton at 920 Ma. *Geological Society, London,*  
2400 *Special Publications* 424, 167–190. <https://doi.org/10.1144/SP424.1>

2401 Eyster, A., Weiss, B.P., Karlstrom, K., Macdonald, F.A., 2019. Paleomagnetism of the Chuar Group and  
2402 evaluation of the late Tonian Laurentian apparent polar wander path with implications for the  
2403 makeup and breakup of Rodinia. *GSA Bulletin.* <https://doi.org/10.1130/B32012.1>

2404 Fang, D., Wang, P., Shen, Z., Tan, X., 1998. Cenozoic paleomagnetic results and Phanerozoic apparent

2405 polar wandering path of Tarim Block. *Sci. China Ser. D Earth Sci.*

2406 Fang, D.-J., Jin, G.-H., Jiang, L.-P., Wang, P.-Y., Wang, Z.-L., 1996. Paleozoic paleomagnetic results and  
2407 the tectonic significance of Tarim Plate. *Acta Geophysica Sinica* 39, 532–542.

2408 Farr, M.R., Gose, W.A., 1991. Paleomagnetism of the Cambrian Moore Hollow Group, Texas: Evidence  
2409 for a primary magnetization carried by detrital magnetite. *J. Geophys. Res.* 96, 9895.  
2410 <https://doi.org/10.1029/91JB00337>

2411 Fezaa, N., Liégeois, J.-P., Abdallah, N., Cherfouh, E.H., De Waele, B., Bruguier, O., Ouabadi, A., 2010.  
2412 Late Ediacaran geological evolution (575–555 Ma) of the Djanet Terrane, Eastern Hoggar,  
2413 Algeria, evidence for a Murzukian intracontinental episode. *Precambrian Res.* 180, 299–327.

2414 Fioretti, A.M., Black, L.P., Foden, J., Visonà, D., 2005. Grenville-age magmatism at the South Tasman  
2415 Rise (Australia): A new piercing point for the reconstruction of Rodinia. *Geology* 33, 769–772.  
2416 <https://doi.org/10.1130/G21671.1>

2417 Fitzsimons, I.C.W., 2003. Proterozoic basement provinces of southern and southwestern Australia, and  
2418 their correlation with Antarctica. Geological Society, London, Special Publications 206, 93–130.  
2419 <https://doi.org/10.1144/GSL.SP.2003.206.01.07>

2420 Flament, N., Williams, S., Müller, R.D., Gurnis, M., Bower, D.J., 2017. Origin and evolution of the deep  
2421 thermochemical structure beneath Eurasia. *Nat. Commun.* 8, 14164.  
2422 <https://doi.org/10.1038/ncomms14164>

2423 French, A.N., Van der Voo, R., 1979. The magnetization of the Rose Hill Formation at the classical site  
2424 of Graham's Fold Test. *J. Geophys. Res.* 84, 7688–7696.  
2425 <https://doi.org/10.1029/JB084iB13p07688>

2426 Fu, X., Zhang, S., Li, Haiyan, Ding, J., Li, Huaikun, Yang, T., Wu, H., Yuan, H., Lv, J., 2015. New  
2427 paleomagnetic results from the Huaibei Group and Neoproterozoic mafic sills in the North China  
2428 Craton and their paleogeographic implications. *Precambrian Res.* 269, 90–106.  
2429 <https://doi.org/10.1016/j.precamres.2015.08.013>

2430 Furnes, H., de Wit, M., Dilek, Y., 2014. Four billion years of ophiolites reveal secular trends in oceanic  
2431 crust formation. *Geoscience Frontiers* 5, 571–603. <https://doi.org/10.1016/j.gsf.2014.02.002>

2432 Gallet, Y., Pavlov, V., 1996. Magnetostratigraphy of the Moyero River Section (North-Western Siberia):  
2433 Constraints On Geomagnetic Reversal Frequency During the Early Palaeozoic. *Geophys. J. Int.*  
2434 125, 95–105. <https://doi.org/10.1111/j.1365-246X.1996.tb06536.x>

2435 Gallet, Y., Pavlov, V., Courtillot, V., 2003. Magnetic reversal frequency and apparent polar wander of the  
2436 Siberian platform in the earliest Palaeozoic, inferred from the Khorbusuonka river section  
2437 (northeastern Siberia). *Geophys. J. Int.* 154, 829–840.

2438 Ganade de Araujo, C.E., Cordani, U.G., Weinberg, R.F., Basei, M.A.S., Armstrong, R., Sato, K., 2014.

2439 Tracing Neoproterozoic subduction in the Borborema Province (NE-Brazil): Clues from U-Pb  
2440 geochronology and Sr-Nd-Hf-O isotopes on granitoids and migmatites. *Lithos* 202–203, 167–  
2441 189. <https://doi.org/10.1016/j.lithos.2014.05.015>

2442 Gao, J., Wang, X.-S., Klemd, R., Jiang, T., Qian, Q., Mu, L.-X., Ma, Y.-Z., 2015. Record of assembly and  
2443 breakup of Rodinia in the Southwestern Altaids: Evidence from Neoproterozoic magmatism in  
2444 the Chinese Western Tianshan Orogen. *J. Asian Earth Sci.* 113, 173–193.  
2445 <https://doi.org/10.1016/j.jseaes.2015.02.002>

2446 Gao, R.F., Huang, H.L., Zhu, Z.W., Liu, H.S., Fan, Y.Q., Qing, X.J., 1983. The study of paleomagnetism  
2447 in northeastern Sino-Korean massif during Pre-late Paleozoic. *Contr. Project of Plate Tectonics in*  
2448 *North China* 1, 265–274.

2449 Garnero, E.J., Lay, T., McNamara, A., 2007. Implications of lower-mantle structural heterogeneity for the  
2450 existence and nature of whole-mantle plumes. *Special Papers-Geological Society of America* 430,  
2451 79.

2452 Ge, R., Zhu, W., Wilde, S.A., He, J., Cui, X., Wang, X., Bihai, Z., 2014. Neoproterozoic to Paleozoic  
2453 long-lived accretionary orogeny in the northern Tarim Craton: accretionary orogeny in northern  
2454 Tarim. *Tectonics* 33, 302–329. <https://doi.org/10.1002/2013TC003501>

2455 Geissman, J.W., Jackson, M., Harlan, S.S., Van Der Voo, R., 1991. Paleomagnetism of Latest Cambrian-  
2456 Early Ordovician and Latest Cretaceous-Early Tertiary rocks of the Florida Mountains, southwest  
2457 New Mexico. *J. Geophys. Res. [Solid Earth]* 96, 6053–6071.

2458 Gernon, T.M., Hincks, T.K., Tyrrell, T., Rohling, E.J., Palmer, M.R., 2016. Snowball Earth ocean  
2459 chemistry driven by extensive ridge volcanism during Rodinia breakup. *Nat. Geosci.* 9, 242.  
2460 <https://doi.org/10.1038/ngeo2632>

2461 Gerya, T., 2014. Precambrian geodynamics: Concepts and models. *Gondwana Res.* 25, 442–463.  
2462 <https://doi.org/10.1016/j.gr.2012.11.008>

2463 Godd ris, Y., Le Hir, G., Macouin, M., Donnadi u, Y., Hubert-Th  ou, L., Dera, G., Aretz, M., Fluteau,  
2464 F., Li, Z.X., Halverson, G.P., 2017. Paleogeographic forcing of the strontium isotopic cycle in the  
2465 Neoproterozoic. *Gondwana Res.* 42, 151–162. <https://doi.org/10.1016/j.gr.2016.09.013>

2466 Goodge, J.W., Fanning, C.M., Fisher, C.M., Vervoort, J.D., 2017. Proterozoic crustal evolution of central  
2467 East Antarctica: Age and isotopic evidence from glacial igneous clasts, and links with Australia  
2468 and Laurentia. *Precambrian Res.* 299, 151–176. <https://doi.org/10.1016/j.precamres.2017.07.026>

2469 Gordon, R.G., Cox, A., O’Hare, S., 1984. Paleomagnetic Euler poles and the apparent polar wander and  
2470 absolute motion of North America since the Carboniferous. *Tectonics* 3, 499–537.  
2471 <https://doi.org/10.1029/TC003i005p00499>

2472 Granot, R., 2016. Palaeozoic oceanic crust preserved beneath the eastern Mediterranean. *Nat. Geosci.* 9,

2473 701–705. <https://doi.org/10.1038/ngeo2784>

2474 Gregory, L.C., Meert, J.G., Bingen, B., Pandit, M.K., Torsvik, T.H., 2009. Paleomagnetism and  
2475 geochronology of the Malani Igneous Suite, Northwest India: Implications for the configuration  
2476 of Rodinia and the assembly of Gondwana. *Precambrian Res.* 170, 13–26.  
2477 <https://doi.org/10.1016/j.precamres.2008.11.004>

2478 Guimarães, I.P., Van Schmus, W.R., de Brito Neves, B.B., Bretas Bittar, S.M., Silva Filho, A.F.,  
2479 Armstrong, R., 2012. U–Pb zircon ages of orthogneisses and supracrustal rocks of the Cariris  
2480 Velhos belt: Onset of Neoproterozoic rifting in the Borborema Province, NE Brazil. *Precambrian*  
2481 *Res.* 192–195, 52–77. <https://doi.org/10.1016/j.precamres.2011.10.008>

2482 Gurnis, M., Turner, M., Zahirovic, S., DiCaprio, L., Spasojevic, S., Müller, R.D., Boyden, J., Seton, M.,  
2483 Manea, V.C., Bower, D.J., 2012. Plate tectonic reconstructions with continuously closing plates.  
2484 *Comput. Geosci.* 38, 35–42. <https://doi.org/10.1016/j.cageo.2011.04.014>

2485 Gurnis, M., Yang, T., Cannon, J., Turner, M., Williams, S., Flament, N., Müller, R.D., 2018. Global  
2486 tectonic reconstructions with continuously deforming and evolving rigid plates. *Comput. Geosci.*  
2487 116, 32–41. <https://doi.org/10.1016/j.cageo.2018.04.007>

2488 Guynn, J., Kapp, P., Gehrels, G.E., Ding, L., 2012. U–Pb geochronology of basement rocks in central  
2489 Tibet and paleogeographic implications. *J. Asian Earth Sci.* 43, 23–50.  
2490 <https://doi.org/10.1016/j.jseaes.2011.09.003>

2491 Guynn, J.H., Kapp, P., Pullen, A., Heizler, M., Gehrels, G., Ding, L., 2006. Tibetan basement rocks near  
2492 Amdo reveal “missing” Mesozoic tectonism along the Bangong suture, central Tibet. *Geology* 34,  
2493 505–508. <https://doi.org/10.1130/G22453.1>

2494 Hadj-Kaddour, Z., Liégeois, J.-P., Demaiffe, D., Caby, R., 1998. The alkaline–peralkaline granitic post-  
2495 collisional Tin Zebane dyke swarm (Pan-African Tuareg shield, Algeria): prevalent mantle  
2496 signature and late agpaitic differentiation. *Lithos* 45, 223–243. [https://doi.org/10.1016/S0024-4937\(98\)00033-4](https://doi.org/10.1016/S0024-4937(98)00033-4)

2498 Haldar, S.K., Deb, M., 2001. Geology and mineralization of Rajpura-Dariba lead-zinc belt, Rajasthan, in:  
2499 Deb, M., Goodfellow, W.D. (Eds.), *Sediment-Hosted Lead-Zinc Deposit Modeling Program*.  
2500 Delhi-Udaipur, Elsevier, New Dehli, pp. 177–187.

2501 Hall, S.A., Evans, I., 1988. Paleomagnetic study of the Ordovician Table Head Group, Port au Port  
2502 Peninsula, Newfoundland. *Can. J. Earth Sci.* 25, 1407–1419. <https://doi.org/10.1139/e88-135>

2503 Halpin, J.A., Daczko, N.R., Kobler, M.E., Whittaker, J.M., 2017. Strike-slip tectonics during the  
2504 Neoproterozoic–Cambrian assembly of East Gondwana: Evidence from a newly discovered  
2505 microcontinent in the Indian Ocean .... *Gondwana Res.*

2506 Halpin, J.A., Jensen, T., McGoldrick, P., Meffre, S., Berry, R.F., Everard, J.L., Calver, C.R., Thompson,

2507 J., Goemann, K., Whittaker, J.M., 2014. Authigenic monazite and detrital zircon dating from the  
2508 Proterozoic Rocky Cape Group, Tasmania: Links to the Belt-Purcell Supergroup, North America.  
2509 *Precambrian Res.* 250, 50–67. <https://doi.org/10.1016/j.precamres.2014.05.025>

2510 Hamilton, M.A., Murphy, J.B., 2004. Tectonic significance of a Llanvirn age for the Dunn Point volcanic  
2511 rocks, Avalon terrane, Nova Scotia, Canada: implications for the evolution of the Iapetus and  
2512 Rheic Oceans. *Tectonophysics* 379, 199–209. <https://doi.org/10.1016/j.tecto.2003.11.006>

2513 Han, Z., Yang, Z., Tong, Y., Jing, X., 2015. New paleomagnetic results from Late Ordovician rocks of the  
2514 Yangtze Block, South China, and their paleogeographic implications. *J. Geophys. Res. [Solid  
2515 Earth]* 120, 4759–4772.

2516 Handke, M.J., Tucker, R.D., Ashwal, L.D., 1999. Neoproterozoic continental arc magmatism in west-  
2517 central Madagascar. *Geology* 27, 351–354. [https://doi.org/10.1130/0091-  
2518 7613\(1999\)027<0351:NCAMIW>2.3.CO;2](https://doi.org/10.1130/0091-7613(1999)027<0351:NCAMIW>2.3.CO;2)

2519 Hargraves, R.B., Dawson, E.M., Houten, F.B., 1987. Palaeomagnetism and age of mid-Palaeozoic ring  
2520 complexes in Niger, West Africa, and tectonic implications. *Geophys. J. Int.* 90, 705–729.  
2521 <https://doi.org/10.1111/j.1365-246X.1987.tb00750.x>

2522 Harlan, S.S., Geissman, J.W., Snee, L.W., 2008. Paleomagnetism of Proterozoic mafic dikes from the  
2523 Tobacco Root Mountains, southwest Montana. *Precambrian Res.* 163, 239–264.  
2524 <https://doi.org/10.1016/j.precamres.2007.12.002>

2525 Hartz, E.H., Torsvik, T.H., 2002. Baltica upside down: A new plate tectonic model for Rodinia and the  
2526 Iapetus Ocean. *Geology* 30, 255–258. [https://doi.org/10.1130/0091-  
2527 7613\(2002\)030<0255:BUDANP>2.0.CO;2](https://doi.org/10.1130/0091-7613(2002)030<0255:BUDANP>2.0.CO;2)

2528 He, T., Zhu, M., Mills, B.J.W., Wynn, P.M., Zhuravlev, A.Y., Tostevin, R., Pogge von Strandmann,  
2529 P.A.E., Yang, A., Poulton, S.W., Shields, G.A., 2019. Possible links between extreme oxygen  
2530 perturbations and the Cambrian radiation of animals. *Nat. Geosci.* 12, 468–474.  
2531 <https://doi.org/10.1038/s41561-019-0357-z>

2532 Heatherington, A.L., Mueller, P.A., Nutman, A.P., 1996. Neoproterozoic magmatism in the Suwannee  
2533 terrane: Implications for terrane correlation. *Geological Society of America Special Papers* 304,  
2534 257–268.

2535 Henry, B., Liégeois, J.P., Nouar, O., Derder, M.E.M., Bayou, B., Bruguier, O., Ouabadi, A., Belhai, D.,  
2536 Amenna, M., Hemmi, A., Ayache, M., 2009. Repeated granitoid intrusions during the  
2537 Neoproterozoic along the western boundary of the Saharan metacraton, Eastern Hoggar, Tuareg  
2538 shield, Algeria: An AMS and U–Pb zircon age study. *Tectonophysics* 474, 417–434.  
2539 <https://doi.org/10.1016/j.tecto.2009.04.022>

2540 Heron, P.J., Murphy, J.B., Nance, D.R., Pysklywec, R.N., 2020. Pannotia’s mantle signature: the quest for

2541 supercontinent identification. Geological Society, London, Special Publications 503.  
2542 <https://doi.org/10.1144/SP503-2020-7>

2543 Hibbard, J.P., van Staal, C.R., Miller, B.V., 2007. Links among Carolina, Avalonia, and Ganderia in the  
2544 Appalachian peri-Gondwanan realm. Geological Society of America Special Papers 433, 291–  
2545 311.

2546 Hochmuth, K., Gohl, K., Uenzelmann-Neben, G., 2015. Playing jigsaw with large igneous provinces—A  
2547 plate tectonic reconstruction of Ontong Java Nui, West Pacific. *Geochem. Geophys. Geosyst.* 16,  
2548 3789–3807.

2549 Hodych, J.P., 1989. Limestones of western Newfoundland that magnetized before Devonian folding but  
2550 after Middle Ordovician lithification. *Geophys. Res. Lett.* 16, 93–96.  
2551 <https://doi.org/10.1029/GL016i001p00093>

2552 Hodych, J.P., Buchan, K.L., 1998. Palaeomagnetism of the ca. 440 Ma Cape St Mary's sills of the Avalon  
2553 Peninsula of Newfoundland: implications for Iapetus Ocean closure. *Geophys. J. Int.* 135, 155–  
2554 164. <https://doi.org/10.1046/j.1365-246X.1998.00263.x>

2555 Hodych, J.P., Cox, R.A., Košler, J., 2004. An equatorial Laurentia at 550 Ma confirmed by Grenvillian  
2556 inherited zircons dated by LAM ICP-MS in the Skinner Cove volcanics of western  
2557 Newfoundland: implications for inertial interchange true polar wander. *Precambrian Res.* 129,  
2558 93–113. <https://doi.org/10.1016/j.precamres.2003.10.012>

2559 Hoffman, P.F., 1991. Did the breakout of Laurentia turn Gondwanaland inside-out? *Science* 252, 1409–  
2560 1412. <https://doi.org/10.1126/science.252.5011.1409>

2561 Hoffman, P.F., Kaufman, A.J., Halverson, G.P., Schrag, D.P., 1998. A Neoproterozoic snowball earth.  
2562 *Science* 281, 1342–1346. <https://doi.org/10.1126/science.281.5381.1342>

2563 Hoffman, P.F., Schrag, D.P., 2002. The snowball Earth hypothesis: testing the limits of global change.  
2564 *Terra Nova* 14, 129–155. <https://doi.org/10.1046/j.1365-3121.2002.00408.x>

2565 Hofmann, M., Linnemann, U., Rai, V., Becker, S., Gärtner, A., Sagawe, A., 2011. The India and South  
2566 China cratons at the margin of Rodinia—Synchronous Neoproterozoic magmatism revealed by  
2567 LA-ICP-MS zircon analyses. *Lithos* 123, 176–187.

2568 Hopper, E., Fischer, K.M., Wagner, L.S., Hawman, R.B., 2017. Reconstructing the end of the  
2569 Appalachian orogeny. *Geology* 45, 15–18. <https://doi.org/10.1130/G38453.1>

2570 Hounslow, M.W., Domeier, M., Biggin, A.J., 2018. Subduction flux modulates the geomagnetic polarity  
2571 reversal rate. *Tectonophysics* 742–743, 34–49. <https://doi.org/10.1016/j.tecto.2018.05.018>

2572 Hu, P.-Y., Zhai, Q.-G., Wang, J., Tang, Y., Wang, H.-T., Hou, K.-J., 2018. Precambrian origin of the  
2573 North Lhasa terrane, Tibetan Plateau: Constraint from early Cryogenian back-arc magmatism.  
2574 *Precambrian Res.* 313, 51–67. <https://doi.org/10.1016/j.precamres.2018.05.014>

- 2575 Hu, X., Garzanti, E., Wang, J., Huang, W., An, W., Webb, A., 2016. The timing of India-Asia collision  
2576 onset--Facts, theories, controversies. *Earth-Sci. Rev.* 160, 264–299.
- 2577 Huang, B., He, Z., Zong, K., Zhang, Z., 2014. Zircon U–Pb and Hf isotopic study of Neoproterozoic  
2578 granitic gneisses from the Alatage area, Xinjiang: constraints on the Precambrian crustal  
2579 evolution in the Central Tianshan Block. *Chin. Sci. Bull.* 59, 100–112.  
2580 <https://doi.org/10.1007/s11434-013-0010-y>
- 2581 Huang, B., Xu, B., Zhang, C., Li, Y., Zhu, R., 2005. Paleomagnetism of the Baiyisi volcanic rocks (ca.  
2582 740Ma) of Tarim, Northwest China: A continental fragment of Neoproterozoic Western  
2583 Australia? *Precambrian Res.* 142, 83–92. <https://doi.org/10.1016/j.precamres.2005.09.006>
- 2584 Huang, B., Yang, Z., Otofujii, Y.-I., Zhu, R., 1999. Early Paleozoic paleomagnetic poles from the western  
2585 part of the North China Block and their implications. *Tectonophysics* 308, 377–402.  
2586 [https://doi.org/10.1016/S0040-1951\(99\)00098-0](https://doi.org/10.1016/S0040-1951(99)00098-0)
- 2587 Huang, B.C., Otofujii, Y., Yang, Z.Y., 1999. Paleomagnetic constraints on the tectonic relationship  
2588 between the Alashan/Hexi Corridor Terrane and the North China Block. *Geophys. Res. Lett.* 26,  
2589 787–790. <https://doi.org/10.1029/1999GL900097>
- 2590 Huang, H., Cawood, P.A., Hou, M., Xiong, F., Ni, S., 2019. Provenance of latest Mesoproterozoic to  
2591 early Neoproterozoic (meta)-sedimentary rocks and implications for paleographic reconstruction  
2592 of the Yili Block. *Gondwana Res.*
- 2593 Huang, K., Opdyke, N.D., Zhu, R., 2000. Further paleomagnetic results from the Silurian of the Yangtze  
2594 Block and their implications. *Earth Planet. Sci. Lett.* 175, 191–202.  
2595 [https://doi.org/10.1016/S0012-821X\(99\)00302-7](https://doi.org/10.1016/S0012-821X(99)00302-7)
- 2596 Huang, Z., Long, X., Kröner, A., Yuan, C., Wang, Y., Chen, B., Zhang, Y., 2015. Neoproterozoic granitic  
2597 gneisses in the Chinese Central Tianshan Block: Implications for tectonic affinity and  
2598 Precambrian crustal evolution. *Precambrian Res.* 269, 73–89.  
2599 <https://doi.org/10.1016/j.precamres.2015.08.005>
- 2600 Iosifidi, A.G., Khramov, A.N., Rodionov, V.P., Pisarevskii, S.A., Popov, V.V., 1999. Geomagnetic  
2601 reversals in the Early Paleozoic: 2. A nonsynchronous record of Middle Ordovician reversals in  
2602 the Berezovskaya section, southern Siberian Platform. *Izv. Phys. Solid Earth* 35, 24–32.
- 2603 Jackson, M., Van der Voo, R., 1985. A Lower Ordovician paleomagnetic pole from the Oneota dolomite,  
2604 Upper Mississippi River Valley. *J. Geophys. Res., Geol. Soc. Am.* 90, 10449.  
2605 <https://doi.org/10.1029/JB090iB12p10449>
- 2606 Jacobs, J., Elburg, M., Läufer, A., Kleinhanns, I.C., Henjes-Kunst, F., Estrada, S., Ruppel, A.S.,  
2607 Damaske, D., Montero, P., Bea, F., 2015. Two distinct Late Mesoproterozoic/Early  
2608 Neoproterozoic basement provinces in central/eastern Dronning Maud Land, East Antarctica: The



2609 missing link, 15–21°E. *Precambrian Res.* 265, 249–272.  
2610 <https://doi.org/10.1016/j.precamres.2015.05.003>

2611 Jacobs, J., Opås, B., Elburg, M.A., Läufer, A., Estrada, S., Ksienzyk, A.K., Damaske, D., Hofmann, M.,  
2612 2017. Cryptic sub-ice geology revealed by a U-Pb zircon study of glacial till in Dronning Maud  
2613 Land, East Antarctica. *Precambrian Res.* 294, 1–14.  
2614 <https://doi.org/10.1016/j.precamres.2017.03.012>

2615 Jarrard, R.D., 2003. Subduction fluxes of water, carbon dioxide, chlorine, and potassium. *Geochem.*  
2616 *Geophys. Geosyst.*, *Geophys. Monogr. Ser.* 4. <https://doi.org/10.1029/2002GC000392>

2617 Jeleńska, M., Bakhmutov, V., Konstantinienko, L., 2005. Paleomagnetic and rock magnetic data from the  
2618 Silurian succession of the Dniester basin, Ukraine. *Phys. Earth Planet. Inter.* 149, 307–320.  
2619 <https://doi.org/10.1016/j.pepi.2004.10.005>

2620 Jeleńska, M., Kaździałko-Hofmokr, M., Bakhmutov, V., Poliachenko, I., Ziólkowski, P., 2015.  
2621 Palaeomagnetic and rock magnetic study of Lower Devonian sediments from Podolia, SW  
2622 Ukraine: remagnetization problems. *Geophys. J. Int.* 200, 557–573.  
2623 <https://doi.org/10.1093/gji/ggu411>

2624 Jian, P., Kröner, A., Jahn, B.-M., Windley, B.F., Shi, Y., Zhang, W., Zhang, F., Miao, L., Tomurhuu, D.,  
2625 Liu, D., 2014. Zircon dating of Neoproterozoic and Cambrian ophiolites in West Mongolia and  
2626 implications for the timing of orogenic processes in the central part of the Central Asian Orogenic  
2627 Belt. *Earth-Sci. Rev.* 133, 62–93. <https://doi.org/10.1016/j.earscirev.2014.02.006>

2628 Jiang, G., Sohl, L.E., Christie-Blick, N., 2003. Neoproterozoic stratigraphic comparison of the Lesser  
2629 Himalaya (India) and Yangtze block (south China): Paleogeographic implications. *Geology* 31,  
2630 917–920. <https://doi.org/10.1130/G19790.1>

2631 Jing, X.-Q., Yang, Z., Tong, Y., Han, Z., 2015. A revised paleomagnetic pole from the mid-  
2632 Neoproterozoic Liantuo Formation in the Yangtze block and its paleogeographic implications.  
2633 *Precambrian Res.* 268, 194–211. <https://doi.org/10.1016/j.precamres.2015.07.007>

2634 Johnson, P.R., Andresen, A., Collins, A.S., Fowler, A.R., Fritz, H., Ghebreab, W., Kusky, T., Stern, R.J.,  
2635 2011. Late Cryogenian–Ediacaran history of the Arabian–Nubian Shield: a review of  
2636 depositional, plutonic, structural, and tectonic events in the closing stages of the northern East  
2637 African Orogen. *J. Afr. Earth. Sci.* 61, 167–232.

2638 Johnson, R.J.E., Van Der Voo, R., 1990. Pre-folding magnetization reconfirmed for the Late Ordovician-  
2639 Early Silurian Dunn Point volcanics, Nova Scotia. *Tectonophysics* 178, 193–205.  
2640 [https://doi.org/10.1016/0040-1951\(90\)90146-Y](https://doi.org/10.1016/0040-1951(90)90146-Y)

2641 Johnson, R.J.E., Van der Voo, R., 1985. Middle Cambrian paleomagnetism of the Avalon Terrane in  
2642 Cape Breton Island, Nova Scotia. *Tectonics* 4, 629–651.

2643 <https://doi.org/10.1029/TC004i007p00629>

2644 Just, J., Schulz, B., de Wall, H., Jourdan, F., Pandit, M.K., 2011. Monazite CHIME/EPMA dating of  
2645 Erinpura granitoid deformation: Implications for Neoproterozoic tectono-thermal evolution of  
2646 NW India. *Gondwana Res.* 19, 402–412. <https://doi.org/10.1016/j.gr.2010.08.002>

2647 Kamo, S.L., Gower, C.F., 1994. Note: U-Pb baddeleyite dating clarifies age of characteristic  
2648 paleomagnetic remanence of Long Range dykes, southeastern Labrador.

2649 Karlsen, K.S., Conrad, C.P., Magni, V., 2019. Deep Water Cycling and Sea Level Change Since the  
2650 Breakup of Pangea. *Geochem. Geophys. Geosyst.* 20, 2919–2935.  
2651 <https://doi.org/10.1029/2019GC008232>

2652 Keppie, J.D., Davis, D.W., Krogh, T.E., 1998. U-Pb geochronological constraints on Precambrian  
2653 stratified units in the Avalon Composite Terrane of Nova Scotia, Canada: tectonic implications.  
2654 *Can. J. Earth Sci.* 35, 222–236. <https://doi.org/10.1139/e97-109>

2655 Keppie, J.D., Dostal, J., 1998. Birth of the Avalon arc in Nova Scotia, Canada: geochemical evidence for  
2656 700–630 Ma back-arc rift volcanism off Gondwana. *Geol. Mag.* 135, 171–181.

2657 Khramov, A.N., Iosifidi, A.G., 2009. Paleomagnetism of the Lower Ordovician and Cambrian  
2658 sedimentary rocks in the section of the Narva river right bank: For the construction of the Baltic  
2659 kinematic model in the Early Paleozoic. *Izv. Phys. Solid Earth* 45, 465–481.

2660 Kirschvink, J.L., Ripperdan, R.L., Evans, D.A., 1997. Evidence for a Large-Scale Reorganization of Early  
2661 Cambrian Continental Masses by Inertial Interchange True Polar Wander. *Science* 277, 541–545.  
2662 <https://doi.org/10.1126/science.277.5325.541>

2663 Knesel, K.M., Cohen, B.E., Vasconcelos, P.M., Thiede, D.S., 2008. Rapid change in drift of the  
2664 Australian plate records collision with Ontong Java plateau. *Nature* 454, 754–757.  
2665 <https://doi.org/10.1038/nature07138>

2666 Konstantinovskaya, E.A., 2002. The mechanism of continental crust accretion: an example of Western  
2667 Kamchatka. *Geotectonics/Geotektonika* 36, 393–411.

2668 Krogh, T.E., Strong, D.F., O'Brien, S.J., Papezik, V.S., 1988. Precise U–Pb zircon dates from the Avalon  
2669 Terrane in Newfoundland. *Can. J. Earth Sci.* 25, 442–453. <https://doi.org/10.1139/e88-045>

2670 Kröner, A., Alexeiev, D.V., Hegner, E., Rojas-Agramonte, Y., Corsini, M., Chao, Y., Wong, J., Windley,  
2671 B.F., Liu, D., Tretyakov, A.A., 2012. Zircon and muscovite ages, geochemistry, and Nd–Hf  
2672 isotopes for the Aktyuz metamorphic terrane: Evidence for an Early Ordovician collisional belt in  
2673 the northern Tianshan of Kyrgyzstan. *Gondwana Res.* 21, 901–927.  
2674 <https://doi.org/10.1016/j.gr.2011.05.010>

2675 Kroner, A., Windley, B.F., Badarch, G., Tomurtogoo, O., Hegner, E., Jahn, B.M., Gruschka, S., Khain,  
2676 E.V., Demoux, A., Wingate, M.T.D., 2007. Accretionary growth and crust formation in the

2677 Central Asian Orogenic Belt and comparison with the Arabian-Nubian shield. *Memoirs-*  
2678 *Geological Society of America* 200, 181.

2679 Lapique, F., Bertrand, J.M., Meriem, D., 1986. A major Pan-African crustal decoupling zone in the  
2680 Timgaouine area (Western Hoggar, Algeria). *Journal of African Earth Sciences* (1983).  
2681 [https://doi.org/10.1016/0899-5362\(86\)90028-x](https://doi.org/10.1016/0899-5362(86)90028-x)

2682 Lenton, T.M., Dahl, T.W., Daines, S.J., Mills, B.J.W., Ozaki, K., Saltzman, M.R., Porada, P., 2016.  
2683 Earliest land plants created modern levels of atmospheric oxygen. *Proc. Natl. Acad. Sci. U. S. A.*  
2684 113, 9704–9709. <https://doi.org/10.1073/pnas.1604787113>

2685 Levashova, N.M., Bazhenov, M.L., Meert, J.G., Kuznetsov, N.B., Golovanova, I.V., Danukalov, K.N.,  
2686 Fedorova, N.M., 2013. Paleogeography of Baltica in the Ediacaran: Paleomagnetic and  
2687 geochronological data from the clastic Zigan Formation, South Urals. *Precambrian Res.* 236, 16–  
2688 30. <https://doi.org/10.1016/j.precamres.2013.06.006>

2689 Li, M., McNamara, A.K., 2013. The difficulty for subducted oceanic crust to accumulate at the Earth's  
2690 core-mantle boundary. *J. Geophys. Res. [Solid Earth]* 118, 1807–1816.

2691 Li, Yianping, McWilliams, M., Sharps, R., Cox, A., Li, Yongan, Li, Q., Gao, Z., Zhang, Z., Zhai, Y.,  
2692 1990. A Devonian paleomagnetic pole from red beds of the Tarim Block, China. *J. Geophys.*  
2693 *Res., Geodyn. Ser.* 95, 19185. <https://doi.org/10.1029/JB095iB12p19185>

2694 Li, Z., Ding, L., Lippert, P.C., Song, P., Yue, Y., van Hinsbergen, D.J.J., 2016. Paleomagnetic constraints  
2695 on the Mesozoic drift of the Lhasa terrane (Tibet) from Gondwana to Eurasia. *Geology* 44, 727–  
2696 730. <https://doi.org/10.1130/G38030.1>

2697 Li, Z., Ding, L., Song, P., Fu, J., Yue, Y., 2017. Paleomagnetic constraints on the paleolatitude of the  
2698 Lhasa block during the Early Cretaceous: implications for the onset of India–Asia collision and  
2699 latitudinal shortening estimates across Tibet and stable Asia. *Gondwana Res.* 41, 352–372.

2700 Li, Z.X., Bogdanova, S.V., Collins, A.S., Davidson, A., De Waele, B., Ernst, R.E., Fitzsimons, I.C.W.,  
2701 Fuck, R.A., Gladkochub, D.P., Jacobs, J., Karlstrom, K.E., Lu, S., Natapov, L.M., Pease, V.,  
2702 Pisarevsky, S.A., Thrane, K., Vernikovskiy, V., 2008. Assembly, configuration, and break-up  
2703 history of Rodinia: A synthesis. *Precambrian Res.* 160, 179–210.  
2704 <https://doi.org/10.1016/j.precamres.2007.04.021>

2705 Li, Z.-X., Evans, D.A.D., Halverson, G.P., 2013. Neoproterozoic glaciations in a revised global  
2706 palaeogeography from the breakup of Rodinia to the assembly of Gondwanaland. *Sediment.*  
2707 *Geol.* 294, 219–232. <https://doi.org/10.1016/j.sedgeo.2013.05.016>

2708 Li, Z.X., Evans, D.A.D., Zhang, S., 2004. A 90° spin on Rodinia: possible causal links between the  
2709 Neoproterozoic supercontinent, superplume, true polar wander and low-latitude glaciation. *Earth*  
2710 *Planet. Sci. Lett.* 220, 409–421. [https://doi.org/10.1016/S0012-821X\(04\)00064-0](https://doi.org/10.1016/S0012-821X(04)00064-0)

- 2711 Li, Z.X., Mitchell, R.N., Spencer, C.J., Ernst, R., Pisarevsky, S., Kirscher, U., Murphy, J.B., 2019.  
2712 Decoding Earth's rhythms: modulation of supercontinent cycles by longer superocean episodes.  
2713 *Precambrian Res.* 323, 1–5.
- 2714 Li, Z.-X., Zhang, L., Powell, C.M., 1995. South China in Rodinia: Part of the missing link between  
2715 Australia–East Antarctica and Laurentia? *Geology* 23, 407–410.  
2716 [2.3.CO;2">https://doi.org/10.1130/0091-7613\(1995\)023<0407:SCIRPO>2.3.CO;2](https://doi.org/10.1130/0091-7613(1995)023<0407:SCIRPO>2.3.CO;2)
- 2717 Li, Z.-X., Zhong, S., 2009. Supercontinent–superplume coupling, true polar wander and plume mobility:  
2718 Plate dominance in whole-mantle tectonics. *Phys. Earth Planet. Inter.* 176, 143–156.  
2719 <https://doi.org/10.1016/j.pepi.2009.05.004>
- 2720 Liégeois, J.P., Black, R., Navez, J., Latouche, L., 1994. Early and late Pan-African orogenies in the Air  
2721 assembly of terranes (Tuareg shield, Niger). *Precambrian Res.* 67, 59–88.  
2722 [https://doi.org/10.1016/0301-9268\(94\)90005-1](https://doi.org/10.1016/0301-9268(94)90005-1)
- 2723 Liégeois, J.P., Latouche, L., Boughrara, M., Navez, J., Guiraud, M., 2003. The LATEA metacraton  
2724 (Central Hoggar, Tuareg shield, Algeria): behaviour of an old passive margin during the Pan-  
2725 African orogeny. *J. Afr. Earth. Sci.* 37, 161–190. <https://doi.org/10.1016/j.jafrearsci.2003.05.004>
- 2726 Liu, L., Gurnis, M., Seton, M., Saleeby, J., Müller, R.D., Jackson, J.M., 2010. The role of oceanic plateau  
2727 subduction in the Laramide orogeny. *Nat. Geosci.* 3, 353–357. <https://doi.org/10.1038/ngeo829>
- 2728 Liu, L., Spasojevic, S., Gurnis, M., 2008. Reconstructing Farallon plate subduction beneath North  
2729 America back to the Late Cretaceous. *Science* 322, 934–938.  
2730 <https://doi.org/10.1126/science.1162921>
- 2731 Liu, X., Zhao, Y., Chen, H., Song, B., 2017. New zircon U–Pb and Hf–Nd isotopic constraints on the  
2732 timing of magmatism, sedimentation and metamorphism in the northern Prince Charles  
2733 Mountains, East Antarctica. *Precambrian Res.* 299, 15–33.  
2734 <https://doi.org/10.1016/j.precamres.2017.07.012>
- 2735 Lixin, B., Rixiang, Z., Harming, W., Bin, G., Jianjun, L., 1998. New Cambrian paleomagnetic pole for  
2736 Yangtze Block. *Sci. China Ser. D Earth Sci.* 41, 66–71. <https://doi.org/10.1007/BF02984514>
- 2737 Llanos, M.P.I., Tait, J.A., Popov, V., Abalmassova, A., 2005. Palaeomagnetic data from Ediacaran  
2738 (Vendian) sediments of the Arkhangelsk region, NW Russia: An alternative apparent polar  
2739 wander path of Baltica for the Late Proterozoic–Early Palaeozoic. *Earth Planet. Sci. Lett.* 240,  
2740 732–747. <https://doi.org/10.1016/j.epsl.2005.09.063>
- 2741 Loucks, V., Elmore, D.R., 1986. Absolute dating of dedolomitization and the origin of magnetization in  
2742 the Cambrian Morgan Creek Limestone, central Texas. *GSA Bulletin* 97, 486–496.  
2743 [2.0.CO;2">https://doi.org/10.1130/0016-7606\(1986\)97<486:ADODAT>2.0.CO;2](https://doi.org/10.1130/0016-7606(1986)97<486:ADODAT>2.0.CO;2)
- 2744 Lubnina, N.V., Iosifidi, A.G., Khramov, A.N., Popov, V.V., Lewandowski, M., 2007. Paleomagnetism of

2745 the Silurian and Devonian sedimentary formations of Podolia, Ukraine, in: Khramov, A.N. (Ed.),  
2746 Paleomagnetism of the Northern Eurasia Sedimentary Basins (IN RUSSIAN). pp. 105–125.

2747 Lubnina, N.V., Pisarevsky, S.A., Puchkov, V.N., Kozlov, V.I., Sergeeva, N.D., 2014. New paleomagnetic  
2748 data from Late Neoproterozoic sedimentary successions in Southern Urals, Russia: implications  
2749 for the Late Neoproterozoic paleogeography of the Iapetan realm. *Int. J. Earth Sci.* 103, 1317–  
2750 1334. <https://doi.org/10.1007/s00531-014-1013-x>

2751 Macdonald, F.A., Prave, A.R., Petterson, R., Smith, E.F., Pruss, S.B., Oates, K., Waechter, F., Trotsuk,  
2752 D., Fallick, A.E., 2013. The Laurentian record of Neoproterozoic glaciation, tectonism, and  
2753 eukaryotic evolution in Death Valley, California. *GSA Bulletin* 125, 1203–1223.  
2754 <https://doi.org/10.1130/B30789.1>

2755 Martin, M.W., Grazhdankin, D.V., Bowring, S.A., Evans, D.A., Fedonkin, M.A., Kirschvink, J.L., 2000.  
2756 Age of Neoproterozoic bilaterian body and trace fossils, White Sea, Russia: implications for  
2757 metazoan evolution. *Science* 288, 841–845. <https://doi.org/10.1126/science.288.5467.841>

2758 Matthews, K.J., Maloney, K.T., Zahirovic, S., Williams, S.E., Seton, M., Müller, R.D., 2016. Global plate  
2759 boundary evolution and kinematics since the late Paleozoic. *Glob. Planet. Change* 146, 226–250.  
2760 <https://doi.org/10.1016/j.gloplacha.2016.10.002>

2761 Matthews, K.J., Williams, S.E., Whittaker, J.M., Müller, R.D., Seton, M., Clarke, G.L., 2015. Geologic  
2762 and kinematic constraints on Late Cretaceous to mid Eocene plate boundaries in the southwest  
2763 Pacific. *Earth-Sci. Rev.* 140, 72–107. <https://doi.org/10.1016/j.earscirev.2014.10.008>

2764 McCabe, C., Channell, J.E.T., 1990. Paleomagnetic results from volcanic rocks of the Shelve Inlier,  
2765 Wales: evidence for a wide Late Ordovician Iapetus Ocean in Britain. *Earth Planet. Sci. Lett.* 96,  
2766 458–468. [https://doi.org/10.1016/0012-821X\(90\)90020-X](https://doi.org/10.1016/0012-821X(90)90020-X)

2767 McCabe, C., Channell, J.E.T., Woodcock, N.H., 1992. Further paleomagnetic results from the Builth  
2768 Wells Ordovician inlier, Wales. *J. Geophys. Res. [Solid Earth]* 97, 9357–9370.

2769 McCabe, C., Van der Voo, R., Wilkinson, B.H., Devaney, K., 1985. A Middle/Late Silurian  
2770 paleomagnetic pole from limestone reefs of the Wabash Formation, Indiana, USA. *J. Geophys.*  
2771 *Res. [Solid Earth]* 90, 2959–2965.

2772 McCausland, P.J.A., Hodych, J.P., 1998. Paleomagnetism of the 550 Ma Skinner Cove volcanics of  
2773 western Newfoundland and the opening of the Iapetus Ocean. *Earth Planet. Sci. Lett.* 163, 15–29.  
2774 [https://doi.org/10.1016/S0012-821X\(98\)00171-X](https://doi.org/10.1016/S0012-821X(98)00171-X)

2775 McCausland, P.J.A., Van der Voo, R., Hall, C.M., 2007. Circum-Iapetus paleogeography of the  
2776 Precambrian–Cambrian transition with a new paleomagnetic constraint from Laurentia.  
2777 *Precambrian Res.* 156, 125–152. <https://doi.org/10.1016/j.precamres.2007.03.004>

2778 McElhinny, M.W., Cowley, J.A., Edwards, D.J., 1978. Palaeomagnetism of some rocks from Peninsular

2779 India and Kashmir. *Tectonophysics* 50, 41–54. [https://doi.org/10.1016/0040-1951\(78\)90198-1](https://doi.org/10.1016/0040-1951(78)90198-1)

2780 McGee, B., Halverson, G.P., Collins, A.S., 2012. Cryogenian rift-related magmatism and sedimentation:  
2781 South-western Congo Craton, Namibia. *J. Afr. Earth. Sci.* 76, 34–49.  
2782 <https://doi.org/10.1016/j.jafrearsci.2012.09.003>

2783 McKenzie, D.P., Parker, R.L., 1967. The North Pacific: an Example of Tectonics on a Sphere. *Nature*  
2784 216, 1276–1280. <https://doi.org/10.1038/2161276a0>

2785 McKenzie, R.N., Hughes, N.C., Gill, B.C., Myrow, P.M., 2014. Plate tectonic influences on  
2786 Neoproterozoic–early Paleozoic climate and animal evolution. *Geology* 42, 127–130.  
2787 <https://doi.org/10.1130/G34962.1>

2788 McKerrow, W.S., Mac Niocaill, C., Ahlberg, P.E., Clayton, G., Cleal, C.J., Eagar, R.M.C., 2000. The  
2789 Late Palaeozoic relations between Gondwana and Laurussia. Geological Society, London, Special  
2790 Publications 179, 9–20. <https://doi.org/10.1144/GSL.SP.2000.179.01.03>

2791 McMenamin, M.A., McMenamin, M.A., McMenamin, D.L.S., 1990. The emergence of animals: the  
2792 Cambrian breakthrough. Columbia University Press.

2793 Meert, J.G., 2014. Ediacaran–Early Ordovician paleomagnetism of Baltica: A review. *Gondwana Res.* 25,  
2794 159–169. <https://doi.org/10.1016/j.gr.2013.02.003>

2795 Meert, J.G., 2003. A synopsis of events related to the assembly of eastern Gondwana. *Tectonophysics*  
2796 362, 1–40. [https://doi.org/10.1016/S0040-1951\(02\)00629-7](https://doi.org/10.1016/S0040-1951(02)00629-7)

2797 Meert, J.G., 2002. Paleomagnetic Evidence for a Paleo-Mesoproterozoic Supercontinent Columbia.  
2798 *Gondwana Res.* 5, 207–215. [https://doi.org/10.1016/S1342-937X\(05\)70904-7](https://doi.org/10.1016/S1342-937X(05)70904-7)

2799 Meert, J.G., Lieberman, B.S., 2008. The Neoproterozoic assembly of Gondwana and its relationship to  
2800 the Ediacaran–Cambrian radiation. *Gondwana Res.* 14, 5–21.  
2801 <https://doi.org/10.1016/j.gr.2007.06.007>

2802 Meert, J.G., Pandit, M.K., Kamenov, G.D., 2013. Further geochronological and paleomagnetic constraints  
2803 on Malani (and pre-Malani) magmatism in NW India. *Tectonophysics* 608, 1254–1267.  
2804 <https://doi.org/10.1016/j.tecto.2013.06.019>

2805 Meert, J.G., Pandit, M.K., Pradhan, V.R., Banks, J., Sirianni, R., Stroud, M., Newstead, B., Gifford, J.,  
2806 2010. Precambrian crustal evolution of Peninsular India: A 3.0 billion year odyssey. *J. Asian*  
2807 *Earth Sci.* 39, 483–515. <https://doi.org/10.1016/j.jseas.2010.04.026>

2808 Meert, J.G., van der Voo, R., Ayub, S., 1995. Paleomagnetic investigation of the Neoproterozoic Gagwe  
2809 lavas and Mbozi complex, Tanzania and the assembly of Gondwana. *Precambrian Res.* 74, 225–  
2810 244. [https://doi.org/10.1016/0301-9268\(95\)00012-T](https://doi.org/10.1016/0301-9268(95)00012-T)

2811 Meffre, S., Direen, N.G., Crawford, A.J., Kamenetsky, V., 2004. Mafic volcanic rocks on King Island,  
2812 Tasmania: evidence for 579 Ma break-up in east Gondwana. *Precambrian Res.* 135, 177–191.

2813 Merdith, A.S., Atkins, S.E., Tetley, M.G., 2019a. Tectonic Controls on Carbon and Serpentinite Storage  
2814 in Subducted Upper Oceanic Lithosphere for the Past 320 Ma. *Front Earth Sci. Chin.* 7, 332.  
2815 <https://doi.org/10.3389/feart.2019.00332>

2816 Merdith, A.S., Collins, A.S., Williams, S.E., Pisarevsky, S., Foden, J.D., Archibald, D.B., Blades, M.L.,  
2817 Alessio, B.L., Armistead, S., Plavsa, D., Clark, C., Müller, R.D., 2017a. A full-plate global  
2818 reconstruction of the Neoproterozoic. *Gondwana Res.* 50, 84–134.  
2819 <https://doi.org/10.1016/j.gr.2017.04.001>

2820 Merdith, A.S., Williams, S.E., Brune, S., Collins, A.S., Müller, R.D., 2019b. Rift and plate boundary  
2821 evolution across two supercontinent cycles. *Glob. Planet. Change* 173, 1–14.  
2822 <https://doi.org/10.1016/j.gloplacha.2018.11.006>

2823 Merdith, A.S., Williams, S.E., Müller, R.D., Collins, A.S., 2017b. Kinematic constraints on the Rodinia to  
2824 Gondwana transition. *Precambrian Res.* 299, 132–150.  
2825 <https://doi.org/10.1016/j.precamres.2017.07.013>

2826 Metcalfe, I., 2013. Gondwana dispersion and Asian accretion: Tectonic and palaeogeographic evolution  
2827 of eastern Tethys. *J. Asian Earth Sci.* 66, 1–33. <https://doi.org/10.1016/j.jseaes.2012.12.020>

2828 Metcalfe, I., 2011. Palaeozoic–Mesozoic history of SE Asia. Geological Society, London, Special  
2829 Publications 355, 7–35. <https://doi.org/10.1144/SP355.2>

2830 Metelkin, D.V., Vernikovskiy, V.A., Kazansky, A.Y., 2012. Tectonic evolution of the Siberian  
2831 paleocontinent from the Neoproterozoic to the Late Mesozoic: paleomagnetic record and  
2832 reconstructions. *Russ. Geol. Geophys.* 53, 675–688. <https://doi.org/10.1016/j.rgg.2012.05.006>

2833 Miller, J.D., Kent, D.V., 1988. Paleomagnetism of the Silurian-Devonian Andreas redbeds: Evidence for  
2834 an Early Devonian supercontinent? *Geology* 16, 195–198.  
2835 [https://doi.org/10.1130/0091-7613\(1988\)016<0195:POTSDA>2.3.CO;2](https://doi.org/10.1130/0091-7613(1988)016<0195:POTSDA>2.3.CO;2)

2836 Mills, B., Watson, A.J., Goldblatt, C., Boyle, R., Lenton, T.M., 2011. Timing of Neoproterozoic  
2837 glaciations linked to transport-limited global weathering. *Nat. Geosci.* 4, 861–864.  
2838 <https://doi.org/10.1038/ngeo1305>

2839 Mills, B.J.W., Krause, A.J., Scotese, C.R., Hill, D.J., Shields, G.A., Lenton, T.M., 2019. Modelling the  
2840 long-term carbon cycle, atmospheric CO<sub>2</sub>, and Earth surface temperature from late  
2841 Neoproterozoic to present day. *Gondwana Res.* 67, 172–186.  
2842 <https://doi.org/10.1016/j.gr.2018.12.001>

2843 Millward, D., Evans, J.A., 2003. U–Pb chronology and duration of late Ordovician magmatism in the  
2844 English Lake District. *J. Geol. Soc. London* 160, 773–781. [https://doi.org/10.1144/0016-764902-](https://doi.org/10.1144/0016-764902-160)  
2845 160

2846 Minh, P., Hieu, P.T., Thuy, N.T.B., Dung, L.T., Kawaguchi, K., Dung, P.T., 2020. Neoproterozoic

2847 granitoids from the Phan Si Pan Zone, NW Vietnam: geochemistry and geochronology  
2848 constraints on reconstructing South China--India Palaeogeography. *Int. Geol. Rev.* 1–16.

2849 Minibaev, R.A. and Sulutdinov, R.M., 1991. Paleomagnetniye kharakteristiki siluriyskikh obrazovani  
2850 sakmarskoy zoni Yuzhnogo Urala. *Bashkirian Natl.Cttee.Ural.Branch Acad.Sci.USSR (Ufa)* 30.

2851 Mitchell, R.N., Kilian, T.M., Evans, D.A.D., 2012. Supercontinent cycles and the calculation of absolute  
2852 palaeolongitude in deep time. *Nature* 482, 208–211. <https://doi.org/10.1038/nature10800>

2853 Moores, E.M., 2002. Pre–1 Ga (pre-Rodinian) ophiolites: Their tectonic and environmental implications.  
2854 *GSA Bulletin* 114, 80–95. [https://doi.org/10.1130/0016-](https://doi.org/10.1130/0016-7606(2002)114<0080:PGPROT>2.0.CO;2)  
2855 [7606\(2002\)114<0080:PGPROT>2.0.CO;2](https://doi.org/10.1130/0016-7606(2002)114<0080:PGPROT>2.0.CO;2)

2856 Moores, E.M., 1991. Southwest U.S.-East Antarctic (SWEAT) connection: A hypothesis. *Geology* 19,  
2857 425–428. [https://doi.org/10.1130/0091-7613\(1991\)019<0425:SUSEAS>2.3.CO;2](https://doi.org/10.1130/0091-7613(1991)019<0425:SUSEAS>2.3.CO;2)

2858 Morgan, W.J., 1968. Rises, trenches, great faults, and crustal blocks. *J. Geophys. Res.* 73, 1959–1982.  
2859 <https://doi.org/10.1029/JB073i006p01959>

2860 Morrison, J., Ellwood, B.B., 1986. Paleomagnetism of Silurian-Ordovician sediments from the Valley  
2861 and Ridge province, northwest Georgia. *Geophys. Res. Lett.* 13, 189–192.

2862 Mulder, J.A., Berry, R.F., Halpin, J.A., Meffre, S., Everard, J.L., 2018a. Depositional age and correlation  
2863 of the Oonah Formation: refining the timing of Neoproterozoic basin formation in Tasmania.  
2864 *Aust. J. Earth Sci.* 65, 391–407. <https://doi.org/10.1080/08120099.2018.1426629>

2865 Mulder, J.A., Everard, J.L., Cumming, G., Meffre, S., Bottrill, R.S., Merdith, A.S., Halpin, J.A., McNeill,  
2866 A.W., Cawood, P.A., 2020. Neoproterozoic opening of the Pacific Ocean recorded by multi-stage  
2867 rifting in Tasmania, Australia. *Earth-Sci. Rev.* 201, 103041.  
2868 <https://doi.org/10.1016/j.earscirev.2019.103041>

2869 Mulder, J.A., Halpin, J.A., Daczko, N.R., 2015. Mesoproterozoic Tasmania: Witness to the East  
2870 Antarctica–Laurentia connection within Nuna. *Geology* 43, 759–762.  
2871 <https://doi.org/10.1130/G36850.1>

2872 Mulder, J.A., Halpin, J.A., Daczko, N.R., Orth, K., Meffre, S., Thompson, J.M., Morrissey, L.J., 2019. A  
2873 Multiproxy provenance approach to uncovering the assembly of East Gondwana in Antarctica.  
2874 *Geology* 47, 645–649. <https://doi.org/10.1130/G45952.1>

2875 Mulder, J.A., Karlstrom, K.E., Halpin, J.A., Merdith, A.S., Spencer, C.J., Berry, R.F., McDonald, B.,  
2876 2018b. Rodinian devil in disguise: Correlation of 1.25–1.10 Ga strata between Tasmania and  
2877 Grand Canyon. *Geology* 46, 991–994. <https://doi.org/10.1130/G45225.1>

2878 Müller, R.D., Cannon, J., Qin, X., Watson, R.J., Gurnis, M., Williams, S., Pfaffelmoser, T., Seton, M.,  
2879 Russell, S.H.J., Zahirovic, S., 2018. GPlates: Building a Virtual Earth Through Deep Time.  
2880 *Geochem. Geophys. Geosyst.* 19, 2243–2261. <https://doi.org/10.1029/2018GC007584>



- 2881 Müller, R.D., Royer, J.-Y., Lawver, L.A., 1993. Revised plate motions relative to the hotspots from  
2882 combined Atlantic and Indian Ocean hotspot tracks. *Geology* 21, 275–278.  
2883 2.3.CO;2">[https://doi.org/10.1130/0091-7613\(1993\)021<0275:RPMRTT>2.3.CO;2](https://doi.org/10.1130/0091-7613(1993)021<0275:RPMRTT>2.3.CO;2)
- 2884 Müller, R.D., Sdrolias, M., Gaina, C., Steinberger, B., Heine, C., 2008. Long-term sea-level fluctuations  
2885 driven by ocean basin dynamics. *Science* 319, 1357–1362.  
2886 <https://doi.org/10.1126/science.1151540>
- 2887 Müller, R.D., Seton, M., Zahirovic, S., Williams, S.E., Matthews, K.J., Wright, N.M., Shephard, G.E.,  
2888 Maloney, K.T., Barnett-Moore, N., Hosseinpour, M., Bower, D.J., Cannon, J., 2016. Ocean Basin  
2889 Evolution and Global-Scale Plate Reorganization Events Since Pangea Breakup. *Annu. Rev.*  
2890 *Earth Planet. Sci.* 44, 107–138. <https://doi.org/10.1146/annurev-earth-060115-012211>
- 2891 Müller, R.D., Zahirovic, S., Williams, S.E., Cannon, J., Seton, M., Bower, D.J., Tetley, M., Heine, C., Le  
2892 Breton, E., Liu, S., Russell, S.H.J., Yang, T., Leonard, J., Gurnis, M., 2019. A global plate model  
2893 including lithospheric deformation along major rifts and orogens since the Triassic. *Tectonics*.  
2894 <https://doi.org/10.1029/2018TC005462>
- 2895 Murphy, J.B., 2002. Geochemistry of the Neoproterozoic metasedimentary Gamble Brook Formation,  
2896 Avalon terrane, Nova Scotia: evidence for a rifted-arc environment along the west Gondwanan  
2897 margin of Rodinia. *J. Geol.* 110, 407–419.
- 2898 Murphy, J.B., Keppie, J.D., Dostal, J., Nance, R.D., 1999. Neoproterozoic-early Paleozoic evolution  
2899 of Avalonia. *Laurentia-Gondwana Connections Before Pangea* 336, 253.
- 2900 Murphy, J.B., Nance, R.D., 1989. Model for the evolution of the Avalonian-Cadomian belt. *Geology* 17,  
2901 735–738. 2.3.CO;2">[https://doi.org/10.1130/0091-7613\(1989\)017<0735:MFTEOT>2.3.CO;2](https://doi.org/10.1130/0091-7613(1989)017<0735:MFTEOT>2.3.CO;2)
- 2902 Murphy, J.B., Pisarevsky, S.A., Nance, R.D., Keppie, J.D., 2004. Neoproterozoic—Early Paleozoic  
2903 evolution of peri-Gondwanan terranes: implications for Laurentia-Gondwana connections. *Int. J.*  
2904 *Earth Sci.* 93, 659–682. <https://doi.org/10.1007/s00531-004-0412-9>
- 2905 Murphy, J.B., Strachan, R.A., Nance, R.D., Parker, K.D., Fowler, M.B., 2000. Proto-Avalonia: A 1.2–1.0  
2906 Ga tectonothermal event and constraints for the evolution of Rodinia. *Geology* 28, 1071–1074.  
2907 2.0.CO;2">[https://doi.org/10.1130/0091-7613\(2000\)28<1071:PAGTEA>2.0.CO;2](https://doi.org/10.1130/0091-7613(2000)28<1071:PAGTEA>2.0.CO;2)
- 2908 Murphy, J.B., Waldron, J.W.F., Kontak, D.J., Pe-Piper, G., Piper, D.J.W., 2011. Minas Fault Zone: Late  
2909 Paleozoic history of an intra-continental orogenic transform fault in the Canadian Appalachians.  
2910 *J. Struct. Geol.* 33, 312–328. <https://doi.org/10.1016/j.jsg.2010.11.012>
- 2911 Murthy, G., Gower, C., Tubrett, M., Pätzold, R., 1992. Paleomagnetism of Eocambrian Long Range  
2912 dykes and Double Mer Formation from Labrador, Canada. *Can. J. Earth Sci.* 29, 1224–1234.  
2913 <https://doi.org/10.1139/e92-098>
- 2914 Nance, R.D., Linnemann, U., 2008. The Rheic Ocean: origin, evolution, and significance. *GSA Today* 18,

2915 4–12.

2916 Nance, R.D., Murphy, J.B., Strachan, R.A., Keppie, J.D., Gutiérrez-Alonso, G., Fernández-Suárez, J.,  
2917 Quesada, C., Linnemann, U., D’lemos, R., Pisarevsky, S.A., 2008. Neoproterozoic-early  
2918 Palaeozoic tectonostratigraphy and palaeogeography of the peri-Gondwanan terranes: Amazonian  
2919 v. West African connections. Geological Society, London, Special Publications 297, 345–383.

2920 Nick, K.E., Elmore, R.D., 1990. Paleomagnetism of the Cambrian Royer Dolomite and Pennsylvanian  
2921 Collings Ranch Conglomerate, southern Oklahoma: An early Paleozoic magnetization and  
2922 nonpervasive remagnetization by weathering. Geol. Soc. Am. Bull. 102, 1517–1525.

2923 Niu, J., Li, Z.-X., Zhu, W., 2016. Palaeomagnetism and geochronology of mid-Neoproterozoic Yanbian  
2924 dykes, South China: implications for a c. 820–800 Ma true polar wander event and the  
2925 reconstruction of Rodinia. Geological Society, London, Special Publications 424, 191–121.  
2926 <https://doi.org/http://doi.org/10.1144/SP424.11>

2927 Noel, J.R., Spariosu, D.J., Dallmeyer, R.D., 1988. Paleomagnetism and  $40\text{Ar}/39\text{Ar}$  ages from the  
2928 Carolina slate belt, Albemarle, North Carolina: Implications for terrane amalgamation with North  
2929 America. Geology 16, 64–68.

2930 O’Brien, S.J., Dunning, G.R., Dube, B., O’Driscoll, C.F., Sparkes, B., Israel, S., Ketchum, J., 2001. New  
2931 insights into the Neoproterozoic geology of the central Avalon Peninsula (parts of NTS map areas  
2932 1N/6, 1N/7 and 1N/3), eastern Newfoundland. Current Research, Government of Newfoundland  
2933 and Labrador, Department of Mines and Energy, Geological Survey 2001, 169–189.

2934 O’Neill, C., Müller, D., Steinberger, B., 2005. On the uncertainties in hot spot reconstructions and the  
2935 significance of moving hot spot reference frames. Geochem. Geophys. Geosyst., Spec. Pap. Geol.  
2936 Soc. Am. 6. <https://doi.org/10.1029/2004GC000784>

2937 Opdyke, N.D., Huang, K., Xu, G., Zhang, W.Y., Kent, D.V., 1987. Paleomagnetic results from the  
2938 Silurian of the Yangtze paraplatform. Tectonophysics 139, 123–132.  
2939 [https://doi.org/10.1016/0040-1951\(87\)90201-0](https://doi.org/10.1016/0040-1951(87)90201-0)

2940 Palin, R.M., Santosh, M., Cao, W., Li, S.S., 2020. Secular change and the onset of plate tectonics on  
2941 Earth. Earth-Sci. Rev.

2942 Pan, B., Brock, G.A., Skovsted, C.B., Betts, M.J., Topper, T.P., Li, G., 2018. *Paterimitra pyramidalis*  
2943 Laurie, 1986, the first tommotiid discovered from the early Cambrian of North China. Gondwana  
2944 Res. 63, 179–185. <https://doi.org/10.1016/j.gr.2018.05.014>

2945 Pandit, M.K., Carter, L.M., Ashwal, L.D., Tucker, R.D., Torsvik, T.H., Jamtveit, B., Bhushan, S.K.,  
2946 2003. Age, petrogenesis and significance of 1 Ga granitoids and related rocks from the Sendra  
2947 area, Aravalli Craton, NW India. J. Asian Earth Sci. 22, 363–381.

2948 Paquette, J.L., Caby, R., Djouadi, M.T., Bouchez, J.L., 1998. U–Pb dating of the end of the Pan-African

2949 orogeny in the Tuareg shield: the post-collisional syn-shear Tioueine pluton (Western Hoggar,  
2950 Algeria). *Lithos* 45, 245–253. [https://doi.org/10.1016/S0024-4937\(98\)00034-6](https://doi.org/10.1016/S0024-4937(98)00034-6)

2951 Parsons, A.J., Hosseini, K., Palin, R.M., Sigloch, K., 2020. Geological, geophysical and plate kinematic  
2952 constraints for models of the India-Asia collision and the post-Triassic central Tethys oceans.  
2953 *Earth-Sci. Rev.* 208, 103084. <https://doi.org/10.1016/j.earscirev.2020.103084>

2954 Pavlov, V., Bachtadse, V., Mikhailov, V., 2008. New Middle Cambrian and Middle Ordovician  
2955 palaeomagnetic data from Siberia: Llandelian magnetostratigraphy and relative rotation between  
2956 the Aldan and Anabar--Angara blocks. *Earth Planet. Sci. Lett.* 276, 229–242.

2957 Pavlov, V., Gallet, Y., 1998. Upper Cambrian to Middle Ordovician magnetostratigraphy from the  
2958 Kulumbe river section (northwestern Siberia). *Phys. Earth Planet. Inter.* 108, 49–59.  
2959 [https://doi.org/10.1016/S0031-9201\(98\)00087-9](https://doi.org/10.1016/S0031-9201(98)00087-9)

2960 Pavlov, V.E., Shatsillo, A.V., Petrov, P.Y., 2015. Paleomagnetism of the upper Riphean deposits in the  
2961 Turukhansk and Olenek uplifts and Uda Pre-Sayan region and the neoproterozoic drift of the  
2962 Siberian Platform. *Izv. Phys. Solid Earth* 51, 716–747.  
2963 <https://doi.org/10.1134/S1069351315050092>

2964 Pavlov, V.E., Veselovskiy, R.V., Shatsillo, A.V., Gallet, Y., 2012. Magnetostratigraphy of the Ordovician  
2965 Angara/Rozhkova River section: Further evidence for the Moyero reversed superchron. *Izv. Phys.*  
2966 *Solid Earth* 48, 297–305. <https://doi.org/10.1134/S1069351312040052>

2967 Pedrosa-Soares, A.C., Noce, C.M., Wiedemann, C.M., Pinto, C.P., 2001. The Aracuai-West-Congo  
2968 Orogen in Brazil: an overview of a confined orogen formed during Gondwanaland assembly.  
2969 *Precambrian Res.* 110, 307–323.

2970 Pehrsson, S.J., Berman, R.G., Eglington, B., Rainbird, R., 2013. Two Neoproterozoic supercontinents  
2971 revisited: The case for a Rae family of cratons. *Precambrian Res.* 232, 27–43.  
2972 <https://doi.org/10.1016/j.precamres.2013.02.005>

2973 Peng, Y., Yu, S., Li, S., Zhang, J., Liu, Y., Li, Y., Santosh, M., 2019. Early Neoproterozoic magmatic  
2974 imprints in the Altun-Qilian-Kunlun region of the Qinghai-Tibet Plateau: Response to the  
2975 assembly and breakup of Rodinia supercontinent. *Earth-Sci. Rev.* 199, 102954.  
2976 <https://doi.org/10.1016/j.earscirev.2019.102954>

2977 Pisarevsky, S., Bylund, G., 1998. Neoproterozoic palaeomagnetic directions in rocks from a key section  
2978 of the Protogine Zone, southern Sweden. *Geophys. J. Int.* 133, 185–200.  
2979 <https://doi.org/10.1046/j.1365-246X.1998.1331497.x>

2980 Pisarevsky, S.A., Elming, S.-Å., Pesonen, L.J., Li, Z.-X., 2014. Mesoproterozoic paleogeography:  
2981 Supercontinent and beyond. *Precambrian Res.* 244, 207–225.  
2982 <https://doi.org/10.1016/j.precamres.2013.05.014>

- 2983 Pisarevsky, S.A., Gladkochub, D.P., Konstantinov, K.M., Mazukabzov, A.M., Stanevich, A.M., Murphy,  
2984 J.B., Tait, J.A., Donskaya, T.V., Konstantinov, I.K., 2013. Paleomagnetism of Cryogenian Kitoi  
2985 mafic dykes in South Siberia: Implications for Neoproterozoic paleogeography. *Precambrian Res.*  
2986 231, 372–382. <https://doi.org/10.1016/j.precamres.2013.04.007>
- 2987 Pisarevsky, S.A., Gurevich, E.L., Khramov, A.N., 1997. Palaeomagnetism of Lower Cambrian sediments  
2988 from the Olenek River section (northern Siberia): palaeopoles and the problem of magnetic  
2989 polarity in the Early Cambrian. *Geophys. J. Int.* 130, 746–756. <https://doi.org/10.1111/j.1365-246X.1997.tb01869.x>
- 2991 Pisarevsky, S.A., Murphy, J.B., Cawood, P.A., Collins, A.S., 2008. Late Neoproterozoic and Early  
2992 Cambrian palaeogeography: models and problems. Geological Society, London, Special  
2993 Publications 294, 9–31. <https://doi.org/10.1144/SP294.2>
- 2994 Pisarevsky, S.A., Natapov, L.M., 2003. Siberia and Rodinia. *Tectonophysics* 375, 221–245.  
2995 <https://doi.org/10.1016/j.tecto.2003.06.001>
- 2996 Pisarevsky, S.A., Wingate, M.T.D., Stevens, M.K., Haines, P.W., 2007. Palaeomagnetic results from the  
2997 Lancer 1 stratigraphic drillhole, Officer Basin, Western Australia, and implications for Rodinia  
2998 reconstructions. *Aust. J. Earth Sci.* 54, 561–572. <https://doi.org/10.1080/08120090701188962>
- 2999 Plavsa, D., Collins, A.S., Foden, J.D., Clark, C., 2015. The evolution of a Gondwanan collisional orogen:  
3000 A structural and geochronological appraisal from the Southern Granulite Terrane, South India.  
3001 *Tectonics* 34, 820–857.
- 3002 Popov, V., Iosifidi, A., Khramov, A., Tait, J., Bachtadse, V., 2002. Paleomagnetism of Upper Vendian  
3003 sediments from the Winter Coast, White Sea region, Russia: implications for the paleogeography  
3004 of Baltica during Neoproterozoic times. *J. Geophys. Res. [Solid Earth]* 107, EPM-10.
- 3005 Popov, V.V., Khramov, A.N., Bachtadse, V., 2005. Palaeomagnetism, magnetic stratigraphy, and  
3006 petromagnetism of the Upper Vendian sedimentary rocks in the sections of the Zolotitsa River  
3007 and in the Verkhotina Hole, Winter Coast of the White Sea, Russia. *Russian Journal of Earth  
3008 Sciences* 7.
- 3009 Powell, C.M., Pisarevsky, S.A., 2002. Late Neoproterozoic assembly of East Gondwana. *Geology* 30, 3–  
3010 6. [https://doi.org/10.1130/0091-7613\(2002\)030<0003:LNAOEG>2.0.CO;2](https://doi.org/10.1130/0091-7613(2002)030<0003:LNAOEG>2.0.CO;2)
- 3011 Powerman, V., Shatsillo, A., Coe, R., Zhao, X., Gladkochub, D., Buchwaldt, R., Pavlov, V., 2013.  
3012 Palaeogeography of the Siberian platform during middle Palaeozoic Times ( 450--400 Ma): new  
3013 palaeomagnetic evidence from the Lena and Nyuya rivers. *Geophys. J. Int.* 194, 1412–1440.
- 3014 Qiantao, B., Shanlin, G., Dihui, L., Zhengren, Y., Chengfa, C., Xiaoquan, L., 2001. A study of the  
3015 Kunlun-Qilian-Qinling suture system. *Acta Geologica Sinica-English Edition* 75, 364–374.
- 3016 Rapalini, A.E., 2006. New late Proterozoic paleomagnetic pole for the Rio de la Plata craton: Implications

3017 for Gondwana. *Precambrian Res.* 147, 223–233. <https://doi.org/10.1016/j.precamres.2006.01.016>

3018 Rapalini, A.E., Cingolani, C.A., 2004. First Late Ordovician Paleomagnetic Pole for the Cuyania  
3019 (Precordillera) Terrane of Western Argentina: a Microcontinent or a Laurentian Plateau.  
3020 *Gondwana Res.* 7, 1089–1104. [https://doi.org/10.1016/S1342-937X\(05\)71086-8](https://doi.org/10.1016/S1342-937X(05)71086-8)

3021 Rapalini, A.E., Tohver, E., Bettucci, L.S., Lossada, A.C., Barcelona, H., Pérez, C., 2015. The late  
3022 Neoproterozoic Sierra de las Ánimas Magmatic Complex and Playa Hermosa Formation,  
3023 southern Uruguay, revisited: Paleogeographic implications of new paleomagnetic and precise  
3024 geochronologic data. *Precambrian Res.* 259, 143–155.  
3025 <https://doi.org/10.1016/j.precamres.2014.11.021>

3026 Raub, T.D., Kirschvink, J.L., Evans, D.A.D., 2007. True polar wander: Linking deep and shallow  
3027 geodynamics to hydro-and biospheric hypotheses. *Treatise on geophysics* 5, 565–589.

3028 Raza, M., Khan, A., Bhardwaj, V.R., Rais, S., 2012. Geochemistry of Mesoproterozoic sedimentary rocks  
3029 of upper Vindhyan Group, southeastern Rajasthan and implications for weathering history,  
3030 composition and tectonic setting of continental crust in the northern part of Indian shield. *J. Asian*  
3031 *Earth Sci.* 48, 160–172.

3032 Robert, B., Besse, J., Blein, O., Greff-Lefftz, M., Baudin, T., Lopes, F., Meslouh, S., Belbadaoui, M.,  
3033 2017. Constraints on the Ediacaran inertial interchange true polar wander hypothesis: A new  
3034 paleomagnetic study in Morocco (West African Craton). *Precambrian Res.* 295, 90–116.  
3035 <https://doi.org/10.1016/j.precamres.2017.04.010>

3036 Robert, B., Domeier, M., Jakob, J., 2020. Iapetan Oceans: An analog of Tethys? *Geology*.

3037 Rodionov, V.P., 1966. Dipole character of the Geomagnetic field in the Late Cambrian and the  
3038 Ordovician in the south of the Siberian Platform. *Geol. Geofiz.* 1, 94–101.

3039 Rodionov, V.P., Dekkers, M.J., Khramov, A.N., Gurevich, E.L., Krijgsman, W., Duermeijer, C.E.,  
3040 Heslop, D., 2003. Paleomagnetism and cyclostratigraphy of the Middle Ordovician Krivolutsky  
3041 suite, Krivaya Luka section, southern Siberian platform: record of non-synchronous NRM-  
3042 components or a non-axial geomagnetic field? *Studia Geophys. Geodaetica* 47, 255–274.

3043 Rodionov, V.P., Khramov, A.N., Pisarevskii, S.A., Popov, V.V., Iosifidi, A.G., 1998. Geomagnetic  
3044 Reversals in the Early Paleozoic. 1. A Late Cambrian Reversal Recorded in the Ichera Section,  
3045 Southern Siberian Platform. *Izv. Phys. Solid Earth* 34, 1009–1017.

3046 Rogers, J.J.W., Santosh, M., 2002. Configuration of Columbia, a Mesoproterozoic Supercontinent.  
3047 *Gondwana Res.* 5, 5–22. [https://doi.org/10.1016/S1342-937X\(05\)70883-2](https://doi.org/10.1016/S1342-937X(05)70883-2)

3048 Ross, M.I., Scotese, C.R., 1988. A hierarchical tectonic model of the Gulf of Mexico and Caribbean  
3049 region. *Tectonophysics*.

3050 Ruppel, A., Jacobs, J., Eagles, G., Läufer, A., Jokat, W., 2018. New geophysical data from a key region in

3051 East Antarctica: Estimates for the spatial extent of the Tonian Oceanic Arc Super Terrane  
3052 (TOAST). *Gondwana Res.* 59, 97–107. <https://doi.org/10.1016/j.gr.2018.02.019>

3053 Safonova, I., Biske, G., Romer, R.L., Seltmann, R., Simonov, V., Maruyama, S., 2016. Middle Paleozoic  
3054 mafic magmatism and ocean plate stratigraphy of the South Tianshan, Kyrgyzstan. *Gondwana*  
3055 *Res.* 30, 236–256. <https://doi.org/10.1016/j.gr.2015.03.006>

3056 Schellart, W.P., Lister, G.S., Toy, V.G., 2006. A Late Cretaceous and Cenozoic reconstruction of the  
3057 Southwest Pacific region: Tectonics controlled by subduction and slab rollback processes. *Earth-*  
3058 *Sci. Rev.* 76, 191–233. <https://doi.org/10.1016/j.earscirev.2006.01.002>

3059 Scherstén, A., Årebäck, H., Cornell, D., Hoskin, P., Åberg, A., Armstrong, R., 2000. Dating mafic–  
3060 ultramafic intrusions by ion-microprobing contact-melt zircon: examples from SW Sweden.  
3061 *Contrib. Mineral. Petrol.* 139, 115–125. <https://doi.org/10.1007/s004100050577>

3062 Schmidt, P.W., Williams, G.E., 2010. Ediacaran palaeomagnetism and apparent polar wander path for  
3063 Australia: no large true polar wander. *Geophys. J. Int.* 182, 711–726.  
3064 <https://doi.org/10.1111/j.1365-246X.2010.04652.x>

3065 Schmidt, P.W., Williams, G.E., 1996. Palaeomagnetism of the ejecta-bearing Bunyeroo Formation, late  
3066 Neoproterozoic, Adelaide fold belt, and the age of the Acraman impact. *Earth Planet. Sci. Lett.*  
3067 144, 347–357. [https://doi.org/10.1016/S0012-821X\(96\)00169-0](https://doi.org/10.1016/S0012-821X(96)00169-0)

3068 Schmidt, P.W., Williams, G.E., 1995. The Neoproterozoic climatic paradox: Equatorial palaeolatitude for  
3069 Marinoan glaciation near sea level in South Australia. *Earth Planet. Sci. Lett.* 134, 107–124.  
3070 [https://doi.org/10.1016/0012-821X\(95\)00106-M](https://doi.org/10.1016/0012-821X(95)00106-M)

3071 Schmidt, P.W., Williams, G.E., Embleton, B.J.J., 1991. Low palaeolatitude of Late Proterozoic  
3072 glaciation: early timing of remanence in haematite of the Elatina Formation, South Australia.  
3073 *Earth Planet. Sci. Lett.* 105, 355–367. [https://doi.org/10.1016/0012-821X\(91\)90177-J](https://doi.org/10.1016/0012-821X(91)90177-J)

3074 Schmidt, P.W., Williams, G.E., McWilliams, M.O., 2009. Palaeomagnetism and magnetic anisotropy of  
3075 late Neoproterozoic strata, South Australia: Implications for the palaeolatitude of late Cryogenian  
3076 glaciation, cap carbonate and the Ediacaran System. *Precambrian Res.* 174, 35–52.  
3077 <https://doi.org/10.1016/j.precamres.2009.06.002>

3078 Scotese, C.R., 2016. PALEOMAP PaleoAtlas for GPlates and the PaleoData Plotter Program,  
3079 PALEOMAP Project. See <http://www.earthbyte.org/paleomap-paleoatlas-for-gplates>.

3080 Scotese, C.R., 2004. A Continental Drift Flipbook. *J. Geol.* 112, 729–741. <https://doi.org/10.1086/424867>

3081 Seton, M., Müller, R.D., Zahirovic, S., Gaina, C., Torsvik, T., Shephard, G., Talsma, A., Gurnis, M.,  
3082 Turner, M., Maus, S., Chandler, M., 2012. Global continental and ocean basin reconstructions  
3083 since 200 Ma. *Earth-Sci. Rev.* 113, 212–270. <https://doi.org/10.1016/j.earscirev.2012.03.002>

3084 Shapiro, M.N., Solov'ev, A.V., 2009. Formation of the Olyutorsky–Kamchatka foldbelt: a kinematic

3085 model. *Russ. Geol. Geophys.* 50, 668–681. <https://doi.org/10.1016/j.rgg.2008.10.006>

3086 Shatsillo, A.V., Paverman, V.I., Pavlov, V.E., 2007. Middle paleozoic segment of the apparent polar  
3087 wander path from the Siberian platform: New paleomagnetic evidence for the Silurian of the  
3088 Nyuya-Berezovskii facial province. *Izv. Phys. Solid Earth* 43, 880–889.  
3089 <https://doi.org/10.1134/S1069351307100102>

3090 Shephard, G.E., Müller, R.D., Seton, M., 2013. The tectonic evolution of the Arctic since Pangea  
3091 breakup: Integrating constraints from surface geology and geophysics with mantle structure.  
3092 *Earth-Sci. Rev.* 124, 148–183. <https://doi.org/10.1016/j.earscirev.2013.05.012>

3093 Shervais, J.W., Dennis, A.J., McGee, J.J., Secor, D., 2003. Deep in the heart of Dixie: Pre-Alleghanian  
3094 eclogite and HP granulite metamorphism in the Carolina Terrane, South Carolina, USA. *J.*  
3095 *Metamorph. Geol.* 21, 65–80.

3096 Shi, R., Yang, J., Wu, C., Wooden, J., 2004. First SHRIMP dating for the formation of the late Sinian  
3097 Yushigou Ophiolite, North Qilian Mountains. *ACTA GEOLOGICA SINICA-CHINESE*  
3098 *EDITION-* 78, 649–657.

3099 Shi, Y., Zhang, W., Kröner, A., Li, L., Jian, P., 2018. Cambrian ophiolite complexes in the Beishan area,  
3100 China, southern margin of the Central Asian Orogenic Belt. *J. Asian Earth Sci.* 153, 193–205.  
3101 <https://doi.org/10.1016/j.jseaes.2017.05.021>

3102 Sigloch, K., Mihalynuk, M.G., 2013. Intra-oceanic subduction shaped the assembly of Cordilleran North  
3103 America. *Nature* 496, 50–56. <https://doi.org/10.1038/nature12019>

3104 Slagstad, T., Kulakov, E., Kirkland, C.L., Roberts, N.M.W., Ganerød, M., 2019. Breaking the Grenville–  
3105 Sveconorwegian link in Rodinia reconstructions. *Terra Nova* 31, 430–437.  
3106 <https://doi.org/10.1111/ter.12406>

3107 Smethurst, M.A., Khramov, A.N., 1992. A new Devonian palaeomagnetic pole for the Russian platform  
3108 and Baltica, and related apparent polar wander. *Geophys. J. Int.* 108, 179–192.  
3109 <https://doi.org/10.1111/j.1365-246X.1992.tb00848.x>

3110 Smethurst, M.A., Khramov, A.N., Pisarevsky, S., 1998. Palaeomagnetism of the Lower Ordovician  
3111 Orthoceras Limestone, St. Petersburg, and a revised drift history for Baltica in the early  
3112 Palaeozoic. *Geophys. J. Int.* 133, 44–56. <https://doi.org/10.1046/j.1365-246X.1998.1331463.x>

3113 Smirnov, A.V., Evans, D.A.D., Ernst, R.E., Söderlund, U., Li, Z.-X., 2013. Trading partners: Tectonic  
3114 ancestry of southern Africa and western Australia, in Archean supercratons Vaalbara and  
3115 Zimgarn. *Precambrian Res.* 224, 11–22. <https://doi.org/10.1016/j.precamres.2012.09.020>

3116 Sohl, L.E., Christie-Blick, N., Kent, D.V., 1999. Paleomagnetic polarity reversals in Marinoan (ca. 600  
3117 Ma) glacial deposits of Australia: Implications for the duration of low-latitude glaciation in  
3118 Neoproterozoic time. *GSA Bulletin* 111, 1120–1139. [2.3.CO;2">https://doi.org/10.1130/0016-](https://doi.org/10.1130/0016-)

3119 7606(1999)111<1120:PPRIMC>2.3.CO;2

3120 Soldati, G., Boschi, L., Piersanti, A., Spada, G., 2001. The effect of global seismicity on the polar motion  
3121 of a viscoelastic Earth. *J. Geophys. Res.* 106, 6761–6767. <https://doi.org/10.1029/2000JB900354>

3122 Song, S., Li, X.-H., 2019. A positive test for the Greater Tarim Block at the heart of Rodinia: Mega-  
3123 dextral suturing of supercontinent assembly: COMMENT. *Geology* 47, e453–e453.

3124 Song, S., Niu, Y., Su, L., Xia, X., 2013. Tectonics of the North Qilian orogen, NW China. *Gondwana*  
3125 *Res.* 23, 1378–1401. <https://doi.org/10.1016/j.gr.2012.02.004>

3126 Song, S., Niu, Y., Zhang, L., Wei, C., Liou, J.G., Su, L., 2009. Tectonic evolution of early Paleozoic HP  
3127 metamorphic rocks in the North Qilian Mountains, NW China: New perspectives. *J. Asian Earth*  
3128 *Sci.* 35, 334–353. <https://doi.org/10.1016/j.jseaes.2008.11.005>

3129 Song, S., Su, L., Li, X.-H., Niu, Y., Zhang, L., 2012. Grenville-age orogenesis in the Qaidam-Qilian  
3130 block: The link between South China and Tarim. *Precambrian Res.* 220–221, 9–22.  
3131 <https://doi.org/10.1016/j.precamres.2012.07.007>

3132 Stampfli, G.M., Borel, G.D., 2002. A plate tectonic model for the Paleozoic and Mesozoic constrained by  
3133 dynamic plate boundaries and restored synthetic oceanic isochrons. *Earth Planet. Sci. Lett.* 196,  
3134 17–33. [https://doi.org/10.1016/S0012-821X\(01\)00588-X](https://doi.org/10.1016/S0012-821X(01)00588-X)

3135 Stearn, J.E.F., Piper, J.D.A., 1984. Sub-Department of Geophysics, University of Liverpool, Liverpool  
3136 L69 3BX (Gt. Britain). *Precambrian Res.* 23, 201–246.

3137 Steinberger, B., Torsvik, T.H., 2008. Absolute plate motions and true polar wander in the absence of  
3138 hotspot tracks. *Nature* 452, 620–623. <https://doi.org/10.1038/nature06824>

3139 Stern, R.J., 1994. Arc Assembly and Continental Collision in the Neoproterozoic East African Orogen:  
3140 Implications for the Consolidation of Gondwanaland. *Annu. Rev. Earth Planet. Sci.* 22, 319–351.  
3141 <https://doi.org/10.1146/annurev.ea.22.050194.001535>

3142 Stern, R.J., Miller, N.R., 2018. Did the transition to plate tectonics cause Neoproterozoic Snowball Earth?  
3143 *Terra Nova* 30, 87–94. <https://doi.org/10.1111/ter.12321>

3144 Strachan, R.A., Collins, A.S., Buchan, C., Nance, R.D., Murphy, J.B., D’Lemos, R.S., 2007. Terrane  
3145 analysis along a Neoproterozoic active margin of Gondwana: insights from U–Pb zircon  
3146 geochronology. *J. Geol. Soc. London* 164, 57–60. <https://doi.org/10.1144/0016-76492006-014>

3147 Sun, L.-S., Huang, B.-C., 2009. New paleomagnetic result for Ordovician rocks from the Tarim Block,  
3148 Northwest China and its tectonic implications.

3149 Surkis, Y.F., Rodionov, V.P., Khramov, A.N., Gurevich, E.L., Westfahl, M., 1999. Geomagnetic  
3150 reversals in the early Paleozoic: 3. Reversals recorded in redbeds of the lower Ordovician Mandra  
3151 section, Siberia. *Izv. Phys. Solid Earth* 35, 347–357.

3152 Sutherland, R., Dickens, G.R., Blum, P., Agnini, C., Alegret, L., Asatryan, G., Bhattacharya, J.,



3153 Bordenave, A., Chang, L., Collot, J., Cramwinckel, M.J., Dallanave, E., Drake, M.K., Etienne,  
3154 S.J.G., Giorgioni, M., Gurnis, M., Harper, D.T., Huang, H.-H.M., Keller, A.L., Lam, A.R., Li, H.,  
3155 Matsui, H., Morgans, H.E.G., Newsam, C., Park, Y.-H., Pascher, K.M., Pekar, S.F., Penman,  
3156 D.E., Saito, S., Stratford, W.R., Westerhold, T., Zhou, X., 2020. Continental-scale geographic  
3157 change across Zealandia during Paleogene subduction initiation. *Geology* 48, 419–424.  
3158 <https://doi.org/10.1130/G47008.1>

3159 Swanson-Hysell, N.L., Maloof, A.C., Kirschvink, J.L., Evans, D.A.D., Halverson, G.P., Hurtgen, M.T.,  
3160 2012. Constraints on Neoproterozoic paleogeography and Paleozoic orogenesis from  
3161 paleomagnetic records of the Bitter Springs Formation, Amadeus Basin, central Australia. *Am. J.*  
3162 *Sci.* 312, 817–884. <https://doi.org/10.2475/08.2012.01>

3163 Tetley, M.G., 2018. Constraining Earth’s plate tectonic evolution through data mining and knowledge  
3164 discovery (PhD). The University of Sydney.

3165 Tetley, M.G., Williams, S.E., Gurnis, M., Flament, N., Müller, R.D., 2019. Constraining absolute plate  
3166 motions since the Triassic. *J. Geophys. Res. [Solid Earth]*. <https://doi.org/10.1029/2019JB017442>

3167 Thomas, R.J., De Waele, B., Schofield, D.I., Goodenough, K.M., Horstwood, M., Tucker, R., Bauer, W.,  
3168 Annells, R., Howard, K., Walsh, G., Rabarimanana, M., Rafahatelo, J.M., Ralison, A.V.,  
3169 Randriamananjara, T., 2009. Geological evolution of the Neoproterozoic Bemarivo Belt, northern  
3170 Madagascar. *Precambrian Res.* 172, 279–300. <https://doi.org/10.1016/j.precamres.2009.04.008>

3171 Thompson, M.D., Grunow, A.M., Ramezani, J., 2010. Cambro-Ordovician paleogeography of the  
3172 Southeastern New England Avalon Zone: Implications for Gondwana breakup. *GSA Bulletin*  
3173 122, 76–88. <https://doi.org/10.1130/B26581.1>

3174 Thorogood, E.J., 1990. Provenance of the pre-Devonian sediments of England and Wales: Sm-Nd  
3175 isotopic evidence. *J. Geol. Soc. London* 147, 591–594. <https://doi.org/10.1144/gsjgs.147.4.0591>

3176 Torsvik, T.H., Ashwal, L.D., Tucker, R.D., Eide, E.A., 2001. Neoproterozoic geochronology and  
3177 palaeogeography of the Seychelles microcontinent: the India link. *Precambrian Res.* 110, 47–59.  
3178 [https://doi.org/10.1016/S0301-9268\(01\)00180-2](https://doi.org/10.1016/S0301-9268(01)00180-2)

3179 Torsvik, T.H., Burke, K., Steinberger, B., Webb, S.J., Ashwal, L.D., 2010a. Diamonds sampled by  
3180 plumes from the core-mantle boundary. *Nature* 466, 352–355.  
3181 <https://doi.org/10.1038/nature09216>

3182 Torsvik, T.H., Cocks, L.R.M., 2017. The integration of palaeomagnetism, the geological record and  
3183 mantle tomography in the location of ancient continents. *Geol. Mag.* 1–19.  
3184 <https://doi.org/10.1017/S001675681700098X>

3185 Torsvik, T.H., Cocks, L.R.M., 2016. *Earth History and Palaeogeography*. Cambridge University Press.

3186 Torsvik, T.H., Cocks, L.R.M., 2009. The Lower Palaeozoic palaeogeographical evolution of the

3187 northeastern and eastern peri-Gondwanan margin from Turkey to New Zealand. Geological  
3188 Society, London, Special Publications 325, 3–21. <https://doi.org/10.1144/SP325.2>

3189 Torsvik, T.H., Dietmar Muller, R., Van der Voo, R., Steinberger, B., Gaina, C., 2008. Global Plate  
3190 Motion Frames: Toward a Unified Model. *Reviews of Geophysics* 46.  
3191 <https://doi.org/10.1029/2007RG000227>

3192 Torsvik, T.H., Domeier, M., 2017. Correspondence: Numerical modelling of the PERM anomaly and the  
3193 Emeishan large igneous province. *Nat. Commun.* 8, 821. [https://doi.org/10.1038/s41467-017-](https://doi.org/10.1038/s41467-017-00125-2)  
3194 [00125-2](https://doi.org/10.1038/s41467-017-00125-2)

3195 Torsvik, T.H., Rehnström, E.F., 2001. Cambrian palaeomagnetic data from Baltica: implications for true  
3196 polar wander and Cambrian palaeogeography. *J. Geol. Soc. London* 158, 321–329.  
3197 <https://doi.org/10.1144/jgs.158.2.321>

3198 Torsvik, T.H., Smethurst, M.A., 1989. GMAP32—Geographic Mapping and Reconstruction System.  
3199 Geol. Surv. of Norway, Oslo 1997.

3200 Torsvik, T.H., Smethurst, M.A., Meert, J.G., Van der Voo, R., McKerrow, W.S., Brasier, Sturt, B.A.,  
3201 Walderhaug, H.J., 1996. Continental break-up and collision in the Neoproterozoic and Palaeozoic  
3202 — A tale of Baltica and Laurentia. *Earth-Sci. Rev.* 40, 229–258. [https://doi.org/10.1016/0012-](https://doi.org/10.1016/0012-8252(96)00008-6)  
3203 [8252\(96\)00008-6](https://doi.org/10.1016/0012-8252(96)00008-6)

3204 Torsvik, T.H., Steinberger, B., Gurnis, M., Gaina, C., 2010b. Plate tectonics and net lithosphere rotation  
3205 over the past 150My. *Earth Planet. Sci. Lett.* 291, 106–112.  
3206 <https://doi.org/10.1016/j.epsl.2009.12.055>

3207 Torsvik, T.H., Tait, J., Moralev, V.M., McKerrow, W.S., Sturt, B.A., Roberts, D., 1995. Ordovician  
3208 palaeogeography of Siberia and adjacent continents. *J. Geol. Soc. London* 152, 279–287.

3209 Torsvik, T.H., Trench, A., 1991. The Lower—Middle Ordovician palaeofield of Scandinavia: southern  
3210 Sweden “revisited.” *Phys. Earth Planet. Inter.* 65, 283–291.

3211 Torsvik, T.H., Trench, A., McKerrow, W.S., 1994. Implications of palaeomagnetic data from the  
3212 Tortworth Silurian inlier (southern Britain) to palaeogeography and Variscan tectonism. *Geophys.*  
3213 *J. Int.* 119, 91–100.

3214 Torsvik, T.H., Trench, A., Svensson, I., Walderhaug, H.J., 1993. Palaeogeographic significance of mid-  
3215 Silurian palaeomagnetic results from southern Britain—major revision of the apparent polar  
3216 wander path for eastern Avalonia. *Geophys. J. Int.* 113, 651–668.

3217 Torsvik, T.H., Van der Voo, R., 2002. Refining Gondwana and Pangea palaeogeography: estimates of  
3218 Phanerozoic non-dipole (octupole) fields. *Geophys. J. Int.* 151, 771–794.  
3219 <https://doi.org/10.1046/j.1365-246X.2002.01799.x>

3220 Torsvik, T.H., van der Voo, R., Doubrovine, P.V., Burke, K., Steinberger, B., Ashwal, L.D., Trønnnes,

3221 R.G., Webb, S.J., Bull, A.L., 2014. Deep mantle structure as a reference frame for movements in  
3222 and on the Earth. *Proc. Natl. Acad. Sci. U. S. A.* 111, 8735–8740.  
3223 <https://doi.org/10.1073/pnas.1318135111>

3224 Torsvik, T.H., Van der Voo, R., Preeden, U., Mac Niocaill, C., Steinberger, B., Doubrovine, P.V., van  
3225 Hinsbergen, D.J.J., Domeier, M., Gaina, C., Tohver, E., Meert, J.G., McCausland, P.J.A., Cocks,  
3226 L.R.M., 2012. Phanerozoic polar wander, palaeogeography and dynamics. *Earth-Sci. Rev.* 114,  
3227 325–368. <https://doi.org/10.1016/j.earscirev.2012.06.007>

3228 Trench, A., Torsvik, T.H., 1991. A revised Palaeozoic apparent polar wander path for Southern Britain  
3229 (Eastern Avalonia). *Geophys. J. Int.* 104, 227–233. [https://doi.org/10.1111/j.1365-](https://doi.org/10.1111/j.1365-246X.1991.tb02506.x)  
3230 [246X.1991.tb02506.x](https://doi.org/10.1111/j.1365-246X.1991.tb02506.x)

3231 Trench, A., Torsvik, T.H., Dentith, M.C., Walderhaug, H., Traynor, J.-J., 1992. A high southerly  
3232 palaeolatitude for Southern Britain in Early Ordovician times: palaeomagnetic data from the  
3233 Treffgarne Volcanic Formation SW Wales. *Geophys. J. Int.* 108, 89–100.

3234 Tretyakov, A.A., Degtyarev, K.E., Kovach, V.P., Kotov, A.B., Salnikova, E.B., Pilitsyna, A.V.,  
3235 Yakovleva, S.Z., 2016. The migmatite–gneiss complex of the Chuya–Kendyktas sialic massif  
3236 (Southern Kazakhstan): Structure and age. *Dokl. Earth Sci.* 467, 236–240.  
3237 <https://doi.org/10.1134/S1028334X16030156>

3238 Tucker, R.D., Ashwal, L.D., Torsvik, T.H., 2001. U–Pb geochronology of Seychelles granitoids: a  
3239 Neoproterozoic continental arc fragment. *Earth Planet. Sci. Lett.* 187, 27–38.  
3240 [https://doi.org/10.1016/S0012-821X\(01\)00282-5](https://doi.org/10.1016/S0012-821X(01)00282-5)

3241 Tucker, R.D., Roig, J.Y., Macey, P.H., Delor, C., Amelin, Y., Armstrong, R.A., Rabarimanana, M.H.,  
3242 Ralison, A.V., 2011. A new geological framework for south-central Madagascar, and its  
3243 relevance to the “out-of-Africa” hypothesis. *Precambrian Res.* 185, 109–130.  
3244 <https://doi.org/10.1016/j.precamres.2010.12.008>

3245 Tung, K., Yang, H.-J., Yang, H.-Y., Liu, D., Zhang, J., Wan, Y., Tseng, C.-Y., 2007. SHRIMP U–Pb  
3246 geochronology of the zircons from the Precambrian basement of the Qilian Block and its  
3247 geological significances. *Chin. Sci. Bull.* 52, 2687–2701. [https://doi.org/10.1007/s11434-007-](https://doi.org/10.1007/s11434-007-0356-0)  
3248 [0356-0](https://doi.org/10.1007/s11434-007-0356-0)

3249 Vaes, B., Van Hinsbergen, D.J.J., Boschman, L.M., 2019. Reconstruction of subduction and back-arc  
3250 spreading in the NW Pacific and Aleutian Basin: Clues to causes of Cretaceous and Eocene plate  
3251 reorganizations. *Tectonics* 38, 1367–1413.

3252 van der Meer, D.G., Spakman, W., van Hinsbergen, D.J.J., Amaru, M.L., Torsvik, T.H., 2010. Towards  
3253 absolute plate motions constrained by lower-mantle slab remnants. *Nat. Geosci.* 3, 36–40.  
3254 <https://doi.org/10.1038/ngeo708>

- 3255 Van der Voo, R., 1990. The reliability of paleomagnetic data. *Tectonophysics* 184, 1–9.  
3256 [https://doi.org/10.1016/0040-1951\(90\)90116-P](https://doi.org/10.1016/0040-1951(90)90116-P)
- 3257 Van der Voo, R., French, R.B., Williams, D.W., 1976. Paleomagnetism of the Wilberns Formation  
3258 (Texas) and the late Cambrian paleomagnetic field for North America. *J. Geophys. Res.* 81,  
3259 5633–5638.
- 3260 van Hinsbergen, D.J.J., Lippert, P.C., Dupont-Nivet, G., McQuarrie, N., Doubrovine, P.V., Spakman, W.,  
3261 Torsvik, T.H., 2012. Greater India Basin hypothesis and a two-stage Cenozoic collision between  
3262 India and Asia. *Proc. Natl. Acad. Sci. U. S. A.* 109, 7659–7664.  
3263 <https://doi.org/10.1073/pnas.1117262109>
- 3264 van Hinsbergen, D.J.J., Torsvik, T.H., Schmid, S.M., Mañenco, L.C., Maffione, M., Vissers, R.L.M.,  
3265 Gürer, D., Spakman, W., 2020. Orogenic architecture of the Mediterranean region and kinematic  
3266 reconstruction of its tectonic evolution since the Triassic. *Gondwana Res.* 81, 79–229.  
3267 <https://doi.org/10.1016/j.gr.2019.07.009>
- 3268 Van Lente, B., Ashwal, L.D., Pandit, M.K., Bowring, S.A., Torsvik, T.H., 2009. Neoproterozoic  
3269 hydrothermally altered basaltic rocks from Rajasthan, northwest India: Implications for late  
3270 Precambrian tectonic evolution of the Aravalli Craton. *Precambrian Res.* 170, 202–222.  
3271 <https://doi.org/10.1016/j.precamres.2009.01.007>
- 3272 van Staal, C.R., Barr, S.M., Brendan Murphy, J., 2012. Provenance and tectonic evolution of Ganderia:  
3273 Constraints on the evolution of the Iapetus and Rheic oceans. *Geology* 40, 987–990.  
3274 <https://doi.org/10.1130/G33302.1>
- 3275 Vernikovskiy, V.A., Vernikovskaya, A.E., 2001. Central Taimyr accretionary belt (Arctic Asia): Meso–  
3276 Neoproterozoic tectonic evolution and Rodinia breakup. *Precambrian Res.* 110, 127–141.  
3277 [https://doi.org/10.1016/S0301-9268\(01\)00184-X](https://doi.org/10.1016/S0301-9268(01)00184-X)
- 3278 Vernikovskiy, V.A., Vernikovskaya, A.E., Kotov, A.B., Sal'nikova, E.B., Kovach, V.P., 2003.  
3279 Neoproterozoic accretionary and collisional events on the western margin of the Siberian craton:  
3280 new geological and geochronological evidence from the Yenisey Ridge. *Tectonophysics* 375,  
3281 147–168. [https://doi.org/10.1016/S0040-1951\(03\)00337-8](https://doi.org/10.1016/S0040-1951(03)00337-8)
- 3282 Vernikovskiy, V.A., Vernikovskaya, A.E., Pease, V.L., Gee, D.G., 2004. Neoproterozoic Orogeny along  
3283 the margins of Siberia. *Geological Society, London, Memoirs* 30, 233–248.  
3284 <https://doi.org/10.1144/GSL.MEM.2004.030.01.18>
- 3285 Veselovskiy, R.V., Arzamastsev, A.A., 2011. Evidence for the Mesozoic endogenous activity in the  
3286 northeastern part of the Fennoscandian Shield. *Dokl. Earth Sci.* 438, 754–758.  
3287 <https://doi.org/10.1134/S1028334X11060377>
- 3288 Vick, H.K., Channell, J.E.T., Opdyke, N.D., 1987. Ordovician docking of the Carolina Slate Belt:

3289 Paleomagnetic data. *Tectonics* 6, 573–583. <https://doi.org/10.1029/TC006i005p00573>

3290 Vizan, H., Carney, J.N., Turner, P., Ixer, R.A., Tomasso, M., Mullen, R.P., Clarke, P., 2003. Late  
3291 Neoproterozoic to Early Palaeozoic palaeogeography of Avalonia: some palaeomagnetic  
3292 constraints from Nuneaton, central England. *Geol. Mag.* 140, 685–705.  
3293 <https://doi.org/10.1017/S001675680300832X>

3294 von Raumer, J.F., Stampfli, G.M., 2008. The birth of the Rheic Ocean—Early Palaeozoic subsidence  
3295 patterns and subsequent tectonic plate scenarios. *Tectonophysics* 461, 9–20.

3296 Walderhaug, H.J., Torsvik, T.H., Eide, E.A., Sundvoll, B., Bingen, B., 1999. Geochronology and  
3297 palaeomagnetism of the Hunnedalen dykes, SW Norway: implications for the Sveconorwegian  
3298 apparent polar wander loop. *Earth Planet. Sci. Lett.* 169, 71–83. [https://doi.org/10.1016/S0012-821X\(99\)00066-7](https://doi.org/10.1016/S0012-821X(99)00066-7)

3299

3300 Walderhaug, H.J., Torsvik, T.H., Halvorsen, E., 2007. The Egersund dykes (SW Norway): a robust Early  
3301 Ediacaran (Vendian) palaeomagnetic pole from Baltica. *Geophys. J. Int.* 168, 935–948.  
3302 <https://doi.org/10.1111/j.1365-246X.2006.03265.x>

3303 Wang, C., Liu, L., Wang, Y.-H., He, S.-P., Li, R.-S., Li, M., Yang, W.-Q., Cao, Y.-T., Collins, A.S., Shi,  
3304 C., Wu, Z.-N., 2015. Recognition and tectonic implications of an extensive Neoproterozoic  
3305 volcano-sedimentary rift basin along the southwestern margin of the Tarim Craton, northwestern  
3306 China. *Precambrian Res.* 257, 65–82. <https://doi.org/10.1016/j.precamres.2014.11.022>

3307 Wang, C.-C., Jacobs, J., Elburg, M.A., Läufer, A., Thomas, R.J., Elvevold, S., 2020. Grenville-age  
3308 continental arc magmatism and crustal evolution in central Dronning Maud Land (East  
3309 Antarctica): Zircon geochronological and HfO isotopic evidence. *Gondwana Res.*  
3310 <https://doi.org/10.1016/j.gr.2019.12.004>

3311 Weil, A.B., Geissman, J.W., Ashby, J.M., 2006. A new paleomagnetic pole for the Neoproterozoic Uinta  
3312 Mountain supergroup, Central Rocky Mountain States, USA. *Precambrian Res.* 147, 234–259.  
3313 <https://doi.org/10.1016/j.precamres.2006.01.017>

3314 Weil, A.B., Geissman, J.W., Van der Voo, R., 2004. Paleomagnetism of the Neoproterozoic Chuar  
3315 Group, Grand Canyon Supergroup, Arizona: implications for Laurentia’s Neoproterozoic APWP  
3316 and Rodinia break-up. *Precambrian Res.* 129, 71–92.

3317 Weil, A.B., Van der Voo, R., Mac Niocaill, C., Meert, J.G., 1998. The Proterozoic supercontinent  
3318 Rodinia: paleomagnetically derived reconstructions for 1100 to 800 Ma. *Earth Planet. Sci. Lett.*  
3319 154, 13–24. [https://doi.org/10.1016/S0012-821X\(97\)00127-1](https://doi.org/10.1016/S0012-821X(97)00127-1)

3320 Wen, B., Evans, D.A.D., Li, Y.-X., 2017. Neoproterozoic paleogeography of the Tarim Block: An  
3321 extended or alternative “missing-link” model for Rodinia? *Earth Planet. Sci. Lett.* 458, 92–106.  
3322 <https://doi.org/10.1016/j.epsl.2016.10.030>

- 3323 Wen, B., Evans, D.A.D., Wang, C., Li, Y.-X., Jing, X., 2019. A positive test for the Greater Tarim Block  
3324 at the heart of Rodinia: Mega-dextral suturing of supercontinent assembly: REPLY. *Geology* 47,  
3325 e454–e454.
- 3326 Wen, B., Evans, D.A.D., Wang, C., Li, Y.-X., Jing, X., 2018. A positive test for the Greater Tarim Block  
3327 at the heart of Rodinia: Mega-dextral suturing of supercontinent assembly. *Geology* 46, 687–690.  
3328 <https://doi.org/10.1130/G40254.1>
- 3329 Wen, B., Li, Y.-X., Zhu, W., 2013. Paleomagnetism of the Neoproterozoic diamictites of the Qiaoenbrak  
3330 formation in the Aksu area, NW China: Constraints on the paleogeographic position of the Tarim  
3331 Block. *Precambrian Res.* 226, 75–90. <https://doi.org/10.1016/j.precamres.2012.10.018>
- 3332 White, C.E., Barr, S.M., Hamilton, M.A., Murphy, J.B., 2020. Age and tectonic setting of Neoproterozoic  
3333 granitoid rocks, Antigonish Highlands, Nova Scotia, Canada: Implications for Avalonia in the  
3334 northern Appalachian orogen. *Can. J. Earth Sci.*
- 3335 White, C.E., Barr, S.M., Miller, B.V., Hamilton, M.A., 2002. Granitoid plutons of the Brookville terrane,  
3336 southern New Brunswick: petrology, age, and tectonic setting.
- 3337 Wilhem, C., Windley, B.F., Stampfli, G.M., 2012. The Altaids of Central Asia: A tectonic and  
3338 evolutionary innovative review. *Earth-Sci. Rev.* 113, 303–341.  
3339 <https://doi.org/10.1016/j.earscirev.2012.04.001>
- 3340 Williams, G.E., Schmidt, P.W., 2015. Low paleolatitude for the late Cryogenian interglacial succession,  
3341 South Australia: paleomagnetism of the Angepena Formation, Adelaide Geosyncline. *Aust. J.*  
3342 *Earth Sci.* 62, 243–253. <https://doi.org/10.1080/08120099.2015.1003967>
- 3343 Williams, S., Flament, N., Dietmar Müller, R., Butterworth, N., 2015. Absolute plate motions since 130  
3344 Ma constrained by subduction zone kinematics. *Earth Planet. Sci. Lett.* 418, 66–77.  
3345 <https://doi.org/10.1016/j.epsl.2015.02.026>
- 3346 Windley, B.F., Alexeiev, D., Xiao, W., Kröner, A., Badarch, G., 2007. Tectonic models for accretion of  
3347 the Central Asian Orogenic Belt. *J. Geol. Soc. London* 164, 31–47. [https://doi.org/10.1144/0016-](https://doi.org/10.1144/0016-76492006-022)  
3348 [76492006-022](https://doi.org/10.1144/0016-76492006-022)
- 3349 Wingate, M.T.D., Giddings, J.W., 2000. Age and palaeomagnetism of the Mundine Well dyke swarm,  
3350 Western Australia: implications for an Australia–Laurentia connection at 755 Ma. *Precambrian*  
3351 *Res.* 100, 335–357. [https://doi.org/10.1016/S0301-9268\(99\)00080-7](https://doi.org/10.1016/S0301-9268(99)00080-7)
- 3352 Wingate, M.T.D., Pisarevsky, S.A., De Waele, B., 2010. Paleomagnetism of the 765 Ma Luakela  
3353 volcanics in Northwest Zambia and implications for Neoproterozoic positions of the Congo  
3354 Craton. *Am. J. Sci.* 310, 1333–1344. <https://doi.org/10.2475/10.2010.05>
- 3355 Wu, C., Zuzva, A.V., Yin, A., Liu, C., Reith, R.C., Zhang, J., Liu, W., Zhou, Z., 2017. Geochronology and  
3356 geochemistry of Neoproterozoic granitoids in the central Qilian Shan of northern Tibet:

- 3357 Reconstructing the amalgamation processes and tectonic history of Asia. *Lithosphere* 9, 609–636.  
3358 <https://doi.org/10.1130/L640.1>
- 3359 Wu, J., Suppe, J., Lu, R., Kanda, R., 2016. Philippine Sea and East Asian plate tectonics since 52 Ma  
3360 constrained by new subducted slab reconstruction methods. *J. Geophys. Res. [Solid Earth]* 121,  
3361 4670–4741.
- 3362 Wu, L., Murphy, J.B., Quesada, C., Li, Z.-X., Waldron, J.W.F., Williams, S., Pisarevsky, S., Collins,  
3363 W.J., 2020. The amalgamation of Pangea: Paleomagnetic and geological observations revisited.  
3364 *GSA Bulletin*. <https://doi.org/10.1130/B35633.1>
- 3365 Xia, B., Zhang, L., Du, Z., Xu, B., 2017. Petrology and age of Precambrian Aksu blueschist, NW China.  
3366 *Precambrian Res.* <https://doi.org/10.1016/j.precamres.2017.12.041>
- 3367 Xiao, W., Windley, B.F., Allen, M.B., Han, C., 2013. Paleozoic multiple accretionary and collisional  
3368 tectonics of the Chinese Tianshan orogenic collage. *Gondwana Res.* 23, 1316–1341.  
3369 <https://doi.org/10.1016/j.gr.2012.01.012>
- 3370 Xiao, W., Windley, B.F., Yong, Y., Yan, Z., Yuan, C., Liu, C., Li, J., 2009. Early Paleozoic to Devonian  
3371 multiple-accretionary model for the Qilian Shan, NW China. *J. Asian Earth Sci.* 35, 323–333.  
3372 <https://doi.org/10.1016/j.jseaes.2008.10.001>
- 3373 Xiao, W.J., Mao, Q.G., Windley, B.F., Han, C.M., Qu, J.F., Zhang, J.E., Ao, S.J., Guo, Q.Q., Clevon,  
3374 N.R., Lin, S.F., Shan, Y.H., Li, J.L., 2010. Paleozoic multiple accretionary and collisional  
3375 processes of the Beishan orogenic collage. *Am. J. Sci.* 310, 1553–1594.  
3376 <https://doi.org/10.2475/10.2010.12>
- 3377 Xu, D., Xia, B., Bakun-Czubarow, N., Bachlinski, R., Li, P., Chen, G., Chen, T., 2008. Geochemistry and  
3378 Sr-Nd isotope systematics of metabasites in the Tunchang area, Hainan Island, South China:  
3379 implications for petrogenesis and tectonic setting. *Mineral. Petrol.* 92, 361–391.  
3380 <https://doi.org/10.1007/s00710-007-0198-0>
- 3381 Xu, D.-R., Xia, B., Li, P.-C., Chen, G.-H., Ma, C., Zhang, Y.-Q., 2007. Protolith natures and U-Pb  
3382 sensitive high mass-resolution ion microprobe (SHRIMP) zircon ages of the metabasites in  
3383 Hainan Island, South China: Implications for geodynamic evolution since the late Precambrian.  
3384 *Island Arc* 16, 575–597.
- 3385 Xu, X., Song, S., Su, L., Li, Z., Niu, Y., Allen, M.B., 2015. The 600–580Ma continental rift basalts in  
3386 North Qilian Shan, northwest China: Links between the Qilian-Qaidam block and SE Australia,  
3387 and the reconstruction of East Gondwana. *Precambrian Res.* 257, 47–64.  
3388 <https://doi.org/10.1016/j.precamres.2014.11.017>
- 3389 Xu, Y., Cawood, P.A., Du, Y., Zhong, Z., Hughes, N.C., 2014. Terminal suturing of Gondwana along the  
3390 southern margin of South China Craton: Evidence from detrital zircon U-Pb ages and Hf isotopes

3391 in Cambrian and Ordovician strata, Hainan Island. *Tectonics* 33, 2490–2504.

3392 Yakubchuk, A., 2017. Evolution of the Central Asian Orogenic Supercollage since Late Neoproterozoic  
3393 revised again. *Gondwana Res.* 47, 372–398. <https://doi.org/10.1016/j.gr.2016.12.010>

3394 Yang, B., Collins, A.S., Blades, M.L., 2019. Middle–late Mesoproterozoic tectonic geography of the  
3395 North Australia Craton: U–Pb and Hf isotopes of detrital zircon grains in the Beetaloo Sub-basin,  
3396 Northern . . . *Journal of the*.

3397 Yang, B., Collins, A.S., Cox, G.M., Jarrett, A.J.M., Denyszyn, S., Blades, M.L., Farkaš, J., Glorie, S.,  
3398 2020. Using Mesoproterozoic sedimentary geochemistry to reconstruct basin tectonic geography  
3399 and link organic carbon productivity to nutrient flux from a Northern Australian large igneous  
3400 Province. *Basin Res.* 60, 175. <https://doi.org/10.1111/bre.12450>

3401 Yang, J.S., Wu, C.L., Chen, S.Y., Shi, R.D., Zhang, J.X., Meng, F.C., Zuo, G.C., Wu, H.Q.,  
3402 Constantinovskaya, E., 2006. Neoproterozoic eclogitic metamorphic age of the Beishan eclogite  
3403 of Gansu, China: evidence from SHRIMP U–Pb isotope dating. *Geology in China* 33, 317–325.

3404 Yang, Z., Otofujii, Y.-I., Sun, Z., Huang, B., 2002. Magnetostratigraphic constraints on the Gondwanan  
3405 origin of North China: Cambrian/Ordovician boundary results. *Geophys. J. Int.* 151, 1–10.  
3406 <https://doi.org/10.1046/j.1365-246X.2002.01656.x>

3407 Yang, Z., Sun, Z., Yang, T., Pei, J., 2004. A long connection (750–380 Ma) between South China and  
3408 Australia: paleomagnetic constraints. *Earth Planet. Sci. Lett.* 220, 423–434.  
3409 [https://doi.org/10.1016/S0012-821X\(04\)00053-6](https://doi.org/10.1016/S0012-821X(04)00053-6)

3410 Yang, Z.-Y., Sun, Z.M., Ma, X.H., Huang, B.C., Dong, J.M., Zhou, Y.X., Zhu, H., 1996. Preliminary  
3411 paleomagnetic results from the Lower Paleozoic of North China (Henan Province) and its  
3412 implications. *Chinese Science Bulletin (in Chinese)* 42, 401.

3413 Yin, A., Harrison, T.M., 2000. Geologic Evolution of the Himalayan-Tibetan Orogen. *Annu. Rev. Earth*  
3414 *Planet. Sci.* 28, 211–280. <https://doi.org/10.1146/annurev.earth.28.1.211>

3415 Young, A., Flament, N., Maloney, K., Williams, S., Matthews, K., Zahirovic, S., Müller, R.D., 2019.  
3416 Global kinematics of tectonic plates and subduction zones since the late Paleozoic Era.  
3417 *Geoscience Frontiers* 10, 989–1013. <https://doi.org/10.1016/j.gsf.2018.05.011>

3418 Yuan, C., Sun, M., Yang, J., Zhou, H., Zhou, M.-F., 2004. Nb-depleted, continental rift-related Akaz  
3419 metavolcanic rocks (West Kunlun): implication for the rifting of the Tarim Craton from  
3420 Gondwana. *Geological Society, London, Special Publications* 226, 131–143.  
3421 <https://doi.org/10.1144/GSL.SP.2004.226.01.07>

3422 Zeng, Y.-C., Chen, Q., Xu, J.-F., Chen, J.-L., Huang, F., Yu, H.-X., Zhao, P.-P., 2018. Petrogenesis and  
3423 geodynamic significance of Neoproterozoic (~925 Ma) high-Fe–Ti gabbros of the RenTso  
3424 ophiolite, Lhasa Terrane, central Tibet. *Precambrian Res.* 314, 160–169.



3425 <https://doi.org/10.1016/j.precamres.2018.06.005>

3426 Zhan, S., Chen, Y., Xu, B., Wang, B., Faure, M., 2007. Late Neoproterozoic paleomagnetic results from  
3427 the Sugetbrak Formation of the Aksu area, Tarim basin (NW China) and their implications to  
3428 paleogeographic reconstructions and the snowball Earth hypothesis. *Precambrian Res.* 154, 143–  
3429 158. <https://doi.org/10.1016/j.precamres.2007.01.001>

3430 Zhang, C.-L., Li, H.-K., Santosh, M., Li, Z.-X., Zou, H.-B., Wang, H., Ye, H., 2012. Precambrian  
3431 evolution and cratonization of the Tarim Block, NW China: Petrology, geochemistry, Nd-isotopes  
3432 and U–Pb zircon geochronology from Archaean gabbro-TTG–potassic granite suite and  
3433 Paleoproterozoic metamorphic belt. *J. Asian Earth Sci.* 47, 5–20.  
3434 <https://doi.org/10.1016/j.jseaes.2011.05.018>

3435 Zhang, C.-L., Li, Z.-X., Li, X.-H., Ye, H.-M., 2009. Neoproterozoic mafic dyke swarms at the northern  
3436 margin of the Tarim Block, NW China: Age, geochemistry, petrogenesis and tectonic  
3437 implications. *J. Asian Earth Sci.* 35, 167–179. <https://doi.org/10.1016/j.jseaes.2009.02.003>

3438 Zhang, C.-L., Zou, H.-B., Li, H.-K., Wang, H.-Y., 2013. Tectonic framework and evolution of the Tarim  
3439 Block in NW China. *Gondwana Res.* 23, 1306–1315. <https://doi.org/10.1016/j.gr.2012.05.009>

3440 Zhang, J., Mattinson, C.G., Meng, F., Wan, Y., Tung, K., 2008. Polyphase tectonothermal history  
3441 recorded in granulitized gneisses from the north Qaidam HP/UHP metamorphic terrane, western  
3442 China: Evidence from zircon U-Pb geochronology. *Geol. Soc. Am. Bull.* 120, 732–749.

3443 Zhang, N., Zhong, S., Leng, W., Li, Z.X., 2010. A model for the evolution of the Earth’s mantle structure  
3444 since the Early Paleozoic. *J. Geophys. Res.*

3445 Zhang, Q.R., Piper, J.D.A., 1997. Palaeomagnetic study of Neoproterozoic glacial rocks of the Yangzi  
3446 Block: palaeolatitude and configuration of South China in the late Proterozoic Supercontinent.  
3447 *Precambrian Res.* 85, 173–199. [https://doi.org/10.1016/S0301-9268\(97\)00031-4](https://doi.org/10.1016/S0301-9268(97)00031-4)

3448 Zhang, S., Evans, D.A.D., Li, H., Wu, H., Jiang, G., Dong, J., Zhao, Q., Raub, T.D., Yang, T., 2013.  
3449 Paleomagnetism of the late Cryogenian Nantuo Formation and paleogeographic implications for  
3450 the South China Block. *J. Asian Earth Sci.* 72, 164–177.  
3451 <https://doi.org/10.1016/j.jseaes.2012.11.022>

3452 Zhang, S., Li, H., Jiang, G., Evans, D.A.D., Dong, J., Wu, H., Yang, T., Liu, P., Xiao, Q., 2015. New  
3453 paleomagnetic results from the Ediacaran Doushantuo Formation in South China and their  
3454 paleogeographic implications. *Precambrian Res.* 259, 130–142.  
3455 <https://doi.org/10.1016/j.precamres.2014.09.018>

3456 Zhang, S.-H., Zhao, Y., Li, X.-H., Ernst, R.E., Yang, Z.-Y., 2017. The 1.33–1.30 Ga Yanliao large  
3457 igneous province in the North China Craton: Implications for reconstruction of the Nuna  
3458 (Columbia) supercontinent, and specifically with the North Australian Craton. *Earth Planet. Sci.*

3459 Lett. 465, 112–125.

3460 Zhao, G., Cawood, P.A., Wilde, S.A., Sun, M., 2002. Review of global 2.1–1.8 Ga orogens: implications  
3461 for a pre-Rodinia supercontinent. *Earth-Sci. Rev.* 59, 125–162. [https://doi.org/10.1016/S0012-](https://doi.org/10.1016/S0012-8252(02)00073-9)  
3462 8252(02)00073-9

3463 Zhao, G., Wang, Y., Huang, B., Dong, Y., Li, S., Zhang, G., Yu, S., 2018. Geological reconstructions of  
3464 the East Asian blocks: From the breakup of Rodinia to the assembly of Pangea. *Earth-Sci. Rev.*  
3465 186, 262–286. <https://doi.org/10.1016/j.earscirev.2018.10.003>

3466 Zhao, P., Chen, Y., Zhan, S., Xu, B., Faure, M., 2014. The Apparent Polar Wander Path of the Tarim  
3467 block (NW China) since the Neoproterozoic and its implications for a long-term Tarim–Australia  
3468 connection. *Precambrian Res.* 242, 39–57. <https://doi.org/10.1016/j.precamres.2013.12.009>

3469 Zhao, X., Coe, R.S., Liu, C., Zhou, Y., 1992. New Cambrian and Ordovician paleomagnetic poles for the  
3470 North China Block and their paleogeographic implications. *J. Geophys. Res., Studi. Geol.* 97,  
3471 1767–1788. <https://doi.org/10.1029/91JB02742>

3472 Zhong, S., Liu, X., 2016. The long-wavelength mantle structure and dynamics and implications for large-  
3473 scale tectonics and volcanism in the Phanerozoic. *Gondwana Res.* 29, 83–104.  
3474 <https://doi.org/10.1016/j.gr.2015.07.007>

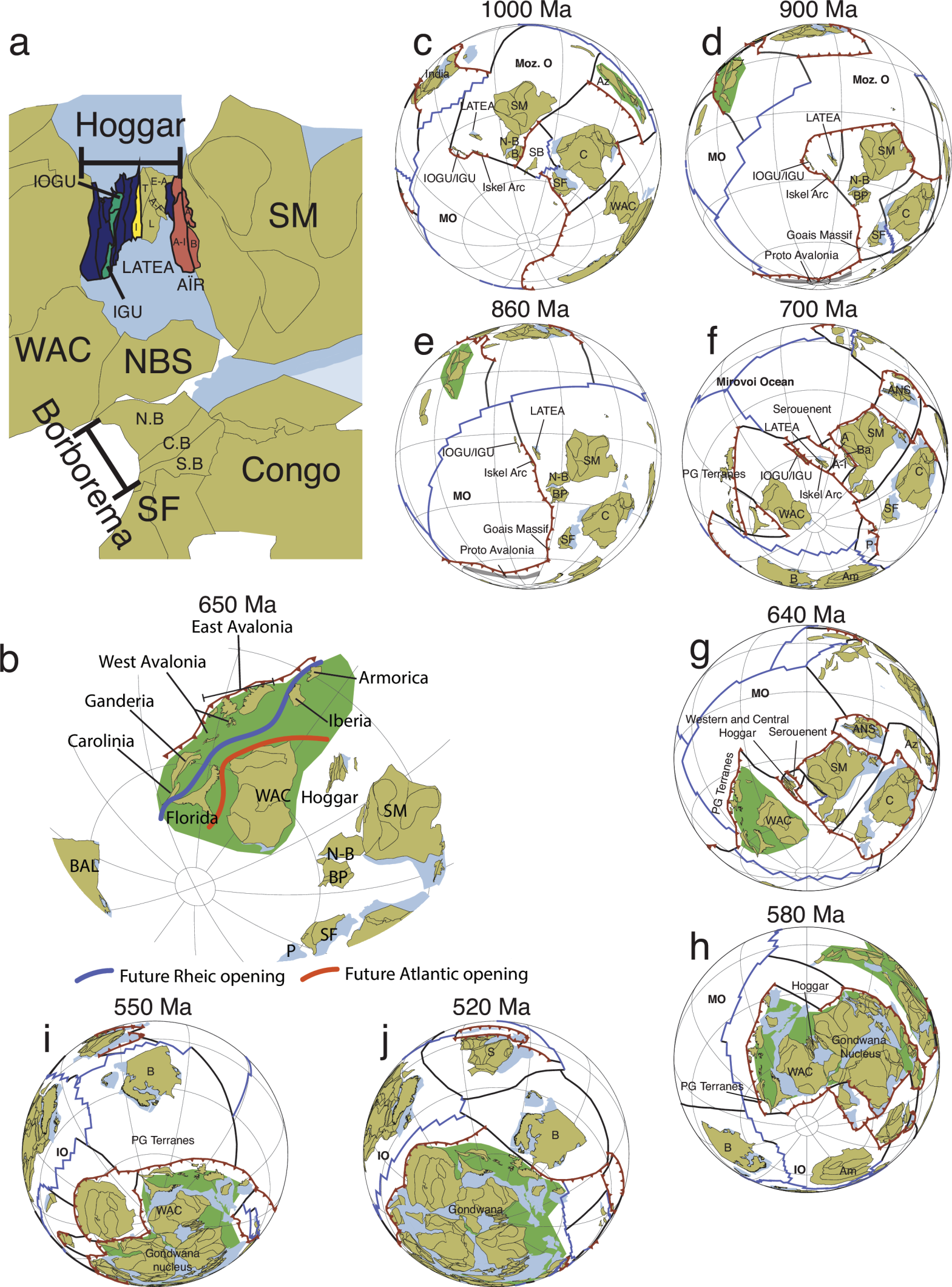
3475 Zhong, S., Rudolph, M.L., 2015. On the temporal evolution of long-wavelength mantle structure of the  
3476 Earth since the early Paleozoic. *Geochem. Geophys. Geosyst.* 16, 1599–1615.

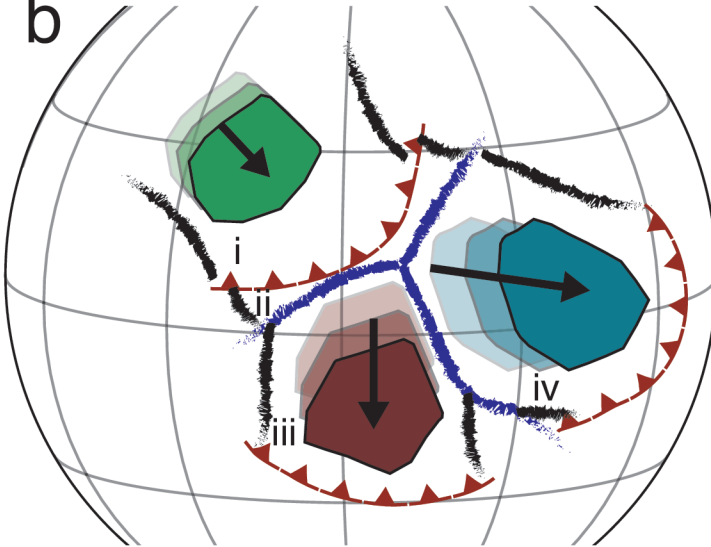
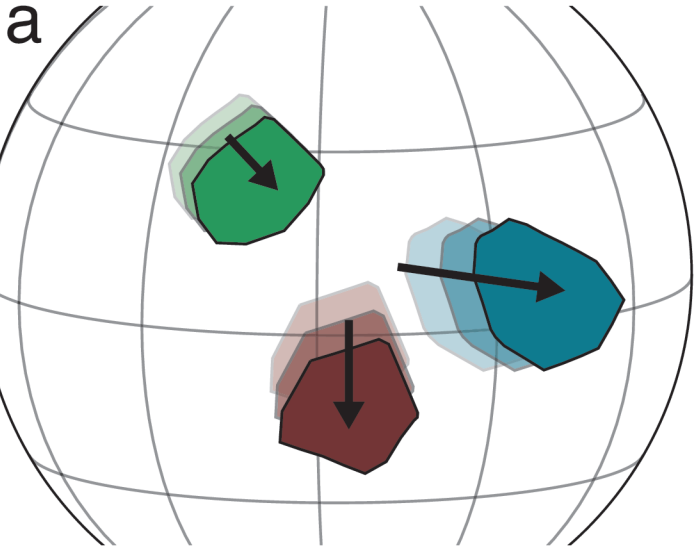
3477 Zhong, S., Zhang, N., Li, Z.-X., Roberts, J.H., 2007. Supercontinent cycles, true polar wander, and very  
3478 long-wavelength mantle convection. *Earth Planet. Sci. Lett.* 261, 551–564.  
3479 <https://doi.org/10.1016/j.epsl.2007.07.049>




3480 Zhu, D.-C., Zhao, Z.-D., Niu, Y., Dilek, Y., Hou, Z.-Q., Mo, X.-X., 2013. The origin and pre-Cenozoic  
3481 evolution of the Tibetan Plateau. *Gondwana Res.* 23, 1429–1454.  
3482 <https://doi.org/10.1016/j.gr.2012.02.002>





3483 Zhu, D.-C., Zhao, Z.-D., Niu, Y., Dilek, Y., Mo, X.-X., 2011. Lhasa terrane in southern Tibet came from  
3484 Australia. *Geology* 39, 727–730. <https://doi.org/10.1130/G31895.1>

3485 Zhu, G.-Y., Ren, R., Chen, F.-R., Li, T.-T., Chen, Y.-Q., 2017. Neoproterozoic rift basins and their  
3486 control on the development of hydrocarbon source rocks in the Tarim Basin, NW China. *J. Asian*  
3487 *Earth Sci.* 150, 63–72. <https://doi.org/10.1016/j.jseaes.2017.09.018>





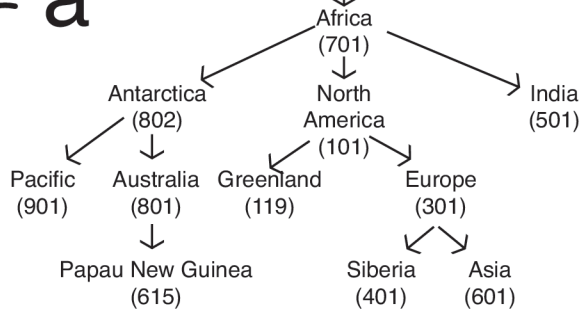
 Transform boundary  
 Mid-ocean ridge  
 Subduction zone

 Direction of movement  
 Old  
 Young  


Relative reference framework

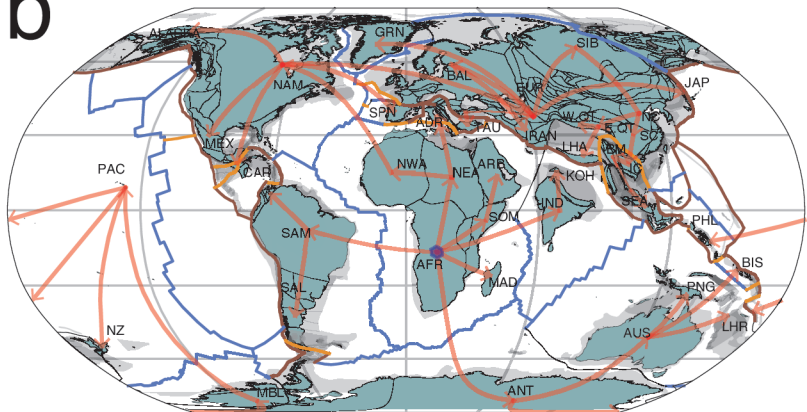
**a**

Absolute reference frame



**b**

50 Ma



Connection to absolute plate motion



Relative rotation framework

Subduction zone

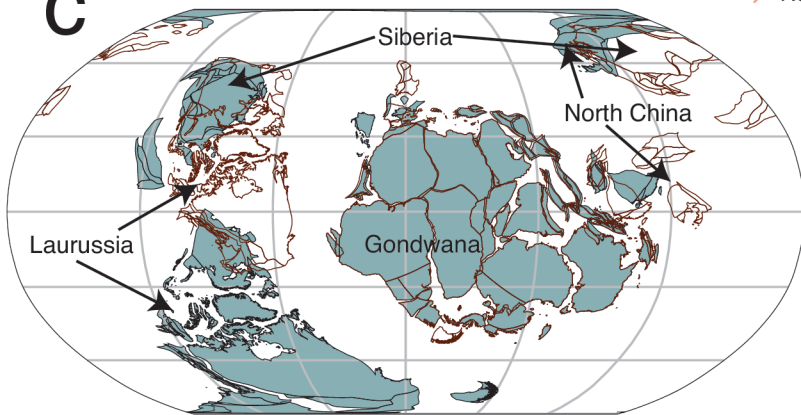
Mid-ocean ridge

Transform boundary

Other plate boundary

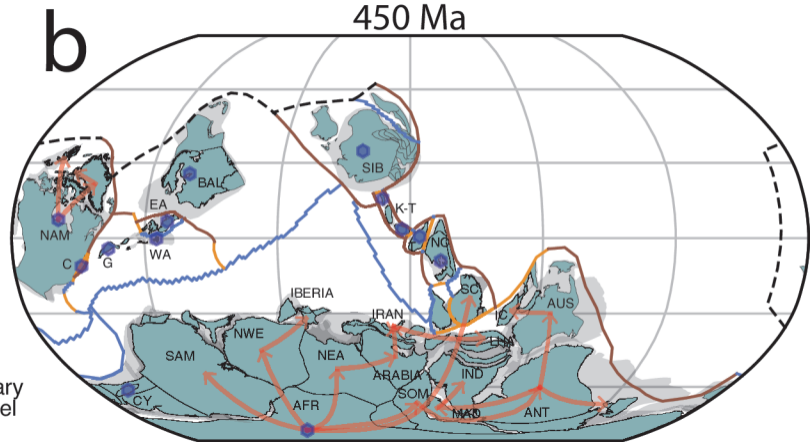
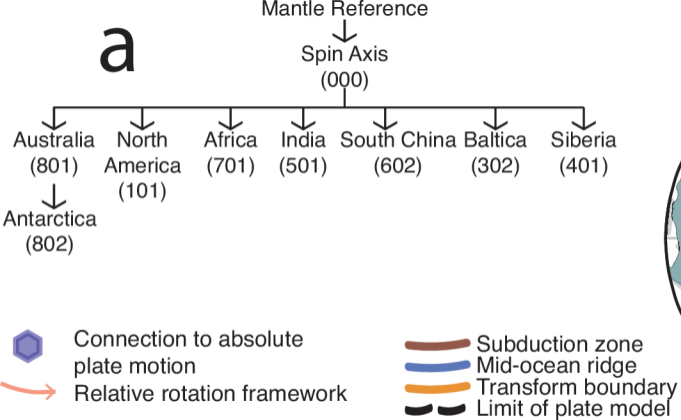
**c**

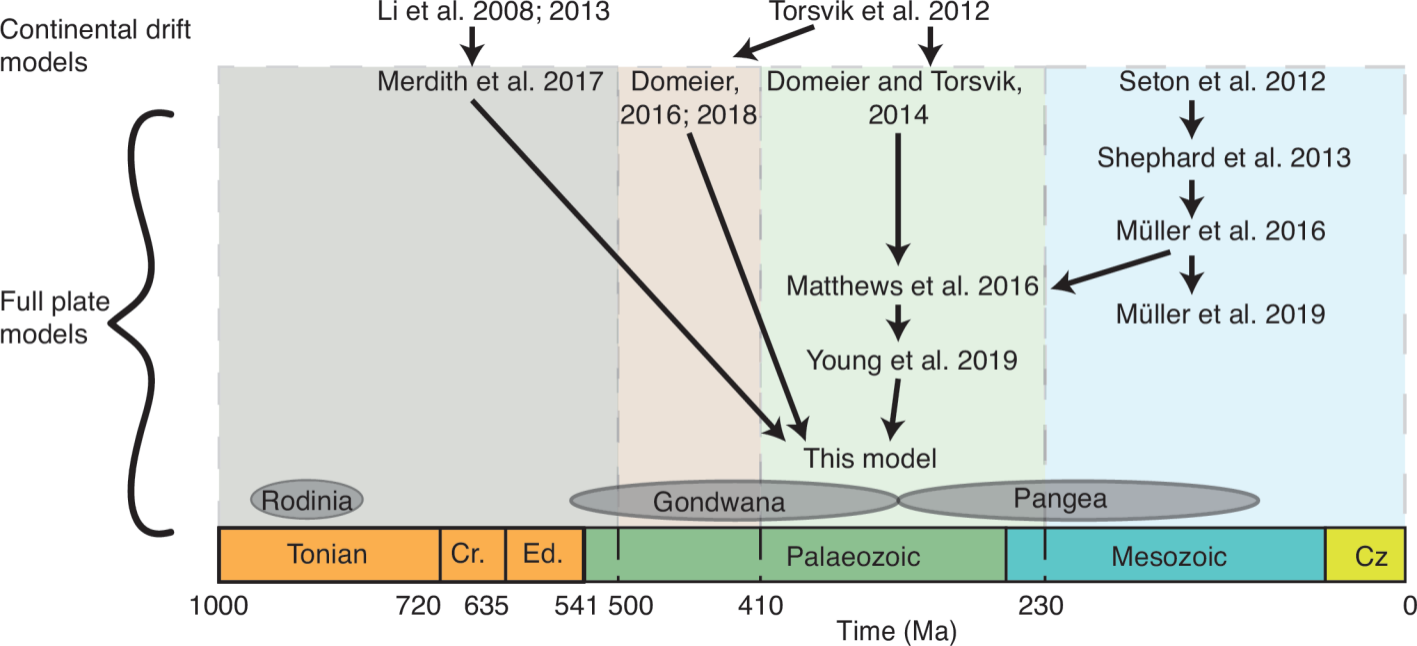
410 Ma

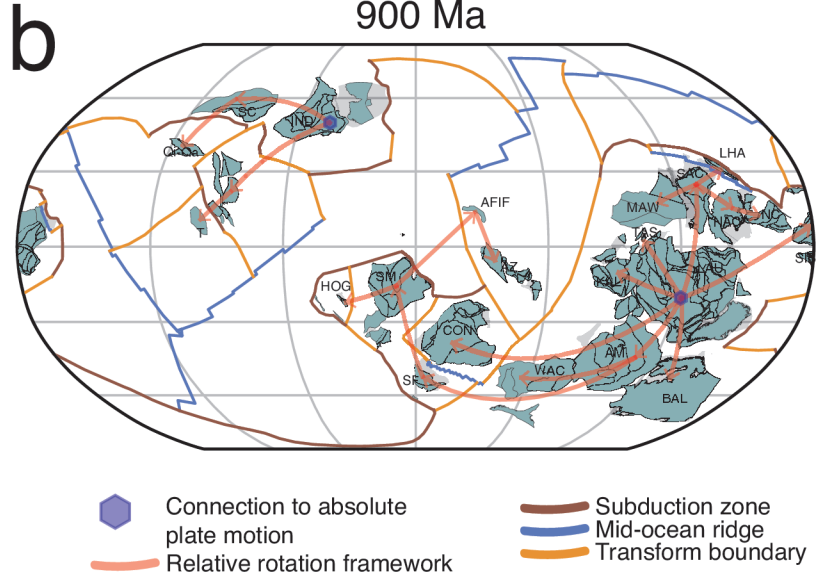
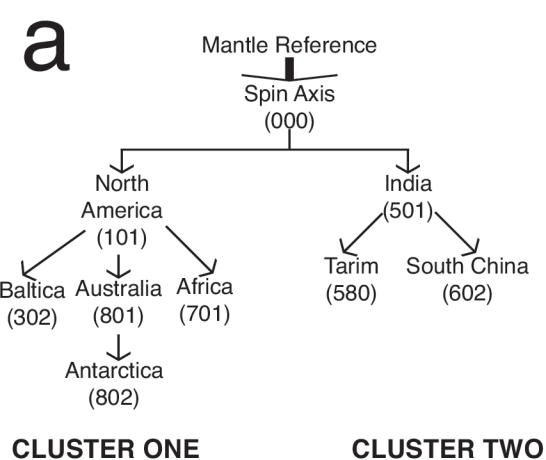


Young et al. (2019)

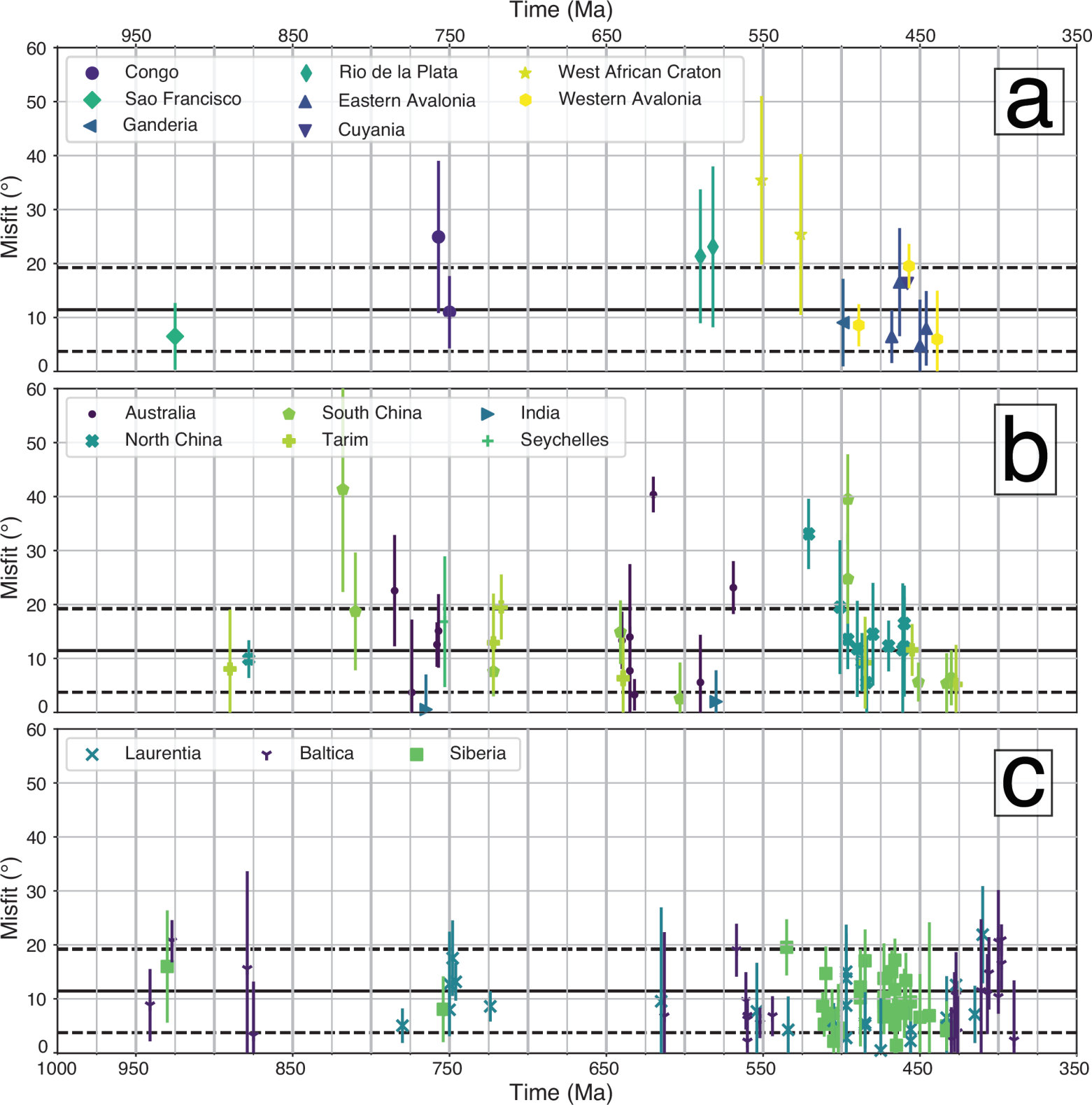
Matthews et al. (2016)

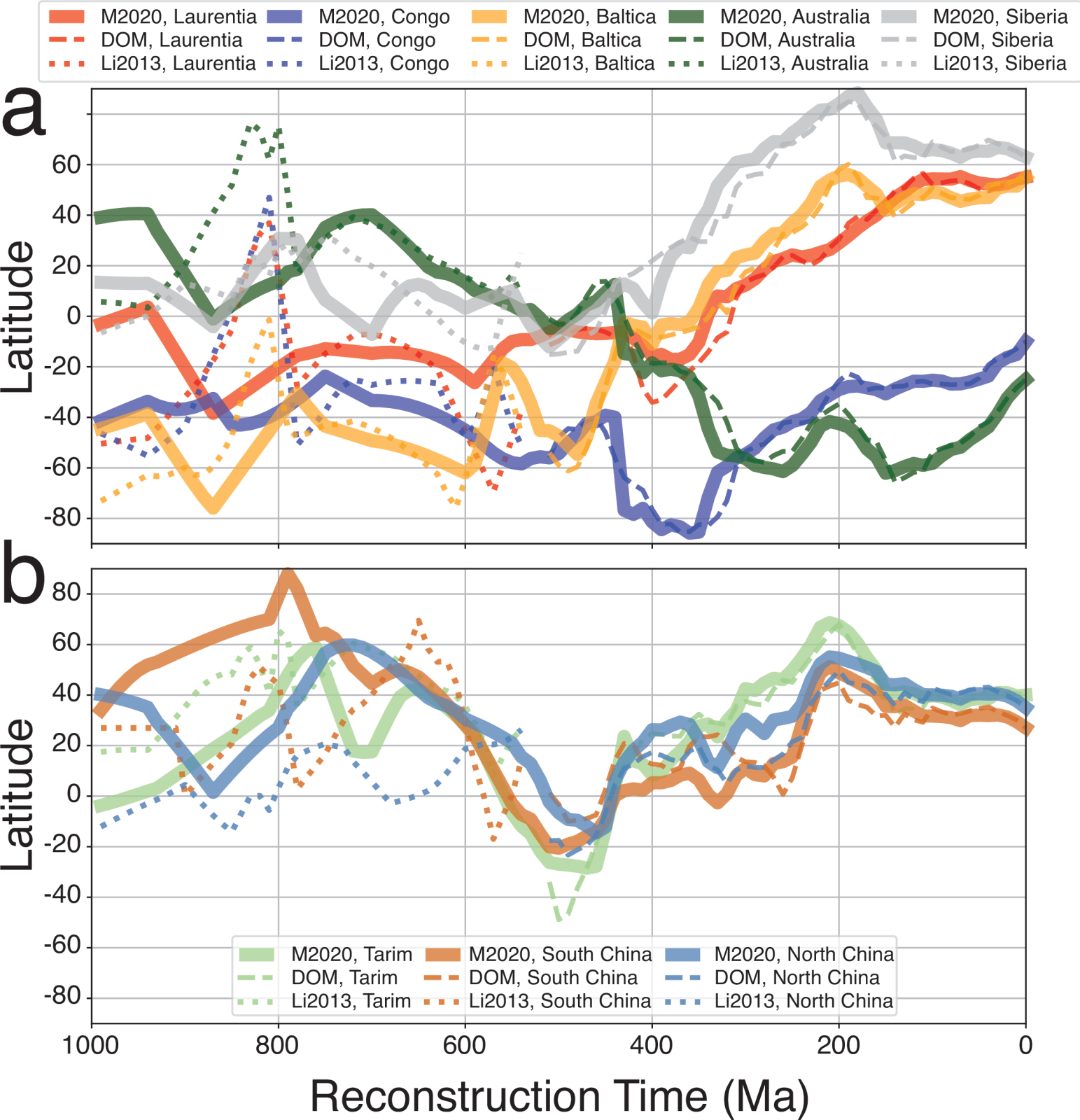






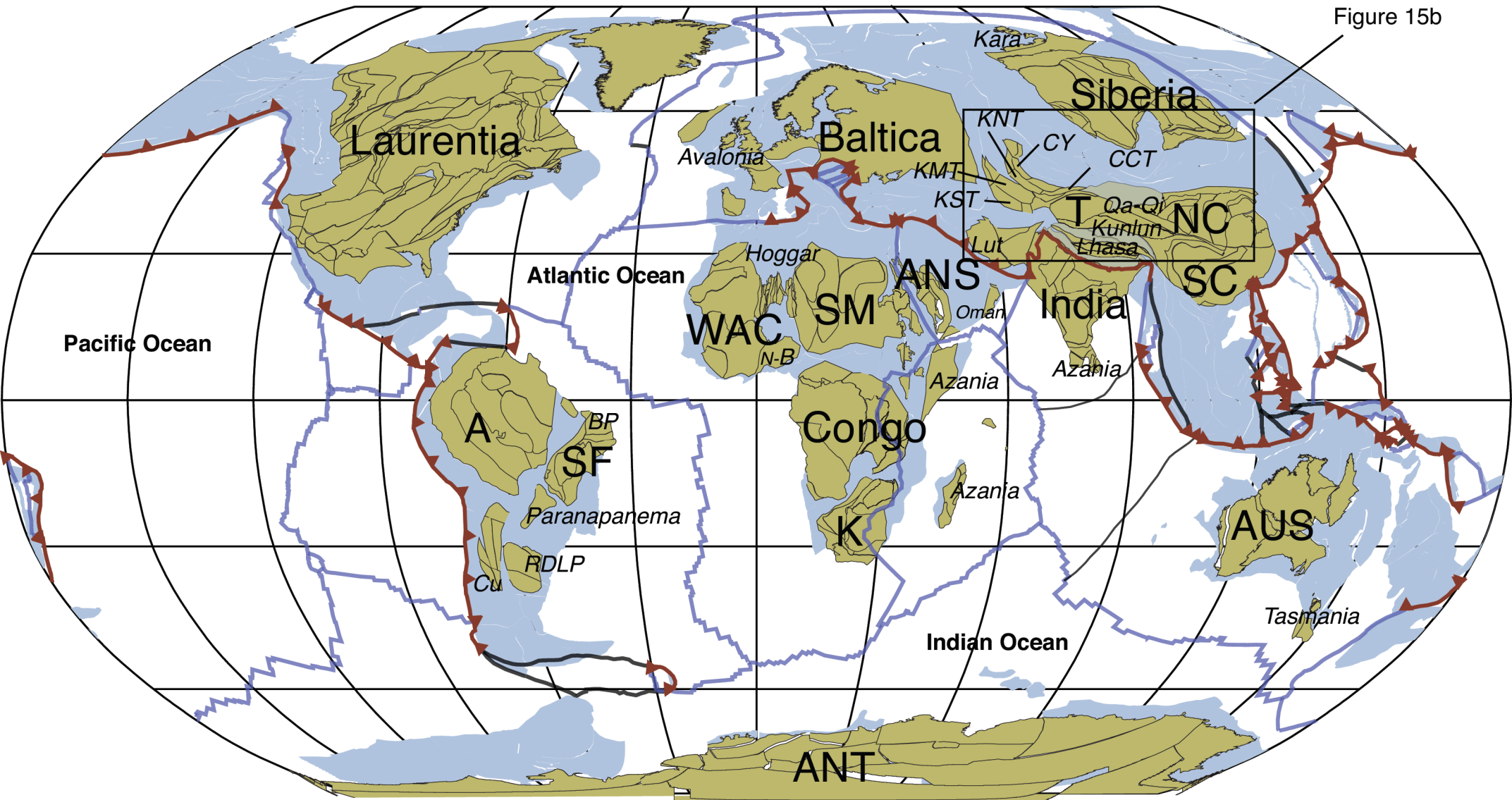






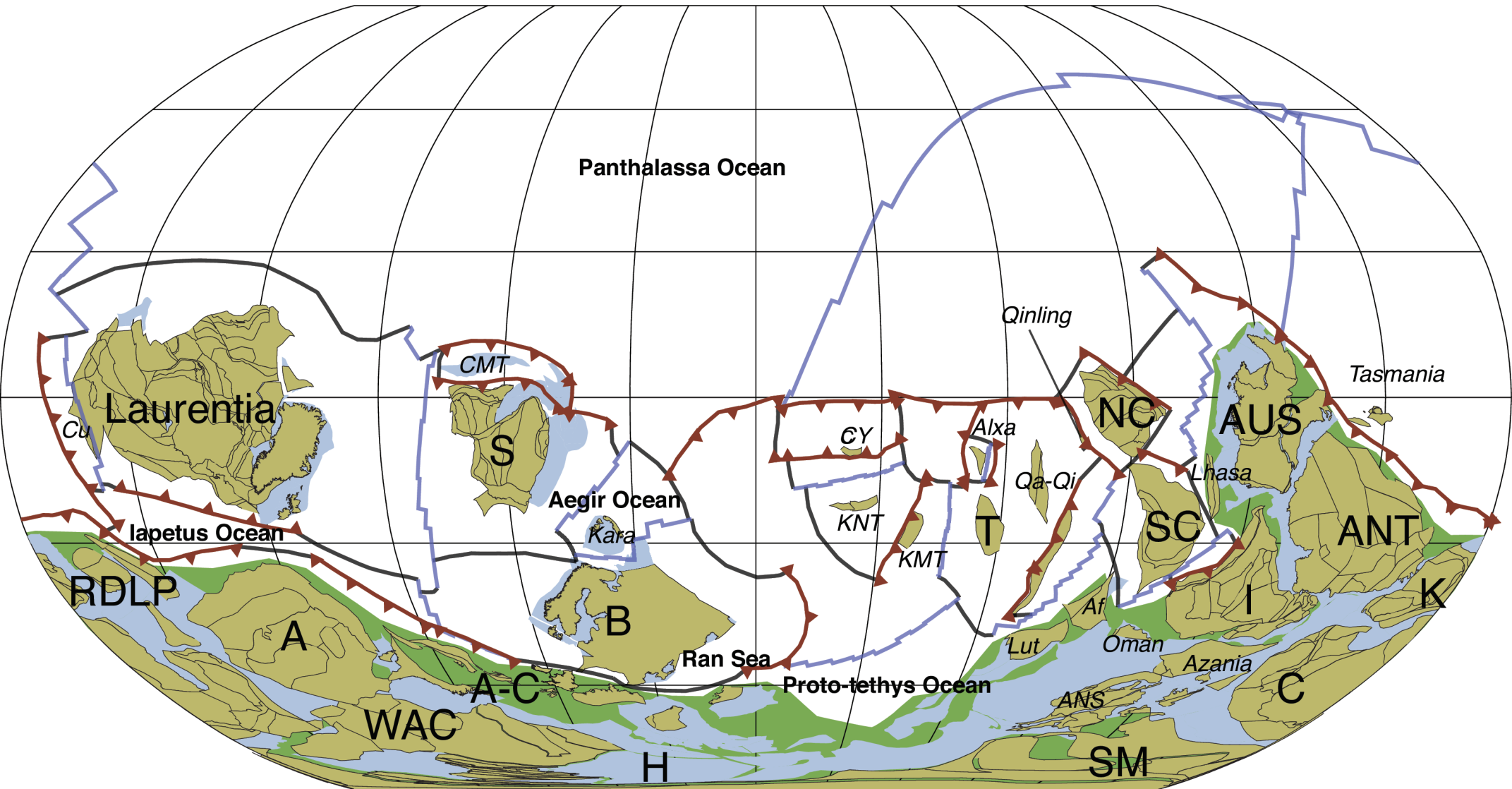
0 Ma

Figure 15b



 Convergent boundary
  Divergent boundary
  Transform boundary

500 Ma



Panthalassa Ocean

Laurentia

CMT

S

Aegir Ocean

Kara

B

Ran Sea

Proto-tethys Ocean

Qinling

NC

AUS

Tasmania

Lhasa

SC

ANT

RDLP

A

A-C

WAC

H

KNT

KMT

T

Alxa

Qa-Qi

Lut

ANS

Af

Oman

Azania

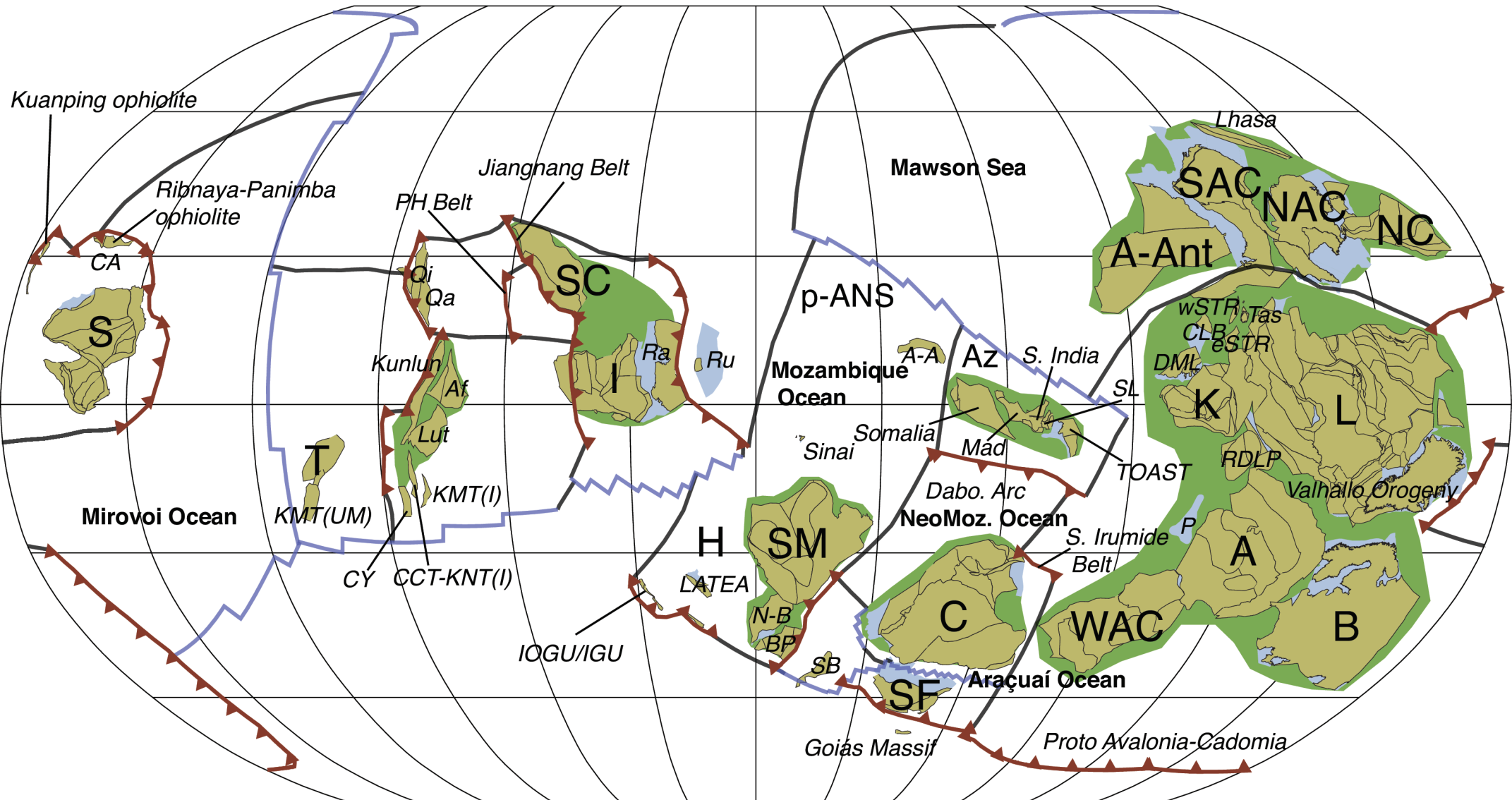
SM

C

K

Convergent boundary      Divergent boundary      Transform boundary

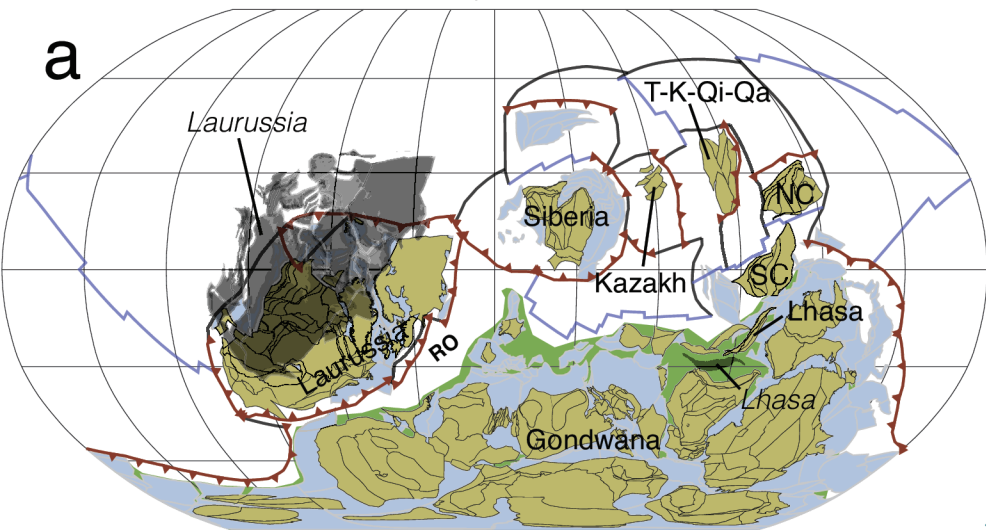
1000 Ma



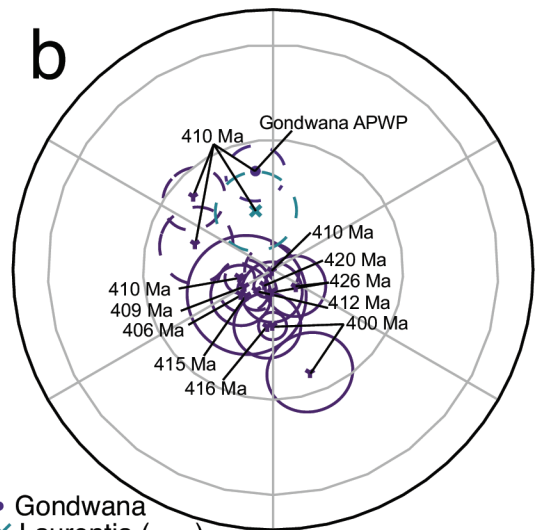
Convergent boundary      Divergent boundary      Transform boundary

# MER20, 410 Ma

a

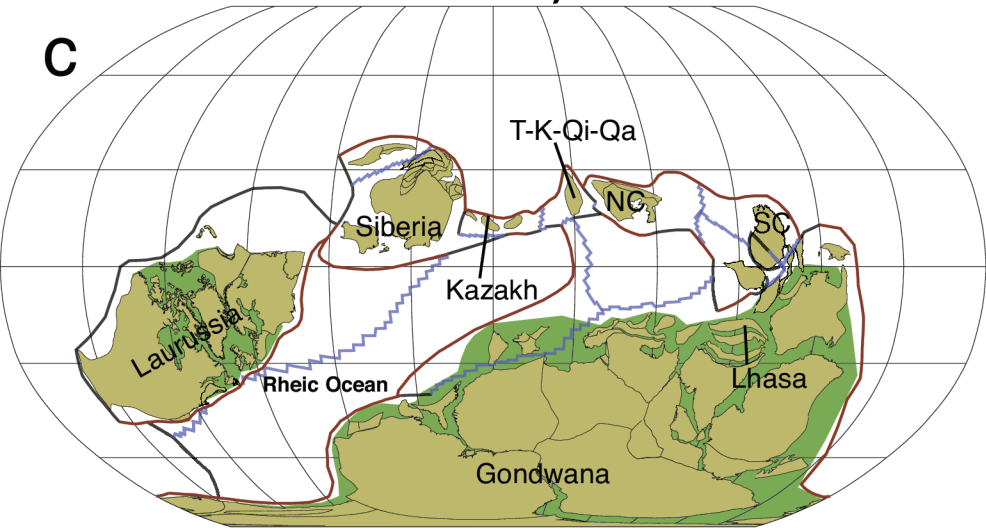


b

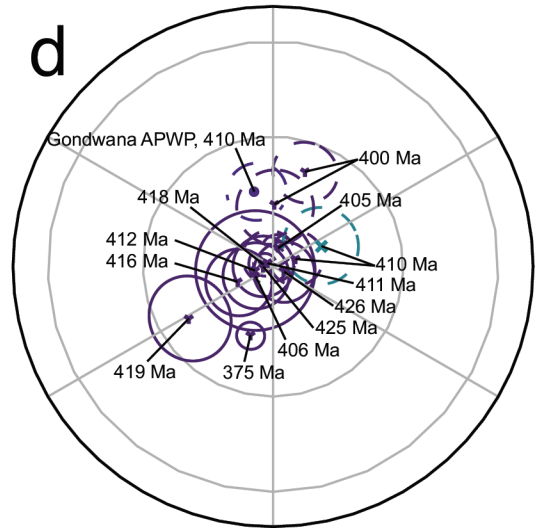


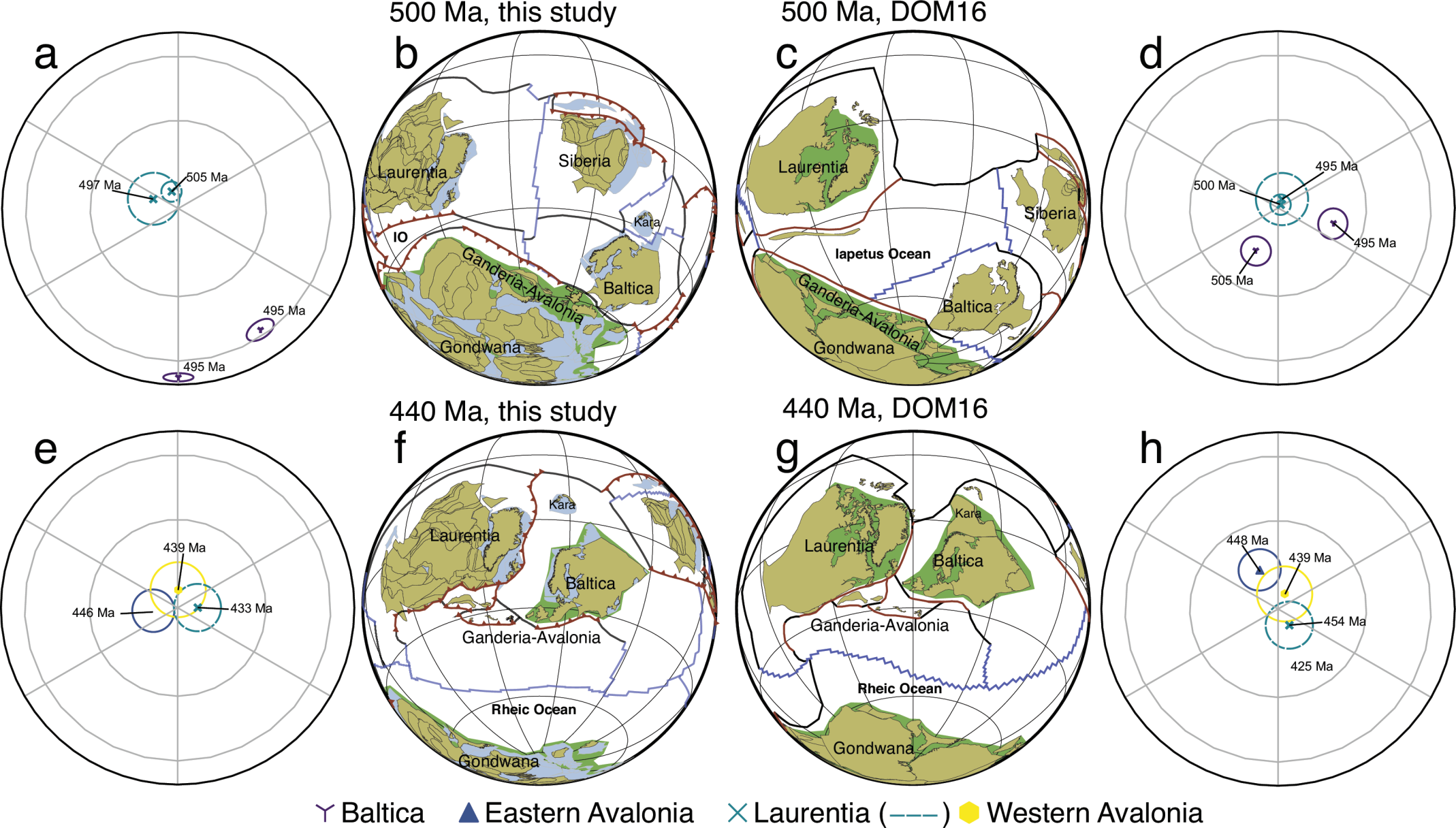
# DOM16/18, 411 Ma

c



d

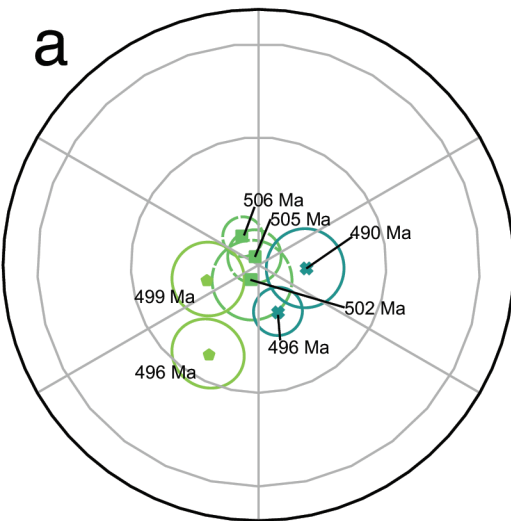




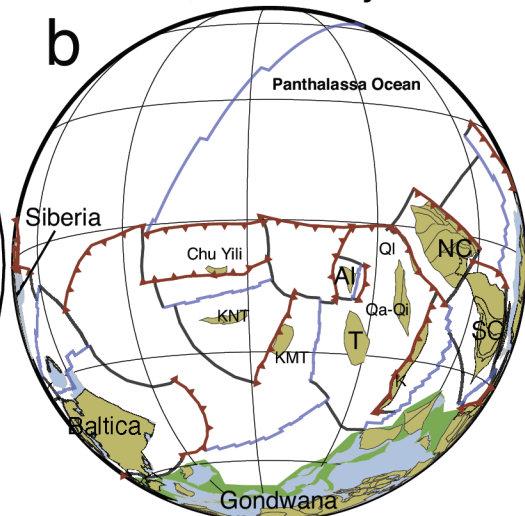
500 Ma, this study

500 Ma, DOM18

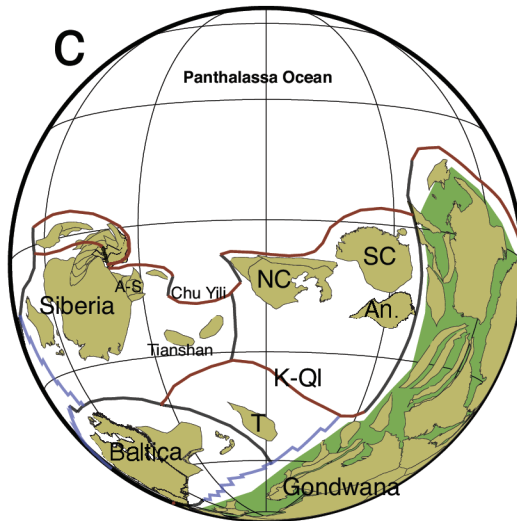
a



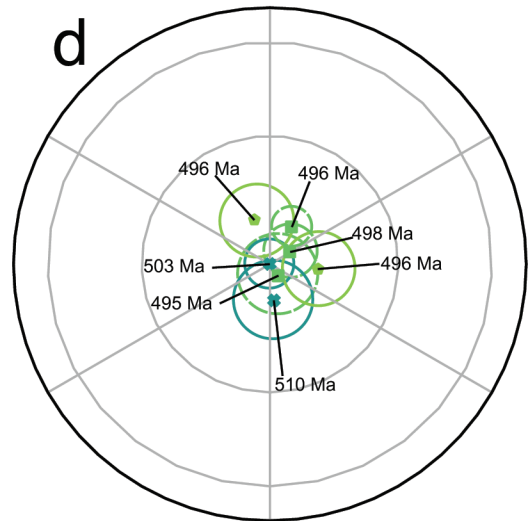
b



c



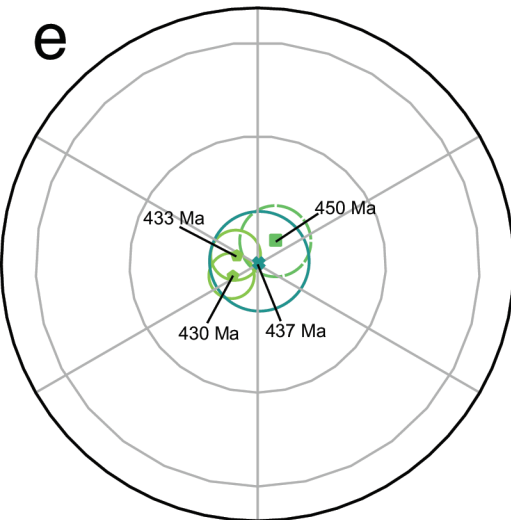
d



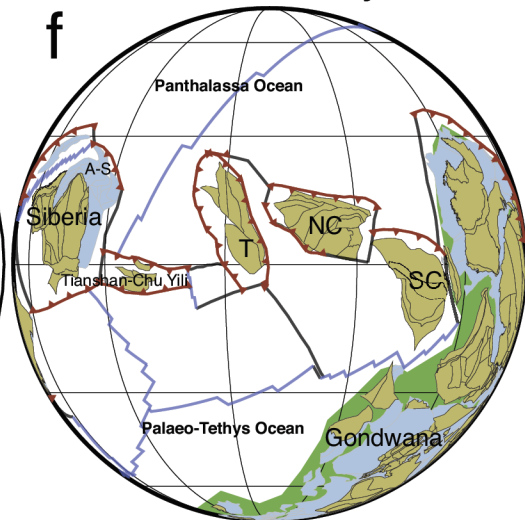
440 Ma, this study

440 Ma, DOM18

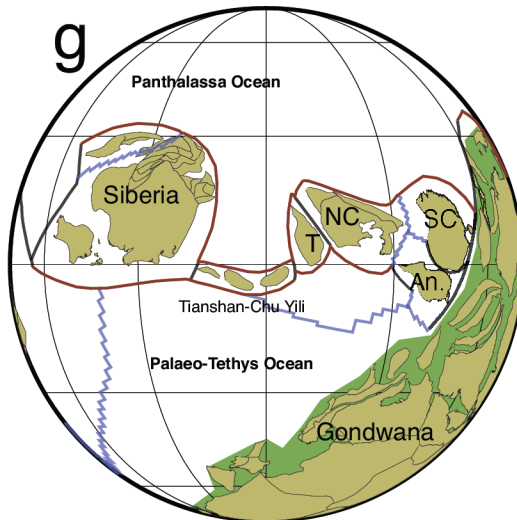
e



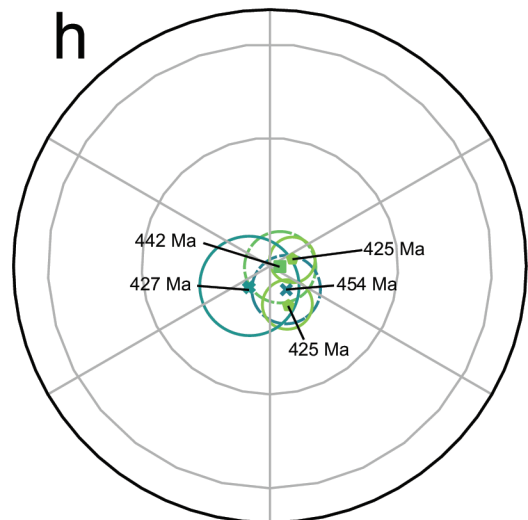
f



g



h



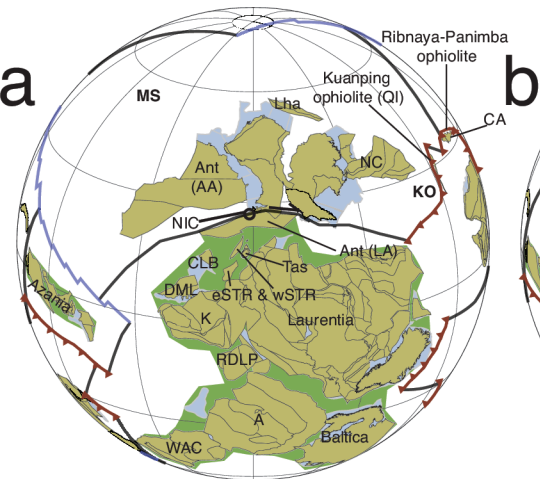
◆ North China

■ Siberia

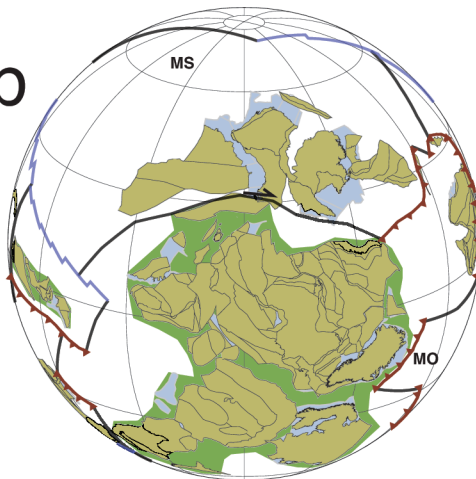
◆ South China



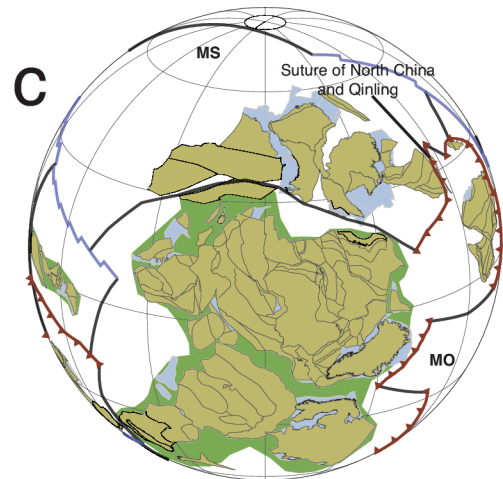
1000 Ma



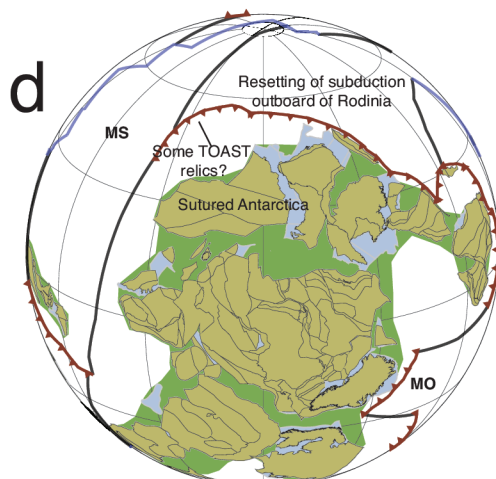
975 Ma



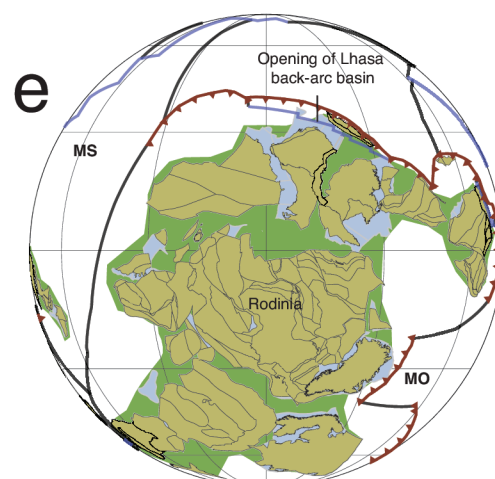
950 Ma



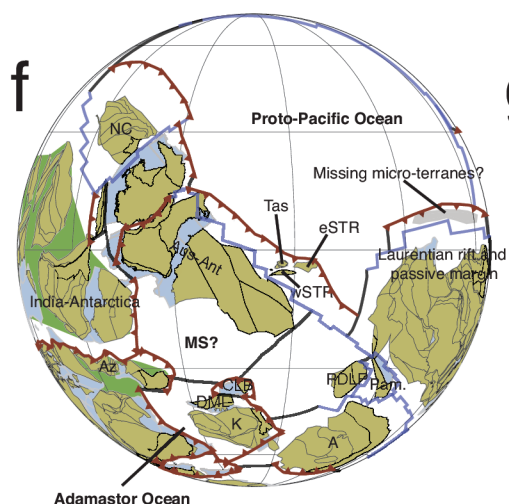
925 Ma



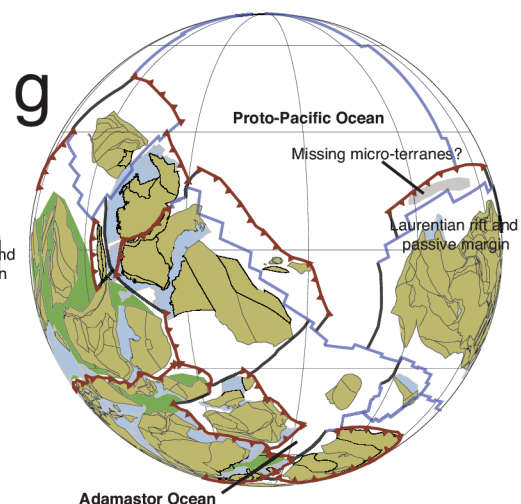
900 Ma

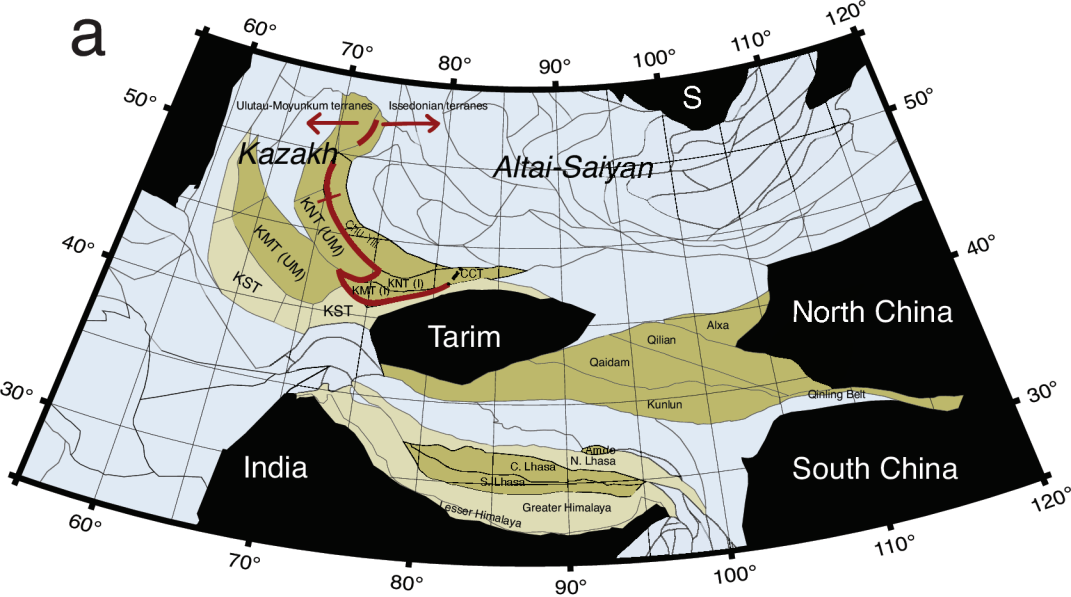


580 Ma



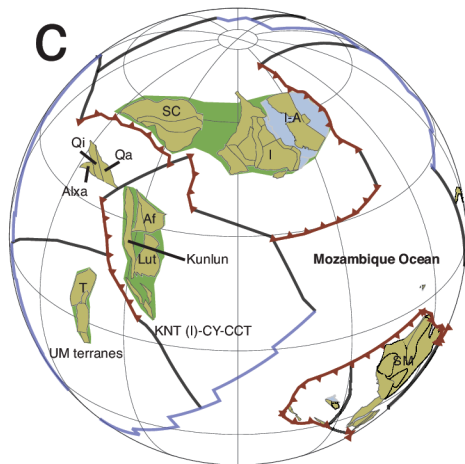
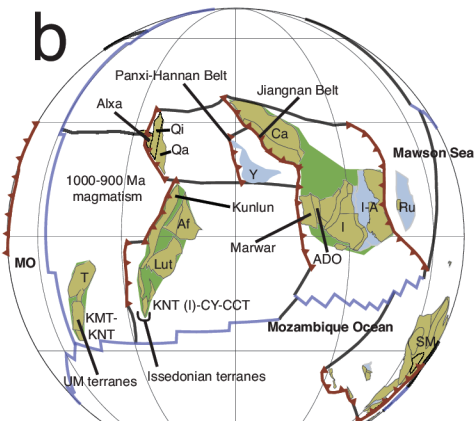
560 Ma





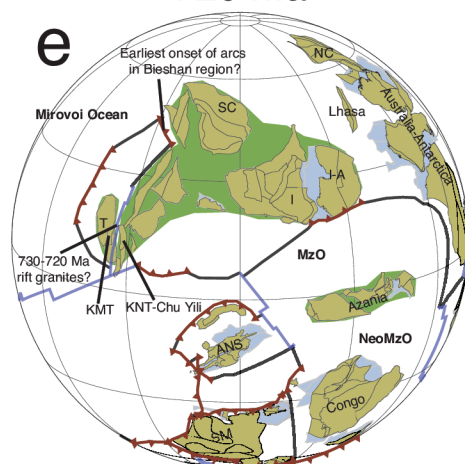
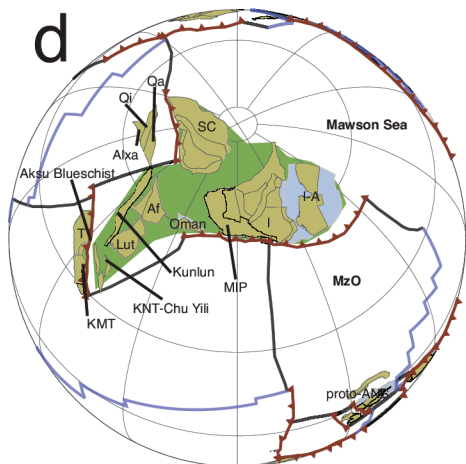
1000 Ma

900 Ma

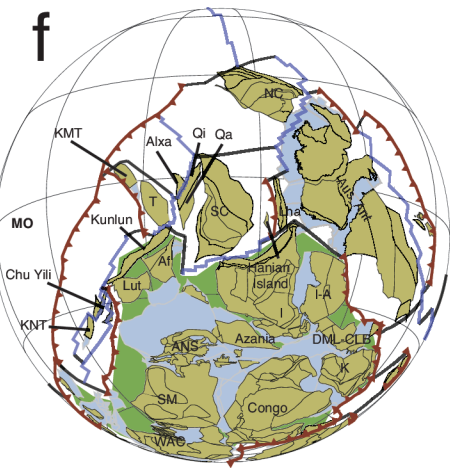


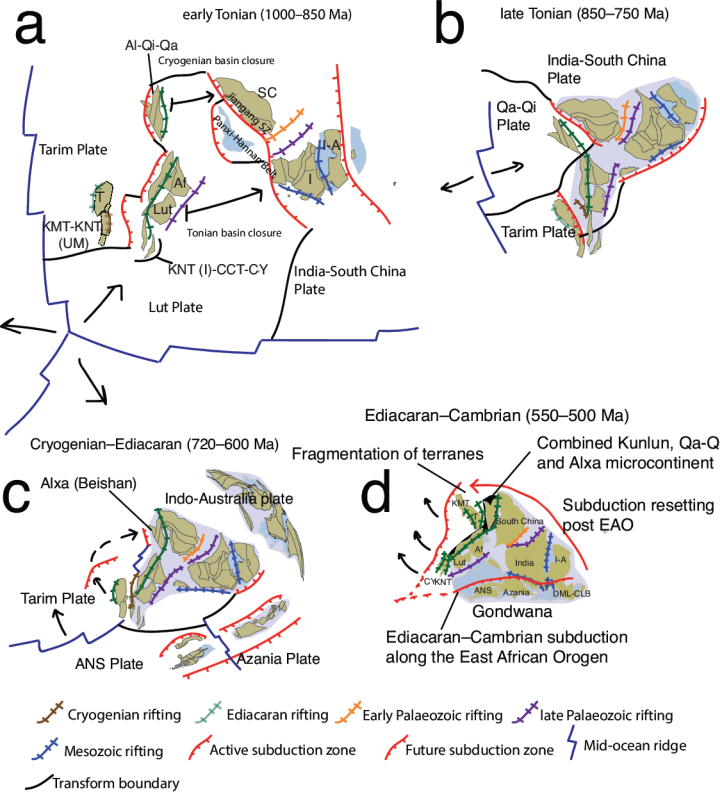
800 Ma

720 Ma



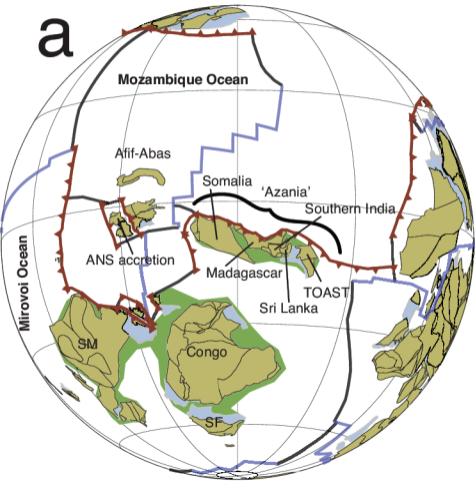
550 Ma





800 Ma

a



520 Ma

b

